Alcoa Environmental

Draft

RI Workplan for the

Alcoa (Point Comfort) / Lavaca Bay Superfund Site

Volume B3: Sediment Transport Study: Radiochemistry Study

Data Report

March 1998

ALCOA

150933

DRAFT

REMEDIAL INVESTIGATION WORK PLAN VOLUME B3
SEDIMENT TRANSPORT STUDY: RADIOCHEMISTRY STUDY

DATA REPORT

ALCOA(POINT COMFORT)/LAVACA BAY SUPERFUND SITE

Prepared for:

ALUMINUM COMPANY OF AMERICA
State Highway 35
Point Comfort, Texas 77978

Prepared By:

PARAMETRIX, INC.
10540 Rockley Road, Suite 300
Houston, Texas 77099

and

Dr. Peter Santschi and Dr. Mead Allison
TEXAS A&M UNIVERSITY at GALVESTON
5007 Avenue U
Galveston, Texas 77551

TABLE OF CONTENTS

APPENDICES

LIST OF TABLES

LIST OF FIGURES

ACRONYM LIST

Alcoa	Aluminum Company of America
AOC	Administrative Order on Consent
BLRA	Baseline Risk Assessment
°C	Degrees Celsius
CAPA	Chlor-Alkali Process Area
CCND	Calhoun County Navigation District
CERCLA	Comprehensive Environmental Response, Compensation, and Liability Act
CF	Constant Flux
CFR	Code of Federal Regulations
CIC	Constant Initial Concentration
cm	centimeter
COC	Chain-of-Custody
COPC	Chemical of Potential Concern
CVAA	Cold Vapor Atomic Absorption
DGPS	Differential Global Positioning System
DMP	Data Management Plan
DQO	Data Quality Objective
EPA	U.S. Environmental Protection Agency
FS	Feasibility Study
GIS	Geographic Information System
HSP	Activity-Specific Health and Safety Plan
IDW	Investigation Derived Waste
L	liter
LOER	Laboratory of Oceanic and Environmental Research
m	meter
mm	millimeter
mg	milligram
mg/kg	milligram per kilogram
MS	Matrix Spike
MSD	Matrix Spike Duplicate
PCO	Alcoa Point Comfort Operations
PMP	Project Management Plan
PSCR	Preliminary Site Characterization Report
QA/QC	Quality Assurance/Quality Control
QAP	Quality Assurance Plan
QAPjP	Quality Assurance Project Plan
RA	Risk Assessment
RCRA	Resource Conservation and Recovery Act
RI	Remedial Investigation
RI/FS	Remedial Investigation/Feasibility Study
RPD	Relative Percent Difference

ACRONYM LIST Continued

SAP	Sampling and Analysis Plan
SCUBA	Self Contained Underwater Breathing Apparatus
SOP	Standard Operating Procedure
SOW	Statement of Work
SSSHP	Site-Specific Safety and Health Plan
TOC	Total Organic Carbon
TNRCC	Texas Natural Resource Conservation Commission
U.S. EPA	United States Environmental Protection Agency

EXECUTIVE SUMMARY

Mercury was released in the late 1960s from a chlor-alkali facility managed by ALCOA and deposited into sediments of Lavaca Bay. Sediments of Lavaca Bay have recorded this event and, as a consequence, typically show well-defined subsurface maxima. The main objectives of this report are to evaluate 1) the potential for transfer of mercury to aquatic ecosystems through a mechanism by which subsurface particle reworking is coupled to sediment resuspension, 2) the impact of an anthropogenically altered sedimentation regime on burial rates of mercury in impacted sediments, and 3) recovery times of mercury contaminated sediments assuming no external inputs. Radiochemical methods, coupled to a numerical simulation approach, provide a means to not only reveal the sedimentation history of the bay, but also to decide if surface sediment concentrations of a contaminant such as mercury can be supported by mixing processes, or if they are an indication of external sources.

This report describes radionuclide and mercury data from sediment cores taken at fifteen stations in Lavaca Bay, collected from January to December 1997, and compare these radionuclide and mercury profiles with those from model simulations and with a database of core x-radiographs and grain size taken from the same locations. To the best of our knowledge, this is the most extensive radiochemical study ever undertaken in the Gulf coast outside the Mississippi River Delta region. X-radiography and grain size investigations can help to 1) provide additional insights into sedimentation patterns by defining the vertical stratigraphy, 2) normalize radiochemical and elemental concentration variations, 3) interpret radiochemical profiles because of strong affinity of tracers for fine-grained particles, and 4) act as tracers to delineate the source material and delivery mechanism for the sediments.

X-radiographs of tray cores were collected from 24 sites[1] to examine shallow (<70 cm depth) stratigraphy of the study area. These images indicate that layering of sediments emplaced by changes in hydrodynamics and sediment supply are preserved at all core depths. At most locations where radiograph images were examined, post-depositional biological disruption of this primary stratification by shelled macrofauna is limited: polychaetes and meiofaunal burrowers are the main bioturbators. Burrow lengths are comparable to the radiochemical surface mixed layer thickness (<10 cm) and support the concept that sediments below this are relatively undisturbed by natural or anthropogenic (e.g., shrimp trawling) mixing.

Basic grain size information (%sand:silt:clay) were obtained for 12-16 one cm depth intervals from 15 cores, with detailed granulometry by Rapid Settling Analyzer (RSA)/Sedigraph from 2-4 intervals/core. Sediment type in the study area varies from clayey sand to clay. Most core sites have a relatively uniform grain size distribution with depth. This consistent sediment source minimizes the effect of grain size on radiochemical activity concentrations. Cores from north of

[1] A total of 24 x-radiography cores were collected. These were comprised of the original 15 stations, 7 additional stations in Cox Bay, and 2 stations that were resampled to assess seasonal effects.

Dredge Island show downcore trends consistent with site changes induced by the creation and maintenance of dredge channels to the plant. Spatial changes are large and detailed granulometry indicate that these changes are a combination of hydrodynamic and source differences. Cox Bay granulometry resembles samples taken from actively infilling dredge channels, reflecting the influence of dredge spoiling in this area.

Age dating of all sediment cores was accomplished by analyzing the profiles of the atmospherically delivered nuclides ^{137}Cs, and, in some cases, $^{239,240}Pu$ (bomb fallout peak in 1963), and ^{210}Pb (half-life of 22 years, steady delivery). Sediment accumulation rates are highest in Cox Bay and at many sites in sediments from the shoreline of CAPA (Chlor-alkali plant area) and north of Dredge Island, and generally decrease away from these sites. Sedimentation rates in these high sedimentation areas are likely enhanced and influenced by anthropogenic activities such as dredging, shoreline erosion, and sheltering by dredge spoil islands.

Particle reworking (i.e., bioturbation or benthic mixing) rates were assessed by analyzing profiles of ^7Be, an atmospherically delivered radionuclide with a half-life of 53 days, in surface sediments. Particle reworking was generally restricted to the upper 2-5 cm of surface sediments, and could be higher and reach deeper (3-7 cm) into the surface sediments in the summer, primarily at sites with higher sedimentation rates. Higher sediment mixing rates were also measured in less impacted open water areas such as south Lavaca Bay and Keller Bay.

Numerical simulations of mercury profiles using sedimentation and mixing parameters derived from radionuclide data can be used to assess if mercury concentrations at the sediment surface can be supported by particle mixing. Peak shapes of mercury profiles in all near-shore sediments support a hypothesis that the input signal passes through a surface mixed layer as defined by the ^7Be data, and then is buried without further disturbance. At most sites, surface mercury concentrations cannot be supported by mixing of the buried layers of high mercury, 15-60 cm below the sediment-water interface. Mercury concentrations in surface sediments are predicted to decrease with recovery half times[2] of 1-9 years, depending on location, assuming there is no on-going source of mercury supply to the surficial sediments.

The data presented in this report demonstrates:

1) Based upon the radiochemistry data (e.g., ^7Be, $^{239,240}Pu$, ^{137}Cs, and ^{210}Pb), grain size data, and x-radiography that the historical mercury in the sediments of Lavaca Bay and Cox Bay is being buried at average sedimentation rates which vary between 0.4 - >2.0 cm/ year, depending upon the location. These rates are consistent with sedimentation rates estimated from mercury peaks using the assumption that the maximum deposition occurred between 1966 and 1969.

---

[2] Recovery half time is the time it takes to decrease the surface concentration to 50%. It is also the inverse of the recovery rate constant times the natural logarithm of 2.

2) The mixed layer depths in the impacted areas of Lavaca Bay are, in general, very shallow using evidence from the sharpness of the mercury peak, the radiography data, and the ^{7}Be data.
3) From the data presented in 1 and 2 above, cores from Cox Bay, and north of Dredge Island show that the mercury at the sediment surface is not a remnant of historical discharges (1966-1969), which are buried deep below.
4) Enhanced sedimentation rates are likely due to anthropogenic activities (i.e. dredge spoil placement, etc.) in Cox Bay and north of Dredge Island and changes in hydrodynamics due to the construction of the ship channel and Dredge Island.
5) Recovery half-time is predicted of the order of 1-9 years (depending upon location) once all external sources are eliminated.

1.0 INTRODUCTION

The Alcoa (Point Comfort)/Lavaca Bay Site was placed on the National Priority List on February 23, 1994, with an effective listing date of March 25, 1994. The Administrative Order on Consent (AOC) was issued on March 31, 1994, under the authority of the Comprehensive Environmental Response, Compensation, and Liability Act (CERCLA), and concerns the conduct of a Remedial Investigation (RI), Baseline Risk Assessment (BLRA), and Feasibility Study (FS) for the Alcoa (Point Comfort)/Lavaca Bay Superfund Site.

Negotiations in support of the development of the AOC were initiated in November of 1993 when Alcoa submitted a proposal to the United States Environmental Protection Agency (EPA) which supported the establishment of a comprehensive administrative mechanism to identify and evaluate areas potentially affected by historical releases of hazardous substances associated with activities at Point Comfort Operations (PCO). The scope of the proposal included the assessment of potential impacts of facility operations on the plant area, Dredge Island, and adjoining areas (e.g., Lavaca Bay system).

The AOC Statement of Work (SOW) for an RI at the Site requires investigations to characterize the environmental setting, the nature and extent of contamination, risks to human health and the environment, and the feasibility of alternative methods to remediate contamination of environmental media. Task III.A.4 of the SOW specifies that "...a program shall be conducted to characterize the surface water bodies on, adjacent to, crossing, or potentially affected by contaminants in the Study Area." As required under subsection (d) of Task III, the characterization shall include:

> *Description of physical characteristics of the sediment including depositional areas, thickness profiles, and physical parameters...*

To meet this requirement, ALCOA initiated a Sediment Transport Study (Alcoa 1997) designed to provide information on (1) the sediment grain size distribution in the study area; (2) the rates of sediment deposition and/or scour at representative locations; and (3) the major hydrometeorological forces affecting sediment transport including current and wind velocities, wave height and period, and salinity, temperature, and turbidity.

Initial attempts to estimate sedimentation rates for Lavaca Bay included the use of sediment traps; however, variable results were achieved. To provide more accurate estimates, a program was initiated (Radiochemistry Study) to collect sediment core samples and date the sediments along a subsurface profile as a means of estimating sediment accumulation and mixing rates.

Natural and anthropogenic radionuclides are powerful geochemical tracers and geochronological tools (e.g., Santschi and Honeyman, 1989). Natural radionuclides include primordial (e.g., U and Th decay series nuclides such as ^{210}Pb) and cosmogenic radionuclides (e.g., ^{7}Be). The latter are delivered to the earth surface through atmospheric processes, while the former are ubiquitous and are produced in-situ. Anthropogenic nuclides include the nuclides produced from bomb tests in the 1950's and 1960's (e.g., ^{137}Cs and $^{239,240}Pu$). Since the production rates in each of the earth's reservoirs is exactly known for many of these nuclides, they can, for example, be used to date sediments and calculate sedimentation rates, and estimate sediment mixing rates. ^{7}Be and ^{210}Pb fluxes from the atmosphere have been measured in Galveston and College Station, over a two year period, and have been found to be primarily controlled by the amount of rain fall (Baskaran et al., 1993a). ^{137}Cs and $^{239,240}Pu$ nuclides have been shown to be useful dating tools in Gulf Coast estuaries (e.g., Ravichandran et al., 1995a,b). Studies of geochemical transport mechanisms of natural radionuclides in these estuaries have been published as well (e.g., Baskaran et al., 1993b).

In this radiochemical investigation of mercury transport in Lavaca Bay, a number of radionuclides, such as ^{7}Be (for deriving sediment mixing rates in surface sediments), ^{137}Cs and $^{239,240}Pu$ (for deriving sedimentation and sediment accumulation rates, as well as verifying sediment mixing rates) have been applied. Natural ^{210}Pb has been useful as an independent geochronometer and also for testing if sediment and mercury accumulation has been continuous or episodical. Most importantly, using a numerical sedimentation and mixing model, it is possible to simulate selected radionuclide and mercury profiles. This should allow for predictions about sediment recovery rates for mercury, provided that any significant external sources of mercury are controlled.

Many recent radiochemical studies of sediment accumulation and mixing in coastal and marine environments (Allison et al., 1995) incorporate geological information to improve interpretation of results. Nittrouer and Sternberg (1981) first showed that the ratio of accumulation rate to mixing rate can be used to predict the extent that physical sedimentary structures (e.g., laminations and beds) are altered by biological mixing. High ratios are indicated by the preservation of these primary features while low ratios show a massive, homogenized stratigraphy. Stratigraphy of modern sediments can be recognized in x-radiographs and petrographic thin-sections. Grain size information also aids in interpretation of radiochemical profiles because of the strong affinity of tracers for fine-grained particles (e.g., Ravichandran et al., 1995a,b). Detailed granulometry has also been used (summarized in Kranck and Milligan, 1985) to identify the sediment source and delivery mechanisms of sediment to the depositional site.

1.1 PURPOSE AND OBJECTIVES

The primary objective of the Radiochemistry Study was to estimate the rate of sedimentation through radioisotope analyses at several locations near Alcoa's Point Comfort Operations adjacent to Lavaca Bay. By collecting sediment core samples and dating the material at various depth strata, it was anticipated that corresponding depths would provide information to estimate deposition rates, thus providing a chronological history of the core sample.

Another objective of the study was to collect x-radiographs and isotope data of the core samples to provide a detailed picture of the sediment accumulation and mixing processes occurring at each location. Radiochemical and x-ray image data, coupled with the total mercury analyses at the corresponding depths, would provide information to support the understanding of current versus historical sources of mercury to Lavaca Bay sediments and provide insights into the potential for future exposure of mercury which has been buried by depositional processes in the Bay.

1.2 STUDY LOCATION

The Radiochemistry Study area encompasses a large portion of Lavaca Bay, with the primary focus being the immediate vicinity of the Alcoa plant and the closed area (Figure 1-1). Alcoa's PCO is located on a portion of the eastern shoreline of Lavaca Bay. Lavaca Bay is located in the western part of the Matagorda Bay system, which includes parts of Matagorda, Calhoun, Victoria and Jackson counties. The Preliminary Site Characterization Report (PSCR, Alcoa 1995) and Ward (1994) contain detailed information on the Matagorda and Lavaca Bay systems.

Within Lavaca Bay and Cox Bay, a total of fifteen locations were sampled for all analyses in the Radiochemistry Study (Figure 1-2). An additional seven stations were sampled for x-radiography only, and three of the original stations[3] were resampled to assess potential seasonality effects. When possible, stations that had been sampled previously (e.g., Phase 2A/2B Investigations) were included in the program to maximize the data available for a specific location.

---

[3] X-radiography negatives were taken at only two of the three stations resampled to evaluate seasonal variability.

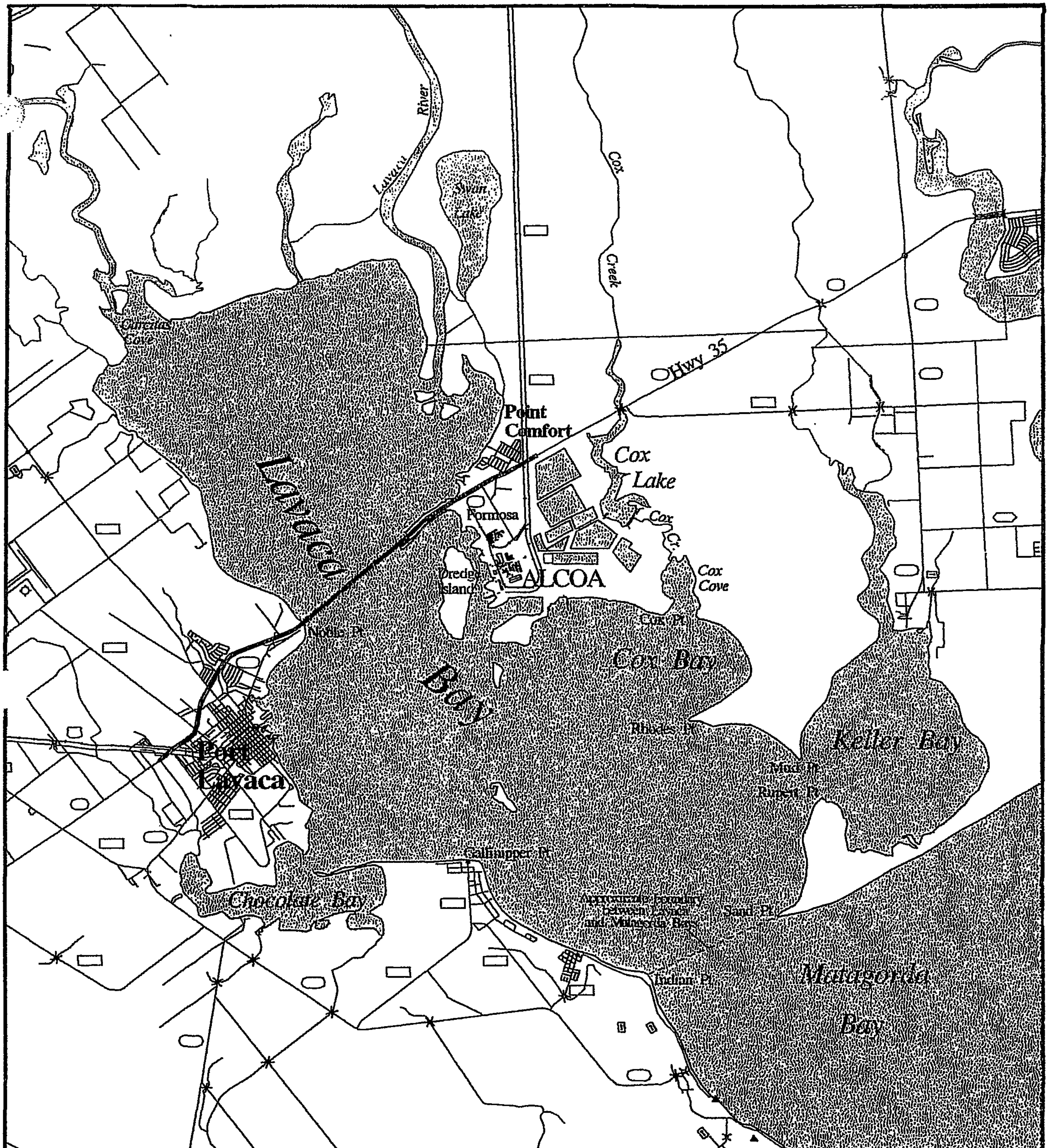

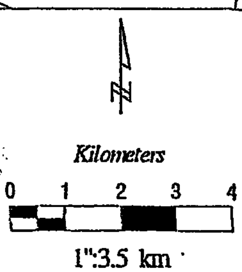

Figure 1-1.
Alcoa PCO Site and Lavaca Bay Location Map

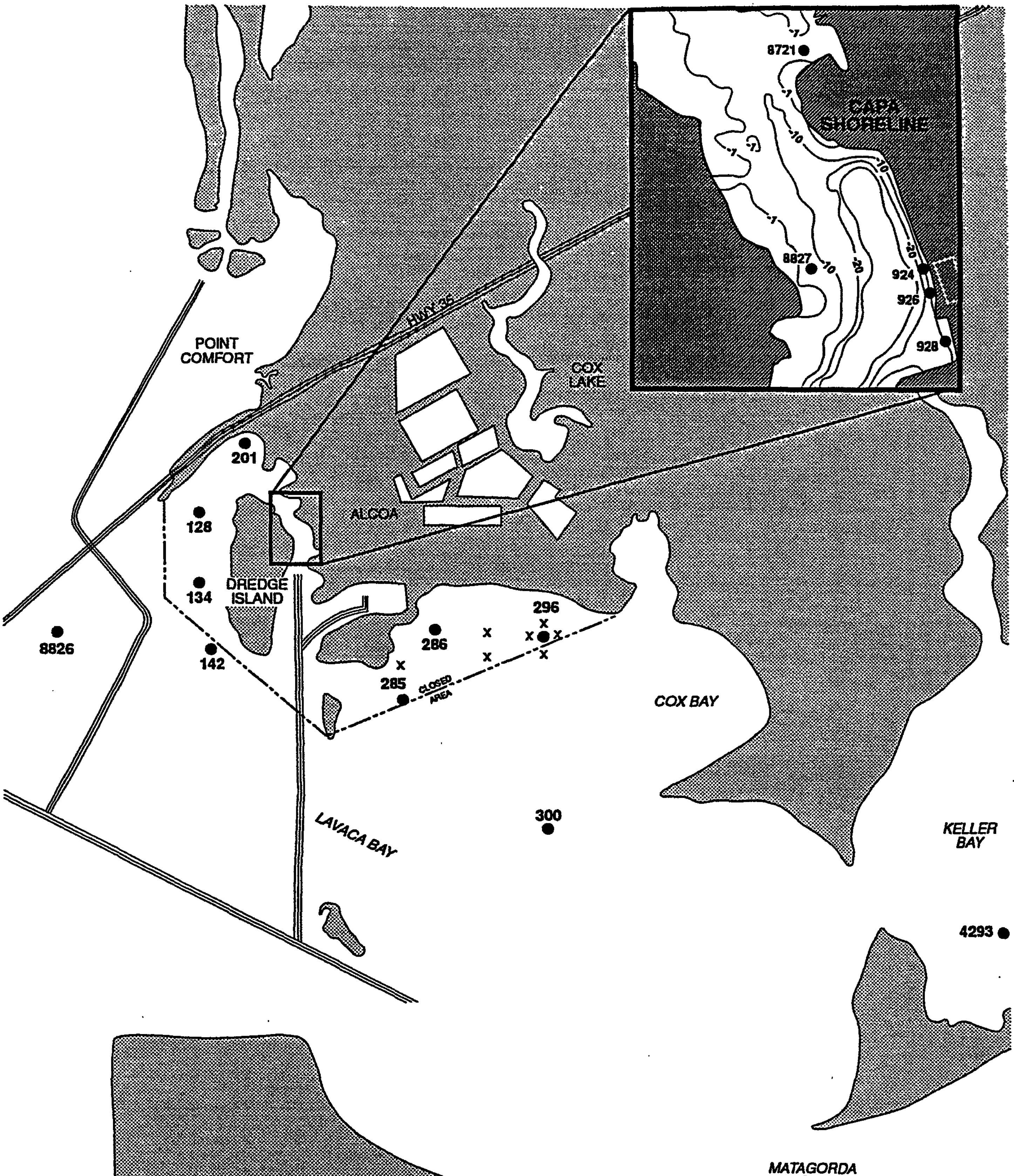

Note: Stations 128, 296 and 286 sampled twice for ^7Be to evaluate seasonal effects

Alcoa Dredge Island/54-2824-107(01) 2/98

KILOMETERS 0 1 2 3

1:75,000

N

● Samples collected for total mercury, TOC, x-radiography and radioisotope analyses

x Samples collected for x-radiography only

Figure 1-2.
Alcoa Point Comfort Operations: Radiochemistry Sampling Locations

2.0 FIELD PROGRAM

The field program for the Radiochemistry Study was designed to collect sediment core samples from several locations in Lavaca Bay for total mercury, radioisotope, and x-radiography analyses. This section first presents the overall study design and then describes the field methods employed in collecting the sediment core samples.

2.1 STUDY DESIGN

The Radiochemistry Study was designed to collect one sediment core for total mercury and radioisotope analyses, and one box core sample for performing x-radiography and grain size analyses at each of fifteen (15) stations located in and around the closed area of Lavaca Bay (see Figure 1-2). Several additional stations (e.g., around Station 296) were sampled for x-radiography to assist in interpreting the stratigraphy results for portions of Cox Bay. Three stations (128, 286, and 296) were sampled on two occasions for ^{7}Be and x-radiography to determine possible seasonal effects on surface mixed layer. Also, additional stations (e.g., South Dredge Island, "Y" Channel Grab, Lower River Channel Grab) were grab sampled for grain size only from various areas to be used for evaluating potential sources of material being deposited into the Alcoa ship channel. These stations are not represented on Figure 1-2, but are discussed with the grain size results.

Sample stations were selected based on areas with a high percentage of fine grained sediments and on a review of the available mercury data for surface and subsurface sediments collected during the Phase 2A and 2B field investigations, and the preliminary results from the hydrodynamic and sediment mixing models for the Bay. Open bay coring sites are therefore not necessarily representative for the bay as a whole. When possible, stations were selected that had been previously sampled so that the data could be compared to the results from previous investigations.

The following sections provide additional detail regarding core sample collection and processing procedures.

2.2 BULK SEDIMENT SAMPLING

Bulk sediments for total mercury and radioisotope analyses were collected using similar procedures as employed during previous field investigations in Lavaca Bay (e.g., Bay System Phase 2A and 2B Investigations). These procedures consist of inserting a 4" ID acrylic core tube into the sediments by SCUBA diver to the desired depth, capping the core tube with an airtight pressure cap, and removing the core tube from the sediment using an electric winch mounted on a 24-foot aluminum research boat. Once on board the boat, the core tubes are secured for transport back to the shore for processing.

The sediment is removed by placing the core tube on a piston-type plunger and extruding the sediment from the top of the core. As the sediment is pushed out of the core, it is measured with a ruler and cut at the desired sample intervals using a stainless-steel spatula and placed into a stainless-steel mixing bowl. The sediments are then homogenized using a stainless-steel spoon and placed into borosilicate glass sample jars for shipment to the analytical laboratory.

The study design for the radiochemistry program included subsampling the sediment cores every 1 cm to provide highly detailed depth profiles. Initially, subsamples from the following 20 depth intervals[4] were analyzed for total mercury: 0-1, 1-2, 2-3, 3-4, 4-5, 5-6, 6-7, 7-8, 8-9, 9-10, 15-16, 20-21, 25-26, 30-31, 35-36, 40-41, 45-46, 50-51, 55-56, 60-61. Later, if strong transitional zones were observed (e.g., total mercury results that changed from 1.2 ppm to 0.1 ppm over a 5 cm depth), additional sample intervals were analyzed to fill in the data gaps.

Prior to shipment, the bulk sediment samples for mercury analysis were stored in a secured refrigerator set at 4°C. Samples for radioisotope analyses were stored at ambient temperature. All samples were logged and tracked using chain-of-custody (COC) forms according to the procedures outlined in the project Quality Assurance Project Plan (QAPjP).

2.3 X-RADIOGRAPHY BOX CORE SAMPLING

To allow x-rays to penetrate the sediment core samples, a special coring device was constructed that yielded a flat cross-section of the sediment core. The coring device was developed by staff at Texas A&M University and was, essentially, an acrylic box core that had three fixed walls and a sliding door to form the fourth wall. When closed, the box core yielded a 1" x 4" x 36" cross-section of the sediment/water interface.

To collect the box core sample, the device was fully inserted into the sediment by SCUBA diver with the sliding door removed. The sliding door was then inserted to close the box core. Next, the diver removed the sediment from around the core to loosen the core from the sediment. The box core was then removed from the sediment, capped on both ends, and secured on the boat for transport back to shore. Once on shore, the box core was stored upright and immediately transported to Texas A&M University's Laboratory for Oceanographic and Environmental Research (LOER) located in Galveston, Texas for analysis.

[4] Note: The core sample compositing scheme for Station STO0128, the first site sampled, consisted of 1 cm intervals for the first five cm (e.g., 0-1, 1-2), then five cm composites for the next 55 cm (e.g. 5-10, 10-15, etc.)

3.0 ANALYTICAL METHODOLOGY

3.1 OVERVIEW

The following sections describe the laboratory procedures used to conduct the total mercury, total organic carbon (TOC), radioisotope, porosity, x-radiography and grain size analyses.

3.2 TOTAL MERCURY ANALYSES

Total mercury analyses were performed by Lancaster Laboratories in Lancaster, Pennsylvania using CVAA, according to method SW7471A. All results were reported on a dry weight basis. Laboratory quality assurance procedures included the use of duplicates, matrix spikes and matrix spike duplicates.

3.3 TOTAL ORGANIC CARBON ANALYSES

Total organic carbon analyses were also performed by Lancaster Laboratories using IR Spectrometry according to method SW9012. Laboratory quality assurance procedures for TOC analyses included laboratory triplicate samples.

3.4 GRAIN SIZE ANALYSES

Sediment grain size analyses were conducted under the direction of Dr. Mead Allison of Texas A&M University's LOER in Galveston, Texas. Sediment samples for grain size analysis were collected from the tray cores following x-radiography. Samples were analyzed for sand:silt:clay ratios by a combination of sieve and pipette analysis.

Detailed granulometric analysis was conducted on selected samples (2-4/core) using Sedigraph/Rapid Settling Analyzer (RSA) analysis. The mud fraction was analyzed with a Sedigraph Model 5100 automated x-ray particle analyzer as a mud/deionized water slurry. The sand fraction was analyzed with a 180-cm-long RSA. Analyses were integrated by the pipette method outlined in Appendix A.

3.5 RADIOISOTOPE ANALYSES

All radioisotope analyses were performed at Texas A&M University's LOER in Galveston, Texas under the direction of Dr. Peter Santschi. In general, sediment samples of approximately 10 grams were used for non-destructive gamma counting in a low-background, high-efficiency, high purity, Germanium (HPGe) well detector for one day, followed by wet chemical extraction procedures and alpha counting for individual radionuclides in selected samples. Alpha counting of samples was carried out on surface barrier detectors for several (3-4) days each. A list of half lives and energies of gamma emitting isotopes is given in Table 3-1. Specific procedures used for counting the individual radionuclides are presented in the following sections and in Appendix B.

Table 3-1. List of gamma emitting radioisotopes.

Isotope	Half Life	Gamma Energy (keV)
^{210}Pb	22 years	46
^{234}Th	24 days	63
^{226}Ra	1600 years	352
^{228}Ra	5.7 years	338,911
^{7}Be	53 days	478
^{137}Cs	30 years	662

3.5.1 Beryllium-7

^{7}Be concentrations were determined by non-destructive gamma counting using 10 grams of sediment according to the procedures given by Schuler et al. (1991).

3.5.2 Lead-210

^{210}Pb concentrations from selected sediment cores were determined by alpha counting using 1 gram of sediment, after complete digestion and chemical separation, according to the procedures given in Santschi et al. (1980), and Ravichandran et al. (1995a,b). In addition, samples from every core were also gamma counted, resulting in another, often less precise, ^{210}Pb value.

3.5.3 Cesium-137

^{137}Cs concentrations were determined by non-destructive gamma counting using approximately 10 grams of sediment according to the procedures given in Wan et al. (1986), and Schuler et al. (1991).

3.5.4 Radium-226

^{226}Ra concentrations were determined by non-destructive gamma counting using approximately 10 grams of sediment according to the procedures given in Santschi et al. (1980) , Baskaran et al. (1995), and Ravichandran et al. (1995a,b). Measured ^{226}Ra activity concentrations, reported from the 351 keV gamma peak (produced by the ^{226}Ra grand daughter nuclide ^{214}Pb), could not always be used to calculate supported ^{210}Pb concentrations, likely due to some ^{222}Rn loss problems in the counting vials. In the case of disagreement between ^{210}Pb activity at depth and the ^{226}Ra concentration (e.g., core 134), the constant ^{210}Pb activity at depth in that core was used for the purpose of calculating excess-^{210}Pb activities.

3.5.5 Radium-228

^{228}Ra concentrations were determined by non-destructive gamma counting using approximately 10 grams of sediment according to the procedures given in Baskaran et al. (1993, 1995), and Ravichandran et al. (1995b). Values were constant within a core, and were not used any further.

3.5.6 Thorium-234

^{234}Th concentrations were determined by non-destructive gamma counting using approximately 10 grams of sediment according to the procedures given in Santschi et al. (1980). Values are reported but were not further used because excess-^{234}Th [$^{234}Th_{xs}$ = ^{234}Th(total) - ^{234}Th(supported)] in surface sediments were zero, within the errors of the measurements. ^{234}Th(supported) activities are equal to those of ^{238}U in the sediments, and are normally determined from both ^{234}Th activities at 5-10 cm below the surface, and from recounting surface sediment samples about 6 months after collection.

3.5.7 Plutonium-239,240

$^{239,240}Pu$ concentrations were determined by wet chemistry followed by alpha counting, according to the procedures given in Santschi et al. (1980, 1984), Baskaran et al. (1995), and Ravichandran et al. (1995b).

3.6 X-RADIOGRAPHY ANALYSES

X-radiography analyses were conducted under the direction of Dr. Mead Allison by Texas A&M University's LOER located in Galveston, Texas. Acrylic (10x4x90cm) box cores were collected from the Lavaca Bay sites and returned to the LOER lab for x-raying on the same day to minimize disturbance and drying of the cores. Trays were x-rayed with a Kramex PX-20N machine at 15mA/70 kV. Fuji sheet negatives were developed in house and scanned into digital form at 300 dpi resolution. Individual x-ray sections of cores were merged digitally to form a single image of each core.

After taking the x-radiographs of the core samples, the box cores were carefully opened by removing the sliding door to expose the sediment. Subsamples of the sediment were collected at discreet depth intervals for use in the detailed grain size analyses (see Section 3.4)

3.7 POROSITY ANALYSES

Porosity (volume fraction of wet sediments occupied by water) was determined from measurements of wet weight and dry weight of sediment samples for the radiochemical analyses, as described in Appendix B.

3.8 LABORATORY QA/QC ANALYSES

This section summarizes analytical data quality for the Radiochemistry Study. The data reviewed in this study are acceptable for use as Level 4 data. Components of the data validation performed are specified in standard operating procedure RAD-SOP-001, "Standard Operation Procedure for Data Validation" (6 March 1996). Data validation included evaluation of the following as appropriate:

- Holding Times and Sample Preservation
- Initial and Continuing Calibration Data
- Reagent and/or Method Blanks
- Laboratory Control Sample and/or Blank Spike Recovery
- Matrix Spike (MS) and Matrix Spike Duplicate (MSD) Recoveries
- Duplicate Sample Relative Percent Differences (RPDs)

Data validation was performed using modified versions of the checklists found in the *RI WORK PLAN for the Alcoa (Point Comfort)/Lavaca Bay Superfund Site, Volume B1: Quality Assurance Plan for Analytical Actives* (October 1995). These checklists contain specific evaluation of the above criteria and are maintained in the Project File. During the validation process, flags were applied to the data to indicate an interferant or recovery problem with the Quality Assurance (QA) samples associated with the samples. Definitions for these flags are provided in Table 3-2.

Table 3-2. Definitions of validation flags applied to the Radiochemistry Study data.

FLAG	DESCRIPTION
J	The analyte was present, but the reported value may not be accurate or precise.
J+	The analyte was present, but the reported value may not be accurate or precise; and there may be a high bias in the value reported (actual concentration may be lower than the reported result).
J-	The analyte was present, but the reported value may not be accurate or precise; and there may be a low bias in the value reported (actual concentration may be higher than the reported result).

These flags indicate that there is a chance that the value was not accurate or precise however, the magnitude of the potential imprecision or inaccuracy was not great enough to reject the value.

4.0 DATA CALCULATIONS

The following sections present the data calculations used to determine values related to modeling of particle reworking, sedimentation, and sediment accumulation rates.

4.1 DETERMINATION OF SEDIMENTATION RATES

Sedimentation rates (in cm/year) can be calculated from time markers, or from profiles of chemicals with a known decay rate (Santschi and Honeyman, 1989). Because compaction is not negligible in some of the sediment cores, or because porosities and densities increase and decrease with depth, it is more reliable to calculate an average sediment accumulation rate (in g cm^{-2} yr^{-1}). An estimate of the average sediment accumulation rate, S_a, can be obtained for the time since 1963 for bomb fallout nuclides, and 1968 for mercury, assuming an average porosity, Ø, and a dry sediment density, ρ, of 2.5 g cm^{-3}, as follows.

$$S_a = S\,(1-Ø)\,\rho \qquad (1)$$

with $S = \Delta x/\Delta t$, Δx = depth interval from surface to peak, Δt = time difference between 1963 (for Cs) or 1968 (for mercury), respectively, and 1997. Alternatively, S_a can be determined from $\Delta m/\Delta t$, with = cumulative mass from surface to the peak = integrated mass of dry sediments per unit area = $\sum \Delta x_i(1-Ø_i)\,\rho$.

Methods applied to date for Lavaca Bay sediments include the following.

1) From bomb fallout nuclide (e.g., ^{137}Cs, $^{239,240}Pu$) peak concentration in 1963

This method could be successfully applied for many (but not all) Lavaca Bay sediment cores, by plotting activity concentrations vs. depth (or mass depth in g cm^{-2}). Sedimentation rates can then be directly calculated from the depth of the ^{137}Cs peak (or Δm) divided by the time difference to 1963. In some of the cores, there were no well-developed peaks of these nuclides. However, the presence of significant amounts of ^{137}Cs at a given depth can be used to constrain sedimentation rates (i.e., put a lower limit on it).

2) *From the $^{210}Pb_{xs}$ (= [^{210}Pb] - [^{226}Ra]) profile.*

^{210}Pb is an atmospherically delivered radionuclide with a half life of 22 years. Sedimentation rates can be calculated, under steady state conditions, and when the sediment inventory of unsupported ^{210}Pb ($^{210}Pb_{xs}$) is close to that expected from atmospheric fallout, from the Constant Initial Concentration (CIC) model (Appleby and Oldfield, 1978; Robbins, 1978), given in eq. 2.

$$[^{210}Pb_{xs}(z)] = [^{210}Pb_{xs}(o)]\,\exp(-\alpha z) \qquad (2a)$$
$$\alpha = (\lambda/S) \qquad (2b)$$

where z = depth in cm (or mass depth in g cm^{-2}), and S = sedimentation rate in cm/yr (or sediment accumulation rate in g cm^{-2} yr^{-1}, respectively) and where λ is the decay constant of ^{210}Pb (=0.031 $year^{-1}$). This method assumes that particle reworking rates are negligible over most of the depth interval of the ^{210}Pb profile, which can be verified by numerical modeling of profiles of radioisotopic and mercury time markers, as described below. If bioturbation were significant over this lower depth range, the $^{210}Pb_{xs}$ activities would still decrease exponentially with depth, but the attenuation coefficient α' would become

$$\alpha' = [(S/2D_b)(1 \pm (1+(4D_b\lambda/S^2))^{1/2})]. \qquad (3)$$

Where D_b is the particle reworking or benthic mixing rate constant. In most Lavaca Bay cores, sediment mixing depths were only of the order of a few cm, and thus, the ^{210}Pb methodology should directly result in estimates of sedimentation rates (i.e., eq. 2b). This model is applicable for sediments where sedimentation rates are either constant or, if variable, initial concentrations vary in proportion to the sediment accumulation rate variations.

If sedimentation rates are variable with time, the Constant Flux (CF) model (Robbins, 1978; Appleby and Oldfield, 1978) could be applied. The interpretation of the $^{210}Pb_{xs}$ data made extensive use of the CIC model, while the CF model results did not improve the interpretation, likely due to the limitations imposed by the finite precision of the ^{210}Pb data. Therefore, the CF model is not further discussed here.

4.2 DETERMINATION OF PARTICLE REWORKING RATES FROM ^7Be PENETRATION

Particle reworking (bioturbation and mixing due to physical processes) rates can be calculated, under steady state conditions, by eq. 4.

$$[^7Be(z)] = [^7Be(o)] \exp(-(\lambda/D_b)^{1/2} z) \qquad (4)$$

D_b was assumed to be constant even though it is often found to be exponentially decreasing with depth. Under such circumstances, there is no analytical solution, since porosity is also decreasing with depth. Model simulations were also carried out using a numerical mixing/sedimentation program in MATLAB (Denham, 1996), which is an improved version of earlier models written BASIC (Crusius, 1992) and FORTRAN (Santschi et al., 1980).

4.3 SEDIMENT AND RADIONUCLIDE BUDGETS

Radionuclide inventories can be calculated from integrating activity concentration (C_i) profiles over the whole depth range, as follows.

$$\text{Inventory (measured)} = \sum C_i^*(1-\text{Ø}_i)^*2.5 \ \{dpm/cm^2\} \qquad (5)$$

with Ø = porosity.

Results of such calculations can then be compared to the average inventory for Lavaca Bay, based on measurements in Houston or Galveston, prorated for the average precipitation of Lavaca Bay, and decay corrected to the year 1997. Discussions of the radionuclide budgets for each of the primary radionuclides measured in this program are provided in Section 5.4.

4.4 GRAIN SIZE TRENDS

Grain size data is reported in phi size classes that are a standard geological simplification (see Folk, 1968) of grain size information into a dimensionless number. The phi scale is related to particle sizes in mm by:

Phi size = $-\log_2 d$, where d= the particle size in mm (6)

Mean grain size and sorting characteristics of a sediment are frequently reduced to a single number using a graphical formula (see Friedman et al., 1992, p. 38). This is a standard method of calculating:

Graphical Mean = $(\phi_{16} + \phi_{50} + \phi_{84}) \div 3$ (7)

Where ϕ_{16}, ϕ_{50}, and ϕ_{84} are the grain sizes in phi for the 16^{th}, 50^{th}, and 84^{th} percentile from a cumulative frequency curve. Graphic Inclusive Standard Deviation is a sorting parameter about this mean calculated as:

Graphic Inclusive Standard Deviation[5] = $(\phi_{84} - \phi_{16}) \div 4) + ((\phi_{95} - \phi_5) \div 6.6)$ (8)

In conjunction with information derived from other textural attributes, compositional attributes, sedimentary structures, and the vertical stratigraphic relationships, grain size analysis provides powerful guidelines for interpreting depositional conditions. As a generalization that holds true for processes in most depositional environments, the mean grain size in a deposit is largely a function of the energy of the processes controlling transport and deposition. In contrast, the degree of sorting of grains in the deposit is a function of the persistence and stability of those energy conditions. The principle exception to this general rule applies when the size of the grains that can be deposited is constrained by the size of the grains in the environment.

[5] Inclusive standard deviation is a graphical sorting technique.

5.0 STUDY RESULTS

This section summarizes the analytical and physical data obtained from the Radiochemistry Study. Section 5.1 presents the total mercury results and Section 5.2 presents the TOC results. The sediment grain size results are presented in Section 5.3 and the radioisotope results are presented in Section 5.4. The results of the x-radiography photos are presented in Section 5.5, and a summary of the laboratory QC analyses is presented in Section 5.6.

5.1 TOTAL MERCURY RESULTS

The results of the total mercury analyses conducted on the radiochemistry core samples are summarized in Table 5-1 and presented in Figures 5-1 through 5-15. With the exception of the samples collected near the ALCOA ship channel, in Keller Bay, and north of the CAPA shoreline, all the cores exhibited mercury profiles that included sharp concentration peaks at depths ranging from 5 to 55 cm. The sediment mercury data are discussed in detail in Section 6.0.

5.2 TOTAL ORGANIC CARBON RESULTS

The results of the TOC analyses conducted on the radiochemistry cores are summarized in Table 5-2 and are also presented in Figures 5-1 through 5-15. These results were used to assist in interpreting the radioisotope analyses and are thus not presented separately.

5.3 GRAIN SIZE AND POROSITY RESULTS

Over 200 measurements (from 1cm core sections) of % sand:silt:clay were made from cuts from the 15 cores collected during this study. Results are presented in graphic form in Figure 5-16 and summarized in Table 5-3. Detailed RSA/Sedigraph results are compiled in Table C-1. Graphic mean and Inclusive Standard Deviation (sorting) calculations were performed for each of the RSA/Sedigraph measurements. Results are summarized in Table C-2 and presented graphically in Figure C-1.

5.3.1 Downcore Trends

Sand:silt:clay ratios were measured for 12-16 depth intervals in each core (Figure 5-16). Downcore variations in grain size are a function of fluctuating bed stress and sediment supply to the site, and, hence may reflect changing sediment deposition rates and/or sediment sources. Downcore plots of %sand and %clay for each core are shown in Figure C-2 to C-70. These data demonstrate that downcore changes for most of the cores are relatively slight when compared with differences between cores. This relative consistency make the Lavaca Bay area an appropriate location for applying particle-reactive radiochemical tracers that are sensitive to the fine-grained sediment content. Grain size changes observed in the interbeds of x-radiograph images exaggerate this downcore variation because the contrast has been increased to improve clarity of internal features.

Table 5-1. Radiochemistry Study - Total Mercury Concentrations (mg/kg dry weight).

Sample Depth (cm)	Total Mercury (mg/kg dry weight)														
	ST00128	ST00134[11]	ST00142	ST00201[12]	ST00285	ST00286	ST00296[13]	ST00300[14]	LVB0924	LVB0926	LVB0928	LVB8721	LVB8826	LVB8827	KLB4293
0- 1	0.31	0.28	0.50	0.37	0.22	0.25	0.23	0.23	8.72	32.83	1.45	0.72	0.13	0.60	0.30
1- 2	0.38	0.62	0.88	0.32	0.25	0.33	0.25	0.21	6.50	75.63	1.42	0.75	0.25	0.48	0.34
2- 3	0.33	0.72	1.16	0.29	0.22	0.40	0.25	0.25	8.02	138.33	2.00	0.77	0.17	0.52	0.24
3- 4	0.39	1.27	1.52	0.27	0.12	0.73	0.25	0.23	5.99	199.60	1.52	0.76	0.16	0.54	0.20
4- 5	0.35	1.53	1.43	0.34	0.33	1.25	0.27	0.26	5.43	154.00	1.61	0.67	0.16	0.52	0.17
5- 6	NT	2.07	1.35	0.46	0.36	1.26	0.25	0.26	7.34	115.50	1.29	0.55	0.14	0.54	0.19
6- 7	NT	1.89	1.42	0.54	0.32	0.43	0.26	0.27	13.26	111.10	1.37	0.65	0.32	0.52	0.18
7- 8	NT	2.37	1.02	0.54	0.29	0.30	0.27	0.28	15.67	82.63	1.63	0.80	0.24	0.59	0.20
8- 9	NT	4.45	0.61	0.49	0.29	0.31	0.25	0.38	28.82	80.39	1.48	0.99	0.25	0.60	0.22
9- 10	0.41[1]	13.12	0.31	0.50	0.27	0.30	0.24	0.41	12.65	106.10	1.55	0.83	0.24	0.61	0.26
15- 16	0.67[2]	0.48	0.12	0.62	0.38	0.21	0.37	1.00	27.31	31.34	1.87	0.78	0.54	0.56	0.21
20- 21	0.74[3]	0.09	0.05	0.69	0.57	0.17	0.45	2.87	15.58	16.90	1.90	0.75	0.63	0.80	0.17
25- 26	1.27[4]	0.07	0.03	1.07	0.54	0.35	0.61	0.77	29.44	33.88	2.32	0.97	0.79	0.84	0.12
30- 31	5.22[5]	0.05	0.02	3.92	0.60	0.36	0.81	0.12	79.46	10.77	2.79	0.86	0.06	0.61	0.06
35- 36	1.17[6]	0.08	0.02	14.24	0.96	0.55	0.68	0.09	7.48	6.10	2.75	0.69	0.01	0.20	0.06
40- 41	0.30[7]	0.04	0.03	2.34	1.35	0.45	1.03	0.06	10.91	8.26	1.55	0.76	0.02	0.04	0.09
45- 46	0.15[8]	0.05	0.01	0.47	1.88	0.45	1.47	0.03	13.91	0.31	3.13	0.90	0.02	0.01	0.09
50- 51	0.12[9]	0.03	0.01	0.19	3.24	0.60	1.69	0.04	4.59	0.05	8.86	0.83	0.01	0.18	0.07
55- 56	0.08[10]	0.03	0.01	0.30	1.56	0.89	3.01	0.06	4.41	0.01	11.20	1.45	0.00	0.02	0.07
60- 61	NT	0.03	0.01	0.18	0.04	2.06	0.10	0.02	1.73	0.40	9.14	1.16	-0.004	0.02	0.03

NT = Not taken.
[1]Actual depth 5-10 cm.
[2]Actual depth 10-15 cm.
[3]Actual depth 15-20 cm.
[4]Actual depth 20-25 cm.
[5]Actual depth 25-30 cm.
[6]Actual depth 30-35 cm.
[7]Actual depth 35-40 cm.
[8]Actual depth 40-45 cm.
[9]Actual depth 45-50 cm.
[10]Actual depth 50-60 cm.

[11]Additional results for Station ST00134 = 10-11 cm (31.15); 11-12 cm (21.10).
[12]Additional results for Station ST00201 = 33-34 cm (7.41); 34-35 cm (20.52); 36-37 cm (4.27); 37-38 cm (11.74).
[13]Additional results for Station ST00296 = 53-54 cm (6.06); 54-55 cm (4.51); 56-57 cm (2.41); 57-58 cm (0.80).
[14]Additional results for Station ST00300 = 18-19 cm (0.61); 19-20 cm (2.78); 21-22 cm (2.04); 22-23 cm (1.74).

Note: Dry weight is estimated for additional depths for stations ST00134, ST00201, and ST00296.

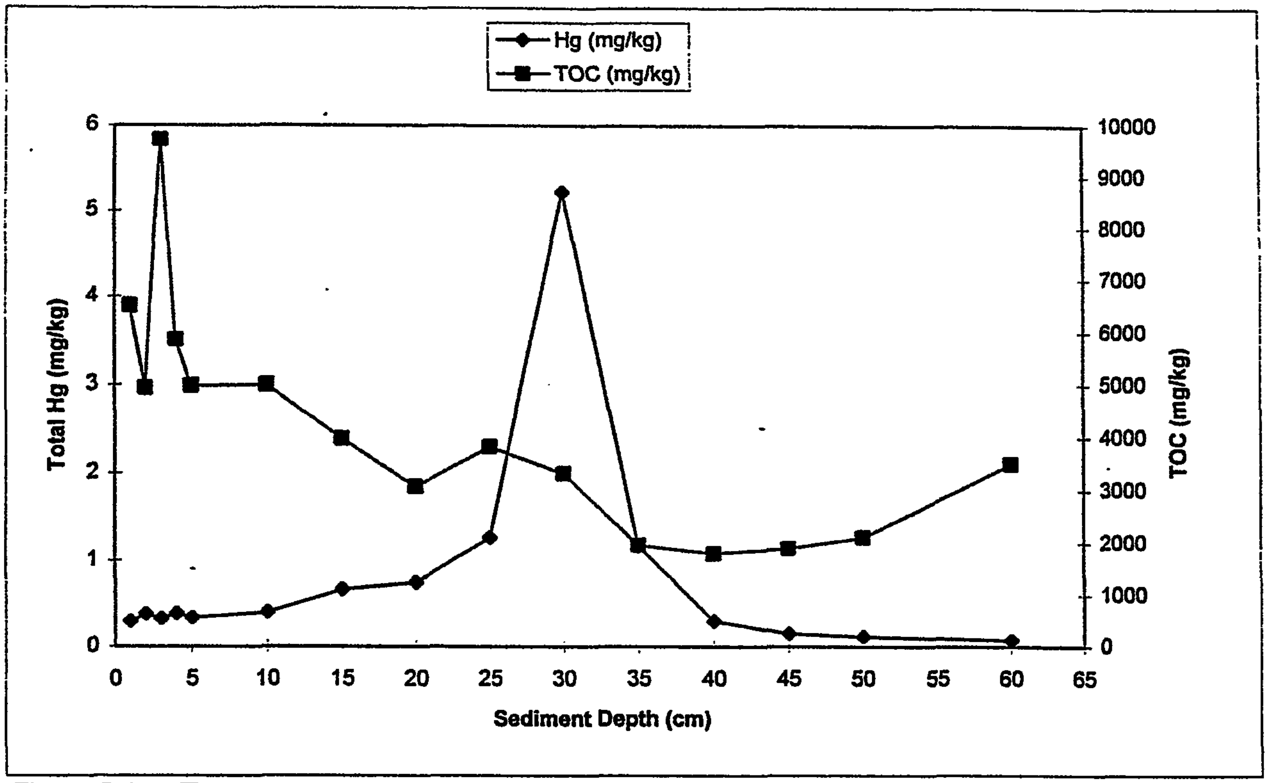

Figure 5-1. Total mercury concentrations (mg/kg dry weight) and TOC (mg/kg) over depth for Station 128.

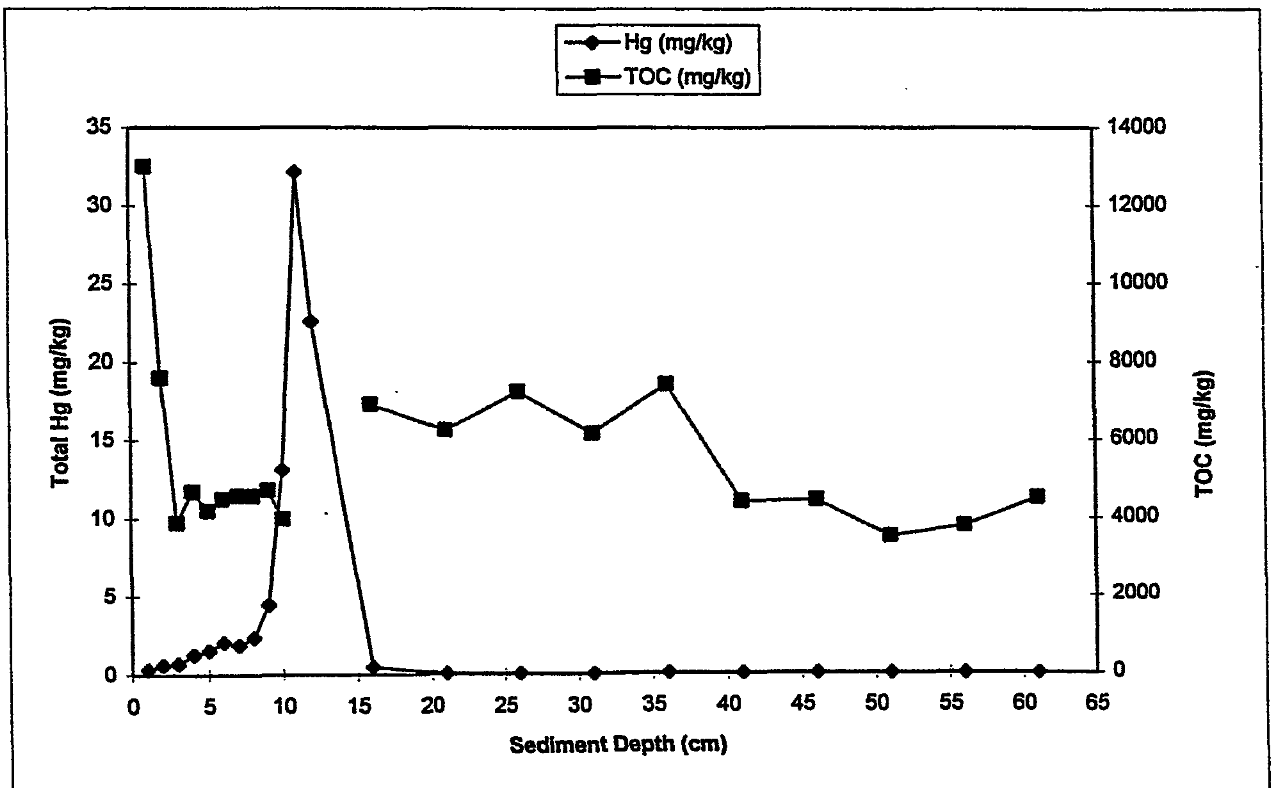

Figure 5-2. Total mercury concentrations (mg/kg dry weight) and TOC (mg/kg) over depth for Station 134.

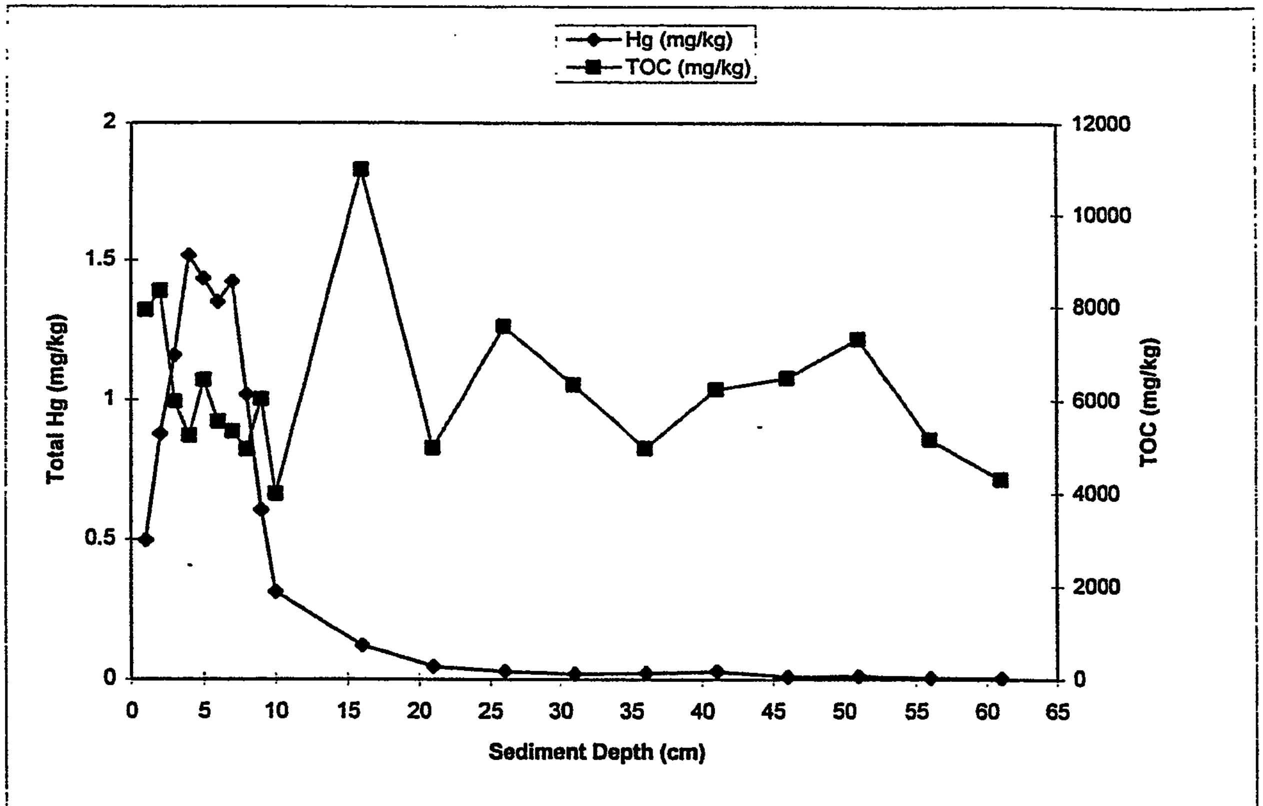

Figure 5-3. Total mercury concentrations (mg/kg dry weight) and TOC (mg/kg) over depth for Station 142.

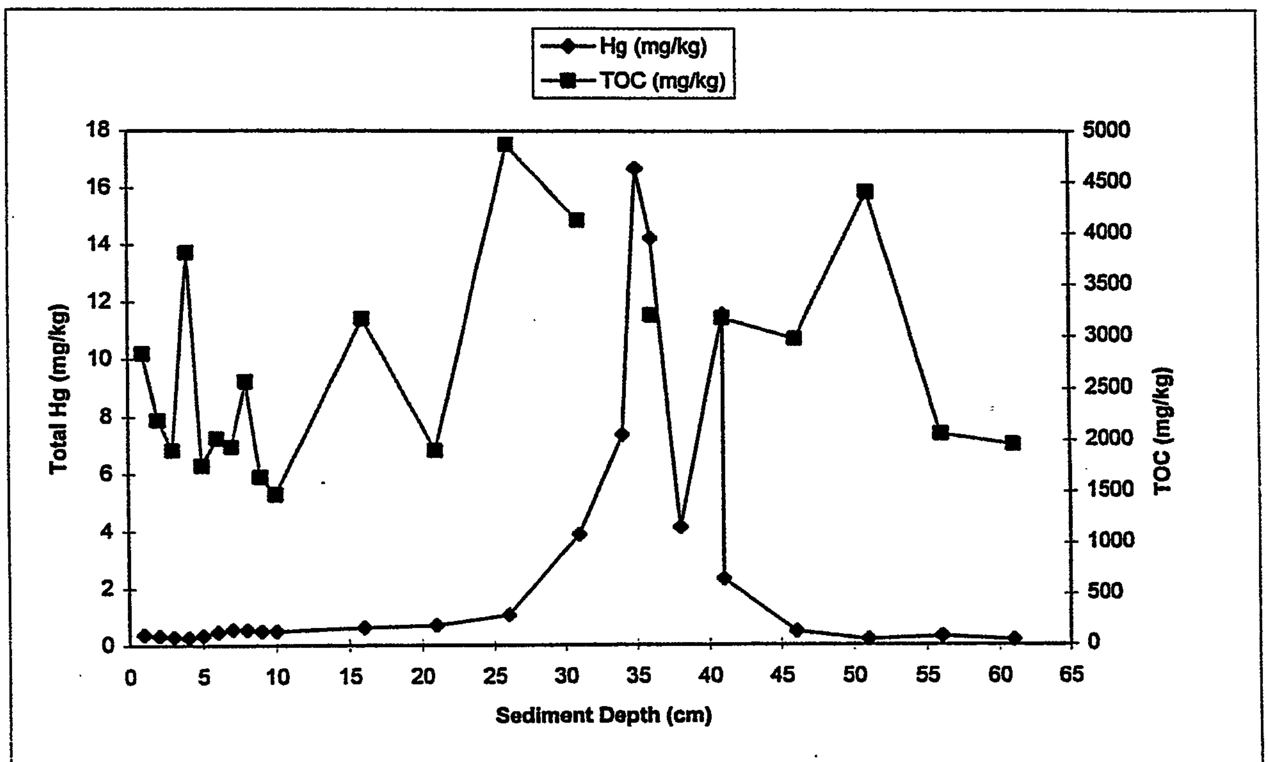

Figure 5-4. Total mercury concentrations (mg/kg dry weight) and TOC (mg/kg) over depth for Station 201.

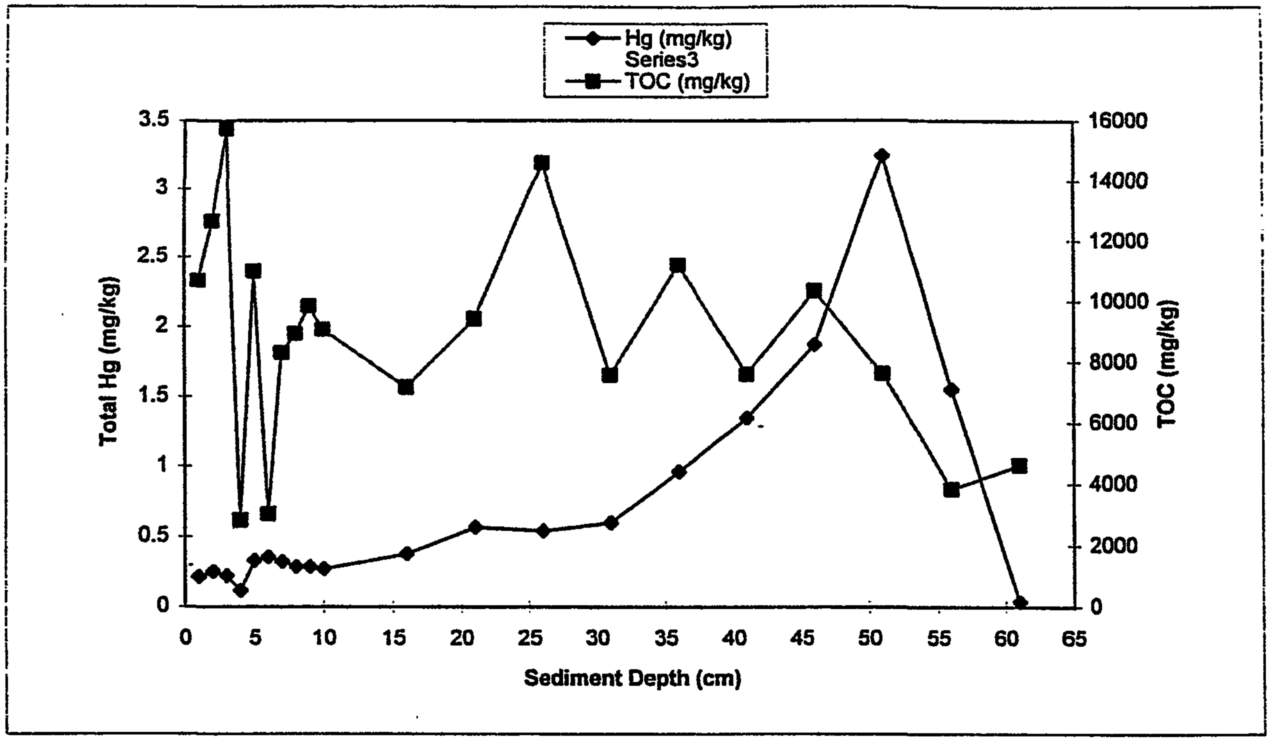

Figure 5-5. Total mercury concentrations (mg/kg dry weight) and TOC (mg/kg) over depth for Station 285.

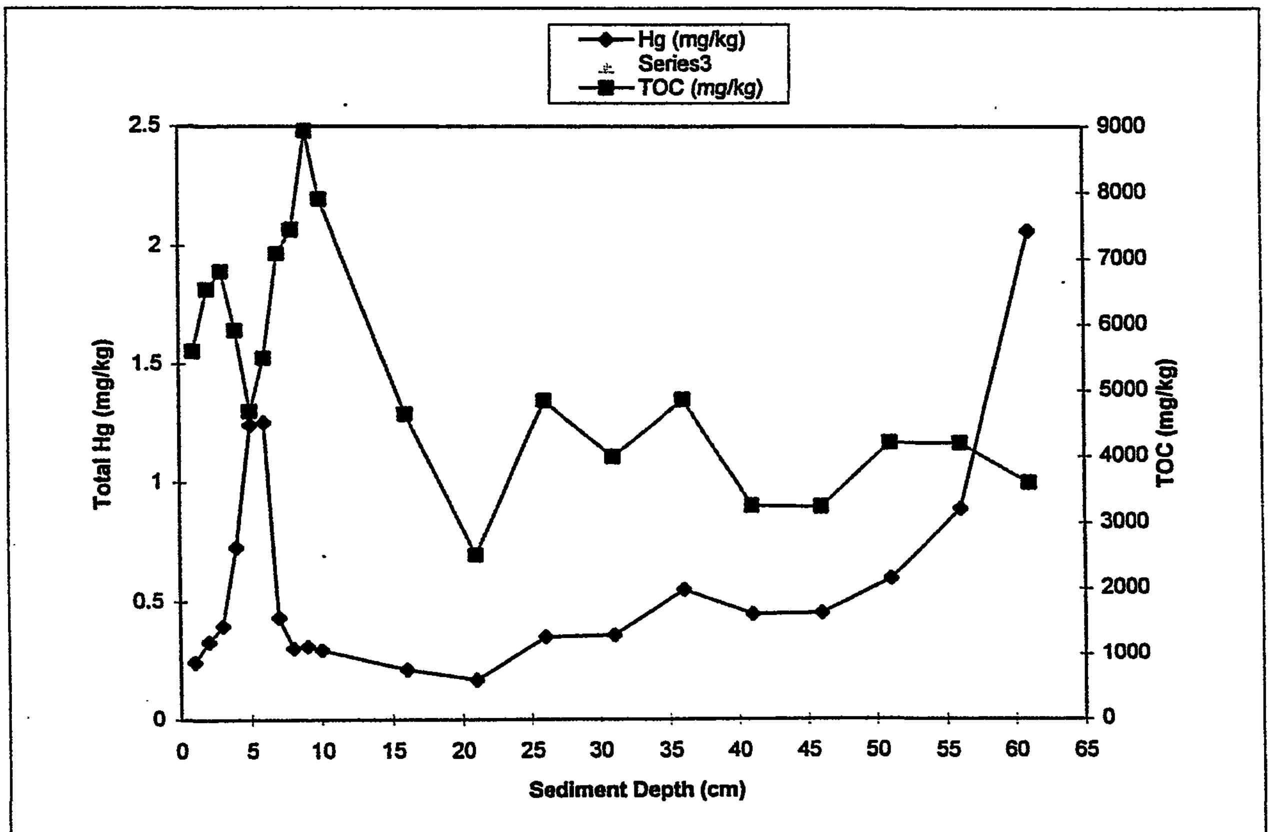

Figure 5-6. Total mercury concentrations (mg/kg dry weight) and TOC (mg/kg) over depth for Station 286.

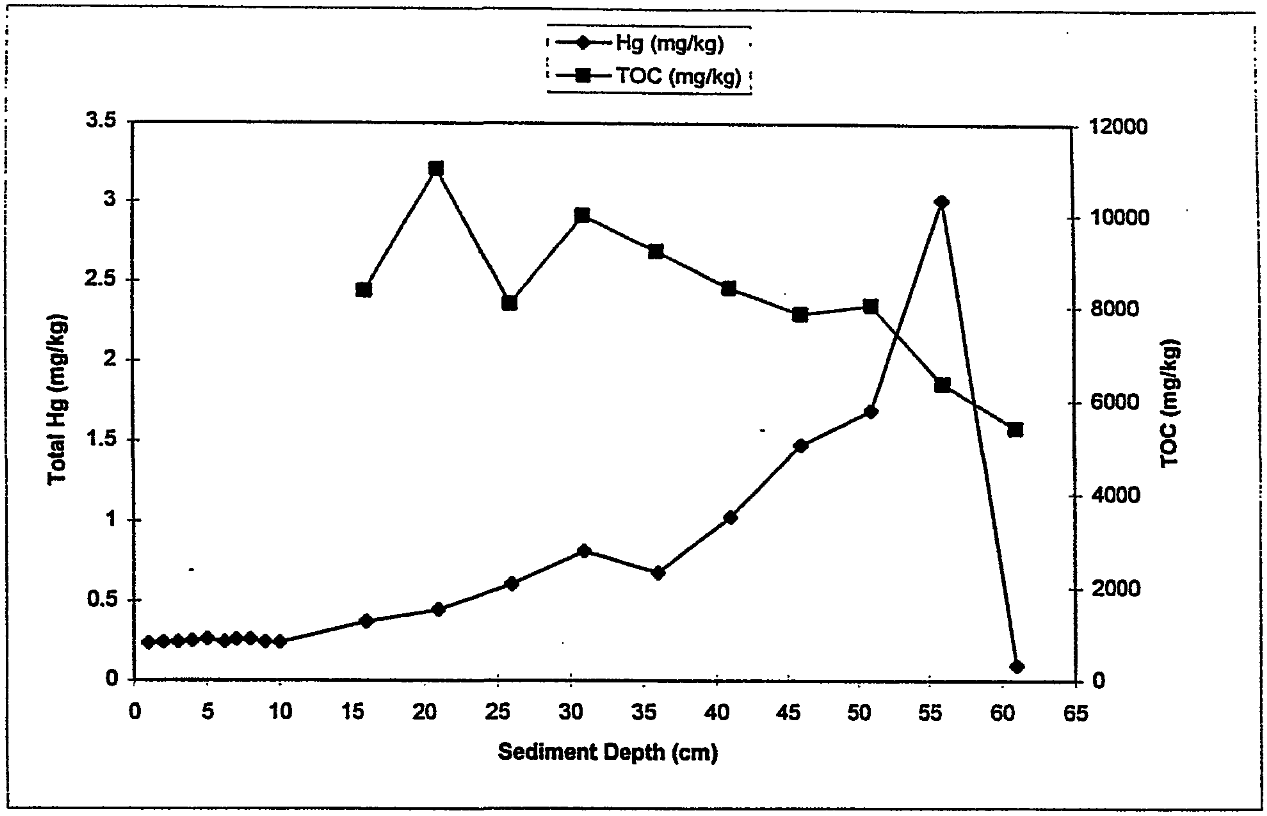

Figure 5-7. Total mercury concentrations (mg/kg dry weight) and TOC (mg/kg) over depth for Station 296.

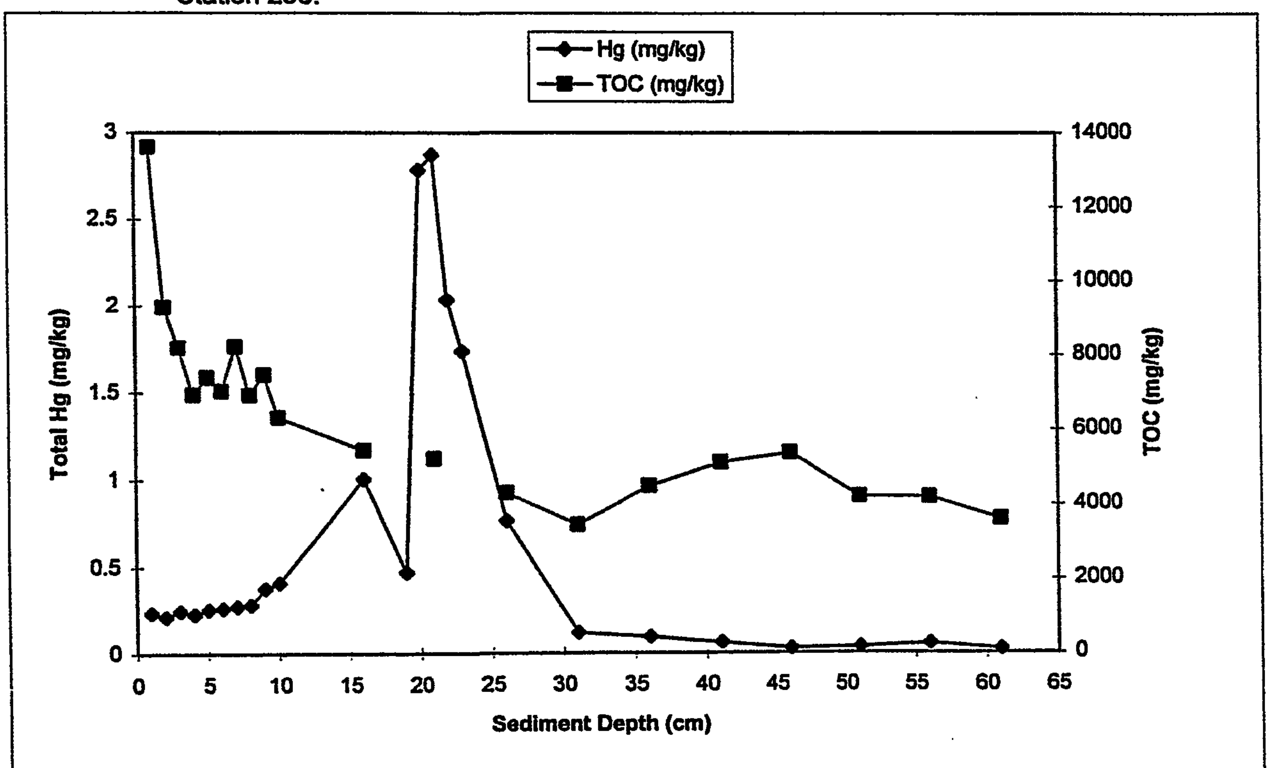

Figure 5-8. Total mercury concentrations (mg/kg dry weight) and TOC (mg/kg) over depth for Station 300.

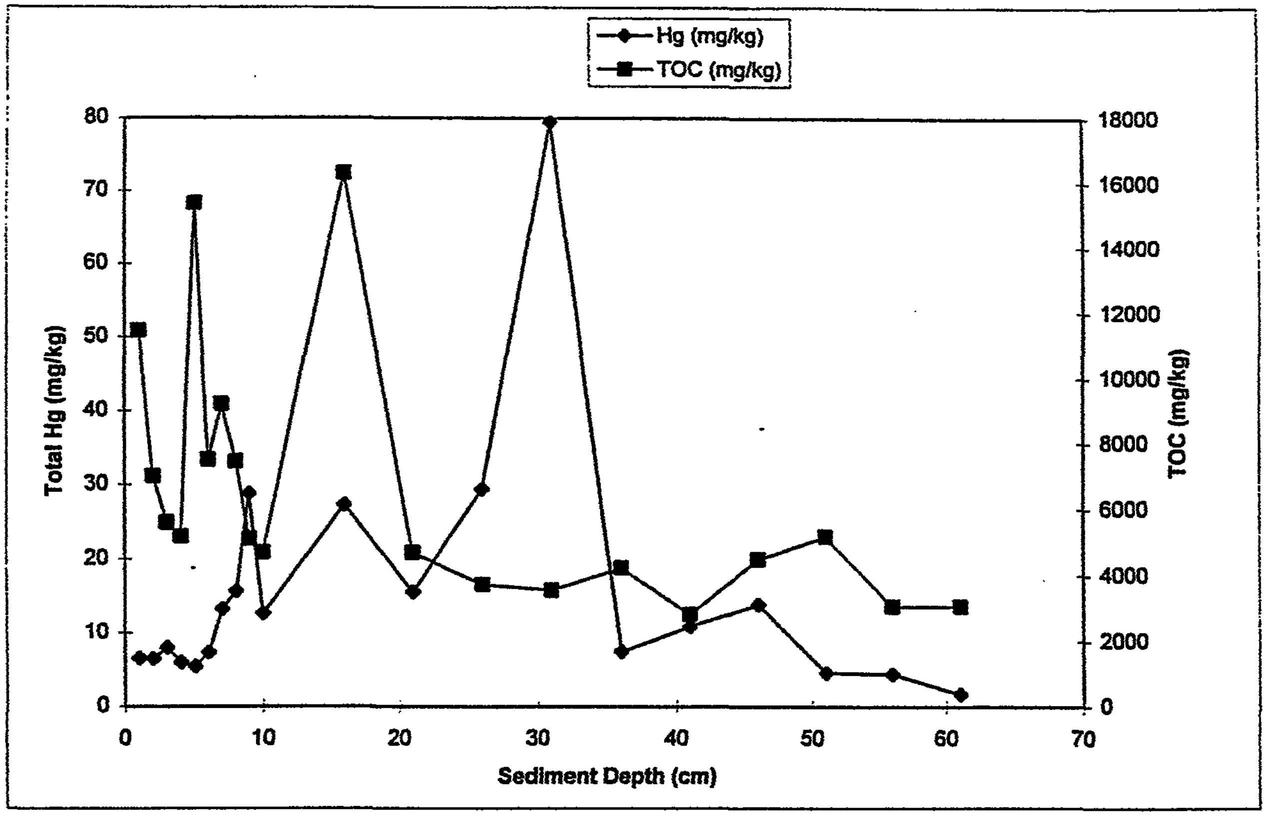

Figure 5-9. Total mercury concentrations (mg/kg dry weight) and TOC (mg/kg) over depth for Station 924.

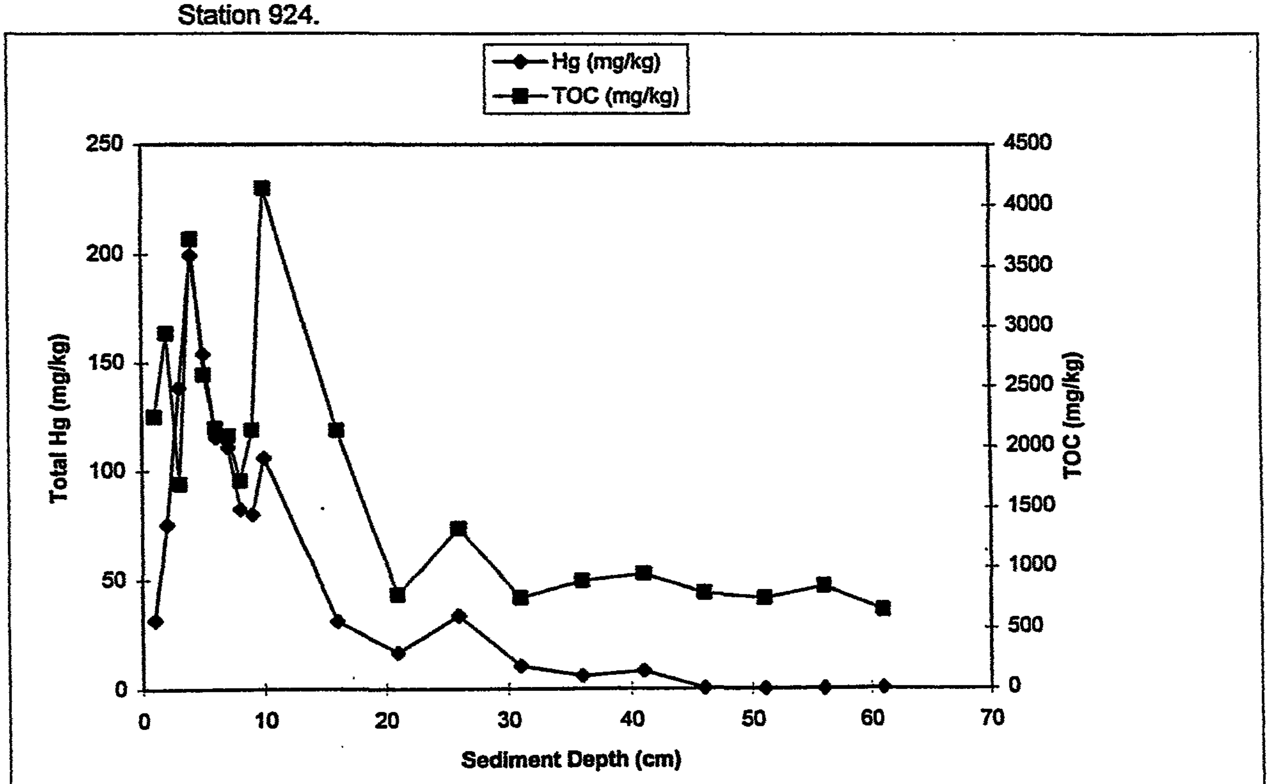

Figure 5-10. Total mercury concentrations (mg/kg dry weight) and TOC (mg/kg) over depth for Station 926.

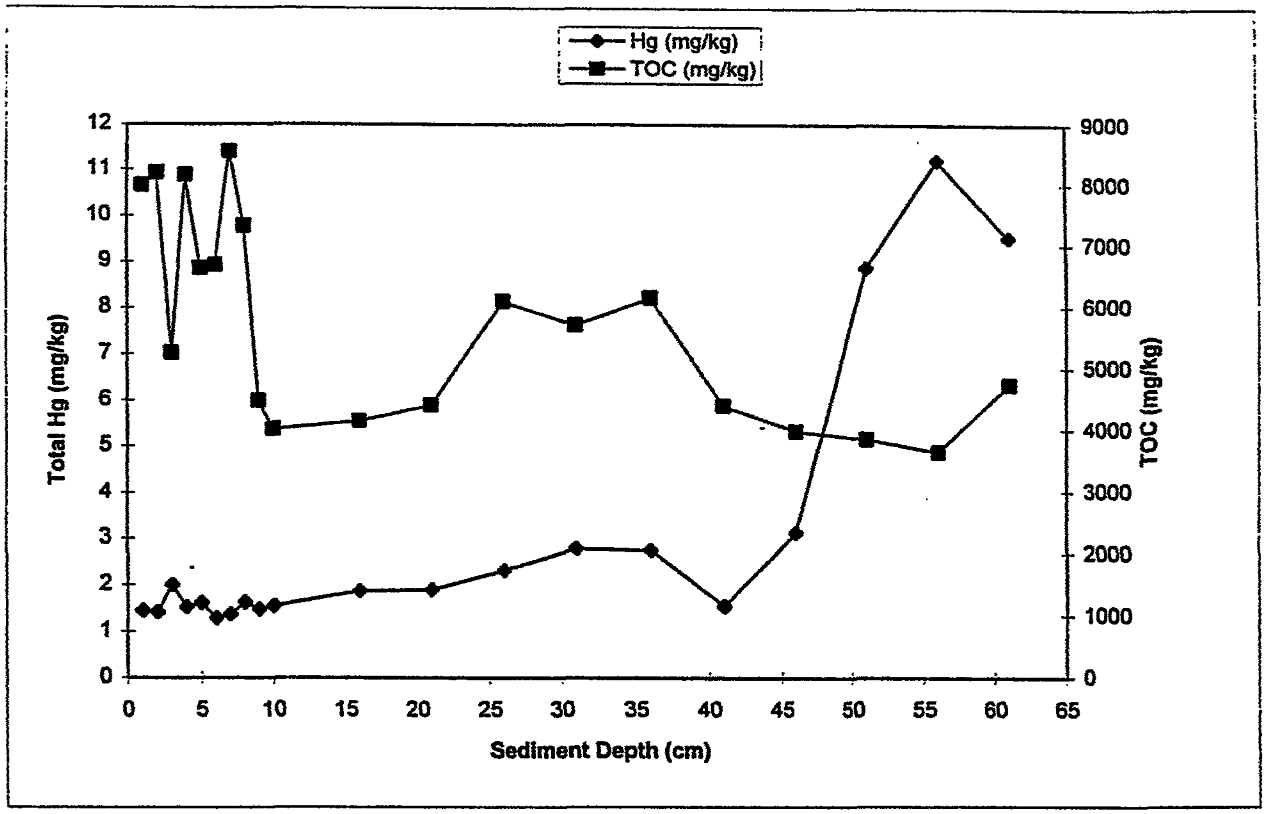

Figure 5-11. Total mercury concentrations (mg/kg dry weight) and TOC (mg/kg) over depth for Station 928.

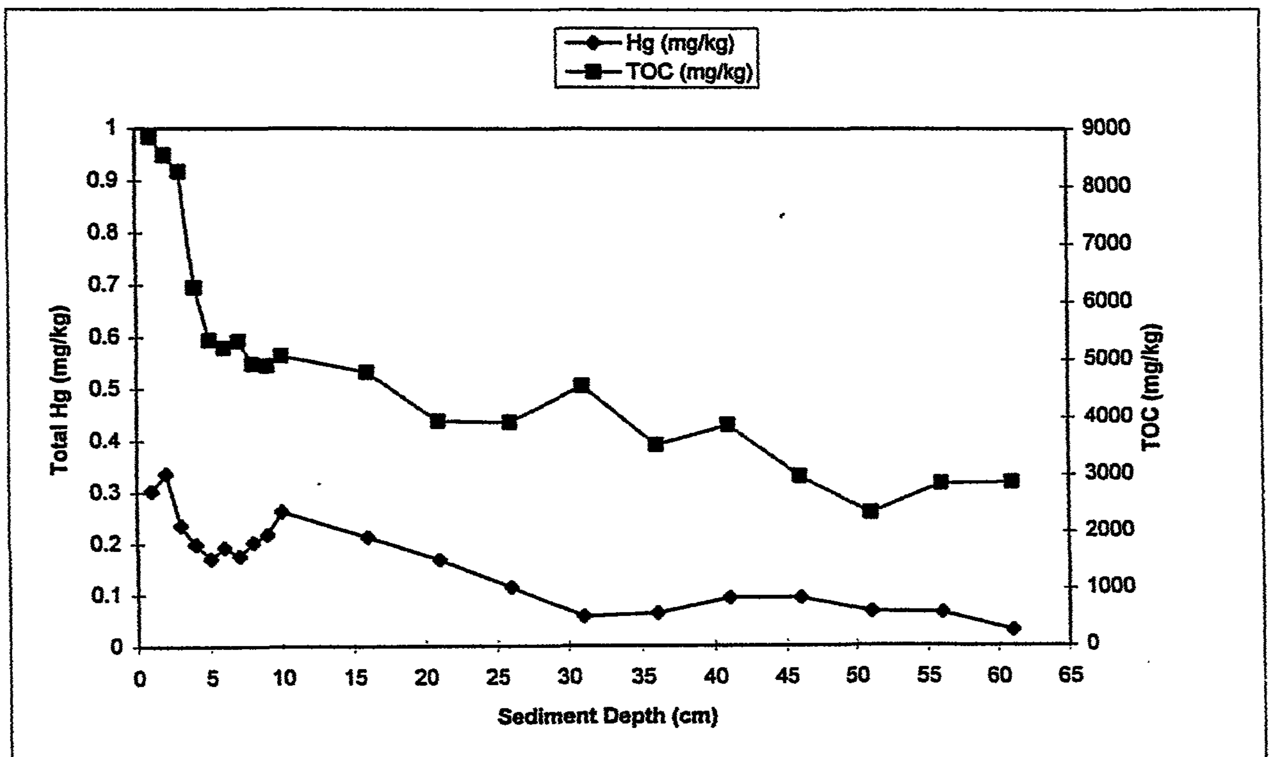

Figure 5-12. Total mercury concentrations (mg/kg dry weight) and TOC (mg/kg) over depth for Station 4293.

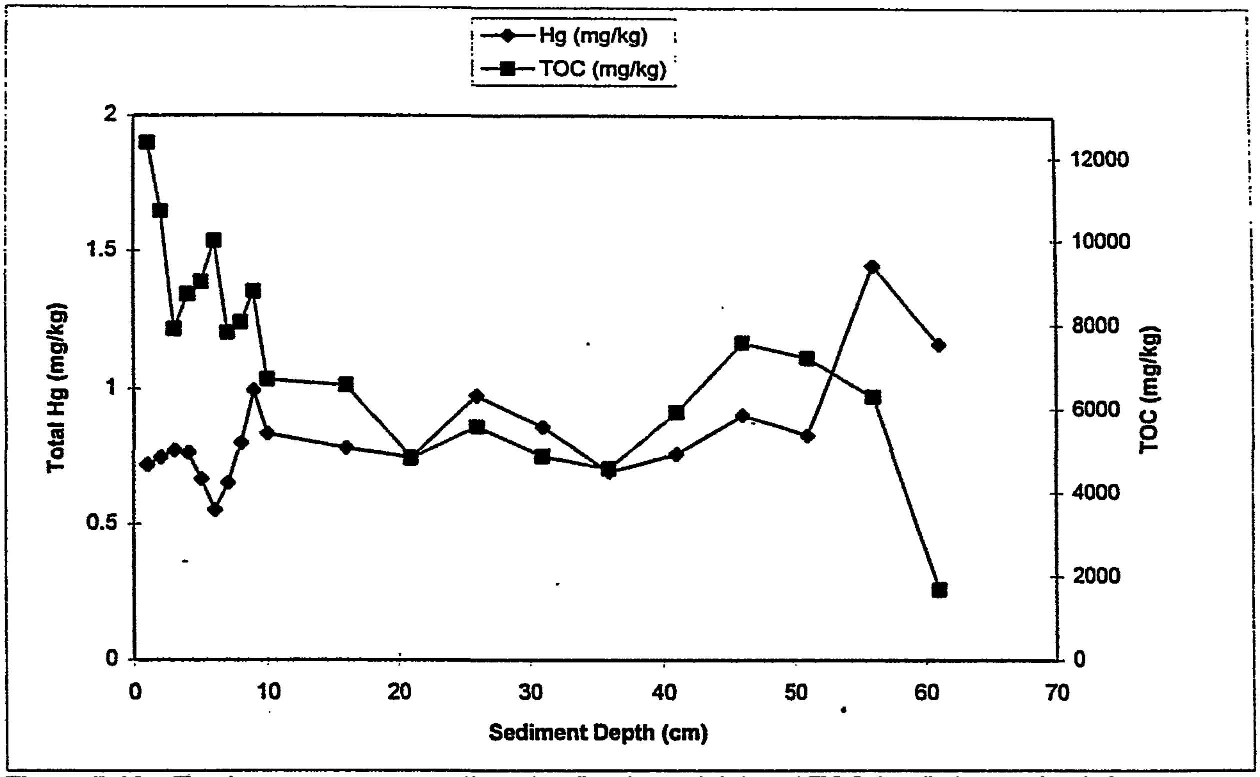

Figure 5-13. Total mercury concentrations (mg/kg dry weight) and TOC (mg/kg) over depth for Station 8721.

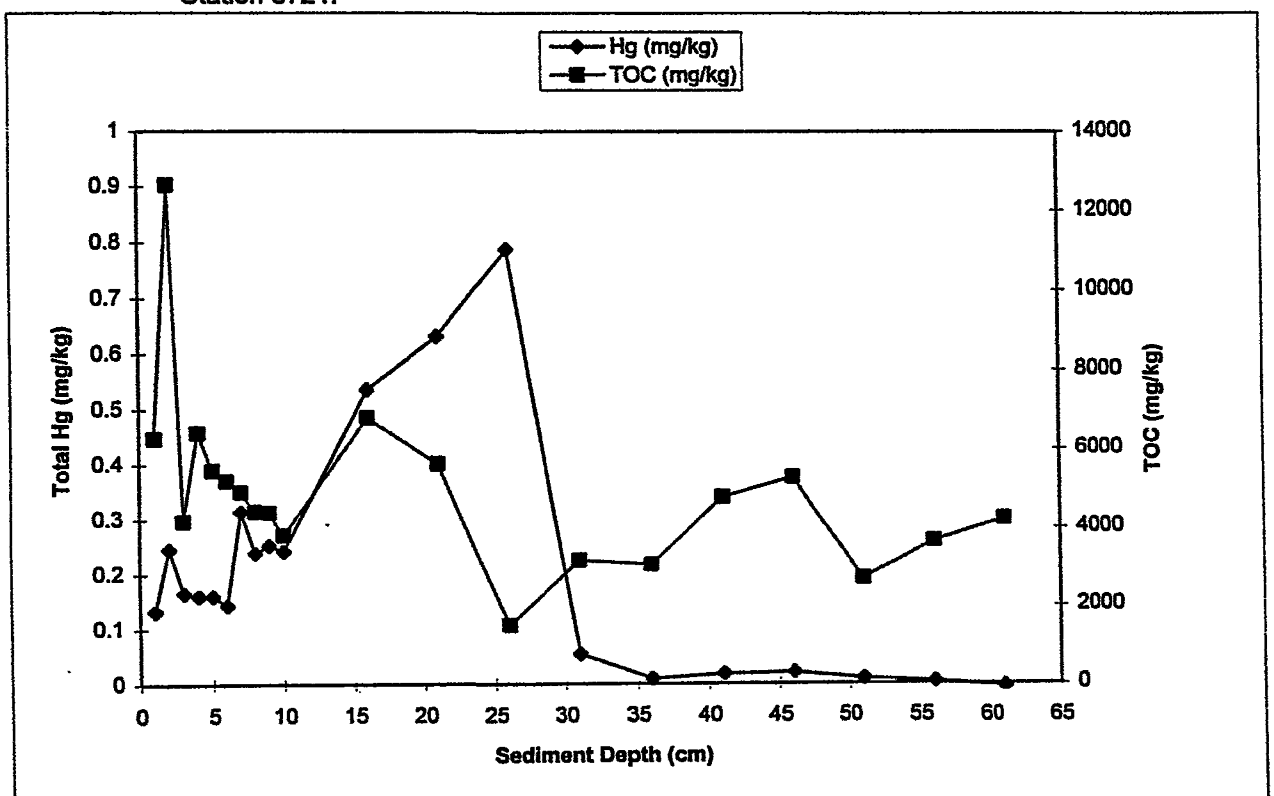

Figure 5-14. Total mercury concentrations (mg/kg dry weight) and TOC (mg/kg) over depth for Station 8826.

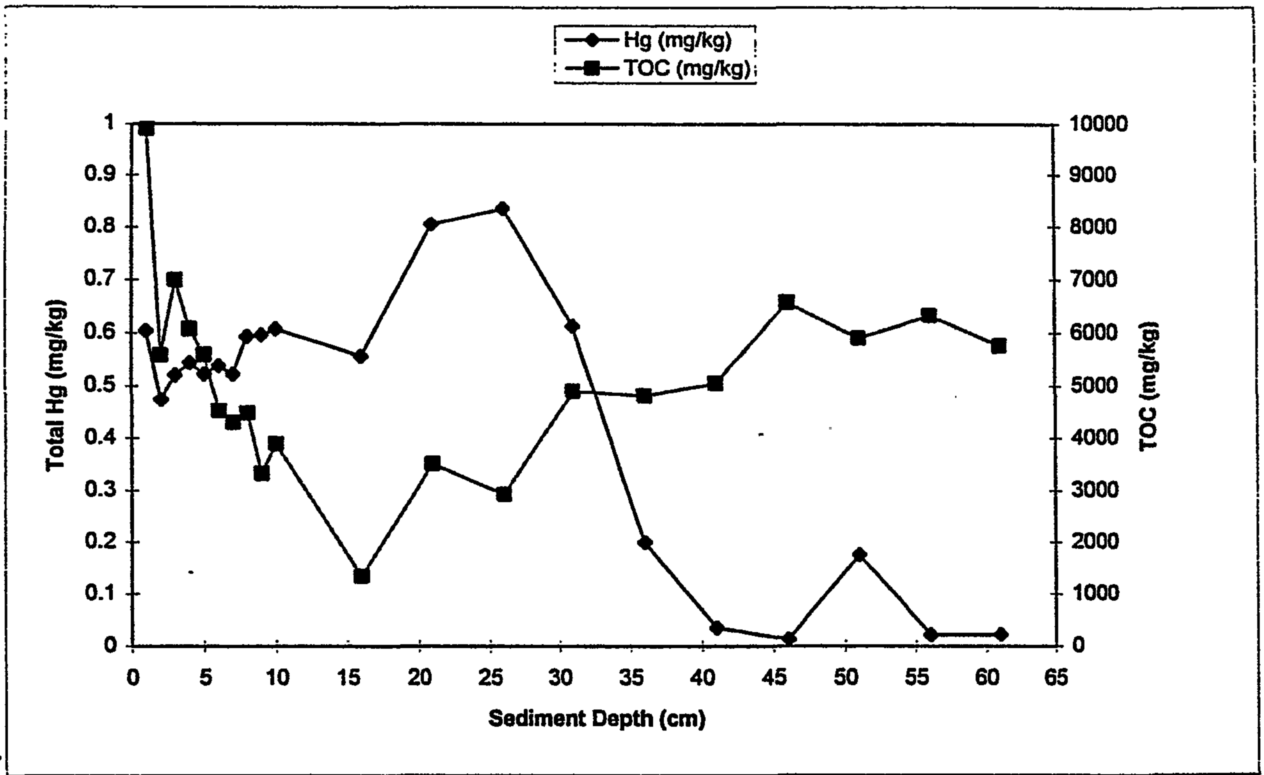

Figure 5-15. Total mercury concentrations (mg/kg dry weight) and TOC (mg/kg) over depth for Station 8827.

Table 5-2. Radiochemistry Study - Total Organic Carbon Results (mg/kg).

	Total Organic Carbon (mg/kg)														
Sample Depth (cm)	ST00128	ST00134	ST00142	ST00201	ST00285	ST00286	ST00296	ST00300	LVB0924	LVB0926	LVB0928	LVB8721	LVB8826	LVB8827	KLB4293
0- 1	6910	13000	7925	2830	10316	5619	NT	13796	10472	2414	7996	12352	6261	9909	8980
1- 2	4940	7610	8324	2190	12635	6536	NT	9304	7016	2945	8194	10699	12634	5576	8545
2- 3	9720	3900	5962	1900	15714	6812	NT	8210	5612	1696	5264	7915	4159	6994	8261
3- 4	5860	4690	5221	3810	2826	5920	NT	6947	5181	3724	8160	8724	6406	6071	6263
4- 5	4980	4200	6423	1750	10958	4688	NT	7409	15369	2598	6639	9004	5451	5584	5359
5- 6	NT	4500	5519	2145	9026	5490	NT	7043	7509	2156	6690	9986	5190	4523	5218
6- 7	NT	4405	5312	1930	8282	7082	NT	8235	9206	2093	8546	7826	4905	4307	5333
7- 8	NT	4580	4930	2560	8913	7440	NT	6935	7465	1722	7333	8061	4411	4484	4934
8- 9	NT	4730	6010	1640	9802	8932	NT	7475	5117	2140	4492	8784	4391	3323	4907
9- 10	4970[1/]	4010	3977	1470	9047	7904	NT	6327	4694	4137	4022	6713	3805	3890	5080
15- 16	3980[2/]	6930	10974	3170	7150	4642	8125	5443	16296	2135	4157	6574	6795	1347	4790
20- 21	3080[3/]	6260	4966	1900	9402	2517	11000	5229	4695	780	4416	4832	5631	3508	3942
25- 26	3830[4/]	7250	7574	4870	14569	4850	8080	4318	3728	1327	6102	5575	1498	2924	3929
30- 31	3330[5/]	6180	6329	4130	7555	3994	9990	3462	3558	754	5717	4871	3174	4896	4554
35- 36	1960[6/]	7440	4963	3210	11181	4865	9220	4494	4224	892	6160	4583	3058	4817	3529
40- 41	1800[7/]	4440	6231	3180	7588	3256	8420	5118	2818	948	4402	5933	4786	5048	3876
45- 46	1900[8/]	4470	6484	2980	10336	3242	7870	5381	4500	792	3981	7584	5285	6573	2975
50- 51	2110[9/]	3540	7312	4410	7611	4212	8050	4222	5186	750	3854	7218	2697	5901	2344
55- 56	3510[10/]	3810	5160	2060	3844	4200	6370	4202	3061	847	3645	6306	3664	6322	2851
60- 61	NT	4520	4288	1960	4609	3602	5420	3617	3065	655	4746	1682	4243	5763	2873

NT = Not Taken.
[1/]Actual depth 5-10 cm.
[2/]Actual depth 10-15 cm.
[3/]Actual depth 15-20 cm.
[4/]Actual depth 20-25 cm.
[5/]Actual depth 25-30 cm.
[6/]Actual depth 30-35 cm.
[7/]Actual depth 35-40 cm.
[8/]Actual depth 40-45 cm.
[9/]Actual depth 45-50 cm.
[10/]Actual depth 50-60 cm.

Figure 5-16. Sand:silt:clay ratios for cores from Lavaca Bay and from the four endmember grab samples.

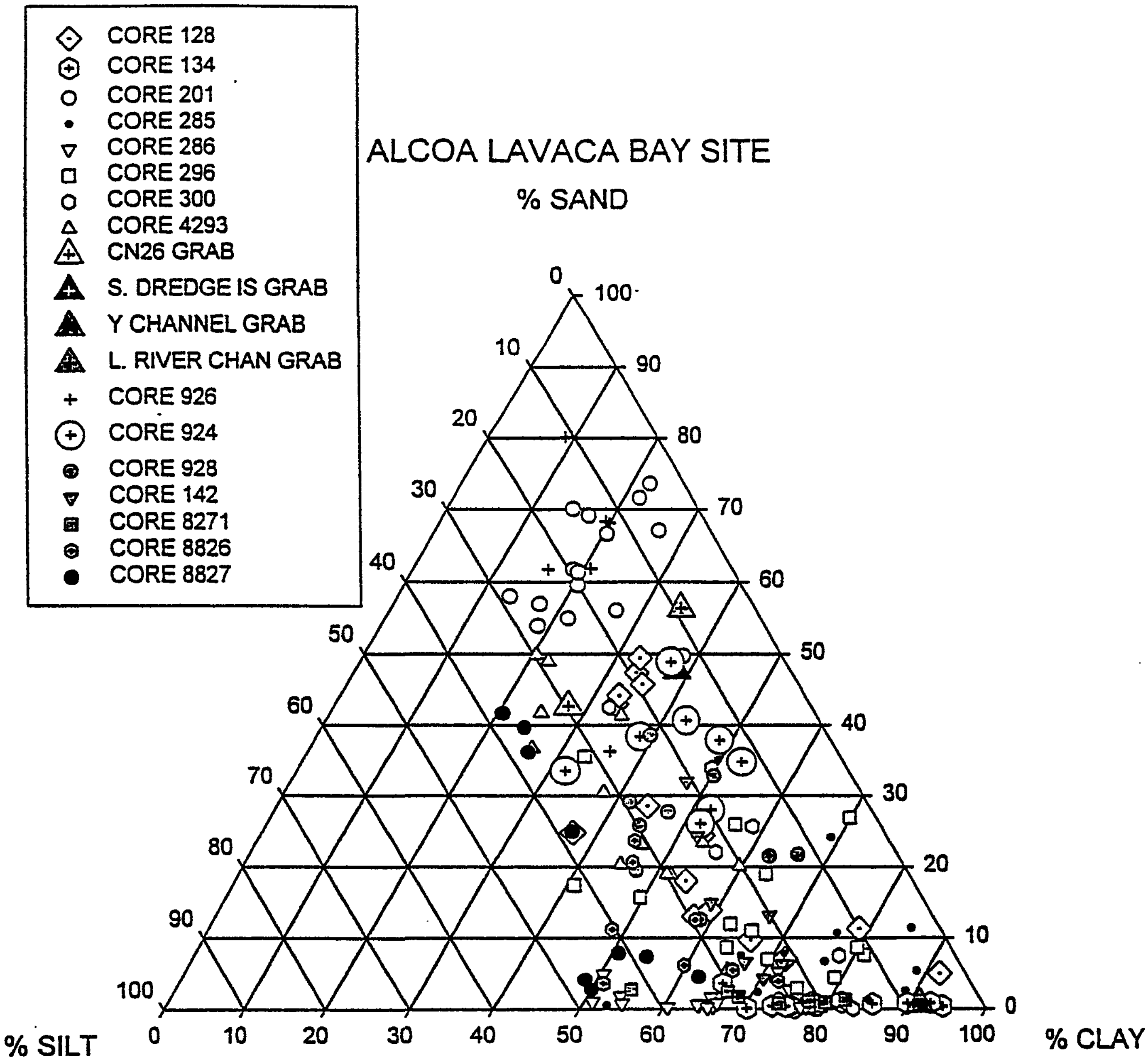

Table 5-3. Results of %sand:silt:clay analyses.

Core 128

Depth	%sand	%silt	%clay
0-1	7.04	21.25	71.71
*1-3	4.99	3.27	91.74
3-4	17.98	27.92	54.1
4-5	42.96	23.94	33.1
7-8	47.39	19.13	33.48
*8-10	24.79	38.19	37.02
12-13	44.18	22.87	32.95
17-18	28.5	27.31	44.19
22-23	24.38	22.57	53.05
27-28	12.98	29.42	57.6
32-33	13.9	26.97	59.13
37-38	9.7	24.2	66.1
42-43	11.3	10	78.7
47-48	49.44	17.67	32.89
*48-50	45.75	19.24	35.01

Core 300

Depth	%sand	%silt	%clay
0-1	1.02	21.69	77.29
1-2	1.31	24.98	73.71
*2-4	0.72	16.92	82.36
4-5	1.16	17.97	80.87
9-10	2.3398	22.65	75.01
*13-15	0.01	16.49	83.50
19-20	7.51	14.41	78.08
*25-27	22.01	22.17	55.82
30-31	22.282	14.98	62.74
40-41	12.051	22.76	65.19
45-46	9.701	10.78	79.52
50-51	25.63	15.87	58.50
*56-58	33.88	16.68	49.44
60-61	42.48	24.95	32.57

Core 285

Depth	%sand	%silt	%clay
0-1	10.68	13.07	76.25
1-2	7.53	26.42	66.05
*2-4	2.55	8.79	88.66
4-5	4.1	24.21	71.69
9-10	0.53	46.56	52.91
19-20	24.11	7	68.89
*20-22	6.71	16.59	76.7
30-31	7.71	20.93	71.36
40-41	5.38	5.97	88.65
50-51	6.23	21.7	72.07
60-61	2.37	27.07	70.56
65-66	1.27	13.98	84.75
70-71	35.15	15.26	49.59
*72-74	11.41	3.58	85.01

Core 924

Depth	%sand	%silt	%clay
0-1	34.76	12.53	52.70
1-2	37.89	13.66	48.45
2-4*	26.81	5.50	67.69
4-5	48.89	14.20	36.91
9-10	40.64	16.42	42.94
13-15*	18.48	17.22	64.30
19-20	28.02	19.72	52.26
25-27*	20.08	16.50	63.42
30-31	38.38	23.29	38.33
40-41	26.02	22.05	51.94
45-46*	31.49	16.39	52.12
50-51	33.49	34.66	31.86

Core 8271

Depth	%sand	%silt	%clay
0-1	2.39	30.62	66.99
2-4*	1.86	6.58	91.56
5-6	1.07	21.39	77.54
9-10	2.74	42.44	54.82
13-15*	1.49	10.37	88.14
18-19	1.67	29.68	68.65
25-27*	2.81	11.78	85.41
30-31	0.78	19.46	79.77
35-36	0.42	20.25	79.32
38-39	0.89	19.50	79.61
40-41	1.26	16.81	81.93
44-46*	0.44	15.49	84.07
52-53	0.77	25.16	74.07

Core 134

Depth	%sand	%silt	%clay
0-1	0.47	21.08	78.45
3-4	0.79	9.45	89.76
4-5	0.38	26.27	73.35
9-10	0.1	23.74	76.16
17-18	0.52	20.58	78.9
*20-22	0.68	13.79	85.53
27-28	0.93	17.42	81.65
32-33	0.33	5.32	94.35
37-38	0.82	6.5	92.68
47-48	0.4	24.14	75.46
52-53	3.6	30.63	65.77
*57-59	0.87	21.17	77.96
63-64	0.33	24.68	74.99
67-68	0.09	29.54	70.37

Core 4293

Depth	%sand	%silt	%clay
0-1	18.89	29.35	51.76
1-2	20.33	34.8	44.87
*2-4	20.07	20.28	59.65
4-5	18.92	29.82	51.26
9-10	5.52	29.07	65.41
*13-15	7.33	20.55	72.12
19-20	23.11	30.76	46.13
*25-27	23.4	23.08	53.52
30-31	30.44	31.68	37.88
40-41	36.77	36.84	26.39
45-46	41.76	33.28	24.96
50-51	49.04	28.75	22.21
*56-58	41.32	24.07	34.61
60-61	49.91	29.68	20.41

Core 286

Depth	%sand	%silt	%clay
0-1	4.9	44.7	50.4
1-2	1.6	33.1	65.3
*2-4	2.7	22.97	74.33
4-5	0.64	35.07	64.29
9-10	0.2	22.17	77.63
17-18	1.81	44.23	53.96
*18-20	0.59	35.34	64.07
*23-25	0.25	39.26	60.49
36-37	0.33	33.53	66.14
46-47	0.99	47.97	51.04
56-57	0.79	32.8	66.41
63-64	0.17	22.95	76.88
*66-68	0.16	34.3	65.54
73-74	0.72	44.61	54.67

Core 928

Depth	%sand	%silt	%clay
0-1	21.66	12.29	66.05
2-4*	37.98	14.21	47.81
5-6	32.77	16.99	50.25
9-10	38.58	21.88	39.55
13-15*	25.76	14.57	59.67
18-19	21.41	15.95	62.64
25-27*	29.77	16.64	53.59
30-31	27.67	25.28	47.05
35-36	19.49	33.31	47.20
38-39	25.77	29.69	44.54
40-41	29.09	29.24	41.67
44-46*	28.51	20.28	51.21

Core 8826

Depth	%sand	%silt	%clay
0-1	3.59	45.37	51.04
2-4*	9.35	30.52	60.13
9-10	23.64	31.38	44.98
13-15*	4.80	25.89	69.31
18-19	6.15	34.13	59.72
25-27*	3.26	21.76	74.98
35-36	12.57	28.84	58.58
40-41	5.44	28.50	66.06
44-46*	1.58	20.23	78.19
50-51	3.88	23.70	72.42
56-57	11.19	40.47	48.34
63-64	20.62	33.18	46.21
70-71	12.50	29.55	57.95

Table 5-3. Results of %sand:silt:clay analyses.

Core 201			
Depth	%sand	%silt	%clay
0-1	54.91	23.47	21.62
1-2	53.9	27.54	18.56
2-3	61.67	19.47	18.86
3-4	58	28.66	13.34
4-5	70.06	15.24	14.7
*5-7	56.03	17.28	26.69
9-10	59.53	20.01	20.46
*12-14	66.63	13	20.37
17-18	69.1	13.89	17.01
22-23	61.3	19.1	19.6
27-28	56.92	25.76	17.32
32-33	67.09	6.45	26.46
37-38	71.54	6.53	21.93
47-48	73.53	4.24	22.23
*57-59	49.7	12.13	38.17

Core 926			
Depth	%sand	%silt	%clay
0-1	68.101	11.96	19.94
1-2	68.35	12.25	19.40
*2-4	55.37	14.37	30.26
4-5	61.808	17.38	20.81
9-10	61.681	22.4	15.92
*13-15	54.94	15.85	29.21
19-20	80.1	11.03	8.87
*25-27	39.84	18.28	41.88
30-31	39.067	22.56	38.37
40-41	36.293	27.99	35.72
*45-46	35.21	18.87	45.92

Core 296			
Depth	%sand	%silt	%clay
0-1	15.71	34.74	49.55
*7-8	10.98	23.37	65.65
17-18	7.61	11.25	81.14
*25-26	25.94	17.74	56.32
*35-36	2.91	21.93	75.16
47-48	7	23.47	69.53
53-54	4.42	16.52	79.06
61-62	8.67	11.56	79.77
64-66	8.67	27.57	63.76
66-67	11.98	25.45	62.57
67-68	26.89	3.25	69.86
68-69	18.98	17.57	63.45
69-70	35.56	31.35	33.09
*70-71	17.43	41.78	40.79

Core 142			
Depth	%sand	%silt	%clay
0-1	31.91	20.77	47.32
2-4*	15.88	16.00	68.12
5-6	6.28	22.05	71.66
9-10	14.92	26.36	58.72
13-15*	4.17	11.24	84.59
18-19	24.24	23.31	52.45
25-27*	2.66	13.72	83.62
35-36	6.57	26.46	66.97
40-41	13.10	20.15	66.75
44-46*	10.83	18.23	70.94
50-51	4.27	25.37	70.36
55-56	5.23	23.03	71.74

Core 8827			
Depth	%sand	%silt	%clay
0-1	24.91	38.23	36.86
2-4*	30.97	10.10	58.93
5-7*	41.64	37.83	20.53
9-10	39.64	36.36	24.00
13-15	34.94	15.18	49.88
18-19	36.13	37.65	26.22
25-27*	17.06	32.86	50.08
35-36	7.86	41.43	50.71
40-41	4.50	33.22	62.28
44-46*	2.95	23.22	73.83
50-51	4.07	47.31	48.62
56-57	2.73	47.27	50.00
60-61	7.35	38.24	54.41

* Detailed Sedigraph data provided in Appendix C, Table C-1.

	%sand	%silt	%clay
CN26 grab	42.67	29.64	27.69
S. Dred. Is grab	47.73	13.98	38.29
Y channel grab	0.70	7.91	91.39
L. River Delta	56.36	9.08	34.56

Two cores, Station 128 (Figure C-2) northwest of Dredge Island and an unimpacted core station (4293) in Keller Bay (Figure C-32), do show an overall downcore trend. Below the surface mixed layer (~5 cm) in 128 the core fines increase downward with a sharp coarsening below 46 cm. A possible interpretation of this trend is that the ship channel dredging in 1949 changed the sedimentation patterns at the site, creating the sharp basal change that is also observed in core 201 (Figure C-9). Since that time, the coarsening at 128 may be an effect of infilling and equilibration of the site.

Porosity was measured in all the cores, and profiles are shown in Figures C-71 to C-86. Data from all the cores except those from the less-impacted stations (cores 4293 and 300) suggest a layering of sediments with intermingled high and low porosity sections that correlates with the layers observed in the x-radiographs. An apparent exception is the porosity profile from core 128 (Figure C-71). However, it likely was produced by averaging over the five times thicker sediment slices which were processed in this core (5 vs 1cm). Porosities from some of the less-impacted stations show a more normal behavior, with porosity decreasing more steadily with depth as a function of overburden-induced consolidation. Porosity is found to correlate significantly with the downcore %clay distribution (Figure C-87). These statistically significant correlations are further improved when the porosity and grain size data are determined in the same core, rather than in two different cores, as was the case for most of the sites. In addition to comparing data points from different cores from the same sites with slightly offset vertical structures, variations in packing density, mineralogy, and organic content could have introduced further variability. However, despite these factors, porosity appears to be an excellent predictor of the percent clay fraction.

5.3.2 Spatial Trends

Sediment type in the sample area varies spatially from clayey sands to clays (Figure 5-16). Silt (4-62 microns) is never the major component. Four grab samples were collected from possible source areas: 1) the erosional north shore of Cox Bay at station CN26, 2) the lower delta of the Lavaca River, 3) the erosional south shore of Dredge Island, and 4) the "Y" part of the Alcoa/CCND navigational channel east of Dredge Island. This was done in order to examine whether observed spatial variations were more a function of different source areas or hydrodynamics. In Figure 5-16 it is apparent that the sand:silt:clay ratio is similar for three of these source areas (endmember) and extremely clay rich in the modern fill of the Y dredge channel.

Detailed Sedigraph/RSA granulometry dividing the grain sizes into 52 size classes were conducted on these endmembers (Figure 5-17) and 2-5 samples per core (procedures detailed in Appendix A). This enables an examination of whether the clay fraction is distinct in the Y dredge channel. Figure 5-18 shows that the endmembers and, excepting a few outliers, all the core samples, group closely together when the clay-sized fraction is subdivided. We interpret this as a result of relatively rapid dispersal of clay-sized material bay-wide, so that even though individual samples have differing amounts of clay, the character of that clay is similar. A secondary factor responsible for the pattern in Figure 5-18 is that the dredge material taken from channel construction is modern infill ultimately derived from endmember sources and also contains underlying Pleistocene material

Figure 5-17. Sedigraph/RSA grain size histogram for the four endmember grab samples collected to identify sediment sources in the study area.

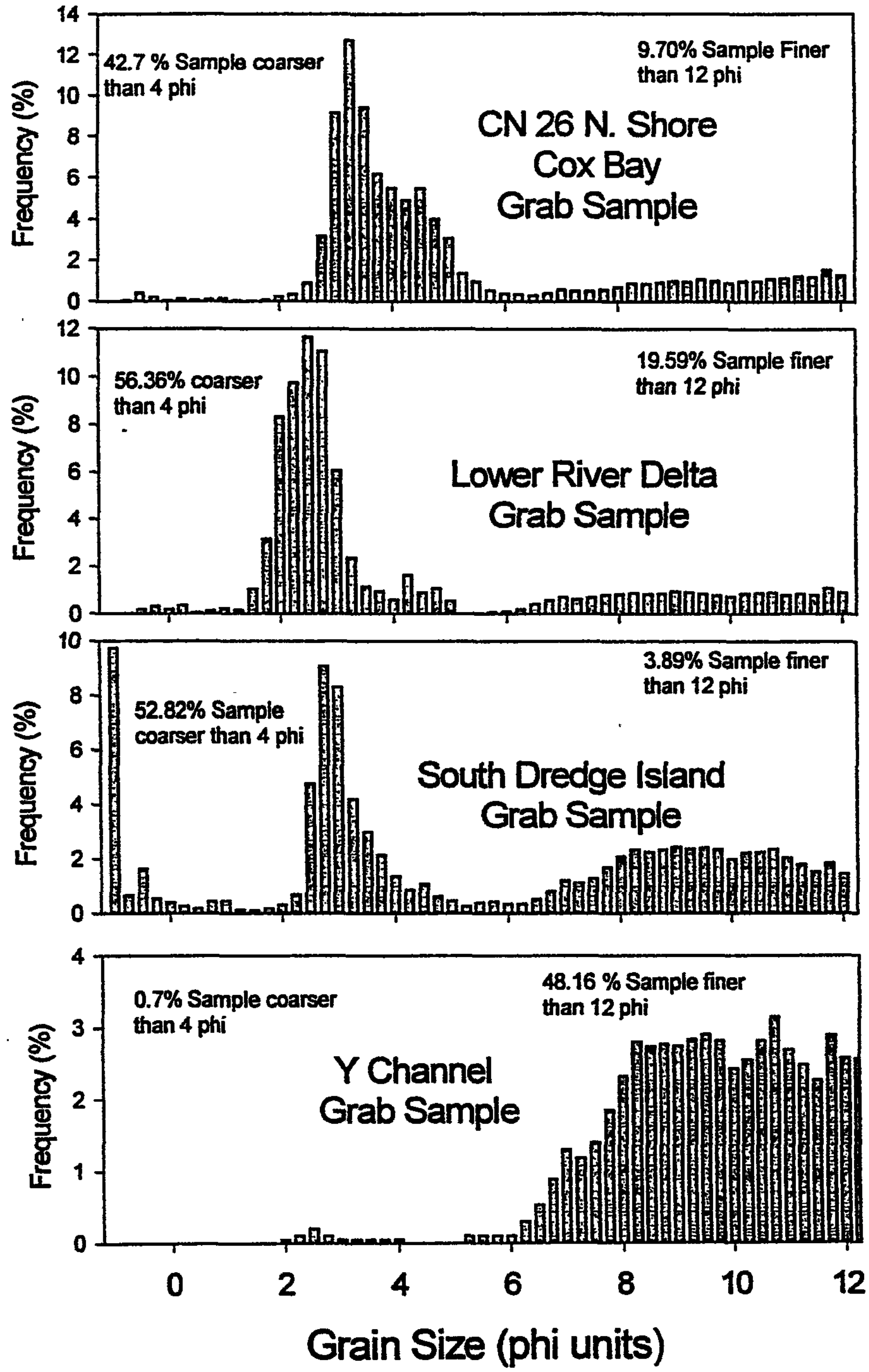

Figure 5-18. Subdivision of clay size fractions for the detailed grain size analyses and for the four endmember grabs.

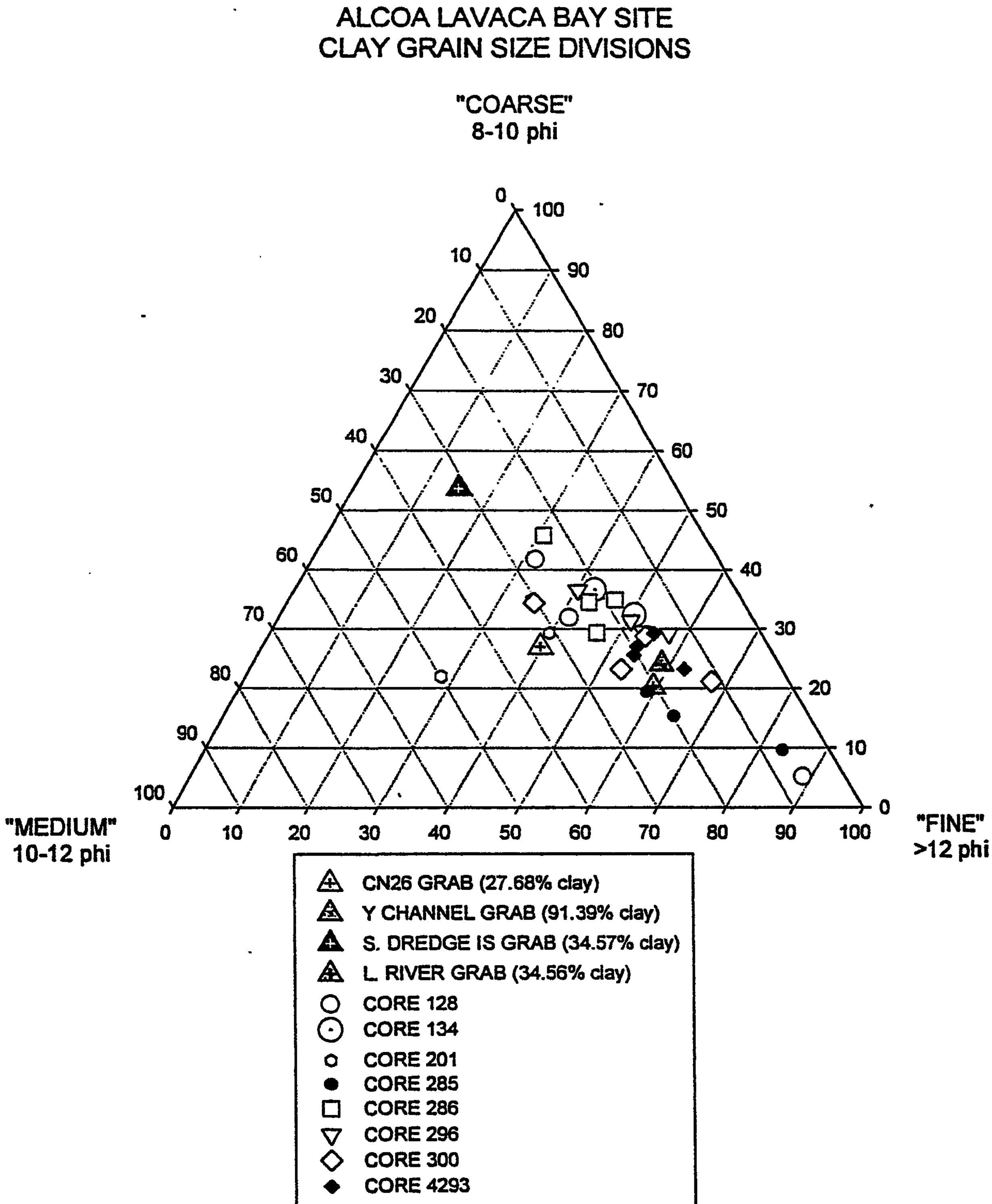

similar to that eroding from the shorelines of Cox Bay. The endmember from south Dredge Island contains slightly more "coarse" clay relative to the mean, perhaps due to selective size sorting of the clay fraction by rainwater runoff.

Figure 5-19 is a different approach utilizing the graphic mean grain size and graphic inclusive standard deviation (sorting) from the Sedigraph/RSA analysis to differentiate granulometry. This plot measures the overall similarity of grain size characteristics. The Y channel dredge material is distinct from the other endmembers with the core samples trending on a line from the two-endmember regions. Samples closest to the dredge material are those from Cox Bay (285, 286) and cores 300 and 134 from Lavaca Bay. The Cox Bay core data, except for samples from the more distal 296, supports the radiochemical evidence of increased sediment accumulation due to dredge spoiling in the area, hence, the granulometry most resembles dredge spoil. The dredge spoil "fingerprint" in upper part of core 300 may reflect redistribution of this material offshore with time. The absence of this fingerprint in all but 1 of 4 samples from 296 may reflect that the spoil dispersal vector was more offshore.

The Sedigraph/RSA analyses show a number of modes in the histogram frequency distribution (Figure 5-17) that each represent a distinct source or mechanism of delivery. Modal data is summarized in Figure 5-20. Six modes of grain size were identified. Of these, the mode at 3.25-3.5 phi (M2) in the sand range and at 8.25-8.5 phi (M4) in the clay range are common to almost all the samples. Bimodal distributions of these modal sizes are typically interpreted by studies of marine and coastal environments as material delivered to the site in two ways: the sand as bedload and the clay as suspended load. A third mode may exist in the fraction finer than 12 phi (0.25 microns) as many of the examples exhibit an increase in frequency of the finest size classes measured (e.g., >12 phi). This mode may be related to the delivery of colloidal matter to the seabed. As a matter of fact, on a percent frequency basis, a large fraction of the Y dredge channel grab and of the Cox Bay sediment samples consist of colloidal material finer than 0.25 μm (>12 phi). The samples that have other modes are interpreted to be receiving sediment from another source area. Core 201 samples show a mode at 2.5-3 phi (M1), which is also observed in the lower river delta endmember grab, suggesting sand from the river is reaching this core or that the eroding adjacent shoreline deposits are composed of older river sands.

5.4 RADIOISOTOPE RESULTS

The following section presents the results of the radioisotope analyses conducted by Texas A&M University along with a discussion of radionuclide budgets for the major isotopes . A detailed listing of all radiochemical results is given in Table C-3. The table shows the core number, sample interval (e.g., 0-1 cm, 1-2 cm, etc.), porosity, the number of counts for each isotope (e.g., ^{137}Cs, ^{210}Pb, etc.), and the standard deviation of the counting statistics.

Figure 5-19. Graphic sorting and mean grain size relationships for detailed graind size samples and for the four endmember grabs.

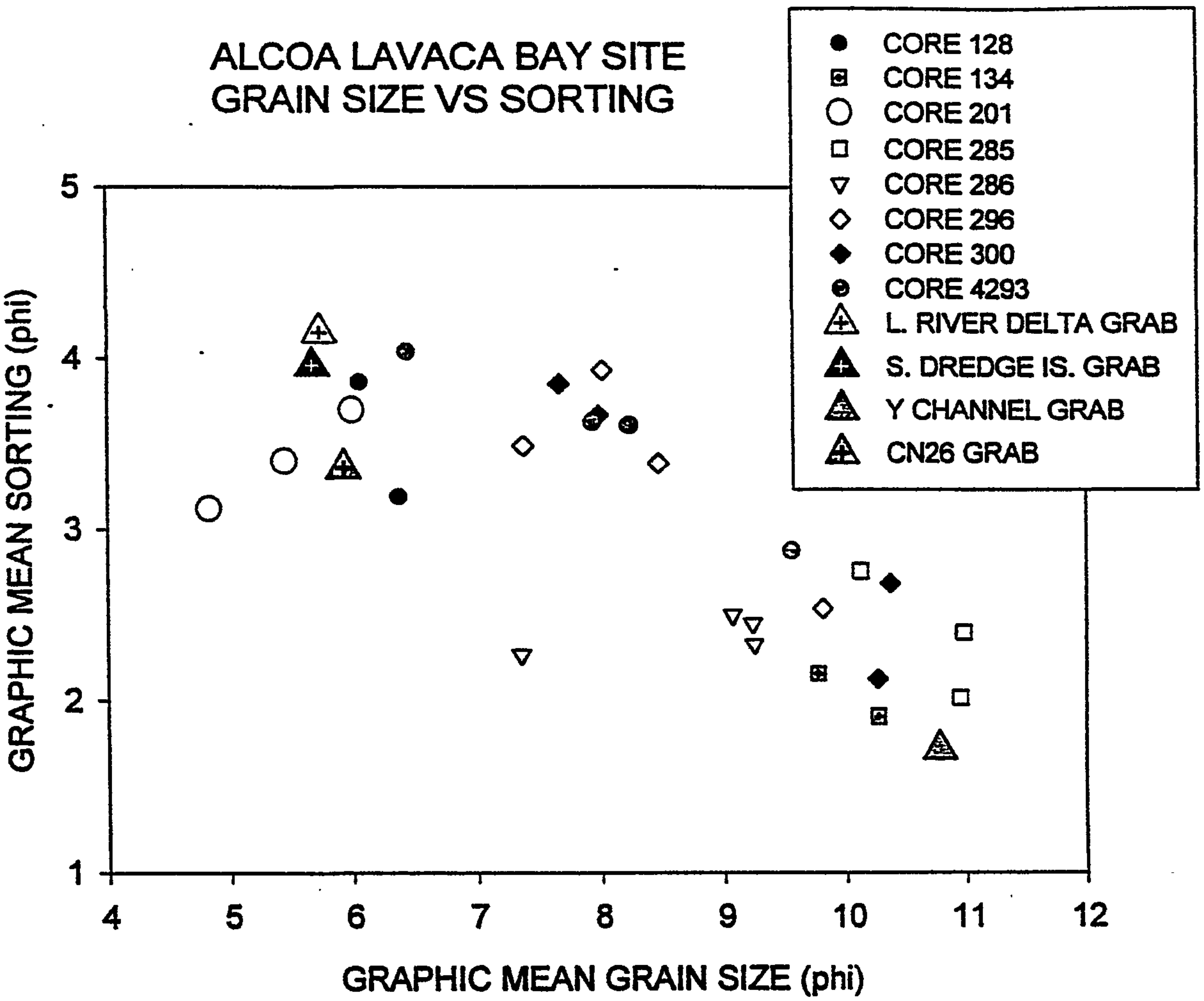

Figure 5-20. Primary and secondary modes of grain size from the detailed granulometry samples in the cores and from the four endmember grabs.

Modes of Sediment Grain Size from ALCOA Lavaca Bay

M1 –2.5-3.0 phi (187.5-125 μ)
M2 –3.25-3.5 phi (109.4-93.8 μ)
M3 –6.75-7.0 phi (9.8-7.8 μ)
M4 –8.25-8.5 phi (3.5-3.0 μ)
M5 –10.25-10.5 phi (0.875-0.75 μ)
M6 – >12 phi (<0.25 μ)

Core & Depth	M1	M2	M3	M4	M5	M6
128 1-3cm		◆			◆	
128 8-10cm		◆		■		
128 48-50cm		◆		■		
134 20-22cm				◆		■
134 57-59cm				◆		■
201 5-7cm	◆	■			■	
201 12-14cm	◆	■		■	■	
201 57-59cm	◆	■		■		
285 2-4cm		■			■	
285 20-22cm		■		◆		■
285 72-74cm	■	■			■	
286 2-4cm			◆			■
286 18-20cm			◆			■
286 23-25cm			◆	■		■
286 66-68cm			◆	■		■
296 7-8cm		◆	■	■		■
296 25-26cm		◆	■	■		
296 35-36cm		◆		■		■
296 70-71cm		◆		■		
300 2-4cm				■		■
300 13-15cm				◆		
300 25-27cm		◆		■		■
300 56-58cm		◆		■		
4293 2-4cm		◆		■		■
4293 13-15cm		◆		■		■
4293 25-27cm		◆		■		■
4293 56-58cm		◆		■		■

Grab Samples of End Member Sediment Sources

	M1	M2	M3	M4	M5	M6
L. River Delta	◆					
S. Dredge Isl.	◆			■	■	
CN26 Shore		◆				
Y Dredge Ch.	■			■	■	■

5.4.1 Beryllium-7

All cores had significant amounts of ^{7}Be in the uppermost sediment layers (Figures C-88 to C-102). Activity concentrations below a level equivalent to 3 times the standard deviation due to counting statistics are considered below the detection limit, and were generally not reported or further considered.

Inventories of ^{7}Be (Figure 5-21, Table 5-4) can be compared to those expected from atmospheric fallout, i.e., 1-4 dpm/cm^2 (average of 3 dpm/cm^2), varying seasonally (Baskaran et al., 1993) and with amount of rainfall. ^{7}Be inventories are significantly correlated with particle reworking rates (D_b) (Figure C-103), suggesting that the mixing intensity is determining its inventory on time scales of a few months. Furthermore, any particle-reactive substance could be expected to be mixed into the sediments on time-scales of months, similarly to this short-lived nuclide.

5.4.2 Lead-210

All cores had significant amounts of ^{210}Pb activities. $^{210}Pb_{xs}$ (calculated as [^{210}Pb] -[^{226}Ra]) activities in surface sediments are significant (i.e., larger than 3 times the propagated standard deviation due to counting statistics), and are, as expected, decreasing with depth. Results, determined from alpha or gamma counting methods, are shown in Figures C-104 to C-120, and are in most cases of sufficient quality to be used to estimate sedimentation rates.

The profiles of $^{210}Pb_{xs}$ can be integrated, and a sediment inventory can be calculated. The observed inventory of $^{210}Pb_{xs}$ was created by atmospheric precipitation, plus riverine flux from drainage basin erosion (expected to be small due to the relatively small size of the catchment basin), and modified by sediment focussing effects (expected to be substantial, at times). In addition, it is assumed that natural radionuclides are efficiently retained in the Bay system, as was shown in a study of another but similar Texas bay, Galveston Bay (Baskaran et al., 1993b). A comparison of the observed inventory with the inventory expected from atmospheric precipitation is useful for a number of reasons, e.g., 1) it can provide additional information useful when interpreting the radionuclide profiles; 2) it can provide useful insights into short- and long-term geochemical transport processes, such as particle mixing and sedimentation rates, as well as focussing processes, which can control the inventories (and therefore, concentrations) of particle-reactive radionuclides and metals, and by extension, also mercury. In the following section, the observed inventory is compared to only the atmospheric inventory since the amounts supplied by the river are not known.

The expected $^{210}Pb_{xs}$ inventory, calculated from atmospheric precipitation of 1m/yr for Lavaca Bay (NOAA, 1996) and a ^{210}Pb deposition rate of 0.84 dpm cm^{-2} yr^{-1} at 1m/yr at this precipitation rate (Baskaran et al., 1993), is about 27 dpm/cm^2, calculated as:

$$\text{Inventory (expected)} = \text{Flux}/\lambda. \tag{9}$$

With λ = decay constant of ^{210}Pb = 0.031 yr^{-1}. While the observed $^{210}Pb_{xs}$ inventories, as presented

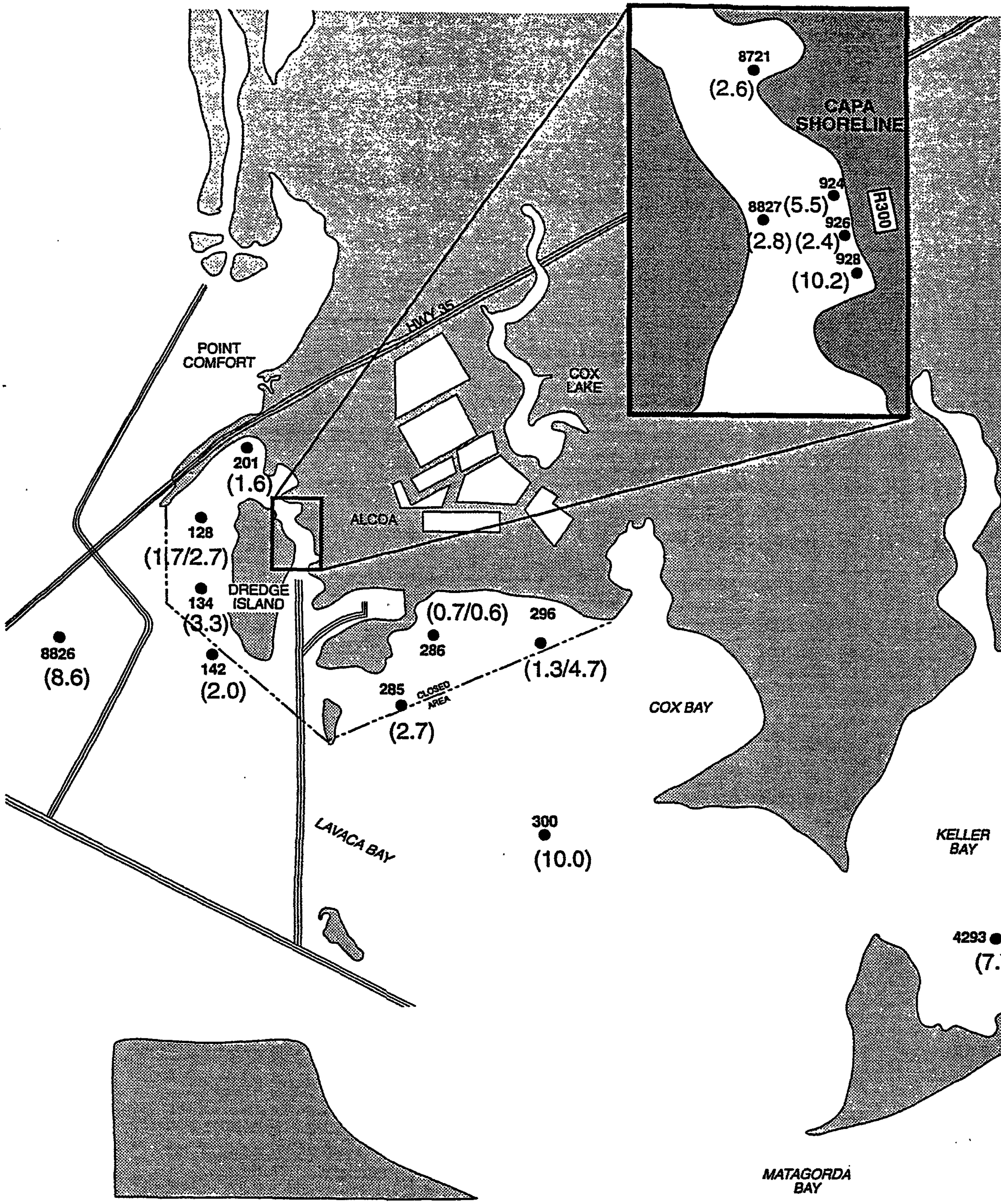

Alcoa Dredge Island/54-2824-55(01) 1/98

KILOMETERS
0 1 2 3
1:75,000

N

● Samples collected for total mercury, TOC, x-radiography and radioisotope analyses

() Be-7 Inventory (dpm/cm^2)

Figure 5-21

Radiochemistry Study - Be-7 Inventories (dpm/cm^2)

Table 5-4. Comparison of transport parameters (i.e., sedimentation, particle reworking rates, D_b, and depths, z_m) and radionuclide inventories.

Station and core #	Date of sampling	Mixed layer depth (cm), based on ^{7}Be penetration	D_b (cm^2/yr), S_s ($g\ cm^{-2}\ yr^{-1}$)	^{7}Be & ^{137}Cs inventory (dpm/cm^2)	$^{210}Pb_{xs}$ inventory (dpm/cm^2)	Porosity, $Ø_o$, $Ø_{min}$ $Ø_{average}$	Sed.rate (cm/yr) from $^{210}Pb/^{137}Cs$/Hg	Hg peak depth (cm)
West	of	Dredge	Island					
128A	1/16/97	4	35,0.85	1.7, 7.9	14	0.84,0.46,0.60	0.7±0.35/ 0.85/1.0	28
128B	8/06/97	7	47,-	2.7,-	-	0.89, -	-	-
134	2/14/97	2	1.8,0.29	3.3,10.3	29	0.88,0.71,0.72	0.45±0.1/ 0.55/0.4	11
142	9/26/97	3	58,0.19	2.0, 7.5	30	0.76,0.70,0.73	0.75±0.35 /0.4/0.2	4-7
201	1/30/97	2	2.3,1.4	1.6, 9.3	32	0.63,0.45,0.47	1.2±0.5 /1.1/1.2	35
Cox	Bay							
285	4/15/97	4	32,1.4	2.7,18.7	64	0.85,0.75,0.75	2.2±0.3 ≥1.8/1.8	50
286A	4/15/97	3	58,1.3	0.7,11.5	63	0.75,0.70,0.68	1.6±0.5/ ≥1.8/2.0	60
286B	8/06/97	3	128,-	0.6,-	-	0.89, -	-	-
296A	2/14/97	3	5.7,1.1	1.25, 15.6	92	0.87,0.75,0.76	1.7± 0.2/ ≥1.8/2.0	55
296B	8/08/97	6	37 (876),-	4.7,-	-	0.88, -	-	55
CAPA	Shore	Line						
924 1/	6/25/97	4	4.2,1.8	5.5,12.8	75	0.86,0.71,0.71	1.2±0.3/ ≥1.8/1.0	31
926 2/	6/25/97	4	23,0.4	2.4,6.3	~2	0.61,0.38,0.44	1.3±1.3/ 0.3/-	4
928 1/	9/26/97	10	314,1.5	10.2,11.2	23.2	0.84,0.56,0.67	0.6±0.15/ ≥1.8/2.0	56
8721 1/	12/17/97	5	52,0.9	2.6,10.0	48	0.86,0.77,0.80	2.0±0.35/ ≥1.8/1.9	56
8827	12/17/97	4	7.3,0.9	2.8,3.1	19	0.80,0.60,0.60	0.8±0.3/ 0.6/0.9	26
Less	Impacted	Sites						
300	5/21/97	7	11,0.34	10.0, 11.3	28	0.88,0.68,0.75	0.4±0.05/ 0.7/0.7	21
4293	5/21/97	7	41,0.7	7.7,9.9	75	0.86,0.61,0.69	1.0±0.4/ ≥0.5/-	2,10, 45
8826	11/20/97	7	22,0.5	8.6,10.8	26	0.89,0.7,0.75	0.9±0.15/ 0.90/0.90	26

1/ Sedimentation rates for these cores are more difficult to estimate due to the presence of mercury and/or cesium at the bottom of the core.
2/ Sedimentation rate for this core is more difficult to estimate due to low concentrations of Cs-137 and Pb-210.

in Figure 5-22, are both below and above the expected 27 dpm cm^{-2}, the observed variability poses the question what process would control the deposition of ^{210}Pb and that of other particle-reactive elements such as mercury. For ^{210}Pb, this can be evaluated as follows. ^{210}Pb accumulation rates can be approximated from the sediment accumulation rate (S_a) and the $^{210}Pb_{xs}$ concentration in surface sediments (C(o)).

$$^{210}Pb \text{ accumulation rates} = C(o) x\, S_a \qquad (10a)$$

As shown in Figure C-121, surface concentrations of $^{210}Pb_{xs}$ are correlated with surface sediment organic carbon concentrations (as a measure of % fine grained sediments), which are themselves significantly correlated with surface porosity (Figure C-122). More importantly, $^{210}Pb_{xs}$ inventories are linearly related to sedimentation rates (Figure C-123).

In this simple case, the distributions and inventories of particle-reactive $^{210}Pb_{xs}$ in surface sediments of Lavaca Bay are thus controlled by 1) sediment accumulation rates, and 2) $^{210}Pb_{xs}(o)$ concentrations in surface sediments. Under steady state conditions, eq 10a can be rewritten in the form of eq 10b. The inventory of $^{210}Pb_{xs}$ is then determined by:

$$^{210}Pb_{xs}\text{-Inventory} = {}^{210}Pb_{xs}(o) x (1-Ø) x \rho_s x S/\lambda \qquad (10b)$$

with

$^{210}Pb_{xs}(o)$ as the excess-^{210}Pb concentration at the sediment surface, in dpm/g,
Ø = average porosity, in cm^3 of water / cm^3 of wet sediments,
ρ_s = dry density of sediment particles, in g dry sediments / cm^3 dry sediments,
S = sedimentation rate in cm/yr
λ = decay constant of ^{210}Pb = 0.031 yr^{-1}.

Since $^{210}Pb_{xs}(o)$ is linearly related to organic carbon concentration (Figure C-121), the inventory of $^{210}Pb_{xs}$ also becomes a function of organic carbon concentration (or porosity or % fine grained sediments) at the sediment surface, provided that most ^{210}Pb is re-adsorbed to sediment particles during organic carbon mineralization when organic carbon concentrations are decreasing with depth.

Average measured surface concentrations of $^{210}Pb_{xs}$ (C(o)) of about 3 dpm/g are in agreement with incoming sediment into Lavaca Bay, and the atmospheric fallout of about 0.84 dpm/cm^2/yr, as can be seen by the following calculation.

$$C(o) = {}^{210}Pb_{xs} \text{ flux/sediment-flux} \qquad (10c)$$

If we assume that 323,000 tons/yr of riverine sediment (J. Connolley, pers. communication, based on Lavaca River Authority data) are coming into the bay every year, and are evenly sedimenting out over the entire area of the bay of 180 km^2, one would get ($3.23x10^{11}$g/yr)/($1.8x10^{12}cm^2$) = 0.2 g/cm^2/yr (equivalent to about 3-4 mm/yr of sedimentation rate).

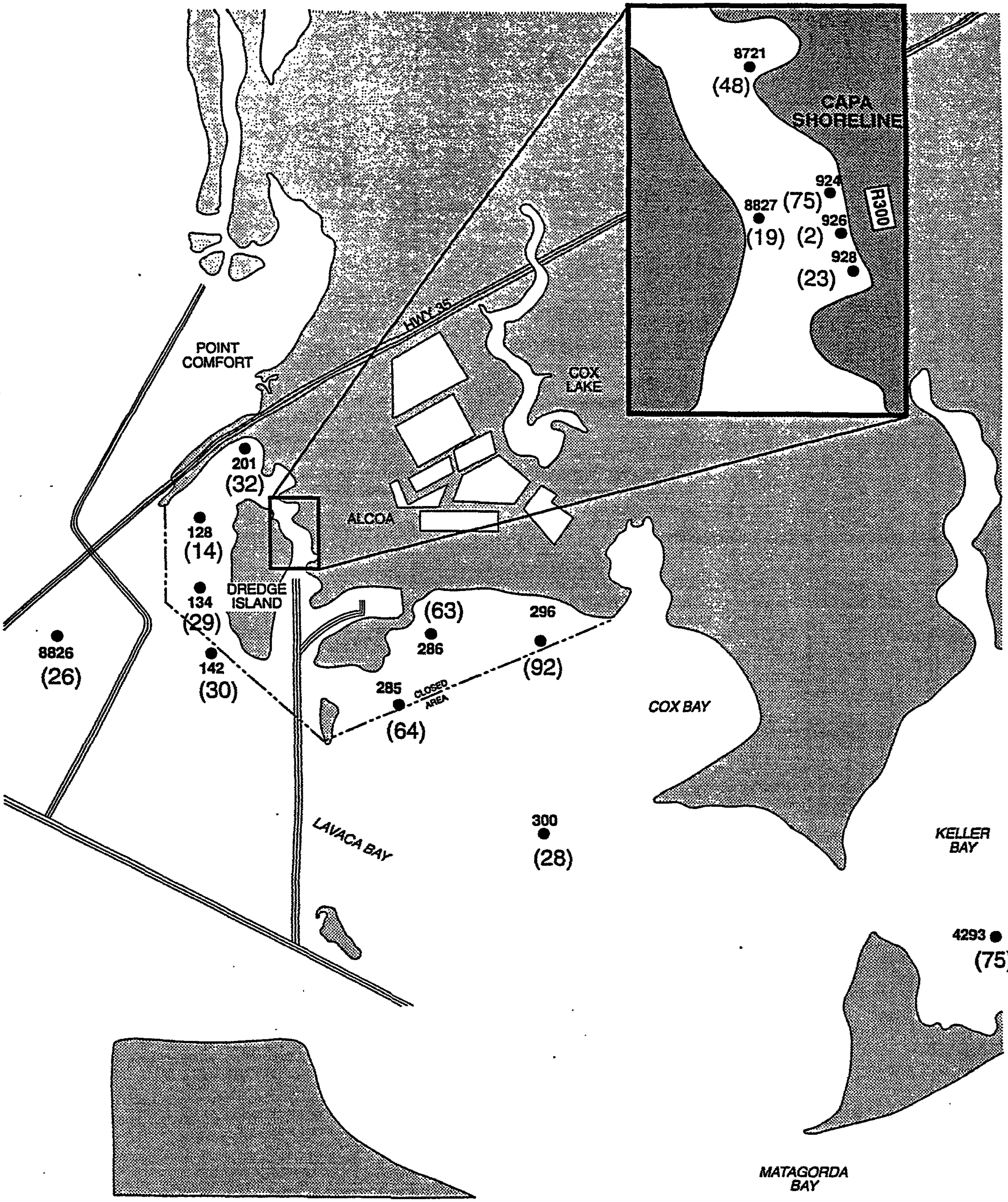

Alcoa Dredge Island/54-2824-55(01) 1/98

KILOMETERS 0 1 2 3
1:75,000

N

● Samples collected for total mercury, TOC, x-radiography and radioisotope analyses

() Excess-Pb-210 Inventory (dpm/cm^2)

Figure 5-22

Radiochemistry Study - Excess Pb-210 Inventories (dpm/cn

$C(o)=(0.84 dpm/cm^2/yr)/(0.2 g/cm^2/yr) \approx 4$ dpm/g. Therefore, the amount of any additional unsupported ^{210}Pb from soil erosion has to be small. This is reasonable since the ratio of drainage basin area to settling basin (Lavaca Bay) area is, according to USGS data, equal to $11{,}900 km^2/180 km^2 = 60$. Using the same approach as that described in Ravichandran et al. (1995), one can estimate an additional inventory from riverine sediments. This additional riverine inventory, however, would enhance the expected total inventory by only 30-40% over that from atmospheric precipitation.

Inventories of the other particle-reactive radionuclides (e.g., ^{137}Cs, $^{239,240}Pu$, ^{7}Be) when compared to those expected from atmospheric deposition, suggest areas of sediment and particle-radionuclide focusing, and mechanisms of tracer entrainment by particle reworking.

5.4.3 Cesium-137

All cores had significant amounts of ^{137}Cs activities (Figures 5-23 to 5-37), to be used to mark the presence of "post-nuclear" sediments, i.e., sediments deposited after 1953.

Inventories of ^{137}Cs (Figure 5-38, Table 5-4) are close, to within a factor of two, to an inventory of about 10 dpm/cm^2, expected from bomb fallout to Houston, Texas, normalized to 1m/yr rainfall, and decay corrected to the year 1997. ^{137}Cs inventories are significantly correlated with sedimentation rates (S) (Figure C-124), indicating that incoming sediments are relatively uniformly labeled with ^{137}Cs, and thus, ^{137}Cs accumulation is mainly determined by sedimentation rates. In addition, its inventory is also determined by surface porosity or organic carbon content (Figures C-125 and C-126), which both are a measure of % clays (e.g., Figure C-87). This relationship explains the often observed higher ^{137}Cs concentrations in the upper few cm of sediments, which also have higher surface porosity, organic carbon and clay contents.

The fact that ^{137}Cs inventories agree, to within a factor of 2, with those from atmospheric fallout alone cannot be taken that this is its only source. To the contrary, it likely indicates that riverine inputs and sediment focussing effects would have compensated for any possible desorption losses to the water which would have occurred after deposition, caused by a lowering of its particle-water partition coefficient, Kd, in salty water.

5.4.4 Radium-226

All cores had significant amounts of ^{226}Ra activities, which could be used at times to calculate $^{210}Pb_{xs}$ activities (see 5.4.2 and remarks in 3.5.4).

5.4.5 Radium-228

All cores had significant and constant activity concentrations of ^{228}Ra. They were not further used in this study.

Figure 5-23. Sediment profiles of Hg and ^{137}Cs in Core 128.

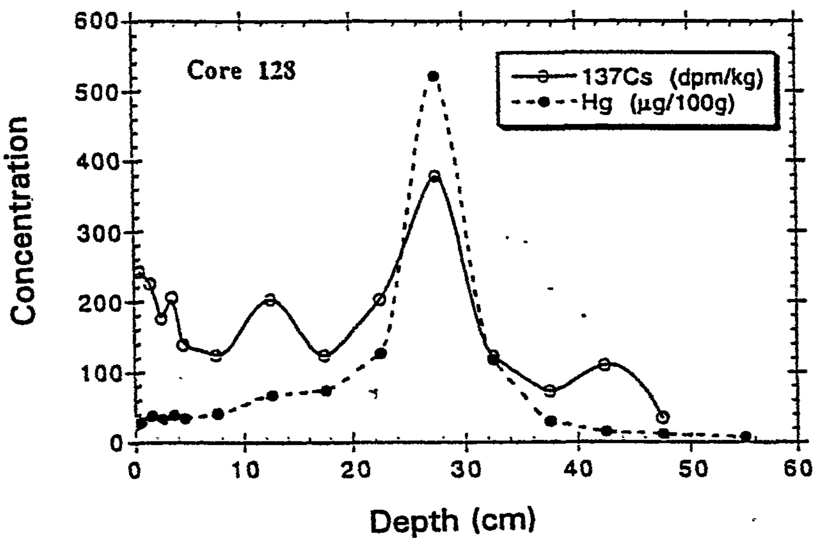

Figure 5-24. Sediment profiles of Hg and ^{137}Cs in Core 134.

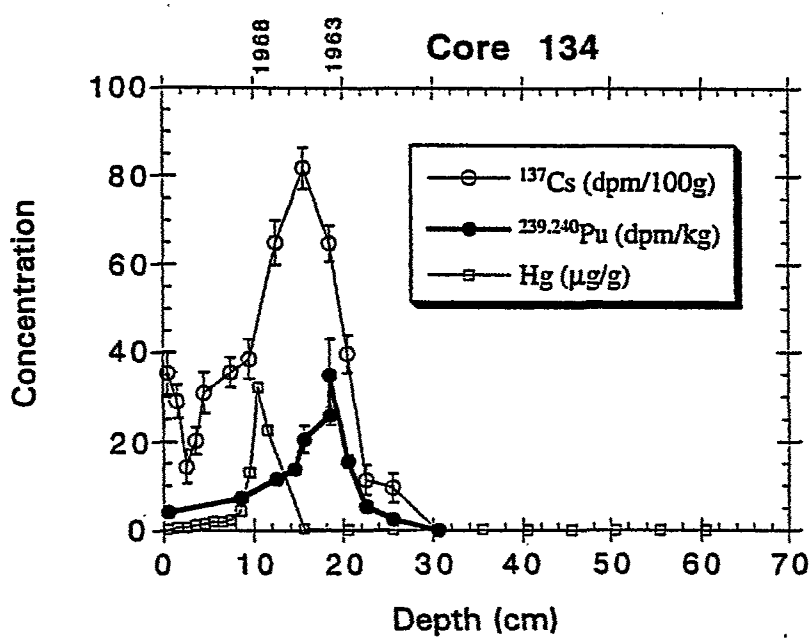

Figure 5-25. Sediment profiles of Hg and ^{137}Cs in Core 142.

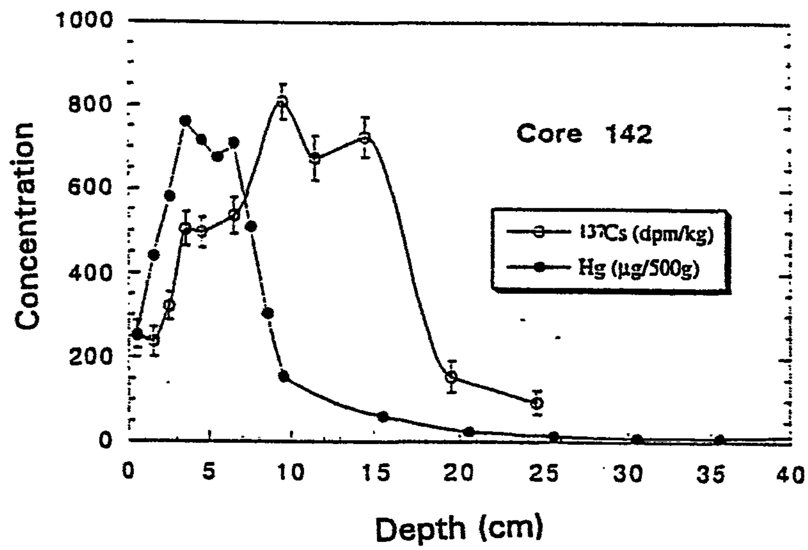

Figure 5-26. Sediment profiles of Hg and ^{137}Cs in Core 201.

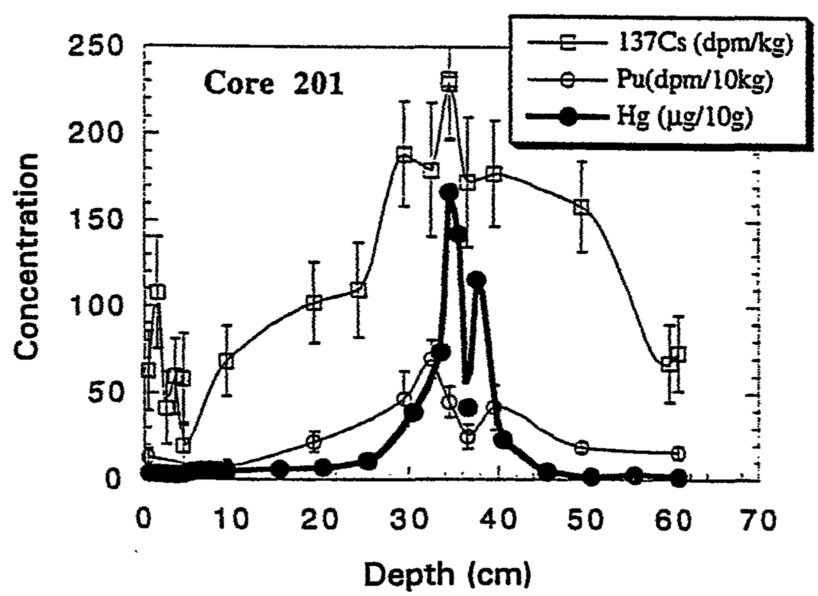

Figure 5-27. Sediment profiles of Hg and ^{137}Cs in Core 285.

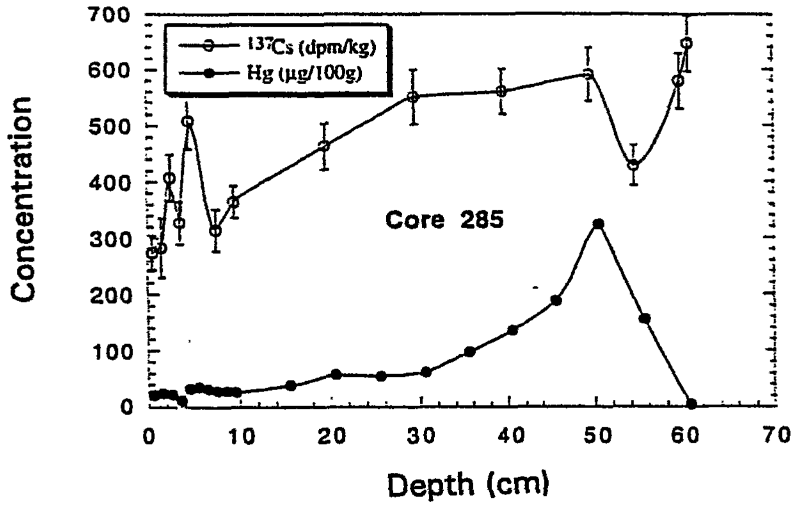

Figure 5-28. Sediment profiles of Hg and ^{137}Cs in Core 286.

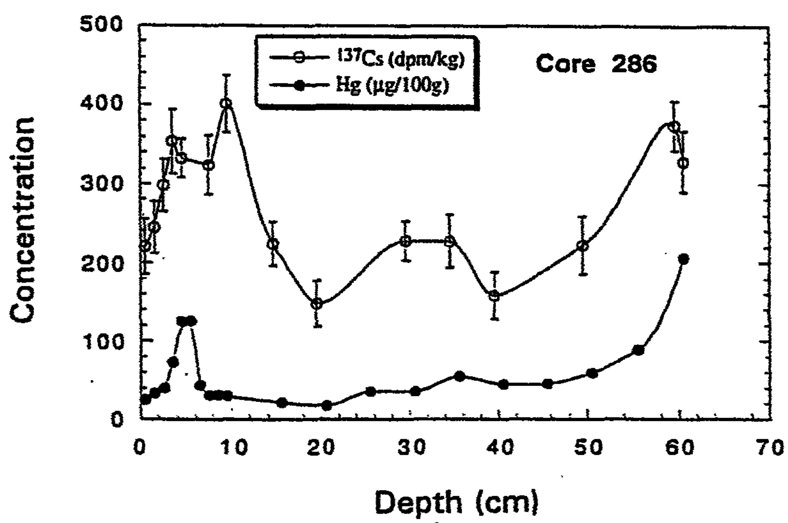

Figure 5-29. Sediment profiles of Hg and ^{137}Cs in Core 296.

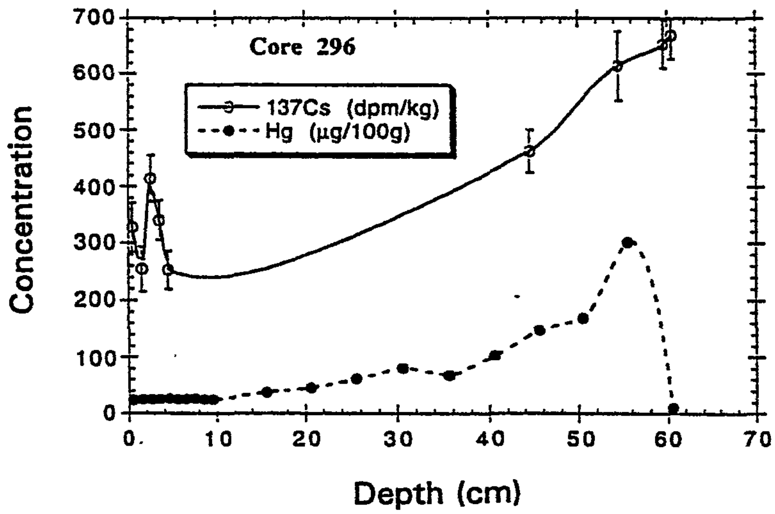

Figure 5-30. Sediment profiles of Hg and ^{137}Cs in Core 300.

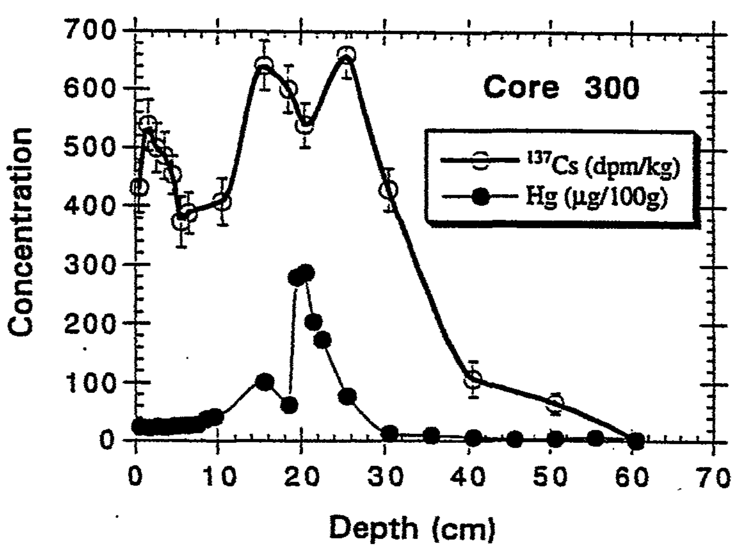

Figure 5-31. Sediment profiles of Hg and ^{137}Cs in Core 924.

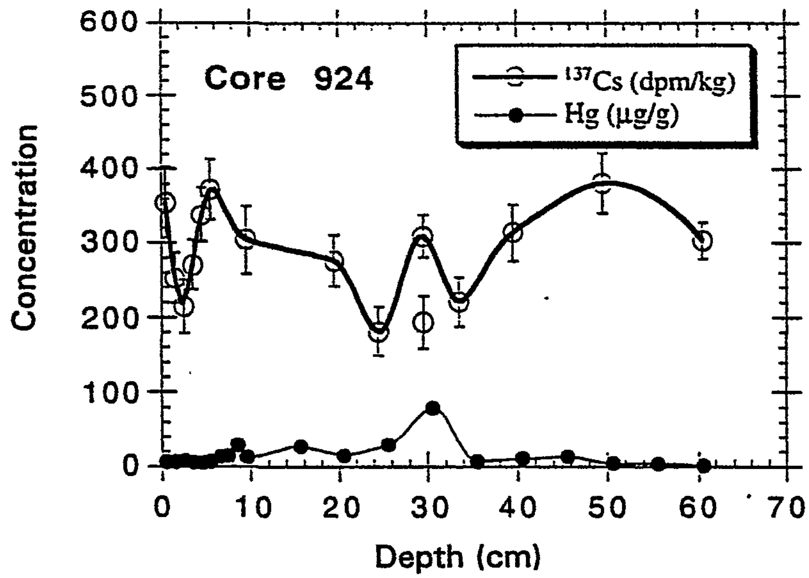

Figure 5-32. Sediment profiles of Hg and ^{137}Cs in Core 926.

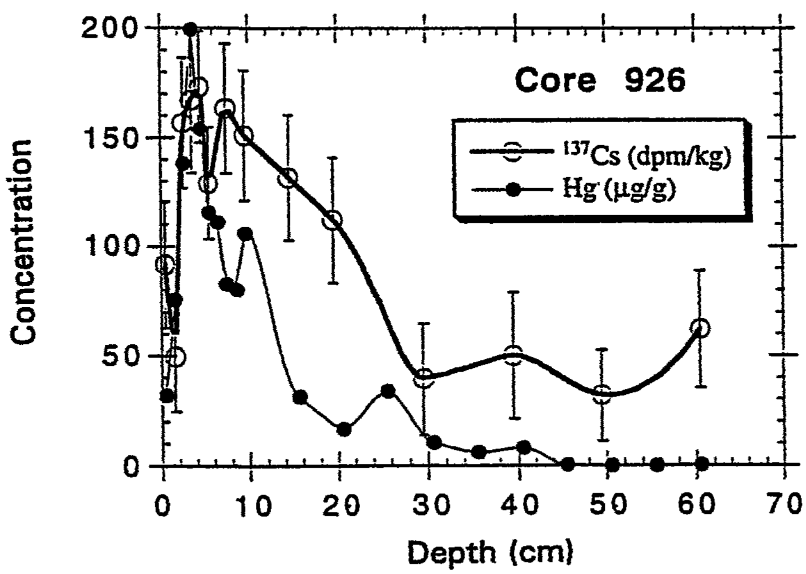

Figure 5-33. Sediment profiles of Hg and ^{137}Cs in Core 928.

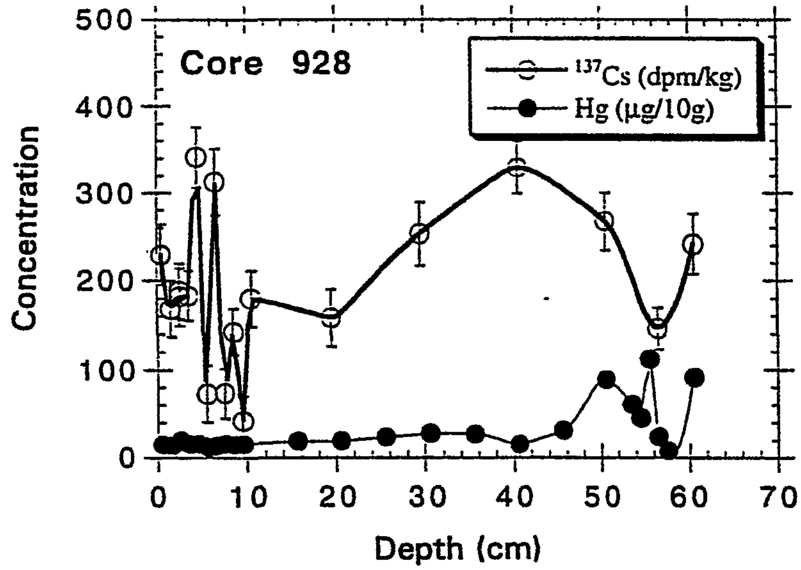

Figure 5-34. Sediment profiles of Hg and ^{137}Cs in Core 4293.

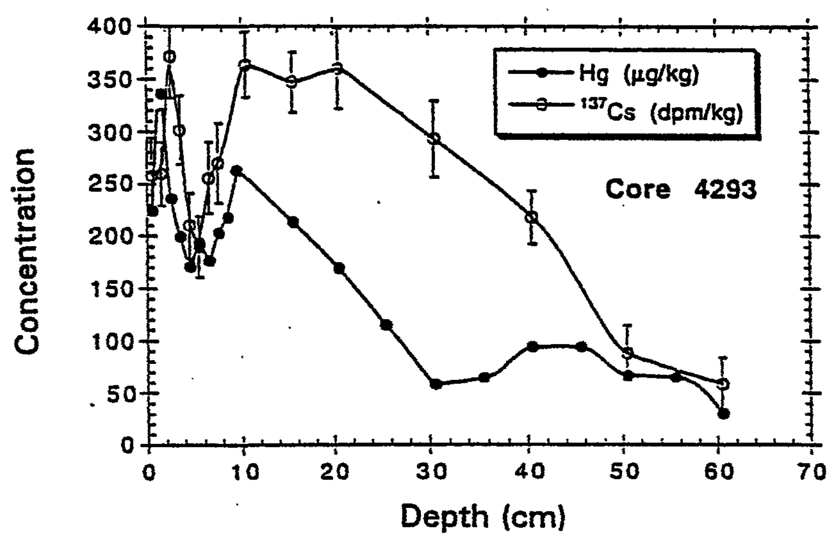

Figure 5-35. Sediment profiles of Hg and ^{137}Cs in Core 8721.

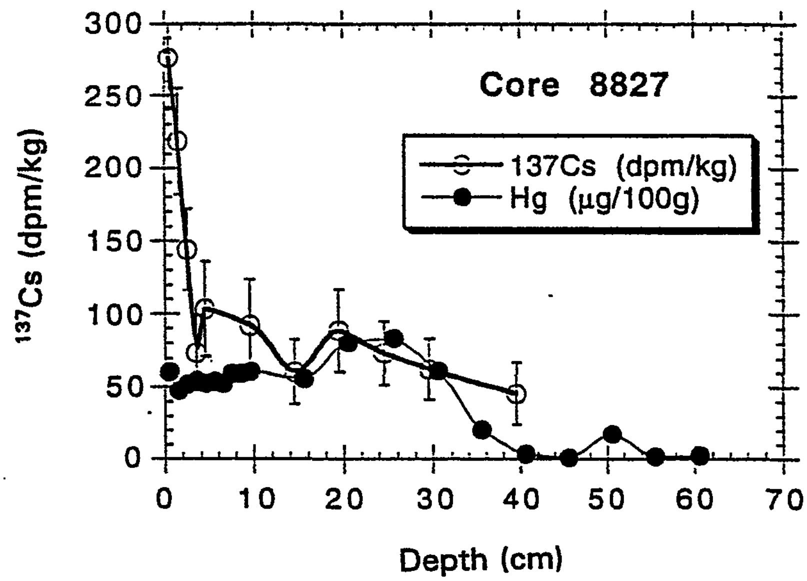

Figure 5-36. Sediment profiles of Hg and ^{137}Cs in Core 8826.

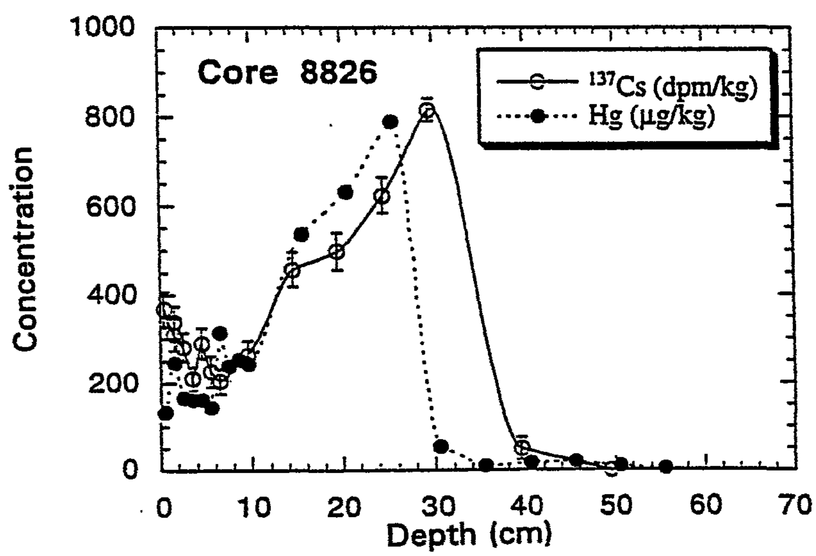

Figure 5-37. Sediment profiles of Hg and ^{137}Cs in Core 8827.

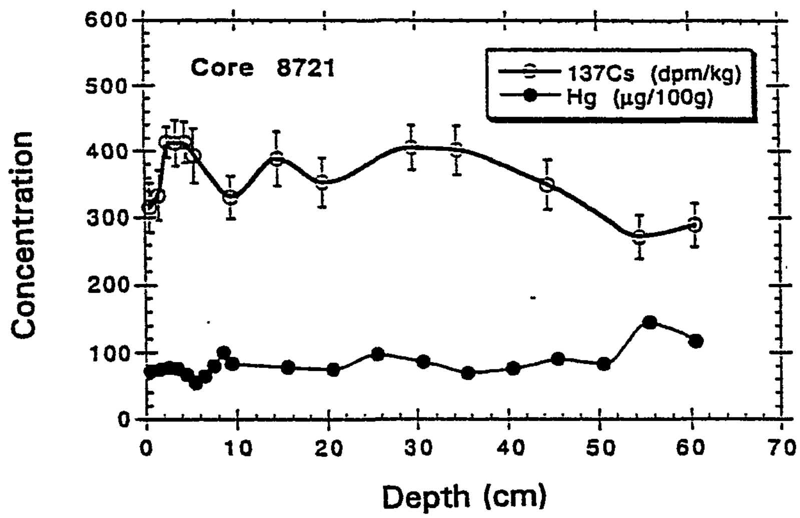

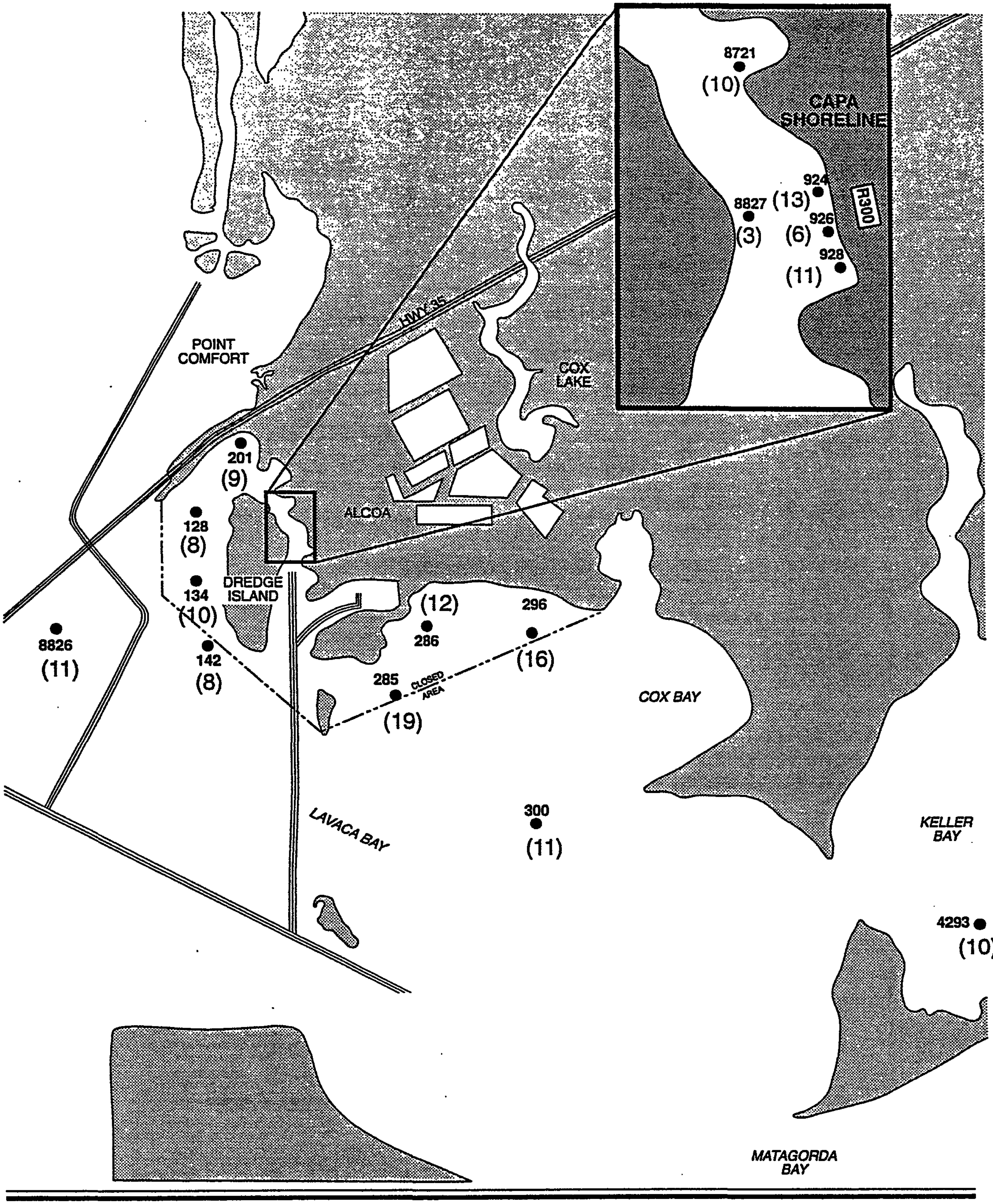

Alcoa Dredge Island/54-2824-55(01) 1/98

KILOMETERS
0 1 2 3
1:75,000

N

● Samples collected for total mercury, TOC, x-radiography and radioisotope analyses

() Cs-137 Inventory (dpm/cm^2)

Figure 5-38

Radiochemistry Study - Cs-137 Inventories (dpm/cm^2)

5.4.6 Thorium-234

All cores had significant and constant activity concentrations of ^{234}Th. Because they were constant, and did not show an increase towards the surface, they were not useful in this study.

5.4.7 Plutonium-239,240

$^{239,240}Pu$ was measured in cores 134 and 201 (Figures 5-39 and 5-40), where it showed significant activity concentrations, and a well developed subsurface peak, coinciding, within the measurement errors, with that of ^{137}Cs, marking the 1963 peak atmospheric fallout from weapons testing. Inventories of $^{239,240}Pu$ (Table 5-4) in cores 134 and 201 are 0.24 and 0.15 dpm/cm^2, respectively. They are very close to the inventories expected from bomb fallout of 0.2 dpm/cm^2 alone (Ravichandran et al., 1995), normalized for 1m/yr rainfall, suggesting that the area north of Dredge Island is effectively capturing other particle-reactive materials, such as mercury.

5.5 X-RADIOGRAPHY RESULTS

X-radiographs were collected from tray cores at 24 sample sites to determine the relative importance of biological and hydrodynamic processes on strata emplacement and preservation in the upper ~70 cm of the sediment. Film negatives were digitized at 300 dpi optical resolution and pieced together with a cm-scale using Adobe Photoshop. The resulting negative images (coarse-grained = white, fine-grained = black) are shown in Figures C-127 through C-151.

Despite differences in the grain size of the cores, an overall pattern of primary physical stratification is apparent. The horizontal layers observed in the x-radiographs (Figure 5-41) represent variations in grain size that influence penetration of x-rays through the sample. In these negative images coarse-grained layers show as white and fine-grained are black. These layers are emplaced at the time of deposition (e.g., primary sedimentary structures) by a combination of temporal variations in bed stress that serve to sort sediment, and by temporal variations in sediment source such as the seasonality of riverine sediment input. Figure 5-42 demonstrates that these layers are continuous over at least meter scales and remain undisturbed below the area of surface mixed layer on seasonal time scales.

The preservation of layering in the cores emplaced at the time of deposition is indicative of limited vertical mixing of stratigraphy by biological and physical processes. Preservation of primary stratification in productive environments like estuaries can be best explained as a function of high sediment accumulation rates (e.g., cm-scale), where rapid burial of primary features limits the period of time they remain in the surface mixed layer. Bioturbation is a secondary (i.e., post-depositional) process that produces disruption and homogenization of laminations giving the x-radiograph a massive appearance that was not observed in the areas examined. Some burrow traces are observed in x-radiograph (Figure 5-41) and are visible because they tend 1) to backfill with sediment that differs from the surrounding material, or 2) to contain fecal pellets or other wall linings produced by the organism. The observed burrow traces are mainly meiofaunal polychaetes

Figure 5-39. Sediment profiles of ^{137}Cs and $^{239,240}Pu$ in Core 134.

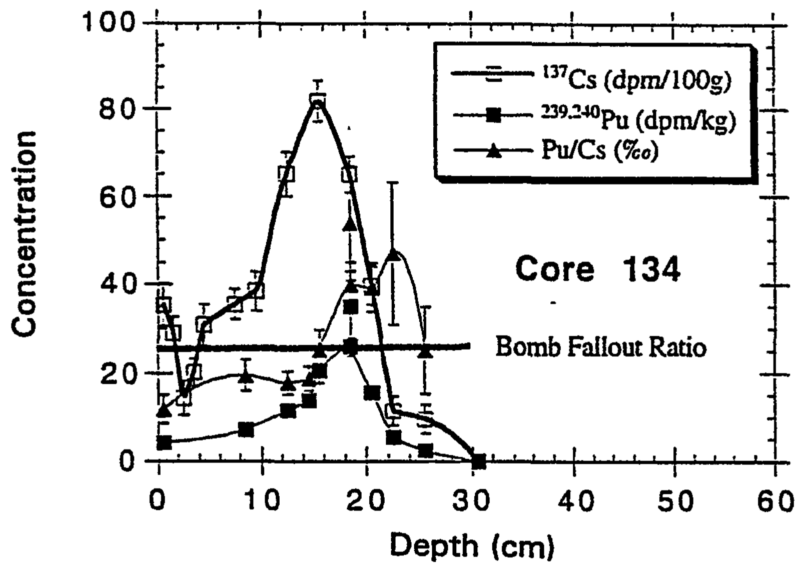

Figure 5-40. Sediment profiles of ^{137}Cs and $^{239,240}Pu$ in Core 201.

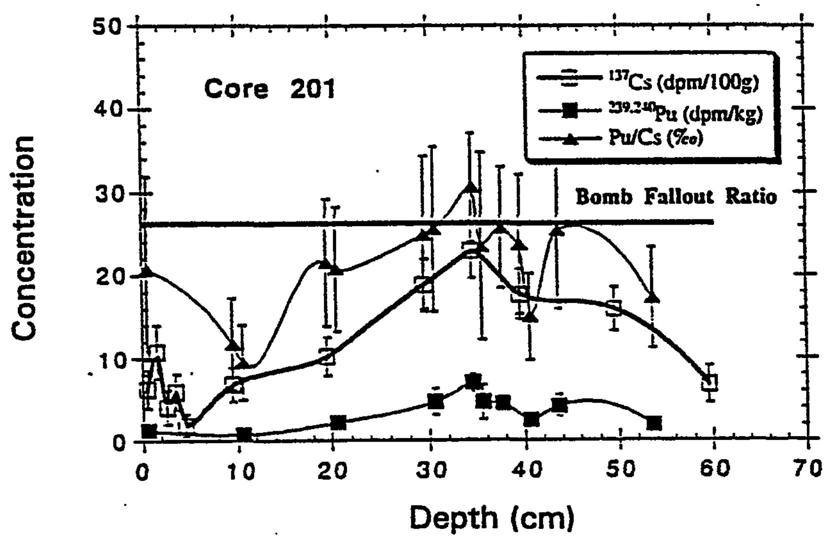

Figure 5-41. X-radiograph negative showing the preservation of primary physical stratification characteristic of the cores from the ALCOA site.

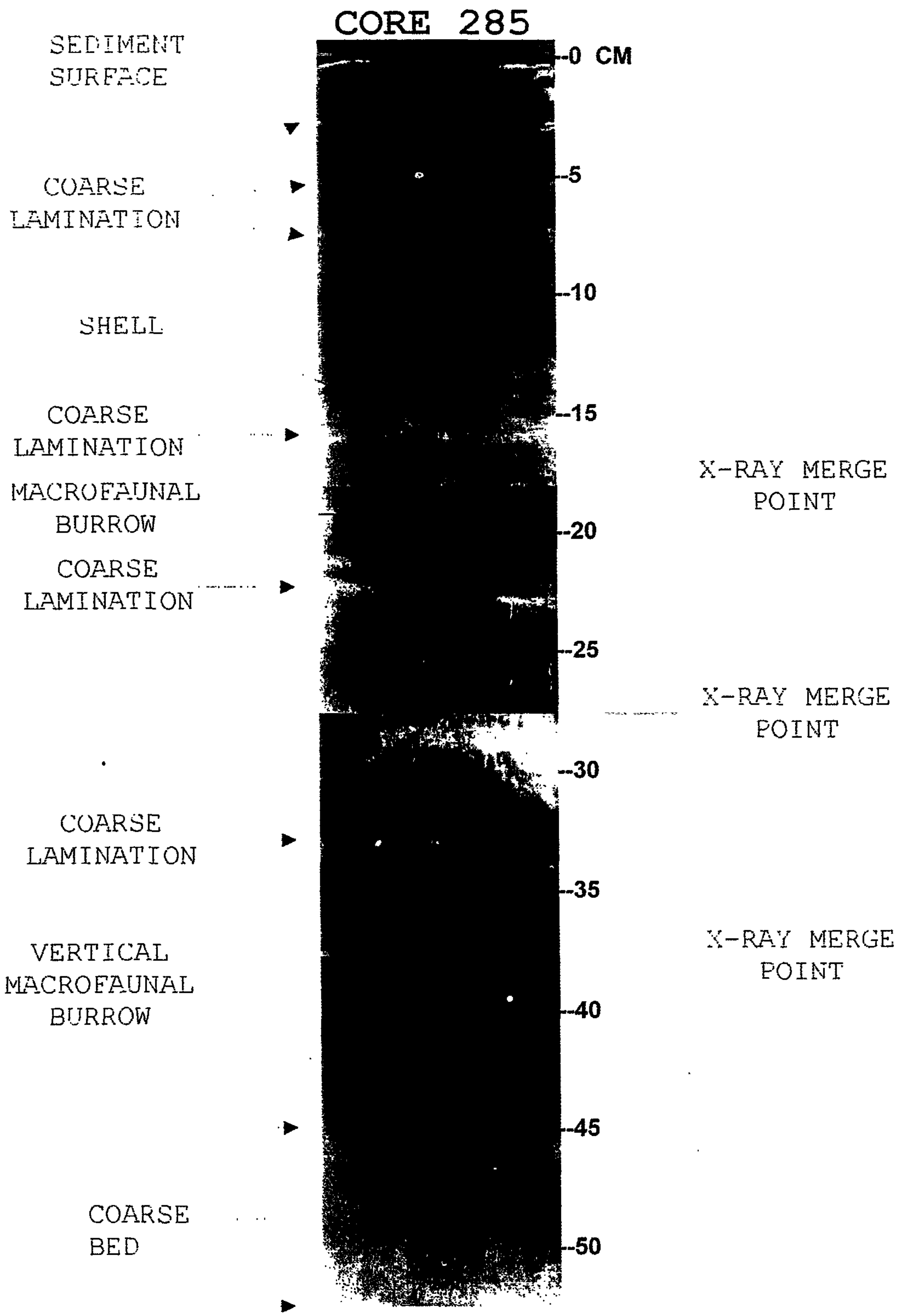

Figure 5-42. X-radiograph negatives of core site 286 taken in April and August showing the preservation of layers over time in the cores except the surface mixed layer.

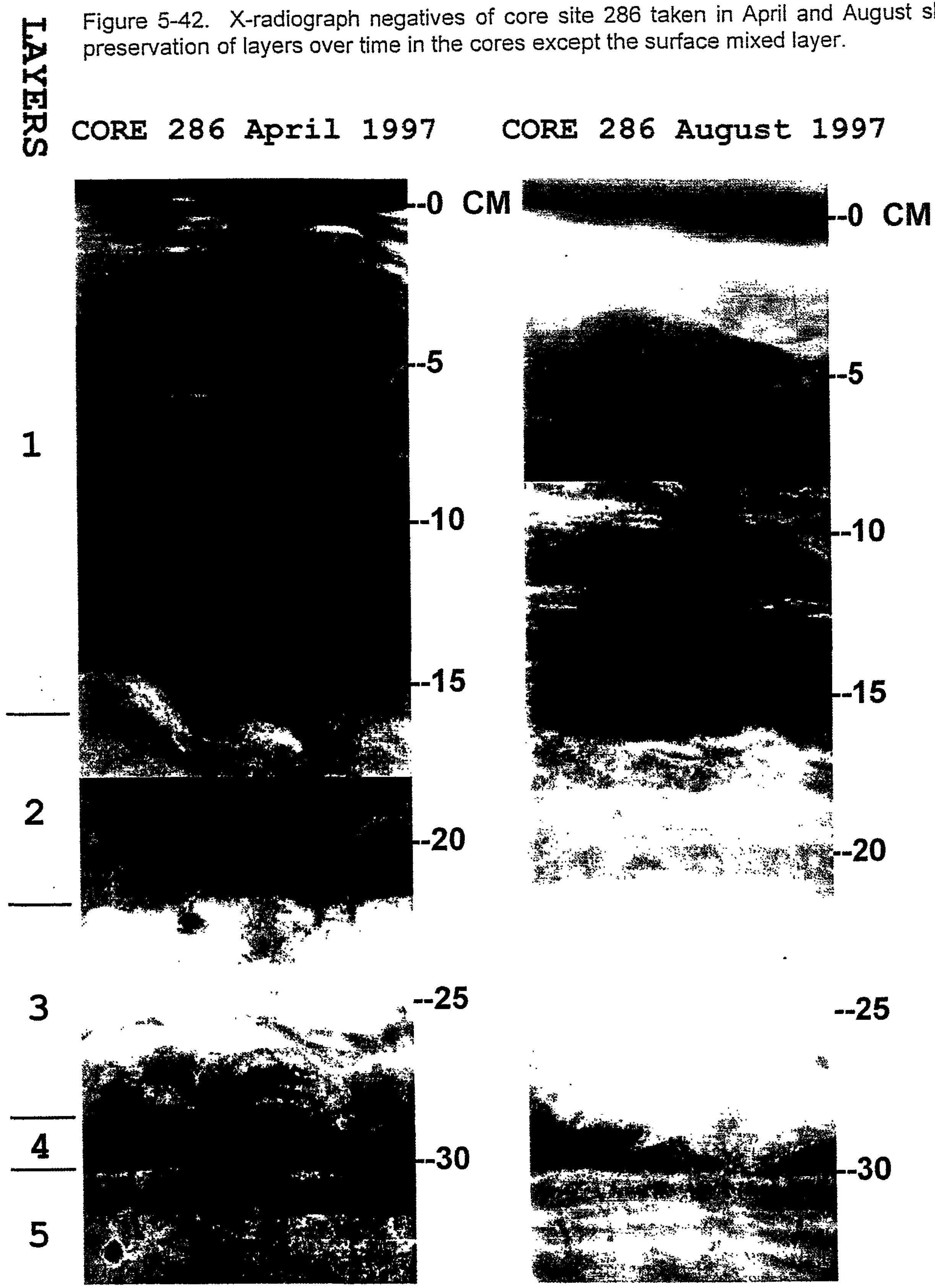

that tend to burrow from the surface to <10cm—macrofaunal burrows in these radiographs that extend to greater depths are rare. The rarity of macrofaunal burrows in the x-radiographs suggests that upmixing of mercury buried at depth by these species is limited. The most burrowing was observed at Station 4293 in Keller Bay.

Primary sedimentary structures are visible in the x-radiographs even within the surface mixed zone (<10 cm) and indicate that mixing rates are relatively modest, a fact confirmed by the radiochemical evidence. This preservation also indicates that anthropogenic sediment mixing (e.g., shrimp trawling) does not influence sediments below a maximum depth of about 3-5 cm, or that the core locations were not impacted by the shrimp trawls.

5.6 LABORATORY QC RESULTS

As mentioned in Section 3.0, the total mercury and total organic carbon analyses were conducted using QAPP-approved analytical methods and were validated to level 4, the highest described for the Alcoa PCO site. The specialized sediment grain size and radioisotope analyses, however, were not conducted under the guidelines of the project QAPP simply due to their highly specialized nature. The results for these analyses are considered of high quality because they were performed under the quality standards recognized by experts in the geochemical field. For the purposes of the Alcoa PCO site, the specialized grain size and radiochemistry data are considered level 2 and will be used for engineering decision making, as well as model preparation, but will not be used for risk assessment purposes.

A summary of the QA/QC procedures applied to the Radiochemistry Study is presented in Section 3.8. Based on data validation, 29 percent of all mercury data reported were flagged. Of the qualified mercury results, 13 percent of the data were flagged as "J+", indicating that the actual concentration may be lower than the reported result. These data were flagged due to elevated recoveries of the matrix spikes, which were not within the control limits for mercury. This signifies that the sample matrix may be affecting the digestion and/or analysis procedures for mercury. An additional 13 percent of the data were flagged as "J", indicating that the results may not be accurate or precise. These data were flagged due to poor agreement between laboratory duplicate analyses, which may be caused by non-homogeneous samples. The remaining 3 percent of the mercury data were flagged "J-", indicating that the reported values may exhibit low bias. These data were flagged because analyses were conducted outside of holding time and/or low recoveries of the matrix spikes. Holding times were exceeded because archive samples were analyzed to help delineate the mercury observed in previous results. This resulted in mercury analysis being conducted approximately 1.5 to 2 months after collection.

Based on data validation, 39 percent of all the TOC data were flagged. The majority of the qualified data was due to analysis conducted out side of hold time. Due to limited volume of samples collected at two core stations, TOC analysis was requested after the completion of radioisotope analyses. As a result, analysis of TOC was conducted out of hold time, therefore twenty percent of the data was flagged "J-". The remaining 19 percent was flagged as "J" due to low precision observed in the replicate analyses of individual samples. The low precision was most likely due to low aliquot weights and/or non-homogeneity for individual samples. The percentage of qualifiers applied due to low precision is similar to that observed in other Alcoa studies (Alcoa 1997).

6.0 DATA DISCUSSION AND CONCLUSIONS

Section 6.0 discusses the data presented in Section 5.0. First, the mercury and radionuclide data are discussed in Section 6.1. Next, the bioturbation rates and depths are discussed in Section 6.2. The model simulations and mercury recovery rates are discussed in Section 6.3. Finally, the overall study conclusions are presented in Section 6.4.

6.1 MERCURY AND RADIONUCLIDE DISTRIBUTIONS AND SEDIMENT ACCUMULATION RATES

Mercury distributions are given in Figures 5-23 to 5-37, along with those of the bomb fallout nuclide ^{137}Cs. All mercury profiles from near-shore sites near the ALCOA plant reveal maxima in mercury concentrations at depths of 5 to 60 cm in the sediments. In general, this layer of maximum mercury concentrations is seen deeper and deeper in the sediments, the closer the core is located towards the shore line. Based on the depth of the mercury layer, five different provinces can be distinguished. 1) Cox Bay, where this layer is situated between 50 and 60 cm depth; 2) CAPA Shoreline, where profiles are more erratic, and peaks show up at 5 to 55 cm depths; 3) Region North of Dredge Island, where this layer is found at 25-35 cm depth; 4) region west of Dredge Island, where this layer is seen more shallow, at 5-11 cm depth; and 5) less impacted stations in different parts of the open bay, where broader peaks with lower mercury concentrations are seen in layers 10-30 cm deep. Maximum documented mercury discharge by the chlor-alkali plant occurred between 1966-1969 (Alcoa, 1995; Palmer-Locarnini and Presley, 1996). If we assume that the mercury peak seen in all the sediments was deposited in 1968, an average sedimentation rate of 0.3 to 2 cm per year, depending on location, can be estimated from these cores. These sedimentation rate estimates can be compared with those determined by the bomb fallout nuclides ^{137}Cs and ^{239,240}Pu, and by unsupported, or excess ^{210}Pb, as described below.

^{137}Cs peaks are usually located below the mercury peaks, as expected from the peak deposition in 1963 (e.g., Santschi et al., 1980, 1989). However, ^{137}Cs peaks are generally not as narrow as those of mercury, indicating greater mobility of this nuclide (e.g., Santschi et al., 1983). This is also evident from a comparison to the more particle-reactive ^{239,240}Pu given in Figures 5-39 and 5-40, which suggests that Pu peaks are more narrow. Furthermore, Pu/Cs ratios in the peak region are enhanced over the bomb fallout ratio of 0.026 in core 134, indicating a lower accumulation rate of Cs than Pu during the 1960's, likely caused by the lower particle-reactivity of Cs. Despite the greater mobility of Cs in seawater environments, most of the ^{137}Cs profiles depict a clear peak, and are thus quite suitable for dating purposes.

An exception is the CAPA core 926, where the mercury and ^{137}Cs peaks are 5-10cm below the surface (Figure 5-32), thus suggesting sedimentation rates of only a few mm/yr, while the $^{210}Pb_{xs}$ derived sedimentation rate (Figure C-115) would, albeit with a low precision, predict their positions deeper in the core. However, due to the low porosity and therefore low and thus imprecise radionuclide activities in this core, no firm conclusions can be drawn from the data for the 926 site or the other CAPA shoreline sediments.

Average sedimentation rates calculated from the known deposition history of Pu and Cs nuclides, shown in Figures 5-39 and 5-40, generally confirm the sedimentation rates calculated from mercury peaks. Apparent sedimentation rates, S, estimated from the peak activity of ^{137}Cs, assuming it was deposited in 1963, the year of the peak bomb fallout, are summarized in Table 5-4. An overview of ^{137}Cs-derived sedimentation rates and mercury peak depths is also given in Figures 6-1 and 6-2. Usually, sedimentation rate estimates calculated from ^{137}Cs peak depths agree with those determined from mercury peak depths and $^{210}Pb_{xs}$ profiles (see later section). Take, for example, Core 201, shown in Figure 5-26, where the value of S is about 1.05 cm/yr when calculated from Cs and Pu, 1.2 cm/yr calculated from mercury, and 1.2±0.5 cm/yr calculated from $^{210}Pb_{xs}$ (see later section). In core 128, the peak concentrations of ^{137}Cs and mercury both occurred at 27.5 (±2.5) cm, giving an estimated value S of 0.9-1.0 cm/yr (Figure 5-23). For calculations of sedimentation rates, it was assumed that the profile had undergone little disturbance since initial deposition, and that compaction was negligible. Even though this was obviously not entirely true since the actual fallout peaks should be slim, this assumption is later verified in the numerical modeling section, and small corrections are applied where needed.

While there should be no ^{137}Cs activity in layers with an inferred date earlier than 1953, when bomb testing began, the greater mobility of ^{137}Cs might have caused tailing in some of the core profiles, which was, however, taken into account in the numerical modeling section.

In all of the cores, ^{210}Pb and ^{226}Ra activities were determined by gamma counting, and in a few of the cores, ^{210}Pb activity concentration was measured by the generally more precise alpha counting technique, after total dissolution of the sediments and chemical separation of the daughter nuclide ^{210}Po. $^{210}Pb_{xs}$ profiles are shown in Figures C-104 to C-120, and show exponentially decreasing activities with depth. This allows us to calculate sedimentation and sediment accumulation rates according to the CIC model as discussed above. Results of these sedimentation rate calculations are given in Table 5-4.

As pointed out before, $^{210}Pb_{xs}$ derived average sedimentation rates from sites with significant $^{210}Pb_{xs}$ activities agree, within the errors, with those determined by the Cs and mercury time marker methods. There was only one exception to this, core 928, where $^{210}Pb_{xs}$ underestimated sedimentation rates from the other methods by a factor of 3, likely due to low activity concentrations and high measurement errors of that method at this site.

In some cases, profiles can also be interpreted assuming that sedimentation rates had varied over time. One example is from Cox Bay where it appears that sedimentation rates have increased in recent times, i.e., they are accumulating more rapidly now near the sediment surface than in the more distant past at depth, as is evident from $^{210}Pb_{xs}$ profiles depicted in Figures C-104 to C-120.

Another example is from the area north and west of Dredge Island. Figures C-105 and C-107 show $^{210}Pb_{xs}$ data from cores 134 and 201, determined by alpha counting. This data could possibly be used to decide if sedimentation had been continuous rather than episodical. There is no indication that the recent sedimentation rate is lower than the average rate.

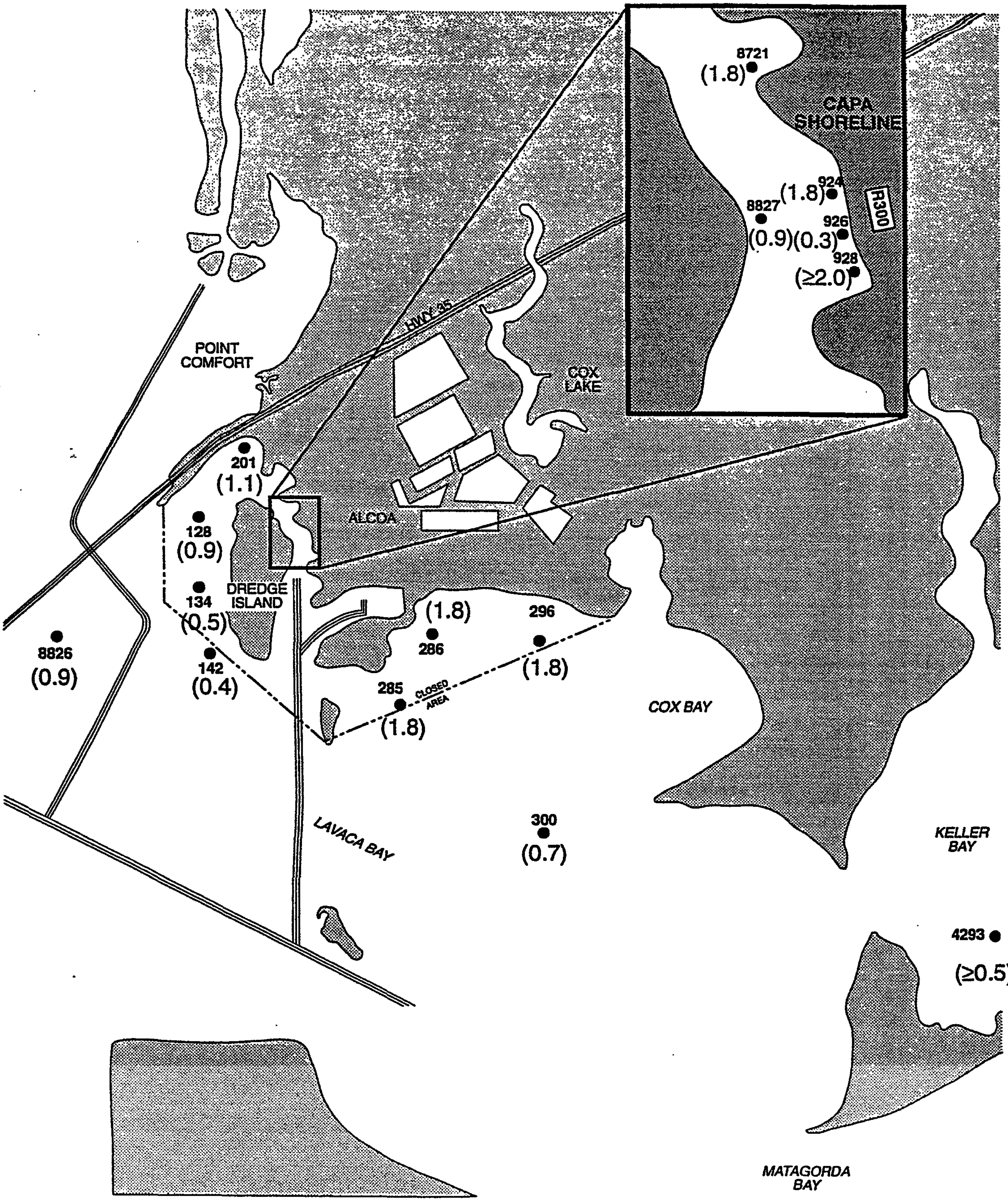

Alcoa Dredge Island/54-2824-55(01) 1/98

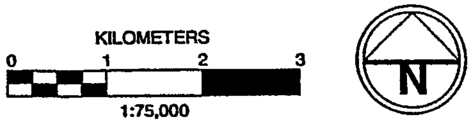

● Samples collected for total mercury, TOC, x-radiography and radioisotope analyses

() Sedimentation rate, S (cm/yr) from Cs-137 peak

Figure 6-1

Radiochemistry Study - Sedimentation Rates from Cs Peak

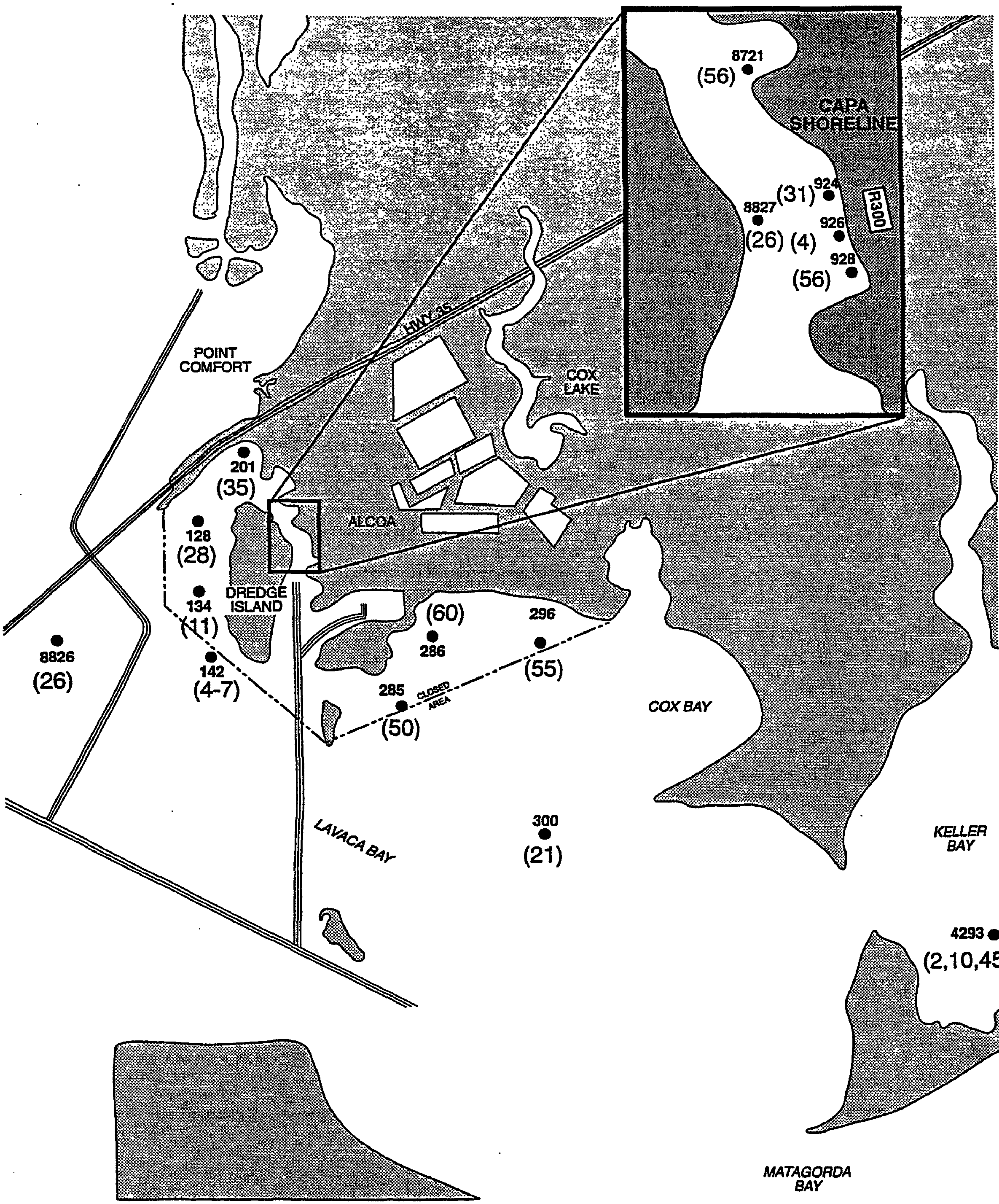

Alcoa Dredge Island/54-2824-55(01) 1/98

KILOMETERS 0 1 2 3

1:75,000

N

● Samples collected for total mercury, TOC, x-radiography and radioisotope analyses

() Mercury Peak Depth (cm)

Figure 6-2

Radiochemistry Study Mercury Peak Depths

Core 134 data from west of Dredge Island are shown in Figure C-105. With the exception of the region between 20 and 24 cm depth, the observed variability of $^{210}Pb_{xs}$ activity appears to be random, suggesting an even sedimentation rate after 1963. The different peak depths of mercury at 11 cm (assigned to 1968) and Pu at 19 cm (assigned to 1963) would be consistent with higher sediment accumulation rates in the 1960's than expected from the average rate of 0.5 cm/yr. The fact that the ^{137}Cs peak at 16 cm appears above the Pu peak at 19 cm (Figure 5-24 and 5-39) might suggest a somewhat higher postdepositional mobility of Cs, as suggested previously. The difference is, however, not significant at the three sigma error level. The near-constant porosity between 19 and 5 cm depth in this core (Figure C-72) would, however, suggest a sedimentation history with little changes in grain size from the 1960's onwards..

In conclusion, ^{210}Pb data from Cox Bay cores are consistent with higher sedimentation rates during the last 1-2 decades than before that time. ^{210}Pb cores from the areas north and west of Dredge Island agree with a lower but more even sedimentation regime in the past several decades.

6.2 PARTICLE REWORKING (BIOTURBATION) RATES AND DEPTHS

The coupling of sedimentation with bioturbation has the consequence that the peak position of a time dependent tracer in the sediments is displaced downwards (e.g., Santschi et al., 1980). Therefore, the dating of the sediments using the peak position of the tracer generally needs to consider the effects of particle reworking and correct for this by modeling the profiles, using measured parameters. At a particle reworking rate of 20 $cm^2\ yr^{-1}$ (near average value observed in Lavaca Bay), a maximum surface mixing depth of 10cm, and an average sediment accumulation rate of 0.5 g $cm^{-2}\ yr^{-1}$, the peak position of the tracer profile would be displaced downwards by about 7 cm (Figure 6-3).

Particle reworking rates and depths, calculated from ^{7}Be penetration into surface sediments, are shown in Figures C-88 to C-102, summarized in Figures 6-4 and 6-5, and tabulated in Table 5-4. In general, particle mixing rates and depths were higher in summer than winter or spring, and were often higher in faster accumulating near-shore sediments, but also in open bay sediments. More slowly accumulating near-shore sediments usually had also a lower particle mixing rate and shallower mixing depth.

Particle mixing rates and depths, like sedimentation rates, are more variable in the CAPA shore line cores than at any of the other sites. Mixing depths range from 4-10 cm. With the exception of core 926, which only showed minimal sediment accumulation of a few mm/yr, all other CAPA cores accumulated sediments at about 1-2 cm/yr, with generally moderate ^{7}Be mixing depths of 4-5 cm, except for core 928, where ^{7}Be penetrated down to 10 cm.

Figure 6-3. Effects of bioturbation on tracer profile in sediments.

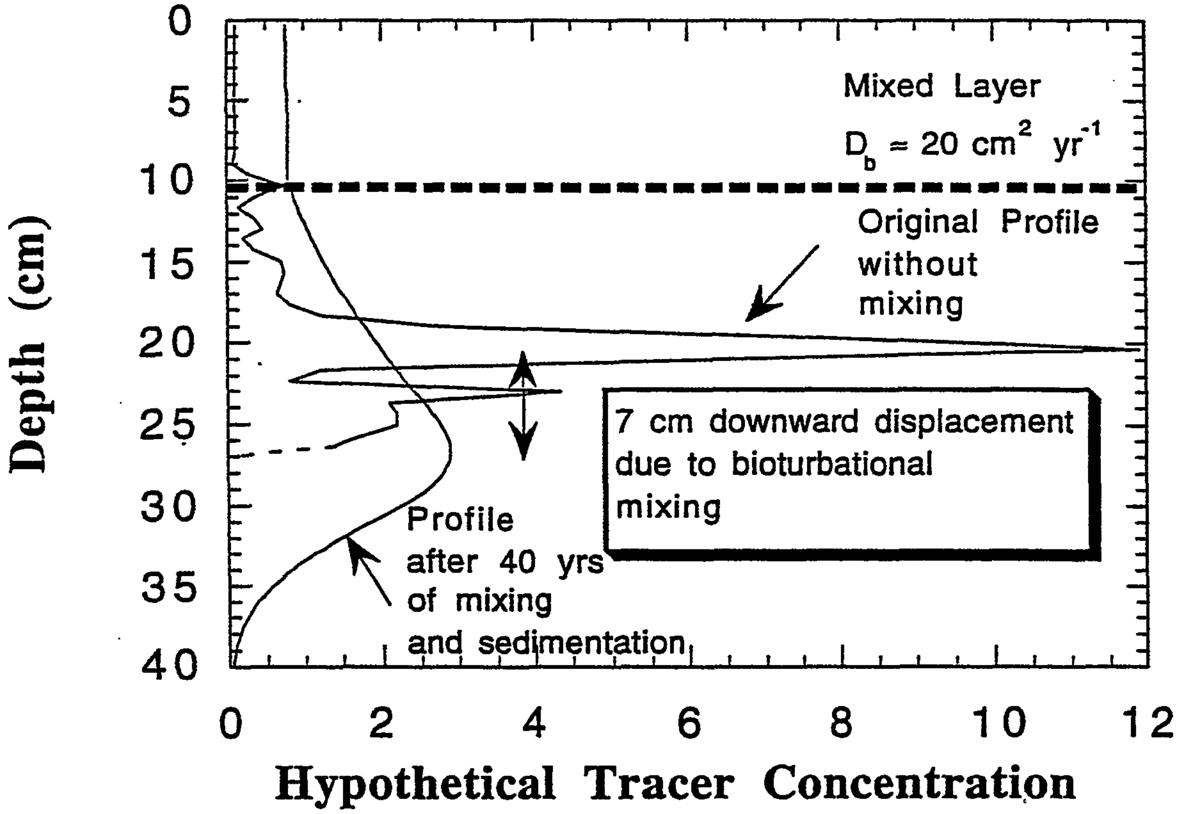

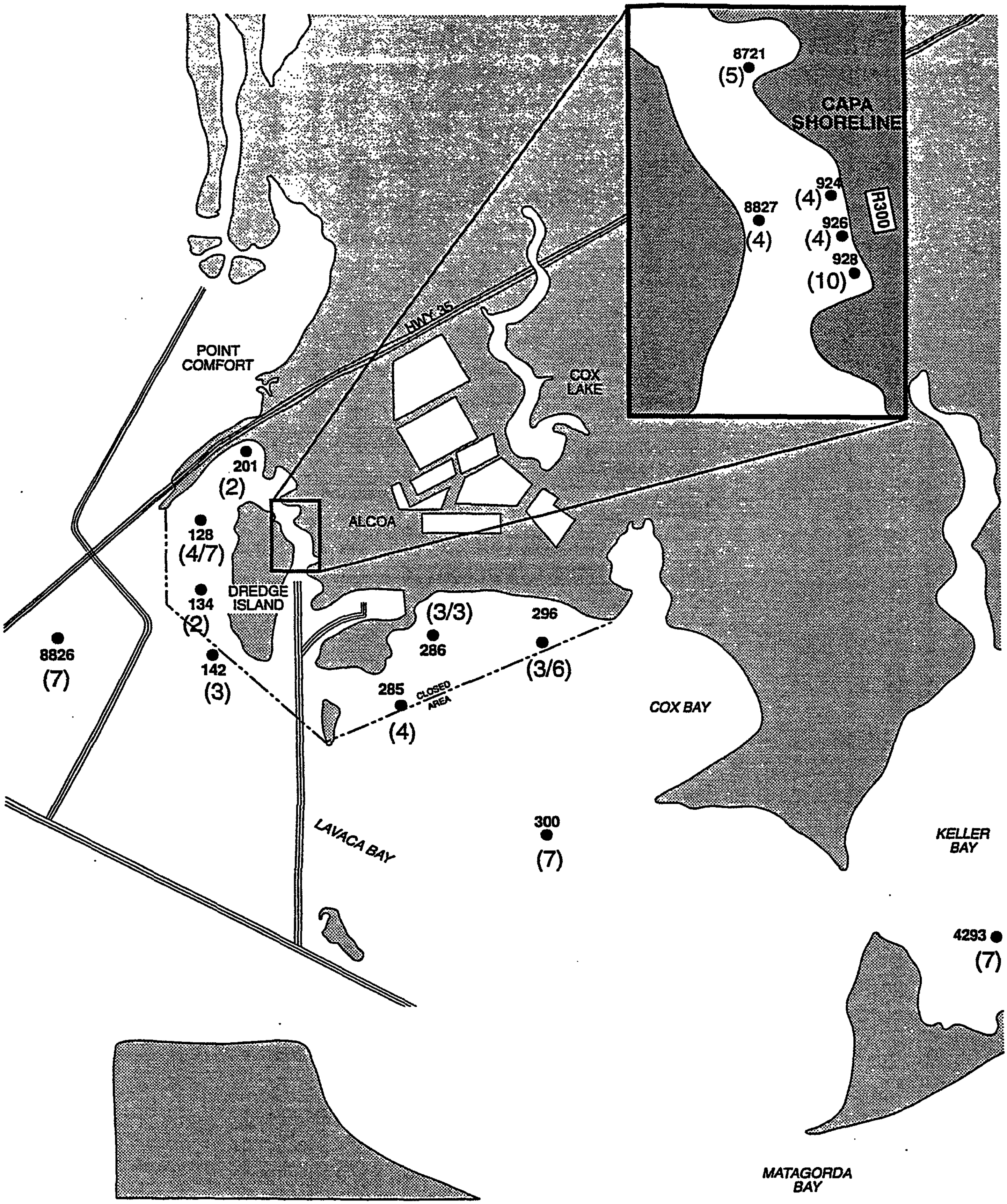

Alcoa Dredge Island/54-2824-55(01) 1/98

KILOMETERS
0 1 2 3
1:75,000

N

● Samples collected for total mercury, TOC, x-radiography and radioisotope analyses

() Mixed Layer Depth, zm (cm)

Figure 6-4

Radiochemistry Study - Mixed Layer Depths

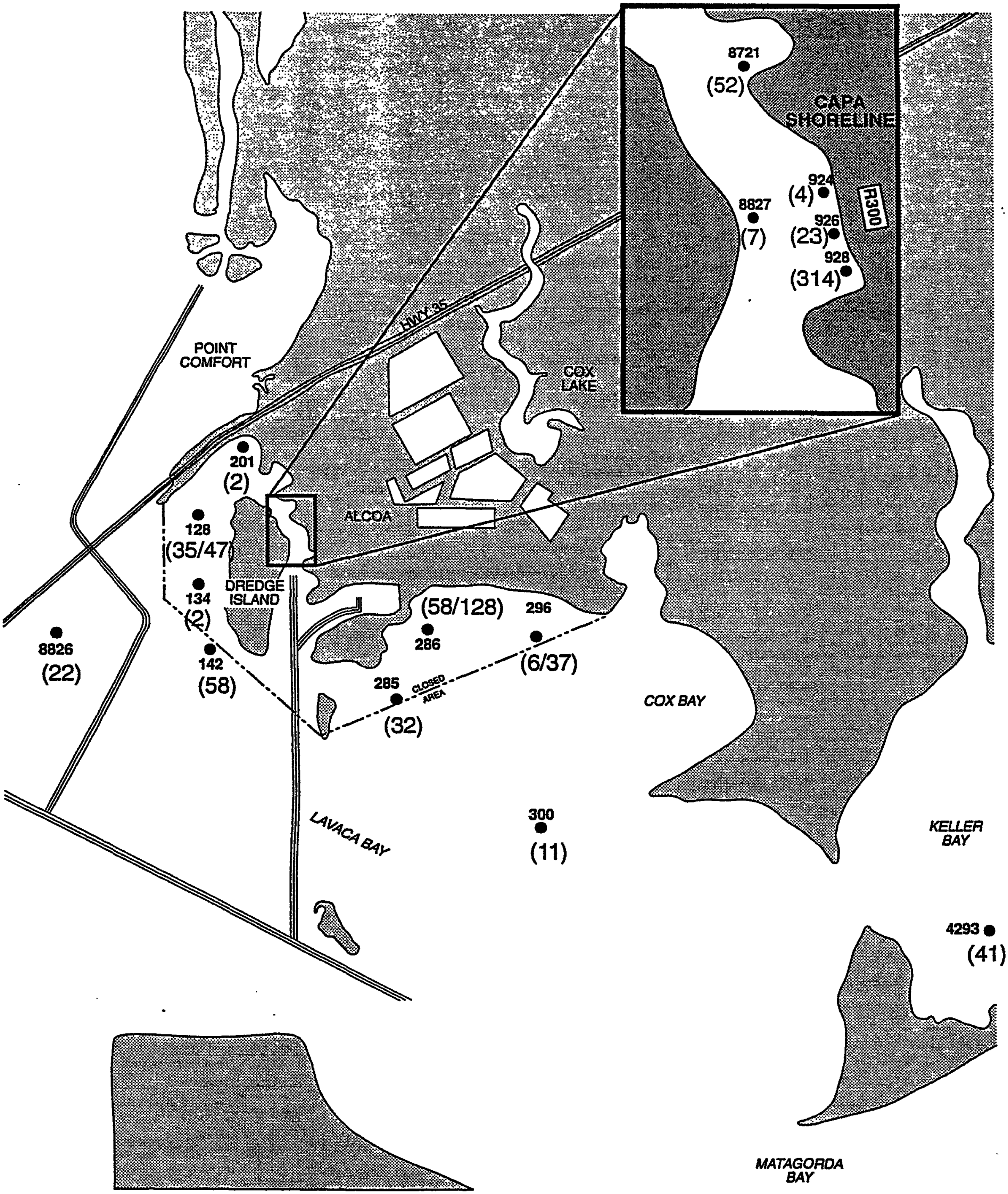

Alcoa Dredge Island/54-2824-55(01) 1/98

KILOMETERS
0 1 2 3
1:75,000

N

● Samples collected for total mercury, TOC, x-radiography and radioisotope analyses

() Particle Reworking Rate, Db (cm^2/yr))

Figure 6-5

Radiochemistry Study - Particle Reworking Rates

6.3 MODEL SIMULATIONS AND MERCURY RECOVERY RATES

6.3.1 Model Simulations

Model simulations were carried out to answer two questions: 1) can mercury at the sediment-water interface be supported by mixing from buried mercury, and 2) how fast would surface sediments recover, i.e., how fast mercury concentrations in surface sediments would decrease after all external sources stop, or be significantly lowered.

Model simulations of radionuclides and mercury profiles were run using a numerical mixing model with constant values of S_a, and time variable mercury and bomb fallout radionuclide fluxes to the sediment-water interface, constant sediment particle reworking rates and depths, particle-water partition coefficients, and porosity. The version used is written in Matlab, and is based on models developed by Crusius (1992) and Santschi et al. (1980). The general approach consisted of first simulating ^{137}Cs (and Pu, when available) profiles, using ^{7}Be based sediment mixing parameters, an average porosity, and a bomb fallout input function (Figure 6-6), and letting the sedimentation rates (S, S_a) vary until simulated model profiles approached measured concentrations profiles (i.e., "eye-ball fit"). More rigorous procedures of least square fits to measured data were not deemed to improve the overall confidence limits due to the data limitations of assumptions involved (e.g., constancy of mixing and sedimentation parameters in time and space). Next, using radionuclide derived sedimentation and mixing parameters and a mercury input function with high fluxes only between 1966 and 1969 were simulated.

Mercury peaks are often very narrow (e.g., in cores 128, 134, 142, 201), suggesting very limited particle reworking during and after emplacement. This puts an important constraint (i.e., upper limit) on the particle mixing rate in any model simulation. It would thus be attractive to simply fit mercury profiles with the assumption that mercury inputs occurred only in 1966-1969, and assume low mixing rates and depths. However, the approach we have chosen in this report verifies the assumption that the peak was caused by historical inputs in the 1960's, and thus, is more rigorous but also more conservative. Furthermore, it constrains sedimentation rates in the period between 1963 (bomb fallout peak) and 1966-1969 (mercury peak). While our approach of basing initial sedimentation rate estimates on the depth of the bomb fallout tracer peaks, and mixing rate and depth estimates on ^{7}Be penetration extent and depths, and agreement between model simulations and actual data is often poorer, we prefer our approach since it is more conservative. In general, the model overestimates the width of the mercury peak. As a result, it is likely that the model overestimates the surface sediment mercury concentrations.

Our approach is demonstrated for cores 128 and 134 in Figures C-152 to C-158. First, the ^{137}Cs (or $^{239,240}Pu$ in case of core 134), profile was simulated using the ^{7}Be derived mixing rates (D_b) and depths (z_m). Particle-water partition coefficient, K_d, and sediment accumulation rate, S_a, values were varied until a satisfactory fit was obtained.

Figure 6-6. Model input function in relative units.

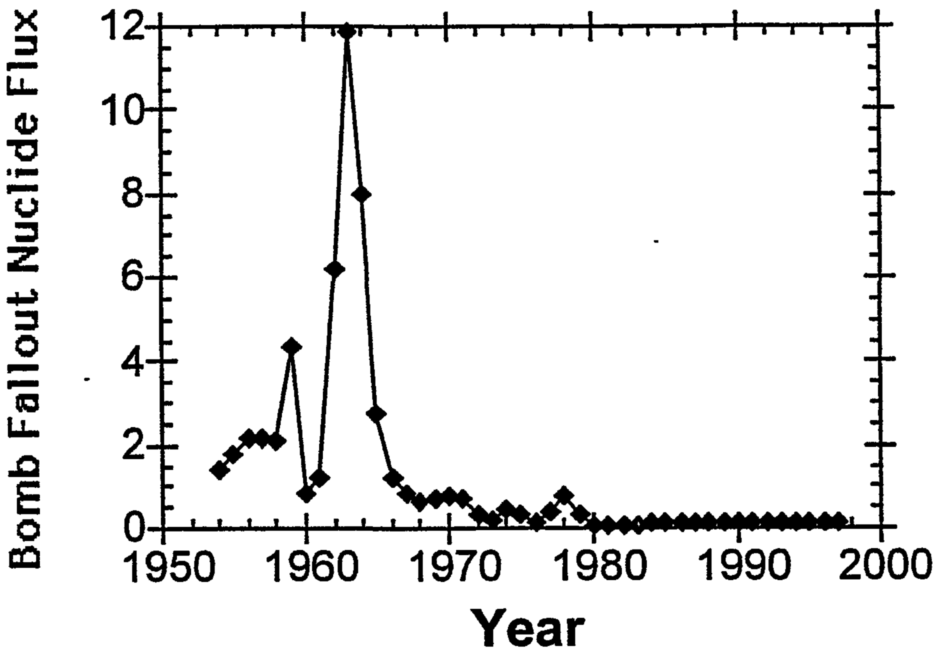

Model outputs are insensitive to assumed Kd values when above 10^4 cm^3 g^{-1}. High values of 1×10^6 were assumed for mercury (and Pu when available), and lower values of 10^2-10^3 cm^3 g^{-1} for the more mobile ^{137}Cs.

This procedure resulted in further refinements of our initial sediment accumulation rate (S_a) estimates given in section 6.1. In general, they came close to the initial estimates, given in section 6.1 Differences between the two S_a estimates were generally within the errors of the estimates. This is due to the relatively high sedimentation rate, moderate particle mixing rates and shallow mixing (mixed layer) depths. Exceptions are sites with low S and S_a values (i.e., 134, 142, 300, 4293, 926). However, at these sites, the overall error in sedimentation rate estimates is higher and agreement between the various estimates derived from ^{137}Cs, $^{239,240}Pu$ and mercury poorer than average. When sites were deemed more important (i.e., 134 and 142), assumed mixing and sedimentation parameters were varied further (i.e., higher values were assumed than were observed) to gain more confidence into the sensitivity of mercury profile simulations on assumed model parameter values. This approach is demonstrated for core 134, where conditions were also run which were not observed, such as deeper mixing rates.

Even though it might look like the surface mercury levels in core 128 predicted by the model (Figures C-152 to C-154) are sufficiently close to the observed levels, and therefore, that historical mercury discharges could account for about 10% of surface mercury at this location, the model overestimates the width of the mercury peak. As a result, it is likely that the model overestimates the surface sediment mercury concentrations. Therefore, surface sediment concentrations of mercury at this location cannot be due to mixing of mercury from the peak depth. The model simulations for core 134 shown in Figures C-155 and C-156 (for ^{137}Cs) and Figure C-157 (for $^{239,240}Pu$) and Figure C-158 (for mercury) do suggest that surface sediment concentrations of mercury could be affected by particle reworking at slightly higher than observed mixed layer depths (i.e., 3-4 cm rather than 2 cm). However, for core 134, as for core 128, the model simulation using the Pu peak (which is slightly deeper and narrower than the ^{137}Cs peak) as a reference date of 1963, overestimates not only the depth of the peak, but also the width of the mercury peak (Figure C-158), suggesting that mixing rates and depths assumed by our model approach are too high, rather than too low. Indeed, when an attempt is made to simulate the mercury peak separately, shown in Figure C-159, lower mixing rates and depths have to be assumed for the late 1960's than were measured in 1997. This again suggests that surface mercury concentrations in this core are likely not a remnant of historical mercury discharges.

While the model runs can reproduce the broad features of radionuclide and mercury profiles, they often do not reproduce elevated surface concentrations of ^{137}Cs (e.g., Figures C-153 and C-156). A possible explanation is the fine-grained nature of the upper few cm of surface sediment in many of the cores, as is evident from the detailed porosity profiles (e.g., Figures C-71, C-72, C-74, C-77, and C-85), and the correlation between porosity and % clay (Figure C-87). As was shown earlier (Figure C-125 and C-126), ^{137}Cs concentrations at the sediment-water interface significantly correlate with porosity or % organic carbon, as proxies of % clay. Indeed, a separate grab sample taken from the ship channel showed an elevated ^{137}Cs concentration of about 300 dpm/kg (Table C-3). This explanation could also apply to mercury and could possibly account for slightly elevated concentrations of mercury over model predictions at some of the sites.

The next example is the ^{137}Cs profile from core 142 from west Dredge Island (Figure C-160). The data for this core are anomalous. The model is unable to describe the mercury data despite one of the better model-data comparisons for ^{137}Cs (Figure C-160). We can only speculate about possible explanations. Mercury in that core showed a maximum at 3.5 cm depth, which might be interpreted as a more recent mercury discharge event (i.e., in the early 1980's) than the main event around 1968. Alternatively, sedimentation rates were not constant, i.e., were higher in the 1960's as a result of dredging activities in the vicinity of the facility, thus causing a wider spread between the mercury peak (1968) and Cs peak (1963). This latter explanation is more likely. In support of the latter interpretation, model simulations of mercury input into sediments, with sedimentation and mixing parameters in agreement with radionuclide data, indicate that the mercury peak should have occurred at 9 cm, rather than at 5 cm (Figure C-161), assuming sedimentation rates were constant in time.

Model simulations are generally suggesting that mercury at the sediment-water interface cannot be a remnant of historical mercury discharges in 1960's, as is, for example, evident from Figures C-162 to C-163 for core 201 from the area north of Dredge Island and Figures C-164 and C-165 for core 296 from Cox Bay. These conclusions about mercury sources hold up despite model simulations which do not reproduce well the ^{137}Cs and mercury for both of these cores. Also, for cores 201 (Figure C-163), 296 (Figure C-165) and 300 (Figure C-167), the model simulations predict a broader peak shape than what is observed. If the model simulations were to fit the sharpness of the mercury peak in these cores, for example, considerably lower mixing rates and depths would have to be assumed, leading to even lower predicted mercury surface concentrations by the model. Only when mixed layer depths are assumed which are considerably deeper than were observed, or lower sedimentation rates than would be consistent with the radionuclide data, could particle reworking account for some significant fraction of the measured surface mercury concentration (Table 6-1). Therefore, it is unlikely that surface mercury in these locations are a remnant of historical discharges. The only exception to this general conclusion is core 926 at CAPA (Figure 5-32, not modeled). However, it holds for all other CAPA cores. As will be shown in section 6.3.2, even in sediments from stations with mercury peaks closer to the sediment surface, mercury concentrations in surface sediments are predicted to recover at rates which are in the same range as those at the other sites with deeper laying mercury peaks.

6.3.2 Mercury Recovery Half Times

In order to obtain a preliminary estimate of mercury recovery half time, the model was run from 1997 onwards into the future, i.e., with time 0 as 1997. The recovery half time is the time required to reduce the concentration of mercury at the surface by one half the initial concentration. A listing of all model parameters, and outputs are given in Tables 6-1, 6-2 and 6-3. Results from these calculations (Figure C-168 to C-172) indicate that significant recovery would occur on a 1-9 year

Table 6-1. Comparison between measured and predicted mercury concentrations at the sediment surface {[Hg](o)}, from model simulations with zero mercury input after 1969.

Core	Measured [Hg](o) at sediment surface (μg/g)	Predicted [Hg](o) (μg/g) from model with ^{7}Be & $^{137}Cs(Pu)$-based parameters	% {Predicted[Hg](o)}/{Measured [Hg(o)]}
128	0.30	0.02	6.7
201	0.37	$1x10^{-6}$	$4x10^{-4}$
300	0.24	0.028	1.2
134	0.35	0.05 or 0.28	14 or 79 (at z_m = 2 or 3 cm)
142	0.50	0.06 or 0.24	12 or 50 (at z_m=2cm, D_b=15 $cm^2\ yr^{-1}$; or z_m=4cm, D_b=30$cm^2\ yr^{-1}$)
296	0.24	(1 or 3)$x10^{-4}$	(0.4 or 1.2)$x10^{-3}$ (at S_a=1.13 or 1.0 g $cm^{-2}\ yr^{-1}$)
300	0.24	0.03	12.5

Table 6-2. List of Parameters used.

Symbol	Parameter	Units	Typical value
S	Sedimentation rate	cm yr^{-1}	1
S_a	Sediment Accumulation rate	g $cm^{-2}\ yr^{-1}$	0.5
$D_b(1)$	Benthic mixing rate in surface mixed layer	$cm^2\ yr^{-1}$	3
$D_b(2)$	Benthic mixing rate in subsurface mixed layer	$cm^2\ yr^{-1}$	0
D_m	Molecular diffusion coefficient	$cm^2\ yr^{-1}$	100
R_1	Benthic mixing rate in surface mixed layer, expressed as sediment exchange rate	g $cm^{-2}\ yr^{-1}$	30
R_2	Benthic mixing rate in subsurface mixed layer, expressed as sediment exchange rate	g $cm^{-2}\ yr^{-1}$	0
z_1	Thickness of surface mixed layer	cm	3
Δz	Box thickness	cm	0.1
Ø	Porosity	-	0.6
Δt	Years for input function	yr	43

Table 6-3. Listing of model runs for mercury.

Run #	Core #	Nucl./ Element	z_m (cm)	S_a ($g\ cm^{-2}\ yr^{-1}$)	D_{b1} ($cm^2\ yr^{-1}$)	R_1 ($g\ cm^{-2}\ yr^{-1}$)	Kd ($cm^3\ g^{-1}$)	Ø
666	128	Hg	4	0.7	35	350	1e6	0.6
667	128	Hg	4	0.85	35	350	1e6	0.6
668	201	Hg	2	1.3	2.3	30	1e6	0.5
669	300	Hg	4	0.34	13	65	1e6	0.8
700	134	Hg	2	0.35	1.8	13	1e6	0.7
701	134	Hg	3	0.35	1.8	13	1e6	0.7
705	296	Hg	5	1.13	33	200	1e6	0.76
706	296	Hg	5	1.0	33	200	1e6	0.76
707	142	Hg	2	0.19	15	100	1e6	0.73
708	142	Hg	4	0.19	30	200	1e6	0.73

time scale. The same recovery times would apply if lower, but non-zero, steady state values would be approached.

A simple algorithm which can predict the recovery half time derived from numerical model calculations is given in eq. 11.

$$T_{½} = (\ln 2) x z_m / S \qquad (11)$$

with $T_{½}$ = recovery half time (yr), z_m = mixed layer depth (cm), and S = sedimentation rate (cm/yr), estimated from the peak position of ^{137}Cs.

The two approaches are compared in Table C-4 and Figure C-173. In this table and figure, recovery half-times determined by numerically modeling mercury distributions into the future are compared to a simple algorithm based on the travel time of mercury through the surface sediment mixed layer (eq.11). The mixed layer depth determines how long surface mercury concentrations are still affected by particle reworking (Reible et al. 1991). Slight differences between the two estimates are likely the result of ignoring 1) particle reworking produced downwards displacement of ^{137}Cs peak positions when estimating sedimentation rates (in cm/yr), 2) the actual kinetics of the mixing process used in the model, and 3) differences in assumed sediment porosities.

Based on these calculations, sediment recovery rates should be relatively rapid, provided that 1) all current external mercury sources were to stop or significantly decrease, and 2) there is no other mercury reservoir in Lavaca Bay sediments which is able to redistribute mercury laterally at a rate equal or slower than the predicted recovery rate for that site. This includes the area of fine-grained sediments in the open less impacted Lavaca Bay, which still show surface mercury concentrations of 0.2 to 0.3 µg/g (e.g., sites 300, 8826 and 4293). If these sites were to recover more slowly than near-shore sites in the closed area (e.g., 134, 201, 128, etc), it would be conceivable that they could affect and prolong recovery at these near-shore sites. The latter assumption therefore needs more scrutiny, and is evaluated below.

Relatively rapid redistribution of mercury contaminated surface sediments is demonstrated by the relatively close positions of the mercury and ^{137}Cs concentration peaks in the sediments from parts of the bay which are further away from the closed area, e.g., cores 8826 (Figure 5-36) and 300 (Figure 5-30). Redistribution of mercury contaminated surface sediments can be viewed mechanistically as a coupled process, where the upper few mm is a mobile phase redistributed over the bay by sedimentation and particle "saltation" over weeks or months time scales. Below this mobile phase is a stationary phase (i.e., a few months, Figure 6-7) of 1-10cm of surface sediments which is actively mixed on time scales of ^{7}Be decay, i.e., a few months. Mercury concentrations in this mixed layer would be homogenized over the time and depth scale given by the ^{7}Be data. According to this conceptual model, it would be the area with the slowest recovery rate which would control the overall recovery. While it is true that redistribution could also be important if mercury is being redistributed faster than it is being buried, because that mercury would be gained fast, and lost at its own intrinsic but slower rate, the recovery rate would still be controlled by the sedimentation and mixing rates occurring at that particular site. Even though that site would have gained more at the beginning, longer term loss rates would be controlled by the ratio of sedimentation rate and mixing depth of that site. However, if another site (e.g., open bay area) would recover more slowly than the site with faster recovery rates (e.g., near-shore site), the latter site would always have a higher mercury concentration in its mixed layer reservoir than it would have without lateral transport. Therefore, it would be the site with the slowest recovery rate which would control overall mercury recovery.

If we assume that cores 300, 4293 and 8826 are representative for areas of Lavaca Bay covered with fine-grained sediments and which also happen to show similar and elevated mercury concentrations at the sediment surface, and that lateral movement of this mobile phase is fast compared to the decrease of mercury in the mixed layer sediments controlled by vertical particle mixing and sedimentation, one could obtain an estimate of their recovery half-time. The recovery half-time, calculated from eq. 11, as (ln2)7cm/(0.7±0.2 cm/yr), is 7 years for concentrations to decline to ½ of their initial value.

We acknowledge that there is some uncertainty in this value given the limited number of cores. However, because of the fact that only the ratio of mixed layer depth to sedimentation rate enters into this calculation, we feel that this recovery half-time of 7 years is a robust estimate.

Figure 6-7. Lateral redistribution of mercury contaminated sediments.

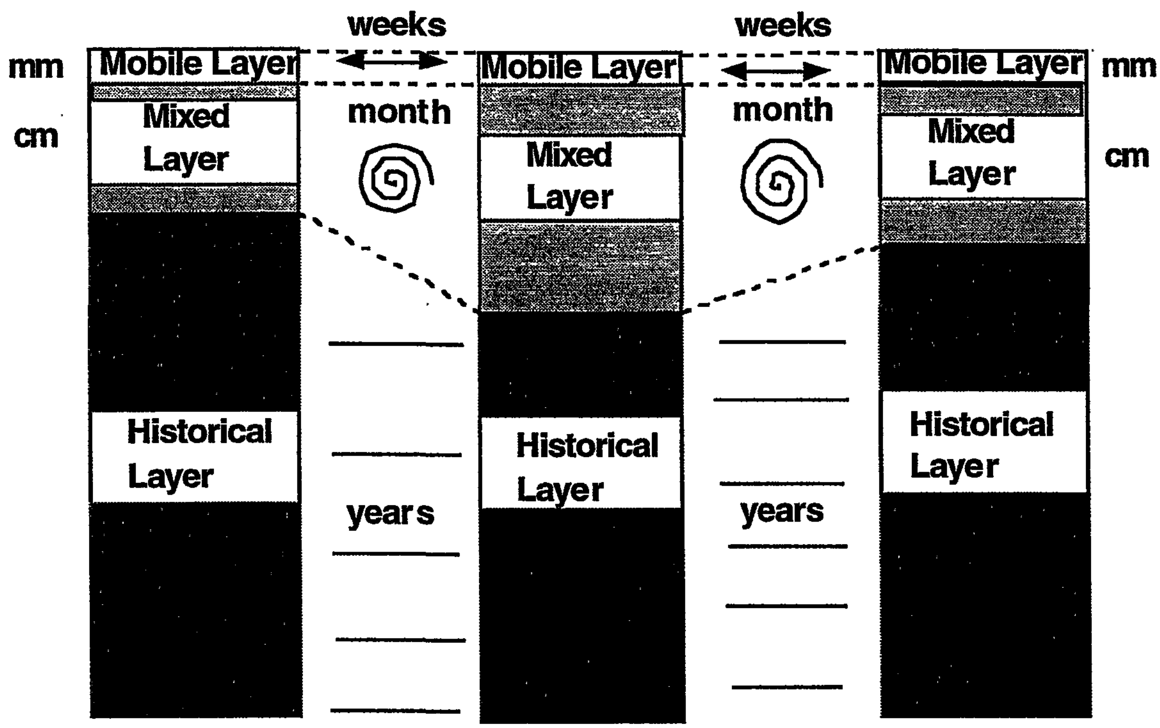

SLOWEST RESERVOIR IS THE ONE WITH THE DEEPEST MIXED LAYER AND LOWEST SEDIMENTATION RATE. IT DETERMINES RECOVERY HALF TIME OF THE TOTAL SYSTEM.

6.4 OVERALL STUDY CONCLUSIONS

Based on the results presented in Section 5.0, and the discussion presented above, the following five conclusions may be made from the Radiochemistry Study:

1) Based upon the radiochemistry data (e.g., ^{7}Be, $^{239,240}Pu$, ^{137}Cs, and ^{210}Pb), grain size data, and x-radiography support the conclusion that historical mercury in the sediments of Lavaca Bay and Cox Bay is being buried at average sedimentation rates which vary between 0.4 - >2.0 cm/ year, depending upon the location. These rates are consistent with sedimentation rates estimated from mercury peaks using the assumption that the maximum deposition occurred between 1966 and 1969.
2) The mixed layer depths in the impacted areas of Lavaca Bay are, in general, very shallow using evidence from the sharpness of the mercury peak, the radiography data, and the ^{7}Be data.
3) From the data presented in 1 and 2 above, cores from Cox Bay, and north of Dredge Island show that the mercury at the sediment surface is not a remnant of historical discharges (1966-1969), which are buried deep below.
4) Enhanced sedimentation rates are likely due to anthropogenic activities (i.e. dredge spoil placement, etc.) in Cox Bay and north of Dredge Island and changes in hydrodynamics due to the construction of the ship channel and Dredge Island.
5) Recovery half-time is predicted of the order of 1-9 years (depending upon location) once all external sources are eliminated.

7.0 REFERENCES

Alcoa, 1995. Preliminary Site Characterization Report for the Alcoa (Point Comfort)/Lavaca Bay Superfund Site. July 1995.

Alcoa, 1996. RI WORK PLAN for the Alcoa (Point Comfort)/Lavaca Bay Superfund Site, Volume B2c: Mercury Reconnaissance Study. Draft Data Report. November 1996.

Alcoa, 1997. RI WORK PLAN (Point Comfort)/ Lavaca Bay Superfund Site, Volume B3: Sediment Transport Study Phase 1A Data Report. January 1997.

Allison, M.A., C.A. Nittrouer, G.C. Kineke. 1995. Seasonal sediment storage on mudflats adjacent to the Amazon River. Marine Geology, 125, 303-328.

Appleby, P.G. and F. Oldfield (1978) The calculation of lead-210 dates assuming a constant rate of supply of unsupported ^{210}Pb to the sediment. Catena, 5, 1-8.

Armstrong, N.E. 1982. Responses of Texas estuaries to freshwater inflows. In: V.S. Kennedy, ed., Estuarine Comparisons. Academic Press, London, pp. 103-120.

Baskaran, M., Asbill, S., Santschi, P.H., Davis, T., Brooks, J., Champ, M., Makeyev, V., and Khlebovich, V. 1995. Distribution of 239, 240Pu and 238Pu Concentrations in Sediments from the Ob and Yenisey Rivers and the Kara Sea, Applied Radiation and Isotopes, 46/11, 1109-1119.

Baskaran, M., C.H. Coleman, and P.H. Santschi. 1993a. Atmospheric depositional fluxes of ^{7}Be and ^{210}Pb at Galveston and College Station, Texas, J. Geophys. Res., 98 (D11), 20,555-20,571.

Baskaran, M. and P.H. Santschi. 1993b. The role of particles and colloids in the transport of radionuclides in coastal environments of Texas. Mar. Chem., 43, 95-114.

Crusius, J.F. 1992. Evaluating the mobility of ^{137}Cs, ^{239,240}Pu, and ^{210}Pb from their distributions in laminated sediments. Ph.D. Dissertation, Columbia University, 261 p.

Denham, C.R. 1996. Zydeco Report to M.B. ten Brink, USGS-WHOI.

Folk, R.L. 1968. Petrology of sedimentary rocks. Hemphill Publishers, Austin, Texas, 170p.

Friedman, G.M., J.E. Sanders, and D.C. Kopaska-Merkel. 1992. Principles of sedimentary deposits. McMillan Publishers, New York, NY. 717 p.

Kranck, K. And T. Milligan. 1985. Origin of grain size spectra of suspension deposited sediment. Geo-Marine Letters, 5, 61-66.

Nittrouer, C.A., and R.W. Sternberg. 1981. The formation of sedimentary strata in an allochthonous shelf environment: the Washington continental shelf. Marine Geology, 42, 201-232.

NOAA. 1996. Climatological Data Annual Summary, Texas, 1996, Volume 101, Number 13, ISSN 0364-6041.

Palmer-Locarnini S.J., and Presley, B.B. 1996. Mercury concentrations in benthic organisms from a contaminated estuary. Mar. Environ. Res., 41, 225-239.

Ravichandran, M., Baskaran, M., Santschi, P.H., and Bianchi, T.S. 1995a. Geochronology of sediments of Sabine-Neches Estuary, Texas, Chemical Geology (Isotope Geoscience)., 125, 291- 306.

Ravichandran, M., M. Baskaran, P.H. Santschi, and T.S. Bianchi. 1995b. History of trace metal pollution in Sabine-Neches estuary, Beaumont, Texas. Environ. Sci. & Tech. 29, 1495-1503.

Reible, D.D., K.T. Valsaraj, and L.J. Thibodeaux (1991) Chemodynamic models for transport of contaminants from sediment beds. In: The Handbook of Environmental Chemistry, Reactions and Processes, Vol. 2, part F, O. Hutzinger, ed., Springer Verlag, New York, pp. 185-228.

Robbins, J.A. (1978) Geochemical and geophysical applications of radioactive lead. In: J.O. Nriagu, ed., The Biogeochemistry of Lead in the Environment. Elsevier, Amsterdam, pp. 285-393.

Santschi, P.H., Y.-H. Li, J. Bell, R.M. Trier, and K. Kawtaluk. 1980. Plutonium in the coastal marine environment. Earth Planet. Sci. Lett. 51, 248-265.

Santschi, P.H., Y.-H. Li, J. Bell, D. Adler, M. Amdurer and U.P. Nyffeler, 1983. The relative mobility of natural (Th, Pb, Po) and fallout (Pu, Cs, Am) radionuclides in the coastal marine environment: Results from model ecosystems (MERL) and Narragansett Bay studies. Geochim. Cosmochim. Acta 47, 201-310.

Santschi, P.H., S. Nixon, M. Pilson, and C. Hunt. 1984. Accumulation of sediments, trace metals (Pb, Cu) and hydrocarbons in Narragansett Bay, Rhode Island, Est. Coast. Shelf Sci. 19(4), 427-450.

Santschi, P.H., and Honeyman, B.D. 1989. Radionuclides in aquatic environments. Radiation Physics and Chemistry 34(2), 213-240.

Santschi, P.H., Li, Y.-H., Bell, J.J., Trier, R.M., and Kawtaluk, K. 1980. Pu in coastal marine environments. Earth Planet. Sci. Lett., 51-248-265.

Schuler, Ch., Wieland, E., Santschi, P.H., Strum, M., Lück, A., Farrenkothen, K., Bollhalder, S., Beer, J., Bonani, G., Hofmann, H.J., Suter, M., and Wölfli, W. 1991. A multi-tracer study of radionuclides in Lake Zurich, Switzerland 1. Comparison of atmospheric and sedimentary fluxes of ^{7}Be, ^{10}Be, ^{210}Pb, ^{210}Po and ^{137}Cs, J. Geophys. Res., 96 (C9), 17051-17065.

Wan, G.J., P.H. Santschi, M. Strum, K. Farrenkothen, E. Werth, and Chr. Schuler. 1987. Natural (^{210}Pb, ^{7}Be) and fallout (^{137}Cs, $^{239,240}Pu$, ^{90}Sr) radionuclides as geochemical tracers of sedimentation in Greifensee, Switzerland, Chemical Geology 63, 181-196.

Ward. 1994. Physical Oceanography of Lavaca Bay: Center for Research in Water Resources. The University of Texas at Austin.

APPENDIX A

Detailed Analytical Procedures for Grain Size Measurements

Sand:Silt:Clay Technique

The grain size separation into major components was conducted following the standard combined sieving and pipette procedures outlined in Folk (1968). Sample intervals were collected from the x-ray trays using a spatula and measuring tape. This sample was placed in deionized water and 1.0 g of sodium metaphosphate was added as a deflocculant. The following analytical steps were followed:

1) Sample beakers were placed in an ultrasonic bath for at least 1 hour to facilitate deflocculation.
2) Samples were poured through a 62.5 micron sieve and funneled into a 1 liter graduated cylinder. Squeeze bottles of deionized water were used wash all finer material through the sieve.
3) Material retained on the sieved was collected, dried at 60C, an weighed to determined weight of sand (coarser than 4 phi) in the sample.
4) Mud (finer than 4 phi) in the graduated cylinder was diluted with deionized water to bring the mixture up to 1 liter.
5) The column was agitated and a 25 ml pipette aliquot (1/40th of the mixture) was collected from the 500 ml mark. This aliquot was dried at 60C to determine weight of silt+clay.
6) The column was put aside and after 1 hr and 57 minutes a second 25ml aliquot (1/39th of the mixture) was collected from the 750 ml mark. This was dried and weighed to determine weight of clay (finer than 8 phi) in the sample.
7) Silt and clay weights are adjusted for the weight of the deflocculant in the sample.

RSA/Sedigraph Analysis

A Rapid Settling Analyzer (RSA) was used to analyze detailed sand granulometry on selected samples. Mud fraction for these samples was analyzed using a Sedigraph model 5100 x-ray particle analyzer. Dual methods are standard because of the relative insensitivity of particle analyzers such as the Coulter Counter and Sedigraph to large (sand) particles. The RSA/Sedigraph is used by many sedimentologists (see results in Allison et al., 1995 for example) because is computer automated. Samples for detailed analysis were separated into sand and mud fractions following the procedures outlined above for sand:silt:clay analysis. Sand was dried and weighed prior to subsampling for RSA. An aliquot of silt+clay+deflocculant was taken by the pipette method described above, and dried and weighed, prior to the Sedigraph analysis of the mud fraction. These two subsamples were used to determine the relative percentage of sand and mud in the sample necessary to reintegrate the data from the two methodologies.

RSA Techniques

The TAMUG RSA unit is a 180-cm-long settling column hooked to an analytical balance that feeds data to a computer for analysis. Software was created inhouse. An aliquot of 1-1.5 g of sand from the sieve was used in the column. The column works on the principle of Stoke's Law of Settling, where, as particle size increases, settling rate increases by the square. Correction for temperature is necessary as it effects the viscosity of the settling fluid. Hence, the time of settling for a particle of known spherical diameter can be predicted. Particles from the sample settle to the bottom of the column and are collected on the pan of the analytical balance where increasing weight with time is monitored by the computer and used to separate fractions into their respective grain size. Size analyses were run to 5 phi (4 phi is the finest sand) to account for non-spherical particles that behave as a silt-sized grain with respect to Stoke's Law. The fraction from 4-5 phi was treated as silt-sized and added to the respective fraction determined from the Sedigraph for the final combination of data. Replicate analyses were run on several samples to determine precision. Replicate values were statistically the same at a 95% confidence interval.

Sedigraph Techniques

The Sedigraph is a product of Micromeritics, Inc. that is used in many industrial purposes (e.g., paints, sewage particulates, machining, etc.) to determine particle sizes in a fluid. The Sedigraph when used for sediment takes a mud-water slurry of concentration of about 10 g/l for analysis. Following collection of the 25 ml aliquot from the graduated cylinder, the remaining solution was allowed to settle for at least 15 days and clear water decanted until a solution of >10 g/l remained. This was homogenized and placed in the Sedigraph. The slurry was diluted to the proper concentration with 0.1% sodium metaphosphate solution. Absorbance % of the x-ray beam is used aas a guide in determining proper concentration. The automated Sedigraph also uses Stoke's Law of settling to determine particle size. Within the analytical chamber the slurry is allowed to settle. The x-ray beam determines the concentration (i.e., % absorbance) relative to a clear water standard (with a 0.1% sodium metaphosphate solution). The beam also moves downward relative to the chamber to speed the calculation of smaller particle sizes. Analyses were run for 47 minutes down to a particle size of 12 phi (0.25 microns). Replicate analyses were run on several samples to determine precision. Replicate values were statistically the same at a 95% confidence interval.

APPENDIX B

Detailed Analytical Procedures for Radiochemistry Program

Overview of Radiochemical Procedures

The radiochemical program includes the following isotopes.

$^{239,240}Pu$:Samples of about 10 g each, by alpha counting, after chemical separation, according to procedures described in Santschi et al. (1980), Santschi et al. (1984), Baskaran et al. (1995) and Ravichandran et al. (1995a).

^{210}Pb: Samples of 1 g each by alpha counting, after complete digestion and chemical separation, according procedures given in Santschi et al. (1980), Santschi et al. (1984), and Ravichandran et al. (1995b). Gamma counted samples will result in another, but often less precise, ^{210}Pb value, to be used for comparison purposes. It is expected that excess-^{210}Pb activity (i.e., [^{210}Pb] - ^{226}Ra]) will be detectable in more than 50% of the sediment samples.

^{226}Ra: Samples of 10 g each by non-destructive gamma counting, according to procedures given in Santschi et al. (1980), Baskaran et al. (1995), and Ravichandran et al. (1995b).

^{234}Th: Samples of 10 g each by non-destructive gamma counting, according to procedures given in Santschi et al. (1980). It is expected that only the top 10 cm of sediments will show measurable excess-^{234}Th activity (i.e., [^{234}Th] - [^{238}U]), but results will be available for all samples, down to about 50 cm.

^{137}Cs: Samples of 10 g each by non-destructive gamma counting, according to procedures given in Wan et al. (1986), and Schuler et al. (1991).

^{7}Be: Samples of 10 g each by non-destructive gamma counting, according to procedures given in Wan et al. (1986), and Schuler et al. (1991).

Porosity is determined from wet and dry weights of the sediment sample, assuming a constant particle density of 2.5 (±0.1) g cm^{-3}.

Details of analytical steps

Dried sediment samples of about 10g size will be used for non-destructive gamma counting in a low-background, high-efficiency high-purity Germanium (HPGe) well detector, followed by wet chemical extraction procedures and alpha counting (or AMS) for individual radionuclides. All 50 samples will thus first be gamma counted and then processed for wet chemical/alpha counting analyses for Pu and Pb isotopes.

The sequence of steps to be followed is as follows:

- gamma counting of samples for 1 day to obtain results for ^{210}Pb (46 keV), ^{234}Th (63 keV), ^{226}Ra (352 keV), ^{7}Be (478 keV), ^{137}Cs (662 keV),
- ^{210}Pb analysis by wet chemistry followed by alpha counting for 1-2 days,
- $^{239,240}Pu$ analysis by wet chemistry (8 days) followed by alpha counting for 1-2 days.

The check list for the Pb and Pu procedures is attached in the appendix. The general procedures which were followed are listed below.

Chemical extraction and separation procedures.

1) ^{210}Pb

1.1) Sample preparation

1. Weigh 1.5g sediment
2. Add spike (^{209}Po or ^{208}Po)
3. Add 10ml conc. HNO_3
4. Add 10ml conc. HF
5. Let solution sit overnight
6. Microwave digestion

1.2) Iron removal

1. Transfer solution to a Teflon beaker
2. Add 5ml conc. Perchloric acid; evaporate
3. Add 5ml conc. HCl; evaporate
4. Add 10ml conc. HCl; evaporate
5. Add 10ml 1M HCl, let dissolve
7. Centrifuge 25min
8. Collect supernatant

1.3) Plating

1. Add 2ml 25% $Na_3C_6H_5O_7$
2. Add 8ml 20% NH_2OH-HCl
3. Raise pH to 2 with conc. NH_4OH, and dilute to 30ml with deionized H_2O
4. Add stirring magnet, cover, heat 15-20min temp between 85-90°C
5. Add Ag square & plate 90min
6. Remove & rinse with deionized H_2O, bag

2) $^{239,240}Pu$

2.1) Leaching of sample

1. Leach 10g of sample with 30ml of 6M HCl
2. Centrifuge HNO_3
3. Repeat above and combine supernate
4. Add ^{242}Pu spike-1ml (0.2842dpm/ml)
5. Dry in hot plate
6. +10ml 8M HNO_3 and centrifuge (1 hr)
7. Dry supernatant
8. 5ml conc. HNO_3, dry
9. 5ml 8M HNO_3 dry (near dry)
10. 8ml 8M HNO_3 and centrifuge. Final supernatant should be < 10ml.

2.2) Column preparation

1. wash w/ 2CV (column volume) deionized water (DIW)
2. Wash w/ 3CV of 6M HCl
3. Wash W/ 3CV of DIW
4. Condition w/ 3CV of 8M HNO_3
5. Repeat step 4 and discard all.

2.3) Elution

1. Load solution
2. Rinse with 1ml 8M HNO_3
3. Repeat step 2
4. Wash w/ 2CV 8M HNO_3
5. Wash w/ 3CV 8M HNO_3
6. Elute w/ 2CV 9M HCl
7. Repeat step 6
8. Keep a beaker below the column and elute w/ 15 ml mix. of 9M HCl+HI
9. Repeat it twice, save the eluate

2.4) Ion Exchange Columns for Pu

1. Dry HCl-HI eluant
2. 5ml conc. HNO_3, dry
3. 6ml 9M HCl + 0.15g $NaNO_2$
4. After fumes cease, centrifuge
5. Wash new column w/ 2CV DIW
6. condition 2CV 9M HCl
7. Repeat
8. Repeat
9. Load samples+ rinse 1ml 9M HCl
10. Wash 2CV 9M HCl

11. Repeat above
12. 45 ml 9M HCl + 1.5ml HI
13. Save eluate

2.5) Electroplating of Pu

1. Dry eluate
2. Add 2ml 5% $NaHSO_4$ +0.5ml $HClO_4$, dry
3. Wash sides w/DIW+1ml conc. HCl; dry
4. 1ml conc. HCl, dry
5. Dissolve in 2-3ml DIW, wait 10min.
6. 4ml 15% Na_2SO_4 in cell+soln. in step 5
7. Plate at 0.5 amp. for 180 m.
8. Add 2ml 4M KOH and continue 2min.
9. Clean cell w/ 1% NH_4OH, rinse w/DIW
10. Dry disc on hot plate, bag

3) Alpha counting procedures

3.1) ^{210}Pb

^{210}Po and ^{239,240}Pu are assayed separately on alpha counters. The Canberra's *Quad Alpha Spectrometer* with ultra-low background surface barrier detectors are used for this purpose. These detectors have an active area of 450 mm^2 and an alpha resolution of 20 keV. The detectors are coupled to a S100 Canberra Multi-Channel Analyzer. The background counts of these detectors are typically about 1-2 counts per day in the regions of interest.

Secular equilibrium between ^{210}Pb and ^{210}Po is assumed to exist before alpha counting for ^{210}Po. A known amount of ^{208}Po spike was added to the sediment samples before digestion. The energies of alpha particles emitted by ^{210}Po is 5.30 MeV and by ^{208}Po is 5.11 MeV (LEDERER and SHIRLEY, 1978). The activity of ^{210}Po (dpm g^{-1}) in the sediment samples was calculated using the formula:

$$^{210}\text{Po Activity (dpm/g)} = \frac{^{210}\text{Po counts (net)}}{^{208}\text{Po counts (net)}} \times \frac{^{208}\text{Po activity added (dpm)}}{\text{Wt. of sample (g)}} \times e^{\lambda t}$$

where, λ = decay constant of ^{210}Po (= 0.693 / 138 days); t = the time between plating and mid-time of counting (in days). The ^{208}Po spike has a relatively short half-life of about 2.8976 years and therefore, it was always decay corrected for the time since it was actually prepared. This was done using the formula:

^{208}Po activity at the time of use (dpm) = ^{208}Po activity when it was prepared (dpm/ml) x vol. of spike (ml) x $e^{-\lambda t}$

where, λ_=_decay constant of Po-208 (=_0.239_y^{-1}); t = time between mid-counting and the time since preparation (in years).

3.2) $^{239,240}Pu$

^{239}Pu and ^{240}Pu are the dominant isotopes from fallout plutonium. ^{239}Pu has a half life of 2.41 x 10^4 years, ^{240}Pu has a half-life of 6.57 x 10^3 years, and the ^{242}Pu isotope, which was used as a yield tracer, has a half-life of 3.76 x 10^5 years. Due to their relatively longer half-lives, decay correction of these isotopes was not needed. The energy levels of alpha particles of ^{242}Pu are 4.90 MeV (74 %) and 4.86 MeV (26 %). The alpha energy levels of ^{239}Pu are 5.16 MeV (73.3 %), 5.15 MeV (15.1 %), and 5.10 MeV (11.5%) and those of ^{240}Pu are 5.16 MeV (75.5 %), 5.12 MeV (24.4 %) and 5.01 MeV (0.091 %). Due to the similar alpha energies of the ^{239}Pu and ^{240}Pu peaks, they are inseparable by an alpha counter. Therefore, the activities of both isotopes are measured together and always written as $^{239,240}Pu$. Since the activities of Pu isotopes are relatively low in the sediments, the background counts in the alpha counter are closely monitored and subtracted from the gross counts. The activity of $^{239,240}Pu$ is calculated as:

$$^{239,240}\text{Pu activity (dpm/kg)} = \frac{^{239,240}\text{Pu counts (net)}}{^{242}\text{Pu counts (net)}} \times \frac{^{242}\text{Pu Activity (dpm)}}{\text{Sample weight (g)}} \times 1000$$

The yield tracer solutions of ^{208}Po, and ^{242}Pu were obtained from the Environmental Measurements Laboratory (courtesy of Dr. Bob Anderson, Lamont Doherty Earth Observatory, NY). They were previously calibrated against standards which are traceable to NBS standards.

The errors associated with the alpha counting method can be calculated as below. If X represents the number of net counts from the isotope of interest, Y represents the number of net counts from the spike isotope, and x and y are the errors of X and Y, respectively, then the propagated error (1 sigma) associated with the counting is:

$$(X / Y) \pm (X/Y) * [(x/X)^2 + (y/Y)^2]^{1/2}$$

where, x is the square root of X and y is the square root of Y.

4) Gamma counting procedures

The list of isotopes to be analyzed is given in Table B-1.

TABLE B-1. LIST OF ISOTOPES

Isotope	Half life	Gamma Energy (keV)
^{210}Pb	22 years	46
^{234}Th	24 days	63
^{226}Ra	1600 years	352
^{228}Ra	5.7 years	338,911
^{7}Be	53 days	478
^{137}Cs	30 years	662

4.1) ^{226}Ra (352 keV) and ^{210}Pb (46 keV)

The ^{226}Ra activities in dry sediment samples are determined by a non destructive gamma counting method. Each section is measured for ^{226}Ra, via its grand-daughter ^{214}Pb, at a photopeak of 352 keV. The gamma counting instrument used has a well-type germanium detector, which consists of a pure germanium closed-end coaxial well crystal of 36 mm depth and 20 mm diameter. The crystal has an active volume of 140.5 cm^3. The resolution of the detector is 1.54 keV for ^{57}Co (122 keV photo peak) and 2.24 keV for ^{60}Co (1332 keV photo peak). The gamma counting system, including the multi-channel analyzer, was previously calibrated with liquid and sediment standards containing ^{210}Pb, ^{234}Th, ^{226}Ra and ^{228}Ra isotopes for various geometries (BASKARAN et al., 1993a). As the geometry increases from 1 ml to 10 ml, the counting efficiency varies almost by a factor of 2.5. There is no background peak observed for ^{226}Ra. The activity of ^{226}Ra in the sediment samples is calculated using the formula:

$$^{226}\mathrm{Ra}\ (\mathrm{dpm/g}) = \frac{^{226}\mathrm{Ra\ Net\ counts}}{\mathrm{Counting\ time\ (min)}} \times \frac{\mathrm{DPM/CPM\ conversion\ factor}}{\mathrm{Sample\ weight\ (g)}}$$

The counting uncertainty (1 standard deviation) was previously determined as 4-8 % for sediment samples, and the final one-sigma-propagated-error (errors from: 1σ_counting error, error due to the background correction, and error from separately conducted calibrations) was always less than 10%. Repeated measurements of the fly-ash sediment standard over long periods of time showed that the stability of the counting system was better than 10%.

Analysis of standard reference material for ^{210}Pb and ^{226}Ra

To ensure that the alpha and gamma counting instruments were well calibrated, and that the microwave digestion method extracted all of the ^{210}Pb in the sediment samples, a Fly Ash sediment standard (a by-product of coal combustion), from the National Bureau of Standards, was measured for Pb-210 and Ra-226. About 1 g of Fly Ash sediment standard was taken in a microwave digestion vessel, digested for Pb-210, plated, and alpha counted. Also, about 5 ml (5.85 g) of the same sediment was taken in a counting vial, and gamma counted for Ra-226. The results indicated that the measured ^{210}Pb activity in this sediment standard was 7.86±0.41 dpm/g while the ^{226}Ra activity was 7.71±0.35 dpm/g. These values are, within the errors, the same as that of the NBS certified ^{226}Ra activity of 7.80±0.51 dpm/g. These results confirm the analytical capability of the alpha and gamma counting instruments, as well as the 100% yield of the microwave digestion technique for ^{210}Pb. Selfadsorption corrections for ^{210}Pb are, however, applied when needed for samples with packing densities in the vial significantly different than 1 g cm^{-3}.

4.2) ^{234}Th (63 keV).

Standard reference materials used for geometry calibrations were obtained from standards obtained by US-EPA-EMSL, as well as liquid standards of ^{238}U. Selfadsorption corrections are applied when needed for samples with packing densities in the vial significantly different than 1 g cm^{-3}. All reported results of [^{234}Th - ^{238}U] are decay corrected to the time of sample collection, with ^{238}U activities taken where ^{234}Th activities remain constant (secular equilibrium) which occurs deeper in the core.

4.3) ^{137}Cs (662 keV).

Standard reference materials used for geometry calibrations were obtained from New England Nuclear Corporation, Dreieich, Germany.

4.4) ^{7}Be (478 keV).

Standard reference materials used for geometry calibrations were obtained from Laboratoire de Meteorologie des Rayonnements Ionisants, Gif-sur-Ivette, France.

5) Details of Porosity and mass depth determination

% of Water is calculated as [Wet weight of sediment - dry weight of sediment] * 100 / [Wet weight of bulk sediments].

The porosity (Ø) of sediments is calculated from the water content using the formula
$Ø = f_w / [f_w + (1-f_w) \rho_w / \rho_s]$

where, f_w = fraction of water content in the bulk sediments (i.e. % water content / 100); ρ_w = density of pore water (assumed to be 1.0 g cm^{-3}); ρ_s = solid density (assumed to be 2.5 g cm^{-3}).

To account for the compaction in the vertical distribution of radionuclides and trace metals, the concentrations are generally plotted against mass depth instead of depth. The cumulative mass depth (g cm^{-2}) in the core is estimated using the formula

Cumulative mass depth = $\sum (1-Ø_i)\ \rho_s\ \Delta z$

with $Ø_i$ = porosity at depth i; ρ_s = density of dry sediments (2.5 g cm^{-3}); Δz = thickness of each section.

APPENDIX C

Supporting Tables and Figures

Table of Contents

Table of Contents Continued

Table of Contents Continued

Table of Contents Continued

Table of Contents Continued

Table of Contents Continued

Table of Contents Continued

Table C-1. Detailed sedigraph data.

Core 128						Core 134				Core 201					
1-3cm		8-10cm		48-50cm		20-22cm		57-59cm		5-7cm		12-14cm		57-59cm	
phi size	%freq	phi size	%freq	phi size	%freq	phi size	%freq	phi size	%freq	phi size	%freq	phi size	%freq	phi size	%freq
-1	0.00	-1	0.00	-1	0.00	-1	0.00	-1	0.00	-1	0.00	-1	0.00	-1	0.00
-0.75	0.00	-0.75	0.00	-0.75	0.00	-0.75	0.00	-0.75	0.00	-0.75	0.78	-0.75	0.05	-0.75	0.00
-0.5	0.00	-0.5	0.22	-0.5	0.00	-0.5	0.01	-0.5	0.01	-0.5	0.21	-0.5	0.02	-0.5	0.00
-0.25	0.00	-0.25	0.00	-0.25	0.00	-0.25	0.01	-0.25	0.01	-0.25	0.00	-0.25	0.08	-0.25	0.00
0	0.00	0	0.00	0	0.00	0	0.01	0	0.01	0	0.30	0	0.00	0	0.00
0.25	0.27	0.25	0.00	0.25	0.09	0.25	0.01	0.25	0.01	0.25	0.48	0.25	0.00	0.25	0.00
0.5	0.04	0.5	0.00	0.5	0.11	0.5	0.01	0.5	0.01	0.5	0.30	0.5	0.00	0.5	0.01
0.75	0.00	0.75	0.02	0.75	0.16	0.75	0.01	0.75	0.02	0.75	0.00	0.75	0.00	0.75	0.06
1	0.00	1	0.00	1	5.03	1	0.02	1	0.01	1	0.00	1	0.00	1	0.11
1.25	0.00	1.25	0.00	1.25	2.22	1.25	0.04	1.25	0.01	1.25	0.25	1.25	0.00	1.25	0.09
1.5	0.00	1.5	0.00	1.5	0.00	1.5	0.09	1.5	0.02	1.5	0.06	1.5	0.23	1.5	0.00
1.75	0.01	1.75	0.12	1.75	0.75	1.75	0.02	1.75	0.00	1.75	0.05	1.75	0.06	1.75	0.00
2	0.00	2	0.10	2	0.68	2	0.03	2	0.00	2	0.19	2	0.24	2	0.01
2.25	0.05	2.25	0.29	2.25	0.00	2.25	0.03	2.25	0.00	2.25	1.35	2.25	1.87	2.25	1.27
2.5	0.15	2.5	0.72	2.5	0.15	2.5	0.05	2.5	0.03	2.5	3.39	2.5	10.83	2.5	7.45
2.75	0.16	2.75	2.37	2.75	2.21	2.75	0.04	2.75	0.09	2.75	17.70	2.75	21.90	2.75	15.65
3	0.17	3	4.24	3	6.64	3	0.06	3	0.17	3	11.35	3	14.79	3	12.34
3.25	0.99	3.25	9.02	3.25	17.02	3.25	0.08	3.25	0.17	3.25	8.19	3.25	6.38	3.25	5.65
3.5	1.55	3.5	6.70	3.5	5.30	3.5	0.07	3.5	0.20	3.5	6.08	3.5	6.04	3.5	3.90
3.75	0.49	3.75	4.53	3.75	5.39	3.75	0.04	3.75	0.12	3.75	5.36	3.75	4.89	3.75	3.25
4	1.65	4	4.69	4	8.48	4	0.00	4	0.53	4	5.45	4	3.63	4	1.22
4.25	0.43	4.25	3.75	4.25	3.36	4.25	0.00	4.25	0.44	4.25	2.36	4.25	1.81	4.25	0.56
4.5	0.00	4.5	2.43	4.5	0.00	4.5	0.07	4.5	0.15	4.5	1.42	4.5	0.74	4.5	0.08
4.75	0.00	4.75	2.17	4.75	0.00	4.75	0.00	4.75	0.19	4.75	1.86	4.75	0.20	4.75	0.00
5	0.00	5	2.53	5	0.47	5	0.00	5	0.23	5	0.17	5	0.20	5	0.26
5.25	0.00	5.25	2.42	5.25	0.20	5.25	0.00	5.25	0.30	5.25	0.43	5.25	0.31	5.25	0.08
5.5	0.00	5.5	2.32	5.5	0.20	5.5	0.10	5.5	0.44	5.5	0.73	5.5	0.51	5.5	0.30
5.75	0.00	5.75	2.32	5.75	0.30	5.75	0.20	5.75	0.59	5.75	0.76	5.75	0.61	5.75	0.53
6	0.00	6	2.21	6	0.40	6	0.30	6	0.89	6	0.69	6	0.56	6	0.60
6.25	0.00	6.25	2.00	6.25	0.40	6.25	0.60	6.25	1.18	6.25	0.63	6.25	0.46	6.25	0.68
6.5	0.39	6.5	1.92	6.5	0.54	6.5	0.86	6.5	1.58	6.5	0.56	6.5	0.49	6.5	0.88
6.75	0.62	6.75	2.17	6.75	0.77	6.75	1.29	6.75	2.28	6.75	0.50	6.75	0.65	6.75	1.16
7	0.18	7	2.31	7	1.02	7	2.05	7	3.02	7	0.43	7	0.74	7	1.43
7.25	0.00	7.25	1.64	7.25	0.96	7.25	2.28	7.25	2.84	7.25	0.40	7.25	0.61	7.25	1.26
7.5	0.00	7.5	1.49	7.5	0.94	7.5	2.71	7.5	2.96	7.5	0.43	7.5	0.66	7.5	1.41
7.75	0.00	7.75	1.82	7.75	1.20	7.75	3.33	7.75	3.55	7.75	0.46	7.75	0.82	7.75	1.70
8	0.17	8	2.04	8	1.24	8	3.73	8	3.88	8	0.43	8	0.84	8	1.86
8.25	0.51	8.25	2.24	8.25	1.42	8.25	3.83	8.25	4.19	8.25	0.40	8.25	0.87	8.25	1.91
8.5	0.80	8.5	2.08	8.5	1.32	8.5	3.43	8.5	3.71	8.5	0.36	8.5	0.74	8.5	1.58
8.75	0.64	8.75	1.82	8.75	1.33	8.75	3.47	8.75	3.55	8.75	0.36	8.75	0.75	8.75	1.60
9	0.34	9	1.61	9	1.53	9	3.48	9	3.70	9	0.36	9	0.71	9	1.67
9.25	0.52	9.25	1.96	9.25	1.43	9.25	3.30	9.25	3.39	9.25	0.59	9.25	0.73	9.25	1.61
9.5	0.93	9.5	1.95	9.5	1.55	9.5	3.40	9.5	3.20	9.5	1.25	9.5	0.71	9.5	1.62
9.75	0.90	9.75	1.74	9.75	1.35	9.75	3.00	9.75	2.88	9.75	2.11	9.75	0.61	9.75	1.46
10	0.99	10	1.15	10	1.09	10	2.45	10	2.22	10	2.44	10	0.49	10	1.33
10.25	1.38	10.25	0.91	10.25	1.15	10.25	2.44	10.25	2.12	10.25	2.48	10.25	0.58	10.25	1.40
10.5	1.08	10.5	0.79	10.5	1.35	10.5	2.25	10.5	1.77	10.5	2.18	10.5	0.69	10.5	1.35
10.75	0.37	10.75	0.80	10.75	1.37	10.75	1.98	10.75	2.02	10.75	1.95	10.75	0.78	10.75	1.37
11	0.00	11	1.00	11	1.09	11	1.50	11	2.01	11	1.62	11	0.69	11	1.33
11.25	0.43	11.25	0.88	11.25	1.07	11.25	1.31	11.25	1.76	11.25	1.29	11.25	0.73	11.25	1.43
11.5	0.58	11.5	0.51	11.5	0.97	11.5	1.21	11.5	1.78	11.5	0.76	11.5	0.68	11.5	1.45
11.75	0.77	11.75	0.27	11.75	1.27	11.75	1.40	11.75	2.44	11.75	0.59	11.75	0.91	11.75	2.00
12	0.31	12	0.41	12	1.04	12	1.04	12	2.12	12	0.36	12	0.73	12	1.66
<12	82.14	<12	11.33	<12	13.44	<12	42.31	<12	31.22	<12	7.16	<12	7.40	<12	11.54

Table C-1. Detailed sedigraph data.

Core 285						Core 286							
2-4cm		20-22 cm		72-74cm		2-4cm		18-20cm		23-25cm		66-68cm	
phi size	%freq	phi size	%freq	phi size	%freq	phi size	%freq	phi size	%freq	phi size	%freq	phi size	%freq
-1	0.00	-1	0.00	-1	0.00	-1	0.00	-1	0.40	-1	0.00	-1	0.00
-0.75	0.01	-0.75	0.00	-0.75	0.00	-0.75	0.08	-0.75	0.01	-0.75	0.00	-0.75	0.00
-0.5	0.02	-0.5	0.01	-0.5	0.00	-0.5	0.00	-0.5	0.00	-0.5	0.00	-0.5	0.00
-0.25	0.01	-0.25	0.00	-0.25	0.00	-0.25	0.00	-0.25	0.00	-0.25	0.05	-0.25	0.00
0	0.01	0	0.00	0	0.00	0	0.00	0	0.00	0	0.01	0	0.00
0.25	0.01	0.25	0.00	0.25	0.01	0.25	0.18	0.25	0.00	0.25	0.00	0.25	0.00
0.5	0.01	0.5	0.14	0.5	0.03	0.5	0.09	0.5	0.00	0.5	0.02	0.5	0.00
0.75	0.01	0.75	0.00	0.75	0.01	0.75	0.00	0.75	0.00	0.75	0.04	0.75	0.00
1	0.01	1	0.06	1	0.56	1	0.00	1	0.00	1	0.03	1	0.00
1.25	0.01	1.25	0.49	1.25	0.10	1.25	0.07	1.25	0.00	1.25	0.02	1.25	0.00
1.5	0.03	1.5	0.17	1.5	0.24	1.5	0.00	1.5	0.02	1.5	0.02	1.5	0.00
1.75	0.14	1.75	0.22	1.75	0.08	1.75	0.10	1.75	0.01	1.75	0.02	1.75	0.00
2	0.09	2	0.15	2	0.20	2	0.27	2	0.01	2	0.00	2	0.02
2.25	0.05	2.25	0.30	2.25	0.62	2.25	0.00	2.25	0.00	2.25	0.00	2.25	0.00
2.5	0.07	2.5	0.56	2.5	1.11	2.5	0.09	2.5	0.02	2.5	0.00	2.5	0.01
2.75	0.24	2.75	1.04	2.75	2.14	2.75	0.11	2.75	0.00	2.75	0.00	2.75	0.02
3	0.63	3	1.35	3	1.95	3	0.00	3	0.00	3	0.00	3	0.00
3.25	0.97	3.25	1.58	3.25	1.98	3.25	0.45	3.25	0.00	3.25	0.03	3.25	0.06
3.5	0.76	3.5	1.26	3.5	1.00	3.5	0.00	3.5	0.00	3.5	0.04	3.5	0.02
3.75	0.44	3.75	1.04	3.75	1.35	3.75	0.00	3.75	0.12	3.75	0.01	3.75	0.03
4	0.34	4	0.75	4	0.99	4	0.00	4	0.22	4	0.10	4	0.03
4.25	0.26	4.25	0.73	4.25	0.79	4.25	0.16	4.25	0.15	4.25	0.00	4.25	0.10
4.5	0.23	4.5	0.70	4.5	0.25	4.5	0.43	4.5	0.30	4.5	0.20	4.5	0.20
4.75	0.21	4.75	0.62	4.75	0.24	4.75	0.74	4.75	0.57	4.75	0.32	4.75	0.10
5	0.17	5	0.00	5	0.12	5	0.44	5	0.58	5	0.70	5	0.39
5.25	0.20	5.25	0.10	5.25	0.00	5.25	0.30	5.25	0.80	5.25	1.10	5.25	0.40
5.5	0.20	5.5	0.40	5.5	0.00	5.5	0.30	5.5	1.30	5.5	1.80	5.5	0.80
5.75	0.20	5.75	0.70	5.75	0.00	5.75	0.60	5.75	2.10	5.75	2.80	5.75	1.30
6	0.30	6	0.90	6	0.00	6	1.10	6	2.90	6	3.80	6	2.00
6.25	0.50	6.25	0.80	6.25	0.00	6.25	1.50	6.25	3.50	6.25	4.40	6.25	2.80
6.5	0.64	6.5	0.75	6.5	0.02	6.5	1.93	6.5	3.75	6.5	4.61	6.5	3.43
6.75	0.90	6.75	1.29	6.75	0.04	6.75	2.70	6.75	4.37	6.75	4.89	6.75	4.63
7	1.17	7	1.90	7	0.02	7	3.51	7	4.82	7	4.68	7	5.55
7.25	1.08	7.25	1.80	7.25	0.68	7.25	3.36	7.25	3.60	7.25	3.48	7.25	4.44
7.5	1.06	7.5	1.76	7.5	0.12	7.5	3.53	7.5	3.18	7.5	3.18	7.5	4.00
7.75	1.33	7.75	1.73	7.75	0.31	7.75	3.73	7.75	3.20	7.75	3.20	7.75	4.13
8	1.38	8	1.66	8	0.11	8	3.45	8	3.45	8	3.18	8	4.14
8.25	1.56	8.25	1.98	8.25	0.29	8.25	3.40	8.25	3.40	8.25	3.40	8.25	4.11
8.5	1.19	8.5	1.85	8.5	0.82	8.5	2.90	8.5	2.90	8.5	3.04	8.5	3.83
8.75	0.80	8.75	1.73	8.75	1.47	8.75	2.67	8.75	2.67	8.75	2.67	8.75	3.87
9	0.70	9	1.67	9	2.98	9	2.50	9	2.50	9	2.23	9	3.90
9.25	0.72	9.25	1.87	9.25	2.80	9.25	2.30	9.25	2.44	9.25	2.15	9.25	3.59
9.5	0.77	9.5	2.16	9.5	3.06	9.5	2.32	9.5	2.47	9.5	2.32	9.5	3.55
9.75	0.75	9.75	1.95	9.75	1.50	9.75	2.25	9.75	2.25	9.75	2.10	9.75	3.00
10	0.68	10	1.50	10	2.05	10	2.05	10	1.77	10	1.64	10	2.32
10.25	0.86	10.25	1.72	10.25	2.15	10.25	2.30	10.25	1.72	10.25	1.58	10.25	2.30
10.5	0.90	10.5	2.10	10.5	2.25	10.5	2.25	10.5	1.80	10.5	1.50	10.5	2.25
10.75	0.91	10.75	2.28	10.75	2.28	10.75	2.28	10.75	1.98	10.75	1.37	10.75	2.13
11	0.82	11	1.90	11	1.90	11	2.04	11	1.77	11	1.09	11	1.63
11.25	0.60	11.25	2.03	11.25	1.79	11.25	2.03	11.25	1.55	11.25	1.19	11.25	1.43
11.5	0.48	11.5	2.17	11.5	1.81	11.5	2.05	11.5	1.57	11.5	1.33	11.5	1.33
11.75	0.51	11.75	3.05	11.75	2.67	11.75	2.80	11.75	2.29	11.75	1.53	11.75	1.91
12	0.26	12	2.87	12	2.35	12	2.48	12	1.96	12	0.78	12	1.70
<12	73.83	<12	42.21	<12	52.73	<12	32.18	<12	25.58	<12	27.41	<12	18.55

Table C-1. Detailed sedigraph data.

Core 296								Core 300							
7-8 cm		25-26cm		35-36cm		70-71cm		2-4cm		13-15cm		25-27cm		56-58cm	
phi size	%freq	phi size	%freq	phi size	%freq	phi size	%freq	phi size	%freq	phi size	%freq	phi size	%freq	phi size	%freq
-1	0.00	-1	0.00	-1	0.00	-1	0.00	-1	0.20	-1	0.00	-1	0.00	-1	0
-0.75	0.00	-0.75	0.14	-0.75	0.00	-0.75	0.00	-0.75	0.00	-0.75	0.00	-0.75	0.00	-0.75	0.01
-0.5	0.00	-0.5	0.15	-0.5	0.00	-0.5	0.00	-0.5	0.00	-0.5	0.00	-0.5	0.01	-0.5	0.00
-0.25	0.00	-0.25	0.17	-0.25	0.00	-0.25	0.00	-0.25	0.00	-0.25	0.00	-0.25	0.00	-0.25	0.00
0	0.04	0	0.00	0	0.00	0	0.00	0	0.00	0	0.00	0	0.04	0	0.00
0.25	0.01	0.25	0.08	0.25	0.00	0.25	0.00	0.25	0.00	0.25	0.00	0.25	0.03	0.25	0.02
0.5	0.02	0.5	1.74	0.5	0.00	0.5	0.00	0.5	0.00	0.5	0.00	0.5	0.06	0.5	0.03
0.75	0.01	0.75	0.73	0.75	0.00	0.75	0.00	0.75	0.00	0.75	0.00	0.75	0.08	0.75	0.07
1	0.04	1	0.00	1	0.00	1	0.00	1	0.12	1	0.00	1	0.08	1	0.90
1.25	0.05	1.25	1.49	1.25	0.09	1.25	0.00	1.25	0.00	1.25	0.00	1.25	0.38	1.25	0.79
1.5	0.13	1.5	1.70	1.5	0.07	1.5	0.02	1.5	0.01	1.5	0.00	1.5	0.36	1.5	0.91
1.75	0.36	1.75	0.75	1.75	0.00	1.75	0.02	1.75	0.02	1.75	0.00	1.75	0.27	1.75	0.80
2	0.17	2	0.32	2	0.00	2	0.32	2	0.00	2	0.00	2	0.27	2	1.24
2.25	0.35	2.25	0.91	2.25	0.04	2.25	0.10	2.25	0.01	2.25	0.00	2.25	0.36	2.25	1.39
2.5	0.52	2.5	1.61	2.5	0.09	2.5	0.14	2.5	0.00	2.5	0.00	2.5	0.43	2.5	1.06
2.75	1.09	2.75	1.32	2.75	0.22	2.75	0.13	2.75	0.01	2.75	0.00	2.75	1.41	2.75	1.29
3	1.64	3	2.17	3	0.39	3	0.30	3	0.01	3	0.00	3	6.49	3	6.25
3.25	2.23	3.25	5.14	3.25	0.34	3.25	1.87	3.25	0.11	3.25	0.00	3.25	4.66	3.25	10.20
3.5	1.99	3.5	3.21	3.5	0.89	3.5	6.47	3.5	0.10	3.5	0.00	3.5	3.82	3.5	5.17
3.75	2.35	3.75	3.88	3.75	0.78	3.75	8.05	3.75	0.13	3.75	0.00	3.75	3.28	3.75	3.72
4	3.65	4	3.07	4	1.25	4	9.37	4	0.10	4	0.00	4	2.66	4	3.49
4.25	2.22	4.25	2.08	4.25	0.74	4.25	5.88	4.25	0.06	4.25	0.00	4.25	1.59	4.25	2.29
4.5	1.20	4.5	0.40	4.5	0.51	4.5	6.36	4.5	0.07	4.5	1.28	4.5	1.10	4.5	2.76
4.75	1.02	4.75	0.20	4.75	0.43	4.75	3.52	4.75	0.02	4.75	0.66	4.75	0.60	4.75	1.31
5	0.00	5	0.20	5	0.50	5	1.64	5	0.23	5	1.26	5	0.53	5	0.29
5.25	0.20	5.25	0.20	5.25	0.80	5.25	0.90	5.25	0.60	5.25	0.20	5.25	0.50	5.25	0.10
5.5	0.40	5.5	0.30	5.5	0.90	5.5	1.00	5.5	0.80	5.5	0.40	5.5	0.80	5.5	0.20
5.75	0.70	5.75	0.40	5.75	0.90	5.75	1.10	5.75	0.90	5.75	0.70	5.75	1.00	5.75	0.30
6	1.00	6	0.50	6	1.00	6	1.40	6	1.10	6	0.90	6	1.00	6	0.40
6.25	1.10	6.25	0.80	6.25	1.20	6.25	1.50	6.25	1.20	6.25	1.00	6.25	0.90	6.25	0.50
6.5	1.18	6.5	1.07	6.5	1.39	6.5	1.39	6.5	1.29	6.5	1.07	6.5	1.18	6.5	0.54
6.75	1.67	6.75	1.54	6.75	1.80	6.75	1.41	6.75	1.80	6.75	1.41	6.75	1.80	6.75	0.64
7	2.19	7	1.90	7	2.48	7	1.61	7	2.19	7	1.90	7	2.19	7	0.88
7.25	1.92	7.25	1.56	7.25	2.52	7.25	1.44	7.25	2.04	7.25	1.68	7.25	1.92	7.25	0.84
7.5	2.12	7.5	1.65	7.5	2.71	7.5	1.53	7.5	2.12	7.5	1.76	7.5	2.00	7.5	0.94
7.75	2.80	7.75	1.87	7.75	2.80	7.75	1.73	7.75	2.40	7.75	2.27	7.75	2.40	7.75	1.20
8	3.04	8	2.07	8	2.76	8	1.93	8	2.62	8	2.76	8	2.62	8	1.24
8.25	3.26	8.25	2.27	8.25	3.12	8.25	1.84	8.25	2.69	8.25	3.26	8.25	2.69	8.25	1.28
8.5	2.90	8.5	1.98	8.5	3.17	8.5	1.32	8.5	2.24	8.5	3.04	8.5	2.38	8.5	1.19
8.75	3.07	8.75	2.00	8.75	2.93	8.75	1.47	8.75	2.13	8.75	3.07	8.75	2.40	8.75	1.33
9	3.20	9	2.23	9	2.50	9	1.95	9	2.23	9	3.06	9	2.37	9	1.39
9.25	3.01	9.25	2.15	9.25	2.15	9.25	1.87	9.25	2.30	9.25	3.01	9.25	2.30	9.25	1.43
9.5	2.94	9.5	2.01	9.5	2.47	9.5	1.55	9.5	2.47	9.5	3.09	9.5	2.32	9.5	1.39
9.75	2.55	9.75	1.95	9.75	2.70	9.75	1.05	9.75	2.40	9.75	2.70	9.75	2.10	9.75	1.20
10	2.05	10	1.64	10	2.18	10	0.95	10	2.05	10	2.32	10	1.77	10	0.95
10.25	2.15	10.25	1.43	10.25	1.87	10.25	1.00	10.25	2.30	10.25	2.44	10.25	1.87	10.25	1.00
10.5	1.95	10.5	1.35	10.5	1.50	10.5	0.90	10.5	2.25	10.5	2.10	10.5	1.95	10.5	0.90
10.75	1.98	10.75	1.37	10.75	1.22	10.75	0.76	10.75	2.43	10.75	1.98	10.75	2.13	10.75	0.91
11	1.77	11	1.09	11	0.68	11	0.82	11	2.31	11	1.63	11	2.04	11	0.54
11.25	1.67	11.25	0.95	11.25	0.36	11.25	0.95	11.25	2.51	11.25	1.43	11.25	2.03	11.25	0.48
11.5	1.57	11.5	0.72	11.5	0.72	11.5	0.84	11.5	2.41	11.5	1.21	11.5	2.05	11.5	0.48
11.75	2.04	11.75	1.15	11.75	1.65	11.75	1.15	11.75	3.18	11.75	1.27	11.75	3.18	11.75	0.38
12	1.70	12	1.04	12	1.83	12	1.04	12	2.61	12	0.91	12	3.00	12	0.26
<12	24.80	<12	28.92	<12	41.33	<12	19.40	<12	41.23	<12	44.22	<12	16.62	<12	33.09

Table C-1. Detailed sedigraph data.

Core 4293										S. Dredge		L.River		"Y"	
2-4cm		13-15cm		25-27cm		56-58cm		CN26 grab		Island Grab		Delta grab		channel grab	
phi size	%freq	phi size	%freq	phi size	%freq	phi size	%freq	phi size	%freq	phi size	%freq	phi size	%freq	phi size	%freq
-1	0.00	-1	0.00	-1	0.00	-1	0.00	-1	0.00	-1	9.73	-1	0.00	-1	0.00
-0.75	0.07	-0.75	0.00	-0.75	0.02	-0.75	0.00	-0.75	0.07	-0.75	0.66	-0.75	0.01	-0.75	0.00
-0.5	0.10	-0.5	0.00	-0.5	0.06	-0.5	0.00	-0.5	0.43	-0.5	1.64	-0.5	0.20	-0.5	0.00
-0.25	0.00	-0.25	0.01	-0.25	0.03	-0.25	0.00	-0.25	0.21	-0.25	0.55	-0.25	0.34	-0.25	0.00
0	0.00	0	0.00	0	0.00	0	0.02	0	0.06	0	0.42	0	0.21	0	0.00
0.25	0.01	0.25	0.00	0.25	0.01	0.25	0.67	0.25	0.17	0.25	0.27	0.25	0.37	0.25	0.00
0.5	0.00	0.5	0.00	0.5	0.07	0.5	0.00	0.5	0.09	0.5	0.18	0.5	0.06	0.5	0.00
0.75	0.00	0.75	0.00	0.75	0.07	0.75	0.27	0.75	0.13	0.75	0.43	0.75	0.16	0.75	0.00
1	0.04	1	0.00	1	0.28	1	0.79	1	0.15	1	0.46	1	0.21	1	0.00
1.25	0.01	1.25	0.13	1.25	0.29	1.25	1.08	1.25	0.05	1.25	0.12	1.25	0.18	1.25	0.00
1.5	0.09	1.5	0.09	1.5	0.18	1.5	2.58	1.5	0.03	1.5	0.10	1.5	1.07	1.5	0.00
1.75	0.02	1.75	0.06	1.75	0.05	1.75	1.44	1.75	0.09	1.75	0.18	1.75	3.17	1.75	0.00
2	0.17	2	0.06	2	0.18	2	2.53	2	0.24	2	0.31	2	8.33	2	0.05
2.25	0.05	2.25	0.08	2.25	0.13	2.25	1.45	2.25	0.36	2.25	0.69	2.25	9.74	2.25	0.10
2.5	0.21	2.5	0.20	2.5	0.05	2.5	2.36	2.5	0.90	2.5	4.77	2.5	11.66	2.5	0.20
2.75	1.16	2.75	0.74	2.75	1.44	2.75	6.11	2.75	3.19	2.75	9.09	2.75	11.07	2.75	0.10
3	3.31	3	2.05	3	4.43	3	6.79	3	9.14	3	8.33	3	6.07	3	0.05
3.25	7.65	3.25	1.63	3.25	7.54	3.25	4.77	3.25	12.71	3.25	4.21	3.25	2.37	3.25	0.05
3.5	4.19	3.5	1.31	3.5	4.99	3.5	5.37	3.5	9.42	3.5	3.00	3.5	1.16	3.5	0.05
3.75	2.97	3.75	0.99	3.75	3.60	3.75	5.05	3.75	6.23	3.75	2.16	3.75	0.99	3.75	0.05
4	2.51	4	0.88	4	3.25	4	3.69	4	5.50	4	1.37	4	0.59	4	0.05
4.25	1.76	4.25	0.75	4.25	2.17	4.25	2.87	4.25	4.92	4.25	0.85	4.25	1.66	4.25	0.00
4.5	0.98	4.5	0.68	4.5	1.39	4.5	2.35	4.5	5.49	4.5	1.10	4.5	0.90	4.5	0.00
4.75	0.58	4.75	0.65	4.75	0.92	4.75	1.27	4.75	4.00	4.75	0.62	4.75	1.08	4.75	0.00
5	0.50	5	0.59	5	0.77	5	1.32	5	3.07	5	0.45	5	0.56	5	0.00
5.25	0.70	5.25	0.60	5.25	0.92	5.25	1.40	5.25	1.37	5.25	0.24	5.25	0.00	5.25	0.10
5.5	1.00	5.5	0.90	5.5	1.15	5.5	1.50	5.5	0.96	5.5	0.39	5.5	0.04	5.5	0.10
5.75	1.00	5.75	1.20	5.75	1.26	5.75	1.30	5.75	0.56	5.75	0.44	5.75	0.08	5.75	0.10
6	1.00	6	1.50	6	1.38	6	1.20	6	0.41	6	0.34	6	0.11	6	0.10
6.25	1.10	6.25	1.50	6.25	1.38	6.25	1.20	6.25	0.37	6.25	0.34	6.25	0.19	6.25	0.30
6.5	1.29	6.5	1.61	6.5	1.35	6.5	1.07	6.5	0.32	6.5	0.52	6.5	0.41	6.5	0.53
6.75	1.41	6.75	1.93	6.75	1.48	6.75	1.03	6.75	0.43	6.75	0.81	6.75	0.58	6.75	0.89
7	1.61	7	2.19	7	1.68	7	1.02	7	0.60	7	1.21	7	0.72	7	1.30
7.25	1.44	7.25	1.68	7.25	1.38	7.25	0.84	7.25	0.53	7.25	1.11	7.25	0.64	7.25	1.19
7.5	1.53	7.5	1.76	7.5	1.22	7.5	0.94	7.5	0.52	7.5	1.26	7.5	0.71	7.5	1.40
7.75	1.87	7.75	2.13	7.75	1.38	7.75	1.07	7.75	0.59	7.75	1.68	7.75	0.81	7.75	1.85
8	1.93	8	2.62	8	1.74	8	1.24	8	0.72	8	2.08	8	0.84	8	2.32
8.25	2.13	8.25	2.83	8.25	1.95	8.25	1.56	8.25	0.89	8.25	2.34	8.25	0.91	8.25	2.81
8.5	1.98	8.5	2.51	8.5	1.67	8.5	1.45	8.5	0.88	8.5	2.25	8.5	0.85	8.5	2.74
8.75	2.00	8.75	2.40	8.75	1.53	8.75	1.33	8.75	0.94	8.75	2.33	8.75	0.86	8.75	2.77
9	1.81	9	2.37	9	1.44	9	1.25	9	0.98	9	2.43	9	0.95	9	2.75
9.25	1.58	9.25	2.30	9.25	1.48	9.25	1.15	9.25	0.96	9.25	2.37	9.25	0.92	9.25	2.84
9.5	1.85	9.5	2.32	9.5	1.42	9.5	1.08	9.5	1.09	9.5	2.40	9.5	0.88	9.5	2.91
9.75	1.95	9.75	2.10	9.75	1.20	9.75	1.05	9.75	1.00	9.75	2.33	9.75	0.79	9.75	2.82
10	1.64	10	1.64	10	0.94	10	0.82	10	0.91	10	1.99	10	0.72	10	2.43
10.25	1.58	10.25	1.72	10.25	1.15	10.25	0.86	10.25	1.01	10.25	2.23	10.25	0.87	10.25	2.56
10.5	1.50	10.5	1.65	10.5	1.20	10.5	0.75	10.5	1.00	10.5	2.26	10.5	0.91	10.5	2.82
10.75	1.52	10.75	1.83	10.75	1.05	10.75	0.76	10.75	1.13	10.75	2.37	10.75	0.92	10.75	3.16
11	1.36	11	1.77	11	0.78	11	0.54	11	1.16	11	2.05	11	0.82	11	2.69
11.25	1.31	11.25	1.79	11.25	0.82	11.25	0.48	11.25	1.24	11.25	1.80	11.25	0.86	11.25	2.48
11.5	1.45	11.5	1.57	11.5	0.83	11.5	0.48	11.5	1.21	11.5	1.53	11.5	0.82	11.5	2.27
11.75	1.91	11.75	2.04	11.75	0.88	11.75	0.76	11.75	1.56	11.75	1.86	11.75	1.11	11.75	2.90
12	1.43	12	1.57	12	0.60	12	0.65	12	1.31	12	1.46	12	0.94	12	2.58
<12	30.72	<12	37.09	<12	32.84	<12	18.40	<12	9.70	<12	3.89	<12	19.59	<12	48.16

Table C-1. Detailed sedigraph data.

Core 928								Core 924							
2-4 cm		13-15 cm		25-27 cm		44-46 cm		2-4 cm		13-15 cm		25-27 cm		44-46 cm	
phi size	%freq	phi size	%freq	phi size	%freq	phi size	%freq	phi size	%freq	phi size	%freq	phi size	%freq	phi size	%freq
-1	13.04	-1	0.37	-1	1.35	-1	0.94	-1	3.85	-1	1.68	-1	0.22	-1	1.82
-0.75	0.00	-0.75	0.14	-0.75	0.00	-0.75	0.50	-0.75	0.00	-0.75	0.06	-0.75	0.02	-0.75	0.04
-0.5	0.00	-0.5	0.21	-0.5	0.27	-0.5	0.79	-0.5	0.00	-0.5	0.00	-0.5	0.00	-0.5	0.02
-0.25	0.15	-0.25	0.31	-0.25	0.00	-0.25	1.08	-0.25	0.00	-0.25	0.00	-0.25	0.00	-0.25	0.02
0	0.00	0	0.04	0	0.04	0	0.00	0	0.07	0	0.00	0	0.05	0	0.10
0.25	0.00	0.25	0.16	0.25	0.00	0.25	0.02	0.25	0.11	0.25	0.15	0.25	0.01	0.25	0.06
0.5	13.62	0.5	0.00	0.5	0.01	0.5	0.00	0.5	0.54	0.5	0.32	0.5	0.17	0.5	0.08
0.75	0.00	0.75	0.11	0.75	0.03	0.75	0.66	0.75	0.33	0.75	0.00	0.75	0.05	0.75	0.01
1	0.00	1	0.05	1	0.32	1	0.39	1	0.05	1	0.12	1	0.00	1	0.15
1.25	0.00	1.25	0.05	1.25	0.22	1.25	0.33	1.25	0.00	1.25	0.03	1.25	0.02	1.25	0.14
1.5	0.00	1.5	0.16	1.5	0.04	1.5	0.10	1.5	0.00	1.5	0.47	1.5	0.01	1.5	0.00
1.75	0.00	1.75	0.00	1.75	0.55	1.75	0.49	1.75	0.00	1.75	0.09	1.75	0.05	1.75	0.01
2	0.00	2	0.11	2	0.72	2	0.71	2	0.00	2	0.00	2	0.00	2	0.34
2.25	0.00	2.25	0.53	2.25	0.48	2.25	0.90	2.25	0.37	2.25	0.35	2.25	0.16	2.25	0.73
2.5	0.00	2.5	0.05	2.5	0.95	2.5	3.28	2.5	0.53	2.5	1.27	2.5	0.27	2.5	0.46
2.75	0.00	2.75	1.98	2.75	2.66	2.75	4.22	2.75	4.04	2.75	3.32	2.75	0.81	2.75	3.34
3	0.00	3	4.30	3	3.93	3	5.43	3	10.57	3	5.89	3	1.64	3	6.78
3.25	0.00	3.25	4.64	3.25	5.03	3.25	6.08	3.25	9.54	3.25	5.53	3.25	23.99	3.25	6.52
3.5	0.00	3.5	3.16	3.5	3.48	3.5	2.93	3.5	4.07	3.5	4.12	3.5	1.12	3.5	4.78
3.75	0.00	3.75	2.10	3.75	2.22	3.75	2.64	3.75	3.90	3.75	2.36	3.75	1.18	3.75	3.11
4	0.00	4	1.66	4	2.17	4	1.69	4	3.88	4	2.27	4	0.81	4	2.66
4.25	0.00	4.25	1.60	4.25	2.29	4.25	2.03	4.25	3.07	4.25	1.81	4.25	0.97	4.25	1.40
4.5	0.10	4.5	1.57	4.5	1.29	4.5	1.03	4.5	1.38	4.5	1.13	4.5	0.52	4.5	2.03
4.75	0.20	4.75	1.88	4.75	1.66	4.75	0.44	4.75	1.20	4.75	1.07	4.75	1.00	4.75	0.22
5	0.10	5	2.43	5	1.33	5	0.41	5	0.85	5	0.85	5	0.88	5	1.10
5.25	0.00	5.25	0.30	5.25	0.20	5.25	0.10	5.25	0.05	5.25	0.14	5.25	0.33	5.25	1.06
5.5	0.20	5.5	0.40	5.5	0.40	5.5	0.20	5.5	0.10	5.5	0.14	5.5	0.40	5.5	1.19
5.75	0.30	5.75	0.40	5.75	0.50	5.75	0.40	5.75	0.16	5.75	0.14	5.75	0.53	5.75	1.06
6	0.30	6	0.51	6	0.60	6	0.59	6	0.31	6	0.27	6	0.73	6	1.00
6.25	0.40	6.25	0.61	6.25	0.50	6.25	0.69	6.25	0.36	6.25	0.47	6.25	1.00	6.25	1.00
6.5	0.40	6.5	0.61	6.5	0.40	6.5	0.79	6.5	0.36	6.5	0.68	6.5	1.20	6.5	1.00
6.75	0.50	6.75	0.81	6.75	0.60	6.75	0.99	6.75	0.41	6.75	0.74	6.75	1.27	6.75	1.19
7	0.50	7	1.01	7	0.99	7	1.29	7	0.52	7	0.88	7	1.40	7	1.26
7.25	0.70	7.25	1.11	7.25	1.09	7.25	1.68	7.25	0.52	7.25	1.08	7.25	1.60	7.25	1.19
7.5	0.90	7.5	1.11	7.5	1.19	7.5	1.98	7.5	0.52	7.5	1.35	7.5	1.93	7.5	1.33
7.75	0.90	7.75	1.21	7.75	1.29	7.75	2.08	7.75	0.52	7.75	1.55	7.75	2.07	7.75	1.59
8	1.00	8	1.52	8	1.39	8	2.18	8	0.47	8	1.82	8	2.20	8	1.92
8.25	1.20	8.25	1.62	8.25	1.49	8.25	2.28	8.25	0.36	8.25	1.96	8.25	2.33	8.25	2.26
8.5	1.40	8.5	1.62	8.5	1.59	8.5	2.18	8.5	0.36	8.5	1.96	8.5	2.47	8.5	2.19
8.75	1.30	8.75	1.72	8.75	1.49	8.75	2.08	8.75	0.47	8.75	2.10	8.75	2.53	8.75	2.12
9	1.20	9	1.72	9	1.39	9	1.98	9	0.47	9	2.10	9	2.53	9	2.12
9.25	1.20	9.25	1.62	9.25	1.39	9.25	1.88	9.25	0.41	9.25	2.10	9.25	2.53	9.25	2.19
9.5	1.30	9.5	1.52	9.5	1.39	9.5	1.88	9.5	0.41	9.5	2.10	9.5	2.53	9.5	2.26
9.75	1.30	9.75	1.42	9.75	1.29	9.75	1.88	9.75	0.47	9.75	1.96	9.75	2.53	9.75	2.19
10	1.20	10	1.52	10	1.19	10	1.78	10	0.52	10	1.76	10	2.47	10	1.99
10.25	1.10	10.25	1.62	10.25	1.39	10.25	1.88	10.25	0.57	10.25	1.89	10.25	2.60	10.25	2.19
10.5	1.20	10.5	1.62	10.5	1.49	10.5	1.68	10.5	0.62	10.5	1.96	10.5	2.53	10.5	2.19
10.75	1.50	10.75	1.62	10.75	1.49	10.75	1.78	10.75	0.67	10.75	2.03	10.75	2.74	10.75	2.32
11	1.50	11	1.82	11	1.39	11	1.78	11	0.72	11	2.03	11	2.80	11	2.26
11.25	1.60	11.25	2.23	11.25	1.59	11.25	2.08	11.25	0.88	11.25	2.30	11.25	3.07	11.25	2.45
11.5	1.70	11.5	2.02	11.5	1.49	11.5	1.98	11.5	0.83	11.5	2.30	11.5	2.94	11.5	2.32
11.75	2.60	11.75	2.63	11.75	1.99	11.75	2.28	11.75	0.67	11.75	2.91	11.75	3.74	11.75	2.79
12	2.30	12	2.43	12	1.59	12	1.78	12	0.16	12	2.30	12	3.07	12	1.99
<12	42.90	<12	34.32	<12	35.69	<12	18.92	<12	38.76	<12	24.13	<12	7.94	<12	13.47

Table C-1. Detailed sedigraph data.

Core 8721								Core 8827							
2-4 cm		13-15 cm		25-27 cm		44-46 cm		2-4 cm		13-15 cm		25-27 cm		44-46 cm	
phi size	%freq	phi size	%freq	phi size	%freq	phi size	%freq	phi size	%freq	phi size	%freq	phi size	%freq	phi size	%freq
-1	0.26	-1	0.14	-1	0.06	-1	0.00	-1	18.33	-1	34.34	-1	0.37	-1	0.06
-0.75	0.00	-0.75	0.01	-0.75	0.01	-0.75	0.00	-0.75	3.48	-0.75	0.00	-0.75	0.29	-0.75	0.02
-0.5	0.00	-0.5	0.00	-0.5	0.00	-0.5	0.01	-0.5	0.32	-0.5	0.44	-0.5	0.00	-0.5	0.00
-0.25	0.00	-0.25	0.00	-0.25	0.00	-0.25	0.01	-0.25	0.63	-0.25	0.13	-0.25	0.00	-0.25	0.00
0	0.01	0	0.00	0	0.00	0	0.00	0	0.00	0	0.00	0	0.00	0	0.02
0.25	0.01	0.25	0.00	0.25	0.01	0.25	0.03	0.25	0.00	0.25	0.00	0.25	0.00	0.25	0.00
0.5	0.02	0.5	0.00	0.5	0.01	0.5	0.00	0.5	3.16	0.5	0.00	0.5	0.00	0.5	0.02
0.75	0.03	0.75	0.00	0.75	0.02	0.75	0.01	0.75	0.00	0.75	0.00	0.75	0.19	0.75	0.00
1	0.03	1	0.07	1	0.03	1	0.01	1	0.00	1	0.03	1	0.16	1	0.00
1.25	0.01	1.25	0.00	1.25	0.00	1.25	0.00	1.25	0.00	1.25	0.00	1.25	0.27	1.25	0.02
1.5	0.00	1.5	0.00	1.5	0.01	1.5	0.03	1.5	0.00	1.5	0.00	1.5	0.08	1.5	0.02
1.75	0.00	1.75	0.00	1.75	0.03	1.75	0.04	1.75	0.00	1.75	0.00	1.75	0.26	1.75	0.02
2	0.00	2	0.00	2	0.03	2	0.00	2	0.00	2	0.00	2	0.21	2	0.02
2.25	0.07	2.25	0.00	2.25	0.05	2.25	0.00	2.25	5.06	2.25	0.00	2.25	0.94	2.25	0.02
2.5	0.05	2.5	0.00	2.5	0.27	2.5	0.05	2.5	0.00	2.5	0.00	2.5	2.89	2.5	0.09
2.75	0.06	2.75	0.09	2.75	0.52	2.75	0.00	2.75	0.00	2.75	0.00	2.75	3.86	2.75	0.40
3	0.25	3	0.21	3	0.57	3	0.06	3	0.00	3	0.00	3	2.36	3	0.76
3.25	0.32	3.25	0.29	3.25	0.65	3.25	0.10	3.25	0.00	3.25	0.00	3.25	1.66	3.25	0.63
3.5	0.40	3.5	0.37	3.5	0.54	3.5	0.09	3.5	0.00	3.5	0.00	3.5	1.76	3.5	0.46
3.75	0.35	3.75	0.30	3.75	0.41	3.75	0.11	3.75	0.00	3.75	0.00	3.75	1.76	3.75	0.40
4	0.55	4	0.50	4	0.50	4	0.10	4	0.00	4	0.00	4	1.14	4	0.59
4.25	0.53	4.25	0.54	4.25	0.42	4.25	0.11	4.25	0.10	4.25	0.00	4.25	0.79	4.25	0.60
4.5	0.33	4.5	0.23	4.5	0.56	4.5	0.58	4.5	0.20	4.5	0.30	4.5	1.14	4.5	0.42
4.75	0.29	4.75	0.26	4.75	0.48	4.75	0.70	4.75	0.30	4.75	0.50	4.75	1.40	4.75	0.34
5	0.34	5	0.21	5	0.45	5	0.44	5	0.40	5	0.80	5	1.24	5	0.47
5.25	0.00	5.25	0.00	5.25	0.28	5.25	0.00	5.25	0.60	5.25	1.10	5.25	1.33	5.25	0.70
5.5	0.10	5.5	0.19	5.5	0.38	5.5	0.30	5.5	0.70	5.5	1.31	5.5	1.74	5.5	1.09
5.75	0.00	5.75	0.39	5.75	0.47	5.75	0.99	5.75	0.80	5.75	1.51	5.75	2.15	5.75	1.19
6	0.00	6	0.68	6	0.66	6	1.29	6	0.90	6	1.51	6	2.46	6	1.39
6.25	0.10	6.25	0.87	6.25	0.85	6.25	1.19	6.25	0.90	6.25	1.51	6.25	2.46	6.25	1.59
6.5	0.19	6.5	0.87	6.5	0.85	6.5	1.09	6.5	0.80	6.5	1.41	6.5	2.46	6.5	1.89
6.75	0.29	6.75	0.97	6.75	0.95	6.75	1.48	6.75	0.80	6.75	1.31	6.75	2.56	6.75	2.09
7	0.29	7	0.97	7	1.14	7	1.68	7	0.80	7	1.20	7	2.66	7	2.39
7.25	0.29	7.25	1.07	7.25	1.23	7.25	1.88	7.25	0.80	7.25	1.31	7.25	2.87	7.25	2.69
7.5	0.29	7.5	1.26	7.5	1.23	7.5	1.88	7.5	0.90	7.5	1.41	7.5	3.18	7.5	2.89
7.75	0.38	7.75	1.36	7.75	1.33	7.75	1.78	7.75	1.10	7.75	1.51	7.75	3.28	7.75	2.89
8	0.58	8	1.46	8	1.61	8	2.08	8	1.30	8	1.71	8	3.38	8	2.89
8.25	0.86	8.25	1.55	8.25	1.71	8.25	2.27	8.25	1.40	8.25	1.81	8.25	3.48	8.25	2.98
8.5	0.96	8.5	1.55	8.5	1.52	8.5	2.08	8.5	1.30	8.5	1.81	8.5	3.38	8.5	2.98
8.75	0.96	8.75	1.46	8.75	1.52	8.75	1.98	8.75	1.30	8.75	1.71	8.75	3.28	8.75	2.98
9	0.96	9	1.36	9	1.61	9	1.98	9	1.40	9	1.51	9	3.18	9	2.89
9.25	0.96	9.25	1.36	9.25	1.61	9.25	1.78	9.25	1.60	9.25	1.61	9.25	3.18	9.25	2.79
9.5	1.05	9.5	1.26	9.5	1.42	9.5	1.78	9.5	1.70	9.5	1.71	9.5	2.97	9.5	2.59
9.75	1.15	9.75	1.16	9.75	1.23	9.75	2.27	9.75	1.80	9.75	1.71	9.75	2.87	9.75	2.69
10	1.34	10	1.07	10	1.23	10	2.47	10	1.70	10	1.61	10	2.77	10	2.79
10.25	1.53	10.25	1.16	10.25	1.42	10.25	2.87	10.25	1.90	10.25	1.81	10.25	2.97	10.25	2.89
10.5	1.53	10.5	1.16	10.5	1.42	10.5	2.87	10.5	2.00	10.5	1.81	10.5	2.87	10.5	2.69
10.75	1.44	10.75	1.07	10.75	1.42	10.75	2.97	10.75	2.00	10.75	1.81	10.75	2.97	10.75	2.79
11	1.25	11	0.97	11	1.33	11	3.07	11	2.00	11	1.71	11	2.97	11	3.08
11.25	1.34	11.25	0.97	11.25	1.42	11.25	3.36	11.25	2.10	11.25	1.91	11.25	3.28	11.25	3.78
11.5	1.34	11.5	0.78	11.5	1.23	11.5	3.26	11.5	1.80	11.5	1.81	11.5	2.97	11.5	3.78
11.75	2.01	11.75	0.68	11.75	1.52	11.75	4.25	11.75	2.10	11.75	2.01	11.75	3.58	11.75	4.88
12	1.92	12	0.58	12	1.33	12	3.36	12	1.60	12	1.51	12	0.00	12	3.88
<12	72.98	<12	68.52	<12	60.44	<12	39.26	<12	29.86	<12	18.88	<12	0.00	<12	20.50

Table C-1. Detailed sedigraph data.

Core 926								Core 8826							
2-4 cm		13-15 cm		25-27 cm		44-46 cm		2-4 cm		13-15 cm		25-27 cm		44-46 cm	
phi size	%freq	phi size	%freq	phi size	%freq	phi size	%freq	phi size	%freq	phi size	%freq	phi size	%freq	phi size	%freq
-1	2.85	-1	3.07	-1	0.73	-1	3.28	-1	0.66	-1	0.19	-1	0.12	-1	0.06
-0.75	0.29	-0.75	0.19	-0.75	0.12	-0.75	0.00	-0.75	0.00	-0.75	0.00	-0.75	0.01	-0.75	0.00
-0.5	0.00	-0.5	0.18	-0.5	0.03	-0.5	0.00	-0.5	0.00	-0.5	0.00	-0.5	0.00	-0.5	0.00
-0.25	1.70	-0.25	0.38	-0.25	0.00	-0.25	0.00	-0.25	0.17	-0.25	0.00	-0.25	0.00	-0.25	0.00
0	0.00	0	0.00	0	0.00	0	0.00	0	0.06	0	0.02	0	0.00	0	0.02
0.25	0.03	0.25	0.29	0.25	0.95	0.25	0.25	0.25	0.03	0.25	0.00	0.25	0.00	0.25	0.11
0.5	0.12	0.5	1.79	0.5	0.22	0.5	0.54	0.5	0.00	0.5	0.00	0.5	0.00	0.5	0.00
0.75	0.60	0.75	0.59	0.75	0.32	0.75	0.02	0.75	0.00	0.75	0.00	0.75	0.04	0.75	0.00
1	1.40	1	0.46	1	0.20	1	0.00	1	0.00	1	0.02	1	0.02	1	0.00
1.25	0.89	1.25	0.37	1.25	0.92	1.25	0.00	1.25	0.18	1.25	0.08	1.25	0.00	1.25	0.02
1.5	2.41	1.5	0.07	1.5	0.00	1.5	0.08	1.5	0.21	1.5	0.01	1.5	0.01	1.5	0.05
1.75	0.00	1.75	0.27	1.75	0.00	1.75	0.00	1.75	0.00	1.75	0.18	1.75	0.10	1.75	0.01
2	1.36	2	0.00	2	0.33	2	0.17	2	0.13	2	0.03	2	0.00	2	0.02
2.25	1.54	2.25	0.53	2.25	1.05	2.25	0.41	2.25	0.00	2.25	0.12	2.25	0.02	2.25	0.10
2.5	2.97	2.5	4.17	2.5	3.40	2.5	1.75	2.5	0.16	2.5	0.12	2.5	0.04	2.5	0.00
2.75	5.02	2.75	7.73	2.75	6.84	2.75	5.67	2.75	1.26	2.75	0.43	2.75	0.30	2.75	0.16
3	12.75	3	12.29	3	7.95	3	8.36	3	1.87	3	0.60	3	0.69	3	0.14
3.25	10.70	3.25	8.93	3.25	7.41	3.25	7.18	3.25	2.34	3.25	1.37	3.25	0.81	3.25	0.39
3.5	6.07	3.5	7.13	3.5	5.50	3.5	4.16	3.5	1.17	3.5	0.91	3.5	0.63	3.5	0.20
3.75	4.69	3.75	6.50	3.75	3.88	3.75	3.33	3.75	1.12	3.75	0.71	3.75	0.46	3.75	0.30
4	2.91	4	3.93	4	3.93	4	2.64	4	2.05	4	1.13	4	0.64	4	0.32
4.25	3.09	4.25	3.87	4.25	3.21	4.25	2.58	4.25	1.63	4.25	1.28	4.25	0.54	4.25	0.41
4.5	1.22	4.5	3.06	4.5	2.42	4.5	2.11	4.5	2.03	4.5	0.84	4.5	0.29	4.5	0.52
4.75	3.07	4.75	2.47	4.75	3.03	4.75	2.10	4.75	1.70	4.75	0.51	4.75	0.40	4.75	0.75
5	3.98	5	0.72	5	0.79	5	2.51	5	3.50	5	0.73	5	0.59	5	0.86
5.25	0.00	5.25	0.00	5.25	0.10	5.25	0.30	5.25	3.13	5.25	0.79	5.25	0.70	5.25	0.79
5.5	0.00	5.5	0.10	5.5	0.10	5.5	0.50	5.5	2.73	5.5	1.09	5.5	1.00	5.5	0.99
5.75	0.00	5.75	0.20	5.75	0.20	5.75	0.50	5.75	2.12	5.75	1.29	5.75	1.19	5.75	1.19
6	0.00	6	0.10	6	0.30	6	0.50	6	1.41	6	1.39	6	1.49	6	1.29
6.25	0.00	6.25	0.10	6.25	0.40	6.25	0.60	6.25	1.21	6.25	1.49	6.25	1.79	6.25	1.29
6.5	0.00	6.5	0.20	6.5	0.40	6.5	0.70	6.5	1.31	6.5	1.69	6.5	1.79	6.5	1.29
6.75	0.00	6.75	0.20	6.75	0.50	6.75	0.81	6.75	1.52	6.75	1.88	6.75	1.69	6.75	1.39
7	0.10	7	0.30	7	0.50	7	0.70	7	1.52	7	1.98	7	1.69	7	1.59
7.25	0.00	7.25	0.20	7.25	0.70	7.25	0.70	7.25	1.52	7.25	1.88	7.25	1.89	7.25	2.09
7.5	0.00	7.5	0.20	7.5	0.80	7.5	0.81	7.5	1.52	7.5	1.98	7.5	2.09	7.5	2.68
7.75	0.00	7.75	0.20	7.75	0.90	7.75	0.81	7.75	1.62	7.75	2.08	7.75	2.19	7.75	2.78
8	0.10	8	0.20	8	1.00	8	0.81	8	1.62	8	2.28	8	2.39	8	2.68
8.25	0.10	8.25	0.20	8.25	1.20	8.25	0.81	8.25	1.52	8.25	2.28	8.25	2.69	8.25	2.78
8.5	0.00	8.5	0.20	8.5	1.20	8.5	0.91	8.5	1.41	8.5	1.98	8.5	2.69	8.5	2.78
8.75	0.10	8.75	0.20	8.75	1.20	8.75	0.81	8.75	1.31	8.75	1.88	8.75	2.59	8.75	2.78
9	0.10	9	0.10	9	1.10	9	0.70	9	1.21	9	1.69	9	2.39	9	2.68
9.25	0.10	9.25	0.10	9.25	1.00	9.25	0.60	9.25	1.21	9.25	1.69	9.25	2.29	9.25	2.48
9.5	0.10	9.5	0.10	9.5	0.90	9.5	0.60	9.5	1.11	9.5	1.69	9.5	2.29	9.5	2.19
9.75	0.00	9.75	0.10	9.75	0.80	9.75	0.50	9.75	1.01	9.75	1.69	9.75	2.19	9.75	2.19
10	0.00	10	0.10	10	0.70	10	0.50	10	1.11	10	1.59	10	2.09	10	2.19
10.25	0.10	10.25	0.10	10.25	0.60	10.25	0.50	10.25	1.41	10.25	1.78	10.25	2.19	10.25	2.38
10.5	0.10	10.5	0.10	10.5	0.40	10.5	0.50	10.5	1.41	10.5	1.49	10.5	2.09	10.5	2.48
10.75	0.10	10.75	0.10	10.75	0.40	10.75	0.50	10.75	1.31	10.75	1.39	10.75	2.09	10.75	2.48
11	0.10	11	0.10	11	0.40	11	0.40	11	1.31	11	1.49	11	2.19	11	2.38
11.25	0.10	11.25	0.10	11.25	0.40	11.25	0.30	11.25	1.52	11.25	1.98	11.25	2.69	11.25	2.88
11.5	0.10	11.5	0.00	11.5	0.20	11.5	0.30	11.5	1.62	11.5	2.18	11.5	2.79	11.5	3.38
11.75	0.10	11.75	0.10	11.75	0.20	11.75	0.30	11.75	2.43	11.75	2.88	11.75	3.98	11.75	4.97
12	0.00	12	0.30	12	0.10	12	0.10	12	2.22	12	2.48	12	3.58	12	4.07
<12	28.94	<12	26.95	<12	30.12	<12	36.75	<12	35.37	<12	40.75	<12	33.55	<12	30.40

Table C-1. Detailed sedigraph data.

Core 142

2-4 cm		13-15 cm		25-27 cm		44-46 cm	
phi size	%freq	phi size	%freq	phi size	%freq	phi size	%freq
-1	1.51	-1	0.18	-1	0.00	-1	0.79
-0.75	0.00	-0.75	0.00	-0.75	0.00	-0.75	0.02
-0.5	0.00	-0.5	0.00	-0.5	0.00	-0.5	0.07
-0.25	0.28	-0.25	0.00	-0.25	0.02	-0.25	0.06
0	0.15	0	0.00	0	0.01	0	0.01
0.25	0.01	0.25	0.00	0.25	0.01	0.25	0.00
0.5	0.00	0.5	0.00	0.5	0.02	0.5	0.01
0.75	0.00	0.75	0.00	0.75	0.02	0.75	0.00
1	0.00	1	0.03	1	0.01	1	0.00
1.25	0.05	1.25	0.09	1.25	0.12	1.25	0.16
1.5	0.00	1.5	0.02	1.5	0.17	1.5	0.01
1.75	0.06	1.75	0.01	1.75	0.08	1.75	0.22
2	0.00	2	0.00	2	0.00	2	0.04
2.25	0.00	2.25	0.02	2.25	0.01	2.25	0.17
2.5	0.49	2.5	0.31	2.5	0.11	2.5	0.28
2.75	2.34	2.75	0.74	2.75	0.37	2.75	1.59
3	3.61	3	0.86	3	0.49	3	2.23
3.25	3.08	3.25	0.88	3.25	0.56	3.25	2.89
3.5	2.26	3.5	0.64	3.5	0.37	3.5	1.27
3.75	2.05	3.75	0.39	3.75	0.30	3.75	1.01
4	0.87	4	0.97	4	0.46	4	1.40
4.25	1.07	4.25	0.96	4.25	0.55	4.25	1.39
4.5	1.48	4.5	0.54	4.5	0.46	4.5	1.31
4.75	0.99	4.75	0.37	4.75	0.43	4.75	0.78
5	1.38	5	0.37	5	0.35	5	0.58
5.25	0.60	5.25	0.40	5.25	0.20	5.25	0.34
5.5	0.79	5.5	0.30	5.5	0.50	5.5	0.42
5.75	0.69	5.75	0.10	5.75	0.60	5.75	0.68
6	0.60	6	0.30	6	0.60	6	0.76
6.25	0.79	6.25	0.69	6.25	0.60	6.25	0.93
6.5	0.99	6.5	0.79	6.5	0.80	6.5	1.10
6.75	0.99	6.75	0.79	6.75	1.00	6.75	1.35
7	0.99	7	0.89	7	1.40	7	1.61
7.25	1.09	7.25	1.09	7.25	1.89	7.25	1.69
7.5	1.19	7.5	1.29	7.5	2.09	7.5	1.86
7.75	1.49	7.75	1.39	7.75	1.79	7.75	2.03
8	1.79	8	1.49	8	1.99	8	2.20
8.25	1.79	8.25	1.59	8.25	2.39	8.25	2.12
8.5	1.39	8.5	1.39	8.5	2.39	8.5	1.86
8.75	1.29	8.75	1.19	8.75	2.19	8.75	1.69
9	1.29	9	1.19	9	1.79	9	1.52
9.25	1.19	9.25	1.29	9.25	1.60	9.25	1.44
9.5	1.09	9.5	1.19	9.5	1.60	9.5	1.35
9.75	1.19	9.75	1.39	9.75	1.69	9.75	1.27
10	1.09	10	1.39	10	1.60	10	1.18
10.25	1.09	10.25	1.39	10.25	1.60	10.25	1.18
10.5	1.29	10.5	1.19	10.5	1.30	10.5	1.18
10.75	1.29	10.75	1.09	10.75	1.10	10.75	1.02
11	1.09	11	1.19	11	1.00	11	0.93
11.25	1.09	11.25	1.29	11.25	1.10	11.25	1.18
11.5	1.09	11.5	1.09	11.5	1.10	11.5	1.18
11.75	1.59	11.75	1.59	11.75	1.40	11.75	1.35
12	1.49	12	1.78	12	1.10	12	0.68
<12	45.97	<12	61.87	<12	56.72	<12	47.63

Table C-2. Graphic mean and Inclusive Standard Deviation Results.

Station	Depth	Graphic Mean	Graphic Standard Deviation	Station	Depth	Graphic Mean	Graphic Standard Deviation
Core 128	1-3	--	--	**Core 924**	2-4	8.15	5.18
	8-10	6.38	3.19		13-15	8.83	3.86
	48-50	6.06	3.86		25-27	8.73	3.97
					45-46	7.87	4.19
Core 134	20-22	10.27	1.91				
	57-59	9.76	2.16	**Core 8271**	2-4	11.93	1.62
					13-15	11.38	2.2
Core 201	5-7	5.45	3.4		25-27	11.22	2.49
	12-14	4.83	3.12		44-46	10.68	2.24
	57-59	6	3.7				
				Core 928	2-4	7.52	4.13
Core 285	2-4	10.95	2.02		13-15	8.38	3.96
	20-22	10.12	2.76		25-27	7.57	3.45
	72-74	10.98	2.4		44-46	7.62	3.69
Core 286	2-4	7.35	2.27	**Core 8827**	2-4	7.05	5.56
	18-20	9.23	2.45		13-15	6.58	5.56
	23-25	9.07	2.5		25-27	7.4	3.04
	66-68	9.24	2.33		44-46	9.82	2.71
Core 296	7-8	8.47	3.39	**Core 926**	2-4	6.3	4.45
	25-26	8.01	3.93		13-15	6.38	4.45
	35-36	9.8	2.54		25-27	6.72	4.11
	70-72	7.37	3.49		45-46	7.4	4.1
Core 300	2-4	10.37	2.69	**Core 142**	2-4	9.37	3.78
	13-15	10.26	2.13		13-15	11.03	2.6
	25-27	7.98	3.67		25-27	10.95	2.48
	56-58	7.66	3.85		44-46	9.81	3.47
Core 4293	2-4	8.23	3.61	**Core 8826**	2-4	9.03	3.53
	13-15	9.55	2.88		13-15	9.82	2.97
	25-27	7.93	3.63		25-27	9.98	3.58
	56-58	6.45	4.04		44-46	10.25	2.52
CN26 grab		5.93	3.36				
S. Dredge Is. grab		5.68	3.96				
L. River Delta		5.74	4.15				
Y channel grab		10.78	1.72				

Table C-3. Radioisotope Analyses - Raw Data

Station 128

SAMPLE	DATE COUNTED	POROSITY	^{137}Cs (dpm/Kg)	ERROR	$^{210}Pb(\gamma)$ (dpm/Kg)	ERROR	^{226}Ra (dpm/Kg)	ERROR	^{7}Be (dpm/Kg)	ERROR
0-1cm	1/25/97	0.843	242.7	35.6	2999.0	299.1	1386.4	76.6	1140.4	284.1
1-2cm	1/26/97	0.774	224.8	36.6	2978.0	321.8	1320.8	79.6	888.4	262.6
2-3cm	1/27/97	0.683	176.1	33.2	2194.1	284.1	1449.8	76.0	613.6	215.4
3-4cm	1/28/97	0.697	205.8	28.8	3042.4	306.7	1242.3	65.7	375.0	196.6
4-5cm	1/29/97	0.672	138.7	28.9	2180.3	299.5	1252.1	64.1	BDL	
5-10cm	1/30/97	0.622	124.8	26.3	1554.1	276.9	1282.1	66.0	BDL	
10-15cm	1/31/97	0.579	202.7	26.9	1210.0	242.0	1098.4	59.0	BDL	
15-20cm	2/14/97	0.537	124.0	20.1	1125.9	190.7	991.7	45.7	BDL	
20-25cm	3/22/97	0.618	234.3	36.1	1773.3	285.2	1453.5	73.8	BDL	
25-30cm	3/20/97	0.652	380.8	39.7	2109.9	307.0	972.1	72.5	BDL	
25-30cm	2/16/97	0.652	378.2	36.9	1370.5	245.1	1061.8	67.8	BDL	
30-35cm	2/20/97	0.498	122.5	24.5	1143.1	259.4	1054.7	66.2	BDL	
35-40cm	2/17/97	0.456	72.1	24.6	1087.0	215.1	1080.1	62.7	BDL	
40-45cm	2/21/97	0.438	109.7	26.6	1592.6	287.4	1050.1	75.4	BDL	
45-50cm	2/18/97	0.464	34.7	24.2	1048.0	217.8	1054.2	62.4	BDL	
50-60cm		0.526								

BDL= below detection limit

Station 128B

SAMPLE	DATE COUNTED	POROSITY	^{137}Cs (dpm/Kg)	ERROR	$^{210}Pb(\gamma)$ (dpm/Kg)	ERROR	^{226}Ra (dpm/Kg)	ERROR	^{7}Be (dpm/Kg)	ERROR
0-1CM	8/11/97	0.889	283.2	41.5	2997.4	344.4	1108.9	74.4	1128.4	133.1
1-2CM	8/10/97	0.841	304.8	37.0	2534.0	293.7	1074.2	70.5	1298.3	129.7
2-3CM	8/12/97	0.806	330.5	34.5	1851.3	292.3	1138.1	66.9	895.4	112.7
3-4CM	8/14/97	0.795	242.3	36.8	3128.9	287.4	848.3	67.9	1250.9	261.9
4-5CM	8/18/97	0.775	359.2	36.7	2721.7	267.3	1265.6	68.3	413.2	101.4
5-6CM	8/19/97	0.750	323.6	36.6	2151.3	335.8	1227.4	76.7	234.9	95.7
6-7CM	8/20/97	0.693	146.0	58.0	2454.3	292.6	1320.3	70.2	BDL	
7-8CM		0.677								
8-9CM		0.656								
9-10CM		0.661								

BDL= below detection limit

Table C-3. Radioisotope Analyses - Raw Data

Station 134

SAMPLE	DATE COUNTED	POROSITY	^{137}Cs (dpm/Kg)	ERROR	$^{210}Pb(\gamma)$ (dpm/Kg)	ERROR	^{226}Ra (dpm/Kg)	ERROR	^{7}Be (dpm/Kg)	ERROR
0-1cm	2/25/97	0.882	354.4	49.0	4125.7	441.9	1571.5	107.9	8054.6	508.1
1-2cm	2/26/97	0.759	289.8	37.3	3080.7	293.1	1249.3	69.2	1561.0	240.5
2-3cm	3/3/97	0.647	144.0	38.4	2356.8	390.0	1699.8	89.8		
3-4cm	3/4/97	0.690	202.8	30.7	2435.3	315.8	1311.4	71.0		
4-5cm	3/5/97	0.719	309.2	46.1	2317.3	361.7	1336.3	89.9		
7-8cm		0.718								
9-10cm	3/6/97	0.737	385.5	44.4	1557.4	316.0	1093.8	74.5		
12-13cm		0.733								
15-16cm		0.704								

Table C-3. Radioisotope Analyses - Raw Data

Station 134

SAMPLE	DATE COUNTED	POROSITY	^{137}Cs (dpm/Kg)	ERROR	$^{210}Pb(\gamma)$ (dpm/Kg)	ERROR	^{226}Ra (dpm/Kg)	ERROR	^{7}BE (dpm/Kg)	ERROR	^{210}PB-(α) (dpm/Kg)	ERROR	$^{239,240}Pu$ (dpm/Kg)	ERROR
0-1cm	2/25/97	0.882	354.4	49.0	4125.7	441.9	1571.5	107.9	8054.6	508.1	3001.3	171.4	4.2	1.0
0-2cm											3638.8	148.8		
1-2cm	2/26/97	0.759	289.8	37.3	3080.7	293.1	1249.3	69.2	1561.0	240.5				
2-3cm	3/3/97	0.647	144.0	38.4	2356.8	390.0	1699.8	89.8	BDL					
2-3cm	4/15/97	0.647	217.7	33.6	2136.7	316.8	1548.1	77.4	BDL					
3-4cm	3/4/97	0.690	202.8	30.7	2435.3	315.8	1311.4	71.0	BDL					
4-5cm	3/5/97	0.719	309.2	46.1	2317.3	361.7	1336.3	89.9	BDL		3306.9	166.5		
5-6cm		0.719												
6-7cm		0.705												
7-8cm	3/24/97	0.718	355.7	34.4	1808.1	319.3	1291.9	74.2	BDL					
8-9cm		0.694											7.2	1.1
9-10cm	3/6/97	0.737	385.5	44.4	1557.4	316.0	1093.8	74.5	BDL		3087.6	235.4		
10-11cm		0.750												
11-12cm		0.751												
12-13cm	3/24/97	0.733	650.1	50.6	1408.1	329.6	1291.4	81.7	BDL		2483.1	180.9	11.6	1.2
13-14cm		0.735												
14-15cm	4/6/97	0.728	790.7	42.9	1859.4	303.2	1245.4	65.2	BDL		2341.6	178.9	13.8	1.2
14-15cm	4/14/97	0.728	809.7	45.0	1259.9	281.9	1483.9	71.3	BDL					
15-16cm	3/31/97	0.704	856.7	51.1	1767.4	286.1	1416.5	75.7	BDL		2037.6	263.7	20.7	3.0
16-17cm		0.719												
17-18cm	4/17/97	0.729	697.2	44.4	2139.9	296.6	1181.9	66.5	BDL					
18-19cm	4/3/97	0.732	668.6	41.8	1236.4	301.0	1069.5	67.7	BDL		1781.9	226.2	25.9	2.0
18-19cm		0.732											35.0	8.1
19-20cm		0.737												
20-21cm	4/1/97	0.705	383.3	41.7	982.7	285.0	1483.4	74.8	BDL		2113.5	273.5	15.6	1.6
21-22cm		0.616												
22-23cm	4/3/97	0.607	125.6	36.4	2163.2	267.9	1334.4	72.7	BDL		1545.2	144.7	5.4	0.9
23-24cm		0.592												
24-25cm		0.657												
25-26cm	4/2/97	0.684	92.7	32.2	1130.8	267.3	1129.5	66.5	BDL		1778.9	110.9	2.4	0.6
26-27cm	4/21/97	0.713	97.5	28.4	1471.5	307.6	1002.5	68.0	BDL					
27-28cm	4/18/97	0.729	111.1	28.4	817.7	253.0	976.0	67.8	BDL					
28-29cm	4/19/97	0.736	0.0	0.0	1268.6	186.1	1202.9	49.9	BDL					
29-30cm		0.742												
30-31cm	4/2/97	0.755	0.0	0.0	2167.4	273.6	1415.7	72.3	BDL		1577.7	141.1	0.0	0.0
30-31cm		0.755									1989.7	114.3		
31-32cm		0.751												
32-33cm		0.745												
33-34cm		0.765												
34-35cm		0.757												
35-36cm	4/7/97	0.758	0	0	1028.2	265.7	1264.6	78.4	BDL		1510.0	74.0		
36-37cm		0.672												
37-38cm		0.671												
38-39cm		0.689												
39-40cm		0.724												
40-41cm	4/8/97	0.725	0.0	0.0	1867.4	284.1	1170.0	78.7	BDL		2105.4	134.3		
41-42cm		0.714												
42-43cm		0.719												
43-44cm		0.743												
44-45cm		0.733												
45-46cm	4/9/97	0.692	0.0	0.0	1703.4	252.2	1279.1	70.8	BDL		1778.2	98.8		
46-47cm		0.727												
47-48cm		0.756												
48-49cm		0.742												
49-50cm		0.747												
50-51cm	11/15/97	0.669	49.4	22.1	1236.7	240.3	1310.0	68.5	BDL		1634.6	95.9		
51-52cm		0.739												
52-53cm		0.728												
53-54cm		0.751												
54-55cm		0.748												
55-56cm	11/14/97	0.730	3.2	19.3	1345.1	262.3	1120.5	61.5	BDL		1655.9	98.4		
56-57cm		0.696												
57-58cm		0.722												
58-59cm		0.731												
59-60cm		0.725												
60-61cm	11/13/97	0.708	38.7	19.3	1431.1	241.0	1440.3	63.4	BDL		1600.4	89.4		

BDL= below detection limit

Table C-3. Radioisotope Analyses - Raw Data

Station 142

SAMPLE	DATE COUNTED	POROSITY	^{137}Cs (dpm/Kg)	ERROR	$^{210}Pb(\gamma)$ (dpm/Kg)	ERROR	^{226}Ra (dpm/Kg)	ERROR	^{7}Be (dpm/Kg)	ERROR
0-1cm	10/13/97	0.757	254.3	33.5	3151.4	305.8	1362.4	71.2	1144.7	243.4
1-2cm	10/14/97	0.722	237.1	35.7	1888.7	285.6	1008.6	73.9	626.0	226.4
2-3cm	10/14/97	0.725	322.8	33.2	1992.6	316.0	1096.7	64.2	635.1	204.9
3-4cm	10/15/97	0.736	503.6	39.5	1523.4	278.3	1102.5	66.3	BDL	
4-5cm	10/16/97	0.746	496.0	36.2	1714.7	291.3	1246.4	68.0	BDL	
5-6cm		0.756								
6-7cm	10/24/97	0.755	536.3	43.2	1719.2	355.1	1076.0	75.6	BDL	
7-8cm		0.755								
8-9cm	11/1/97	0.760	538.4	39.5	1535.3	326.5	1217.0	70.5	BDL	
9-10cm	10/18/97	0.732	810.2	43.4	1327.4	265.6	1091.9	62.1	BDL	
10-11cm		0.734								
11-12cm	10/28/97	0.755	674.0	52.9	1151.3	296.4	1025.6	75.3	BDL	
12-13cm		0.748								
13-14cm		0.741								
14-15cm	10/19/97	0.759	742.9	48.9	2304.9	338.4	1180.5	72.6	BDL	
15-16cm		0.758								
16-17cm	11/2/97	0.744	626.5	46.7	1193.6	309.8	1056.4	74.2	BDL	
17-18cm		0.688								
18-19cm		0.734	538.4	39.5	1535.3	326.5	1217.0	70.5	BDL	
19-20cm	10/27/97	0.716	155.0	38.1	1646.7	348.1	1140.0	82.8	BDL	
20-21cm		0.703								
21-22cm		0.669								
22-23cm	11/3/97	0.721	108.5	32.0	1086.3	331.8	1185.0	76.8	BDL	
23-24cm		0.735								
24-25cm	10/21/97	0.708	94.1	29.4	1576.1	316.5	1097.9	73.6	BDL	
25-26cm		0.740								
26-27cm		0.752								
27-28cm		0.757								
28-29cm		0.752								
29-30cm	11/3/97	0.749	72.9	30.2	976.8	327.6	1290.4	75.6	BDL	
30-31cm		0.746								
31-32cm		0.685								
32-33cm		0.714								
33-34cm		0.726								
34-35cm		0.725								
35-36cm		0.720								
36-37cm		0.707								
37-38cm		0.714								
38-39cm		0.721								
39-40cm		0.728								
40-41cm		0.736								
41-42cm		0.697								
42-43cm		0.715								
43-44cm		0.744								
44-45cm		0.746								
45-46cm		0.742								
46-47cm		0.752								
47-48cm		0.750								
48-49cm		0.746								
49-50cm		0.759								
50-51cm		0.743								
51-52cm		0.755								
52-53cm		0.751								
53-54cm		0.760								
54-55cm		0.731								
55-56cm		0.618								
56-57cm		0.599								
57-58cm		0.583								
58-59cm		0.655								
59-60cm		0.700								
60-61cm		0.671								

BDL= below detection limit

Table C-3. Radioisotope Analyses - Raw Data

Station 201

SAMPLE	DATE COUNTED	POROSITY	^{137}Cs (dpm/Kg)	ERROR	$^{210}Pb(\gamma)$ (dpm/Kg)	ERROR	^{226}Ra (dpm/Kg)	ERROR	^{7}Be (dpm/Kg)	ERROR	$^{210}PB\text{-}(\alpha)$ (dpm/Kg)	ERROR	$^{239,240}Pu$ (dpm/Kg)	ERROR
0-1cm	2/1/97	0.625	62.6	23.0	2396.4	308.2	1290.1	69.5	1320.0	238.5	1764.1	112.4	1.3	0.5
1-2cm	2/2/97	0.494	107.7	32.2	1456.3	306.1	1415.0	82.9	309.5	152.6				
2-3cm	2/3/97	0.427	41.1	20.7	1122.4	222.5	1436.1	65.9	BDL					
3-4cm	2/4/97	0.392	59.4	21.7	1221.7	284.5	1300.1	67.8	BDL					
4-5cm	2/5/97	0.391	19.4	13.4	1501.4	246.6	1271.6	62.0	BDL					
4-5cm	4/13/97	0.391	57.8	26.5	1153.5	285.3	1185.4	72.6	BDL					
5-6cm		0.451												
6-7cm		0.455												
7-8cm		0.446												
8-9cm		0.449												
9-10cm	2/6/97	0.449	68.3	20.2	1102.3	222.2	1201.3	71.2	BDL		1439.9	127.0	0.8	0.3
10-11cm		0.458												
11-12cm		0.448												
12-13cm		0.449												
13-14cm		0.446												
14-15cm		0.449												
15-16cm		0.464												
16-17cm		0.503												
17-18cm		0.547												
18-19cm		0.474												
19-20cm	2/7/97	0.451	102.2	23.4	1036.6	215.9	1078.2	60.3	BDL		1260.3	93.7	2.2	0.6
20-21cm		0.435												
21-22cm		0.426												
22-23cm		0.416												
23-24cm		0.432												
24-25cm	4/10/97	0.465	109.8	27.4	1037.1	224.6	1301.8	66.6	BDL					
25-26cm		0.474												
26-27cm		0.449												
27-28cm		0.501												
28-29cm		0.559												
29-30cm	2/10/97	0.592	188.7	30.1	1173.0	273.2	1676.6	74.8	BDL		1840.0	181.5	4.7	1.6
29-30cm		0.592									1882.1	103.6		
30-31cm		0.613												
31-32cm		0.546												
32-33cm	3/23/97	0.544	179.3	38.5	1219.9	312.6	1365.9	86.8	BDL		1451.5	115.5	7.0	1.1
32-33cm		0.544											4.7	2.1
33-34cm		0.550												
34-35cm	2/19/97	0.564	229.1	32.6	1655.8	291.7	1178.4	70.2	BDL		1378.3	101.2	4.5	0.9
34-35cm	4/11/97	0.564	231.8	34.2	1301.0	321.9	1438.9	73.5	BDL					
35-36cm		0.544												
36-37cm	3/23/97	0.532	172.1	37.6	1702.7	345.0	1418.7	83.9	BDL		1314.7	147.5	2.5	0.7
37-38cm		0.540												
38-39cm		0.511												
39-40cm	2/11/97	0.536	177.2	30.5	1000.2	250.7	1165.3	69.1	BDL		1279.5	105.6	4.2	1.3
40-41cm		0.487												
41-42cm		0.507												
42-43cm		0.527												
43-44cm		0.556												
44-45cm		0.521												
45-46cm		0.513												
46-47cm		0.498												
47-48cm		0.441												
48-49cm		0.442												
49-50cm	2/12/97	0.438	158.6	26.2	783.4	222.3	1119.3	59.4	BDL		1371.4	149.6	1.9	0.3
49-50cm		0.438									1354.7	93.5		
50-51cm		0.380												
51-52cm		0.393												
52-53cm		0.434												
53-54cm		0.417												
54-55cm		0.398												
55-56cm		0.390												
56-57cm		0.382												
57-58cm		0.418												
58-59cm		0.382												
59-60cm	2/13/97	0.407	67.8	22.5	1510.5	265.9	1152.8	66.0	BDL					
60-61cm	4/12/97	0.454	73.5	21.9	1295.0	257.5	1196.8	60.1	BDL		982.2	137.4	1.6	0.4

BDL= below detection limit

Table C-3. Radioisotope Analyses - Raw Data

Station 285

SAMPLE	DATE COUNTED	POROSITY	^{137}Cs (dpm/Kg)	ERROR	$^{210}Pb(\gamma)$ (dpm/Kg)	ERROR	^{226}Ra (dpm/Kg)	ERROR	^{7}Be (dpm/Kg)	ERROR	^{210}PB-(α) (dpm/Kg)	ERROR	^{210}PB-(α) $(dpm/Kg)_{repeat}$	ERROR
0-1cm	4/23/97	0.794	274.2	31.0	2604.5	310.5	1205.5	66.8	1674.7	116.5	4026.3	269.5	3558.4	153.9
1-2cm	4/24/97	0.847	283.1	52.6	3763.5	447.5	1164.3	96.6	2877.8	342.1				
2-3cm	4/25/97	0.829	407.6	40.4	3872.6	347.0	1406.2	78.8	756.8	109.4				
3-4cm	4/26/97	0.720	327.8	37.7	3719.9	358.6	1446.5	78.8	203.3	74.5	3356.3	269.9	3204.8	180.6
4-5cm	4/27/97	0.789	508.1	49.3	4505.7	482.4	1337.0	95.8	121.9	95.8				
5-6cm		0.793												
6-7cm		0.793									3256.5	254.7	3687.1	195.7
7-8cm	5/6/97	0.798	314.9	38.0	3123.1	318.8	1367.2	75.1	206.6	102.8				
7-8cm	5/17/97	0.798	377.2	31.1	3747.8	235.3	1198.0	60.3	BDL					
8-9cm		0.786												
9-10cm	4/28/97	0.795	365.6	28.0	2406.6	238.0	1056.8	50.7	BDL		3874.4	350.1	3879.2	174.6
10-11cm		0.785												
11-12cm		0.775												
12-13cm		0.774									3189.3	322.4	3063.6	162.8
13-14cm		0.744												
14-15cm		0.739												
15-16cm		0.750									3500.1	242.4	3206.2	203.4
15-16cm											3086.2	215.4	3428.8	144.3
16-17cm		0.761												
17-18cm		0.756												
18-19cm		0.735									3021.3	203.5	2889.3	188.6
19-20cm	4/30/97	0.756	463.6	40.7	2973.3	319.0	1101.8	71.0	BDL					
20-21cm		0.749												
21-22cm		0.748									3485.5	188.2	3140.3	116.0
22-23cm		0.752												
23-24cm		0.749												
24-25cm		0.751									3283.0	253.7	2793.6	156.6
25-26cm		0.756												
26-27cm		0.752												
27-28cm		0.768									3436.9	247.7	3115.3	152.5
28-29cm		0.761												
29-30cm	5/2/97	0.763	551.2	49.3	2633.0	349.0	1209.1	77.3	BDL					
30-31cm		0.669									2956.9	245.7	2796.3	152.5
31-32cm		0.710												
32-33cm		0.734												
33-34cm		0.730									2854.3	172.1	2691.2	115.3
34-35cm	5/14/97	0.745	549.8	46.6	2539.5	312.7	815.6	74.4	BDL					
35-36cm		0.753												
36-37cm		0.745									2545.3	285.3	3057.4	130.4
36-37cm											3188.7	233.9	3115.8	146.3
37-38cm		0.690												
38-39cm		0.728												
39-40cm	5/3/97	0.754	560.7	40.3	2179.7	299.1	1069.1	67.2	BDL		2810.4	203.5	2710.6	144.9
40-41cm		0.747												
41-42cm		0.743												
42-43cm		0.726									2356.4	174.9	2570.0	127.7
43-44cm		0.739												
44-45cm	5/12/97	0.754	623.1	44.3	1961.5	320.3	1197.8	70.0	BDL					
45-46cm		0.747									2648.5	210.7	2744.7	139.4
46-47cm		0.744												
47-48cm	5/16/97	0.688	490.5	38.6	1777.2	285.1	1244.6	71.7	BDL					
48-49cm		0.699									2119.3	167.4	2485.6	155.9
49-50cm	5/4/97	0.730	590.3	47.8	1780.6	304.9	1220.9	78.8	BDL					
50-51cm		0.717												
51-52cm		0.695									2584.1	182.3	2436.9	101.9
52-53cm	5/15/97	0.705	455.7	39.3	2036.3	313.4	1159.2	70.5	BDL					
52-53cm	9/2/97	0.705	514.4	40.9	2000.5	322.5	1422.4	72.5	BDL					
53-54cm		0.732												
54-55cm	5/9/97	0.746	429.0	35.6	1702.1	236.4	1163.0	66.4	BDL		2076.1	202.6	2003.1	235.0
55-56cm		0.694												
56-57cm		0.720												
57-58cm		0.711									1985.6	167.5	2588.4	161.9
57-58cm											2118.5	119.8	2095.1	130.2
58-59cm		0.686												
59-60cm	5/5/97	0.735	578.9	49.5	1596.9	333.6	1224.1	86.2	BDL					
60-61cm	5/8/97	0.752	646.2	50.3	2199.2	335.9	1334.1	82.4	BDL		1987.1	144.8	2333.9	142.1

BDL= below detection limit

Table C-3. Radioisotope Analyses - Raw Data

Staion 286

SAMPLE	DATE COUNTED	POROSITY	^{137}Cs (dpm/Kg)	ERROR	$^{210}Pb(\gamma)$ (dpm/Kg)	ERROR	^{226}Ra (dpm/Kg)	ERROR	^{7}Be (dpm/Kg)	ERROR
0-1cm	4/24/97	0.754	219.8	35.2	3196.0	339.5	1315.4	72.9	508.2	108.6
1-2cm	4/25/97	0.776	244.2	33.2	3158.4	309.3	1298.3	70.3	244.3	83.7
2-3cm	4/26/97	0.760	298.0	33.3	3079.0	340.6	1279.0	70.5	278.0	95.3
3-4cm	4/27/97	0.740	353.7	40.7	2363.4	356.6	1252.4	78.4	BDL	
4-5cm	4/28/97	0.738	332.4	24.2	1884.2	217.3	1465.3	54.9	BDL	
5-6cm		0.752								
6-7cm		0.742								
7-8cm	5/7/97	0.792	324.1	37.3	3614.0	293.9	1165.6	64.6	BDL	
8-9cm		0.811								
9-10cm	4/30/97	0.797	400.8	35.7	3480.6	322.8	930.1	68.0	BDL	
10-11cm		0.775								
11-12cm		0.783								
12-13cm		0.738								
13-14cm		0.729								
14-15cm	5/7/97	0.670	223.9	27.9	3140.7	307.2	1190.8	67.2	BDL	
15-16cm		0.643								
16-17cm		0.657								
17-18cm		0.663								
18-19cm		0.703								
19-20cm	5/1/97	0.588	148.2	29.5	1997.3	303.2	1586.4	73.8	BDL	
20-21cm		0.568								
21-22cm		0.563								
22-23cm		0.614								
23-24cm		0.605								
24-25cm		0.645								
25-26cm		0.653								
26-27cm		0.687								
27-28cm		0.703								
28-29cm		0.677								
29-30cm	5/3/97	0.658	227.6	25.2	1990.5	254.8	1309.8	59.8	BDL	
29-30cm	5/17/97	0.658	241.6	22.8	1728.3	210.0	1369.8	53.6	BDL	
30-31cm		0.655								
31-32cm		0.612								
32-33cm		0.643								
33-34cm		0.676								
34-35cm	5/8/97	0.703	227.3	33.7	2159.1	273.5	1263.4	73.6	BDL	
35-36cm		0.698								
36-37cm		0.670								
37-38cm		0.646								
38-39cm		0.640								
39-40cm	5/4/97	0.633	158.4	30.3	2042.3	279.0	1245.4	66.7	BDL	
40-41cm		0.638								
41-42cm		0.628								
42-43cm		0.641								
43-44cm		0.640								
44-45cm	5/14/97	0.626	181.0	32.0	2066.5	316.5	1288.5	67.7	BDL	
45-46cm		0.639								
46-47cm		0.625								
47-48cm		0.644								
48-49cm		0.655								
49-50cm	5/5/97	0.667	222.4	36.7	1767.2	323.2	1379.6	79.8	BDL	
50-51cm		0.663								
51-52cm		0.662								
52-53cm		0.677								
53-54cm		0.697								
54-55cm	5/12/97	0.630	179.8	33.2	2140.9	293.3	1444.3	66.7	BDL	
55-56cm		0.642								
56-57cm		0.645								
57-58cm	5/15/97	0.665	298.0	32.0	1482.4	294.0	1279.4	67.7	BDL	
58-59cm		0.682								
59-60cm	5/6/97	0.700	373.7	31.5	1615.7	246.7	1267.5	66.8	BDL	
59-60cm	5/16/97	0.700	284.6	31.4	2097.7	291.1	1294.3	64.3	BDL	
60-61cm	5/9/97	0.691	328.1	38.7	2271.4	297.0	1147.2	72.4	BDL	

BDL=below detection limit

Table C-3. Radioisotope Analyses - Raw Data

Station 286B

SAMPLE	DATE COUNTED	POROSITY	^{137}Cs (dpm/Kg)	ERROR	$^{210}Pb(\gamma)$ (dpm/Kg)	ERROR	^{226}Ra (dpm/Kg)	ERROR	^{7}Be (dpm/Kg)	ERROR
0-1cm	8/21/97	0.889	265.76	32.80	2709.42	312.68	1275.40	71.30	528.25	101.05
1-2cm	8/22/97	0.841	190.06	23.14	2264.57	244.15	1345.94	60.40	508.58	71.67
2-3cm	8/23/97	0.806	134.22	36.95	2673.71	523.14	1323.03	86.32	349.68	110.66
3-4cm	8/25/97	0.795	269.88	28.11	2549.24	290.63	1172.08	58.07	BDL	
4-5cm		0.775								
5-6cm		0.750								
6-7cm		0.693								
7-8cm		0.677								
8-9cm		0.656								
9-10cm		0.661								

BDL= below detection limit

Table C-3. Radioisotope Analyses - Raw Data

Station 296

SAMPLE	DATE COUNTED	POROSITY	^{137}Cs (dpm/Kg)	ERROR	^{210}Pb (dpm/Kg)	ERROR	^{226}Ra (dpm/Kg)	ERROR (dp	^{7}Be (dpm/Kg)	ERROR	^{210}PB-(∝) (dpm/Kg)	ERROR	^{210}PB-(∝) $(dpm/Kg)_{repeat}$	ERROR
0-1cm	3/10/97	0.869	327.6	43.1	3339.5	341.4	1061.5	75.8	2269.2	293.9	4331.9	239.5	4471.0	161.0
1-2cm	3/11/97	0.823	254.9	39.6	3023.9	375.3	1324.0	80.2	763.2	230.5				
2-3cm	3/12/97	0.813	413.9	40.8	3006.1	343.3	1089.4	73.5	356.5	206.0				
3-4cm	3/17/97	0.794	339.8	35.6	2820.8	341.6	1228.7	67.0	BDL		4343.9	328.1	4367.0	181.8
3-4cm		0.794									4473.7	286.7	4221.0	196.2
4-5cm	3/20/97	0.780	253.4	33.6	2203.4	362.8	1063.8	69.1	BDL					
5-6cm		0.771												
6-7cm		0.776									3778.4	236.8	3973.8	208.1
7-8cm		0.786												
8-9cm		0.753												
9-10cm		0.746									3279.0	196.5	3245.7	176.2
10-11cm	4/5/97	0.747	256.9	35.3	2708.7	369.5	1379.1	80.1	BDL					
11-12cm		0.747												
12-13cm		0.735									3488.1	149.6	3484.7	167.8
13-14cm		0.749												
14-15cm		0.761												
15-16cm		0.764									3870.9	153.1	3726.0	210.0
16-17cm		0.760												
17-18cm		0.752												
18-19cm		0.744									3285.4	139.9	3365.2	152.8
18-19cm		0.744												
19-20cm		0.746												
20-21cm	4/7/97	0.750	318.7	46.6	2493.7	340.5	1355.2	83.7	BDL					
21-22cm		0.763									3458.3	247.5	3611.1	162.9
21-22cm		0.763									3786.7	194.2	3827.2	193.2
22-23cm		0.763												
23-24cm		0.765												
24-25cm		0.759									3498.0	204.7	3236.5	143.5
25-26cm		0.751												
26-27cm		0.749												
27-28cm		0.764									3220.8	315.8	2946.2	162.5
28-29cm		0.764												
29-30cm		0.755												
30-31cm	4/2/97	0.766	466.8	40.9	2583.6	311.5	1493.7	86.7	BDL		3361.9	265.2	3371.3	170.8
31-32cm		0.765												
32-33cm		0.773												
33-34cm		0.775									3385.7	197.6	3400.7	178.4
33-34cm		0.775												
34-35cm		0.782												
35-36cm		0.778												
36-37cm		0.773									3429.2	206.7	3628.7	131.1
37-38cm		0.752												
38-39cm		0.753												
39-40cm		0.758									3457.9	225.3	3700.4	180.0
40-41cm	4/4/97	0.777	498.3	44.0	2739.7	338.6	1363.1	76.0	BDL					
40-41cm	8/9/97	0.777	541.3	50.9	2041.0	462.0	1339.5	91.3	BDL					
41-42cm		0.780												
42-43cm		0.764									3506.2	259.1	2971.3	136.7
43-44cm		0.755												
44-45cm	3/27/97	0.762	462.6	37.2	2814.8	333.0	1411.3	72.0	BDL					
45-46cm		0.758									2946.4	203.1	3197.5	166.9
46-47cm		0.758												
47-48cm		0.761												
48-49cm		0.757									2932.0	231.6	2571.3	201.7
49-50cm	4/1/97	0.746	423.0	37.4	2219.4	306.5	1230.2	66.8	BDL					
50-51cm		0.747												
51-52cm		0.733									2901.9	228.0	2778.9	167.5
52-53cm		0.713												
53-54cm		0.737												
54-55cm	3/26/97	0.743	615.5	61.9	2415.2	491.9	1290.3	108.7	BDL		2179.7	188.7	2379.7	268.4
55-56cm		0.734												
56-57cm		0.736												
57-58cm		0.753									2235.8	173.4	2474.4	156.4
58-59cm		0.757												
59-60cm	3/28/97	0.739	653.1	42.8	1491.2	302.5	1563.3	76.3	BDL					
60-61cm	3/31/97	0.752	670.0	42.2	1968.6	291.3	1399.9	71.8	BDL		2128.4	176.8	2343.6	144.5

BDL= below detection limit

Table C-3. Radioisotope Analyses - Raw Data

Station 296B

SAMPLE	DATE COUNTED	POROSITY	^{137}Cs (dpm/Kg)	ERROR	$^{210}Pb(\gamma)$ (dpm/Kg)	ERROR	^{226}Ra (dpm/Kg)	ERROR	^{7}Be (dpm/Kg)	ERROR
0-1cm	8/26/97	0.882	167.76	38.77	3423.22	345.47	1144.20	74.20	581.12	115.23
0-1cm	9/5/97	0.882	297.02	39.49	2894.23	331.40	1234.55	72.01	764.08	102.64
1-2cm	8/27/97	0.848	294.97	36.05	2588.75	358.79	1278.38	69.00	2977.73	260.87
2-3cm	8/28/97	0.825	288.12	34.32	2832.64	359.19	1222.02	68.33	1830.53	249.38
3-4cm	8/29/97	0.812	323.87	36.90	2308.74	358.74	1137.24	68.90	1499.48	267.46
4-5cm	8/30/97	0.846	295.10	37.54	4041.69	354.55	821.40	64.72	1032.41	246.67
5-6cm	8/31/97	0.816	319.38	37.14	2982.54	361.53	1259.96	65.09	619.39	211.47
6-7cm	9/1/97	0.817	400.22	39.79	2948.98	433.50	1112.93	73.56	BDL	
7-8cm		0.782								
8-9cm		0.775								
9-10cm		0.772								

BDL= below detection limit

Table C-3. Radioisotope Analyses - Raw Data

Station 300

SAMPLE	DATE COUNTED	POROSITY	^{137}Cs (dpm/Kg)	ERROR	^{210}Pb (dpm/Kg)	ERROR	^{226}Ra (dpm/Kg)	ERROR	^{7}Be (dpm/Kg)	ERROR
0-1cm	5/29/97	0.884	430.9	42.5	3810.3	380.5	1062.7	75.0	8692.0	382.5
0-1cm	8/7/97	0.884	477.7	44.3	5445.8	677.4	1170.7	84.9	3320.3	339.3
1-2cm	5/31/97	0.863	538.3	44.0	3779.5	360.3	1178.3	73.1	10266.0	413.2
2-3cm	6/2/97	0.840	499.0	41.4	3604.0	378.5	1014.6	72.8	4080.3	327.9
3-4cm	6/4/97	0.818	486.2	39.8	3062.2	312.8	1293.8	71.5	709.7	202.8
4-5cm	6/6/97	0.806	453.1	33.1	3556.5	283.7	900.3	58.8	466.2	158.6
5-6cm	6/8/97	0.809	373.2	43.4	3560.6	359.3	1089.8	81.1	747.5	199.9
6-7cm	6/10/97	0.806	388.3	35.6	3685.5	326.7	1041.2	70.9	194.4	164.2
7-8cm		0.808								
8-9cm		0.810								
9-10cm		0.805								
10-11cm	6/12/97	0.788	408.0	40.1	3469.4	331.1	1181.3	67.2	BDL	
11-12cm		0.774								
12-13cm		0.768								
13-14cm		0.766								
14-15cm		0.765								
15-16cm	6/26/97	0.759	641.2	42.9	2524.0	293.3	1142.9	66.6	BDL	
16-17cm		0.766								
17-18cm		0.763								
18-19cm	6/28/97	0.762	600.8	40.3	1598.5	316.1	1216.0	73.9	BDL	
19-20cm		0.766								
20-21cm	6/14/97	0.761	538.9	37.5	1226.7	244.2	1144.8	60.6	BDL	
20-21cm	8/8/97	0.761	648.9	38.9	1183.6	280.6	1072.7	64.3	BDL	
21-22cm		0.754								
22-23cm		0.751								
23-24cm		0.747								
24-25cm		0.747								
25-26cm	6/29/97	0.750	660.2	40.2	2571.7	308.3	1193.9	65.0	BDL	
26-27cm		0.746								
27-28cm	6/30/97	0.751	583.8	36.8	961.9	258.4	1029.4	61.9	BDL	
28-29cm		0.752								
29-30cm		0.736								
30-31cm	6/16/97	0.679	429.1	36.5	1482.5	313.3	1182.4	69.0	BDL	
31-32cm		0.674								
32-33cm		0.676								
33-34cm		0.681								
34-35cm		0.704								
35-36cm		0.720								
36-37cm		0.715								
37-38cm		0.686								
38-39cm		0.729								
39-40cm		0.747								
40-41cm	6/19/97	0.748	106.4	30.7	1211.4	279.4	1042.2	70.5	BDL	
41-42cm		0.740								
42-43cm		0.740								
43-44cm		0.746								
44-45cm		0.751								
45-46cm		0.746								
46-47cm		0.757								
47-48cm		0.753								
48-49cm		0.751								
49-50cm		0.743								
50-51cm	6/21/97	0.750	63.8	18.1	1120.1	261.6	1137.6	66.0	BDL	
51-52cm		0.733								
52-53cm		0.729								
53-54cm		0.718								
54-55cm		0.705								
55-56cm		0.729								
56-57cm		0.721								
57-58cm		0.697								
58-59cm		0.708								
59-60cm		0.693								
60-61cm	6/24/97	0.677	0.0	0.0	1029.9	228.6	1009.0	55.4	BDL	

BDL= below detection limit

Table C-3. Radioisotope Analyses - Raw Data

Station 924

SAMPLE	DATE COUNTED	POROSITY	^{137}Cs (dpm/Kg)	ERROR	^{210}Pb (dpm/Kg)	ERROR	^{226}Ra (dpm/Kg)	ERROR	^{7}Be (dpm/Kg)	ERROR
0-1cm	7/1/97	0.857	354.4	49.0	4125.7	441.9	1571.5	107.9	8054.6	508.1
1-2cm	7/3/97	0.773	252.7	33.5	1869.3	291.9	773.0	64.2	2442.4	263.8
2-3cm	7/5/97	0.760	215.0	35.9	2358.4	303.0	1089.6	66.9	911.4	216.5
3-4cm	7/7/97	0.776	270.9	33.1	2328.5	276.6	931.4	67.8	BDL	
4-5cm	7/9/97	0.804	338.0	36.7	2674.9	295.0	943.3	66.2	BDL	
5-6cm	7/12/97	0.819	373.0	40.8	2365.3	333.0	1049.5	73.0	BDL	
6-7cm		0.814								
7-8cm		0.799								
8-9cm		0.790								
9-10cm	7/14/97	0.764	304.6	46.0	2190.2	334.0	1109.6	78.3	BDL	
10-11cm		0.746								
11-12cm		0.735								
12-13cm		0.732								
13-14cm		0.729								
14-15cm		0.732								
15-16cm		0.753								
16-17cm		0.717								
17-18cm		0.662								
18-19cm		0.673								
19-20cm	7/16/97	0.715	276.3	34.5	2098.1	327.7	839.6	75.8	BDL	
20-21cm		0.695								
21-22cm		0.712								
22-23cm		0.711								
23-24cm		0.672								
24-25cm	7/31/97	0.661	181.4	32.3	1682.9	286.2	1142.2	63.2	BDL	
25-26cm		0.677								
26-27cm		0.694								
27-28cm		0.675								
28-29cm		0.677								
29-30cm	7/18/97	0.661	309.1	28.2	1229.3	262.4	951.3	53.8	BDL	
29-30cm	9/7/97	0.661	194.1	34.9	1649.7	296.4	1188.3	75.6	BDL	
30-31cm		0.645								
31-32cm		0.656								
32-33cm		0.667								
33-34cm	7/30/97	0.671	221.3	33.1	1766.2	313.4	1069.3	65.3	BDL	
34-35cm		0.649								
35-36cm		0.684								
36-37cm		0.673								
37-38cm		0.697								
38-39cm		0.645								
39-40cm	7/21/97	0.698	314.4	37.9	1794.4	266.8	958.4	69.4	BDL	
40-41cm		0.575								
41-42cm		0.619								
42-43cm		0.611								
43-44cm		0.703								
44-45cm		0.691								
45-46cm		0.689								
46-47cm		0.674								
47-48cm		0.694								
48-49cm		0.728								
49-50cm	7/23/97	0.724	381.6	40.7	1902.4	244.1	1028.5	68.7	BDL	
50-51cm		0.735								
51-52cm		0.726								
52-53cm		0.718								
53-54cm		0.714								
54-55cm		0.681								
55-56cm		0.700								
56-57cm		0.725								
57-58cm		0.715								
58-59cm		0.738								
59-60cm		0.743								
60-61cm	7/25/97	0.716	303.6	24.8	1265.9	169.2	1009.1	47.1	BDL	
Y(0-5cm)	7/19/97	0.893	295.4	32.3	2942.1	290.7	722.1	54.3	3094.9	256.2

BDL=below detection limit

Table C-3. Radioisotope Analyses - Raw Data

Station 926

SAMPLE	DATE COUNTED	POROSITY	^{137}Cs (dpm/Kg)	ERROR	^{210}Pb (dpm/Kg)	ERROR	^{226}Ra (dpm/Kg)	ERROR	^{7}Be (dpm/Kg)	ERROR
0-1cm	7/2/97	0.610	91.8	29.1	1178.8	283.9	964.8	64.1	1398.9	244.6
1-2cm	7/4/97	0.500	49.5	24.9	932.2	239.1	848.1	63.8	169.3	235.5
2-3cm	7/6/97	0.583	156.7	29.7	1014.5	235.6	1128.7	66.6	348.2	179.6
3-4cm	7/8/97	0.564	167.1	33.2	940.1	292.2	1328.3	72.3	366.6	206.6
4-5cm	7/11/97	0.502	173.3	25.4	910.8	199.5	1174.8	57.6	BDL	
5-6cm	7/13/97	0.476	129.1	25.6	1028.2	261.6	1038.1	72.9	BDL	
6-7cm		0.494								
7-8cm	8/1/97	0.483	163.2	29.6	1274.6	240.5	1231.7	73.8	BDL	
8-9cm		0.480								
9-10cm	7/15/97	0.534	151.1	29.7	1079.7	251.6	1109.5	66.7	BDL	
10-11cm		0.574								
11-12cm		0.620								
12-13cm		0.621								
13-14cm		0.619								
14-15cm	8/4/97	0.512	131.7	28.8	1516.3	262.6	1267.9	65.6	BDL	
15-16cm		0.509								
16-17cm		0.549								
17-18cm		0.570								
18-19cm		0.542								
19-20cm	7/17/97	0.485	112.3	28.7	1253.8	267.2	1188.0	64.1	BDL	
20-21cm		0.473								
21-22cm		0.374								
22-23cm		0.336								
23-24cm		0.378								
24-25cm		0.432								
25-26cm		0.422								
26-27cm		0.385								
27-28cm		0.384								
28-29cm		0.383								
29-30cm	7/20/97	0.345	39.6	25.4	1159.1	200.4	1005.8	65.2	BDL	
30-31cm		0.361								
31-32cm		0.341								
32-33cm		0.335								
33-34cm		0.330								
34-35cm		0.348								
35-36cm		0.364								
36-37cm		0.336								
37-38cm		0.332								
38-39cm		0.373								
39-40cm	7/22/97	0.411	50.1	28.8	1287.1	218.3	1222.7	69.8	BDL	
40-41cm		0.402								
41-42cm		0.416								
42-43cm		0.428								
43-44cm		0.432								
44-45cm		0.449								
45-46cm		0.468								
46-47cm		0.450								
47-48cm		0.451								
48-49cm		0.450								
49-50cm	7/24/97	0.435	BDL		2072.6	284.7	1182.9	72.2	BDL	
49-50cm	9/6/97	0.435	31.9	20.8	956.6	261.7	1252.5	72.6	BDL	
50-51cm		0.407								
51-52cm		0.425								
52-53cm		0.412								
53-54cm		0.422								
54-55cm		0.425								
55-56cm		0.424								
56-57cm		0.404								
57-58cm		0.402								
58-59cm		0.405								
59-60cm		0.397								
60-61cm	7/27/97	0.380	62.2	26.8	935.7	238.2	1106.8	74.5	BDL	

BDL=below detection limit

Table C-3. Radioisotope Analyses - Raw Data

Station 928

SAMPLE	DATE COUNTED	POROSITY	^{137}Cs (dpm/Kg)	ERROR	^{210}Pb(γ) (dpm/Kg)	ERROR	^{226}Ra (dpm/Kg)	ERROR	^{7}Be (dpm/Kg)	ERROR	^{210}PB-(α) (dpm/Kg)	ERROR	^{239,240}Pu (dpm/Kg)	ERROR
0-1cm	10/2/97	0.836	229.3	34.0	1661.0	308.9	1169.7	68.3	2838.4	271.5				
1-2cm	10/3/97	0.724	168.2	31.7	1776.3	289.0	1182.2	71.5	1748.9	233.7				
2-3cm	10/4/97	0.733	182.0	33.1			1125.0	68.0	1357.4	229.0				
2-3cm	10/8/97	0.733	188.2	31.0	2316.0	304.1	1303.2	70.7	939.7	219.5				
3-4cm	10/4/97	0.754	183.2	28.4	1972.7	279.7	1149.6	63.0	1846.3	216.9				
4-5cm	10/6/97	0.792	340.9	34.8	2380.8	287.5	1034.0	65.9	1990.0	244.9				
5-6cm	10/5/97	0.677	72.7	32.1	1859.7	306.4	1283.9	75.0	1251.5	246.9				
6-7cm	10/7/97	0.784	312.4	38.4	3266.7	312.4	1144.4	68.2	2186.8	271.1				
7-8cm	10/9/97	0.739	73.0	27.8	1904.8	311.0	1522.9	70.5	919.0	191.2				
8-9cm	10/11/97	0.698	142.4	25.9	2074.2	256.5	1266.2	57.8	686.9	149.1				
9-10cm	10/12/97	0.588	42.2	27.8	1484.5	300.5	1416.9	82.0	488.4	205.9				
10-11cm	10/13/97	0.672	179.6	31.7	1830.4	291.8	1342.2	76.1	BDL					
11-12cm		0.631												
12-13cm		0.684												
13-14cm		0.692												
14-15cm		0.649												
15-16cm		0.564												
16-17cm		0.615												
17-18cm		0.649												
18-19cm		0.619												
19-20cm	10/27/97	0.590	157.7	32.1	1563.9	277.0	1212.0	74.2	BDL					
20-21cm		0.586												
21-22cm		0.641												
22-23cm		0.638												
23-24cm		0.555												
24-25cm		0.526												
25-26cm		0.669												
26-27cm		0.693												
27-28cm		0.675												
28-29cm		0.670												
29-30cm	10/22/97	0.692	252.7	35.6	1534.8	290.1	1152.9	74.0	BDL					
30-31cm		0.711												
31-32cm		0.746												
32-33cm		0.749												
33-34cm		0.740												
34-35cm		0.739												
35-36cm		0.746												
36-37cm		0.744												
37-38cm		0.753												
38-39cm		0.745												
39-40cm		0.739												
40-41cm	11/7/97	0.747	329.1	29.7	2495.5	227.7	1153.9	62.4	BDL					
41-42cm		0.781												
42-43cm		0.758												
43-44cm		0.694												
44-45cm		0.673												
45-46cm		0.639												
46-47cm		0.655												
47-48cm		0.631												
48-49cm		0.606												
49-50cm		0.615												
50-51cm	11/6/97	0.587	267.1	32.9	1235.8	305.7	1217.2	79.1	BDL					
51-52cm		0.588												
52-53cm		0.587												
53-54cm		0.602												
54-55cm		0.598												
55-56cm		0.604												
56-57cm	11/8/97	0.591	146.2	23.8	1284.7	236.3	1209.3	63.6	BDL					
57-58cm		0.586												
58-59cm		0.569												
59-60cm		0.578												
60-61cm	10/20/97	0.579	241.8	34.0	1223.9	274.6	1310.4	73.4	BDL					

BDL= below detection limit

Table C-3. Radioisotope Analyses - Raw Data

Station 4293

SAMPLE	DATE COUNTED	POROSITY	^{137}Cs (dpm/Kg)	ERROR	^{210}Pb (dpm/Kg)	ERROR	^{226}Ra (dpm/Kg)	ERROR	^{7}Be (dpm/Kg)	ERROR
0-1cm	5/28/97	0.859	257.7	36.3	2961.9	350.1	1023.0	69.4	3121.4	301.8
0-1cm	8/5/97	0.859	271.3	35.3	3799.7	336.0	1165.9	73.7	1232.2	255.4
1-2cm	5/30/97	0.843	259.8	30.4	3347.6	288.5	998.4	59.4	4042.3	258.2
2-3cm	6/1/97	0.832	371.1	39.6	3870.3	379.1	1230.1	74.0	3774.5	318.2
3-4cm	6/3/97	0.811	301.5	33.0	2602.6	318.9	1137.1	61.3	2156.5	235.7
4-5cm	6/5/97	0.786	210.3	31.4	2766.5	302.7	1157.7	66.1	1039.5	219.8
5-6cm	6/7/97	0.756	189.8	29.1	3603.6	291.3	1120.4	60.8	868.6	194.3
6-7cm	6/9/97	0.741	255.8	34.2	3577.2	313.1	1260.1	74.4	428.9	195.1
7-8cm	6/11/97	0.758	270.0	38.3	3659.5	372.2	1322.8	79.0	BDL	
8-9cm		0.754								
9-10cm		0.748								
10-11cm	6/13/97	0.745	364.1	31.2	3158.3	283.7	1328.0	66.8	BDL	
11-12cm		0.737								
12-13cm		0.745								
13-14cm		0.751								
14-15cm		0.751								
15-16cm	6/27/97	0.747	347.0	28.8	2059.4	260.1	1252.8	56.9	BDL	
16-17cm		0.728								
17-18cm		0.757								
18-19cm		0.768								
19-20cm		0.778								
20-21cm	6/15/97	0.768	359.9	38.0	1939.4	337.2	1345.2	73.4	BDL	
21-22cm		0.730								
22-23cm		0.724								
23-24cm		0.664								
24-25cm		0.668								
25-26cm	7/28/97	0.729	382.1	41.7	2372.2	500.4	1397.9	78.2	BDL	
26-27cm		0.751								
27-28cm		0.745								
28-29cm		0.705								
29-30cm		0.694								
30-31cm	6/18/97	0.703	293.1	36.4	1649.1	292.3	1268.3	72.4	BDL	
30-31cm	8/6/97	0.703	374.2	37.0	2851.9	381.3	1202.1	68.8	BDL	
31-32cm		0.702								
32-33cm		0.669								
33-34cm		0.631								
34-35cm		0.625								
35-36cm		0.622								
36-37cm	7/29/97	0.637	385.8	54.7	4734.7	259.1	621.8	63.9	BDL	
36-37cm	11/19/97	0.637	375.0	60.0	4525.3	253.5	576.6	55.6	BDL	
37-38cm		0.638								
38-39cm		0.646								
39-40cm		0.641								
40-41cm	6/20/97	0.670	218.0	25.5	2140.5	276.3	1376.3	63.1	BDL	
41-42cm		0.674								
42-43cm		0.658								
43-44cm		0.647								
44-45cm		0.627								
45-46cm		0.615								
46-47cm		0.576								
47-48cm		0.599								
48-49cm		0.615								
49-50cm		0.615								
50-51cm	6/22/97	0.618	88.0	26.4	1080.2	242.0	1061.4	70.7	BDL	
51-52cm		0.611								
52-53cm		0.616								
53-54cm		0.598								
54-55cm		0.594								
55-56cm		0.593								
56-57cm		0.597								
57-58cm		0.591								
58-59cm		0.609								
59-60cm		0.619								
60-61cm	6/25/97	0.606	58.5	25.4	1968.9	282.1	1064.2	63.3	BDL	

BDL= below detection limit

Table C-3. Radioisotope Analyses - Raw Data

Station 8721

SAMPLE	DATE COUNTED	POROSITY	^{137}Cs (dpm/Kg)	ERROR	$^{210}Pb(\gamma)$ (dpm/Kg)	ERROR	^{226}Ra (dpm/Kg)	ERROR	^{7}Be (dpm/Kg)	ERROR
0-1cm	12/20/97	0.857	315.3	37.4	2841.7	341.9	834.7	72.8	1699.6	272.6
1-2cm	12/21/97	0.848	333.4	37.4	3227.8	348.4	949.7	70.5	2159.5	296.8
2-3cm	12/23/97	0.847	413.6	23.1	3133.9	189.7	959.1	40.7	1260.6	151.8
3-4cm	12/26/97	0.854	412.0	34.9	3952.6	295.2	1102.4	63.4	854.0	242.5
4-5cm	12/27/97	0.857	413.4	31.2	3525.4	262.6	1037.1	54.4	524.7	157.9
5-6cm	12/29/97	0.845	393.2	41.3	2879.7	333.4	1064.4	70.9	BDL	
6-7cm		0.828								
7-8cm		0.817								
8-9cm		0.813								
9-10cm	12/30/97	0.822	330.9	31.9	3302.9	313.2	1131.8	63.0	BDL	
10-11cm										
11-12cm										
12-13cm										
13-14cm										
14-15cm	1/1/98	0.830	389.2	41.2	3051.5	342.8	1043.0	76.0	BDL	
15-16cm										
16-17cm										
17-18cm										
18-19cm										
19-20cm	1/7/98	0.812	353.6	36.9	2466.7	309.1	916.9	61.9	BDL	
20-21cm										
21-22cm										
22-23cm										
23-24cm										
24-25cm										
25-26cm										
26-27cm										
27-28cm										
28-29cm										
29-30cm	1/9/98	0.802	405.1	34.4	2604.7	285.0	806.2	58.5	BDL	
30-31cm										
31-32cm										
32-33cm										
33-34cm										
34-35cm	1/10/98	0.812	401.7	37.1	3012.1	319.0	878.1	59.7	BDL	
35-36cm										
36-37cm										
37-38cm										
38-39cm										
39-40cm										
40-41cm										
41-42cm										
42-43cm										
43-44cm										
44-45cm	1/11/98	0.809	349.6	37.3	2701.8	313.7	1033.0	67.4	BDL	
45-46cm										
46-47cm										
47-48cm										
48-49cm										
49-50cm		0.802								
50-51cm										
51-52cm										
52-53cm										
53-54cm										
54-55cm	1/11/98	0.769	271.9	32.7	1943.9	288.1	1128.4	63.2	BDL	
55-56cm										
56-57cm										
57-58cm										
58-59cm										
59-60cm		0.774								
60-61cm	1/10/98	0.781	289.1	32.6	1939.1	295.9	1195.9	69.1	BDL	

BDL=below detection limit

Table C-3. Radioisotope Analyses - Raw Data

Station 8826

SAMPLE	DATE COUNTED	POROSITY	^{137}Cs (dpm/Kg)	ERROR	^{210}Pb(γ) (dpm/Kg)	ERROR	^{226}Ra (dpm/Kg)	ERROR	^{7}Be (dpm/Kg)	ERROR
0-1cm	11/26/97	0.886	368.83	40.05	4315.90	320.76	1208.12	78.03	6949.29	354.75
1-2cm	11/27/97	0.847	310.85	37.27	2765.63	294.14	957.27	69.75	5127.37	327.04
1-2cm	12/2/97	0.847	338.80	37.01	3091.02	295.39	988.73	71.80	4260.80	344.37
2-3cm	11/28/97	0.792	282.56	32.80	2629.57	291.27	1116.63	63.43	1460.24	239.33
3-4cm	11/29/97	0.754	209.59	27.80	2654.06	249.81	1188.39	59.58	401.60	183.66
4-5cm	11/30/97	0.735	290.70	34.74	2033.26	359.85	1261.39	66.22	177.23	134.54
5-6cm	12/1/97	0.735	225.93	36.08	3073.56	287.37	1244.87	74.10	715.93	246.13
6-7cm	12/4/97	0.733	203.59	28.72	2256.43	335.50	1115.69	67.60	755.44	197.07
7-8cm		0.740								
8-9cm		0.737								
9-10cm	12/1/97	0.709	284.15	33.28	2435.41	311.72	1198.37	72.00	BDL	
10-11cm		0.712								
11-12cm		0.735								
12-13cm		0.746								
13-14cm		0.732								
14-15cm	12/9/97	0.759	457.94	38.27	1956.82	287.10	1326.75	66.31	BDL	
15-16cm		0.774								
16-17cm		0.775								
17-18cm		0.785								
18-19cm		0.771								
19-20cm	12/2/97	0.760	498.59	41.14	2358.55	280.12	1041.97	67.63	BDL	
20-21cm		0.734								
21-22cm		0.723								
22-23cm		0.729								
23-24cm		0.741								
24-25cm	12/9/97	0.746	623.86	39.74	1855.62	277.01	1067.23	64.22	BDL	
25-26cm		0.759								
26-27cm		0.752								
27-28cm		0.753								
28-29cm		0.755								
29-30cm	12/5/97	0.743	815.72	25.95	1668.23	153.69	1010.45	37.85	BDL	
30-31cm		0.734								
31-32cm		0.742								
32-33cm		0.725								
33-34cm		0.685								
34-35cm		0.668								
35-36cm		0.690								
36-37cm		0.713								
37-38cm		0.708								
38-39cm		0.729								
39-40cm	12/8/97	0.748	49.66	25.27	1442.34	286.36	988.74	67.28	BDL	
40-41cm		0.764								
41-42cm		0.770								
42-43cm		0.769								
43-44cm		0.778								
44-45cm		0.774								
45-46cm										
46-47cm		0.754								
47-48cm		0.761								
48-49cm										
49-50cm	12/8/97	0.769	BDL		1411.31	287.01	1099.90	65.89	BDL	
50-51cm										
51-52cm										
52-53cm										
53-54cm										
54-55cm		0.698								
55-56cm										
56-57cm										
57-58cm										
58-59cm										
59-60cm										
60-61cm										

BDL= below detection limit

Table C-4. Comparison of characteristic recovery half-times ($t_{1/2}$, time for surface concentration to decrease to 50% of present-day value) determined by numerically modeling mercury distributions into the future, and a simple algorithm based on the travel time of mercury through the surface sediment mixed layer, which determines how long mercury concentrations are affected by particle reworking. Slight differences between the two estimates are likely the result of ignoring 1) particle reworking produced downwards displacement of ^{137}Cs peak positions when estimating sedimentation rates (cm/yr), 2) the actual kinetics of the mixing process used in the model, and 3) differences in assumed sediment porosities.

Core	$T_{1/2}$(numerical model) (yr)	z_m (cm)	S (cm/yr)	$T_{1/2}=(\ln 2) x z_m/S$ (yr)
201	0.98	2	1.1	1.26
128	3.57	4	0.85	3.29
134	9.1	4	0.55	5.11
134	3.5	2	0.55	2.52
300	8.75	7	0.7	7
142	----	3	0.4	5.25
296	----	3	1.8	1.19
296	----	6	1.8	2.31

Figure C-1. **Graphic sorting and mean grain size relationships for detailed grain size samples and endmember grabs.**

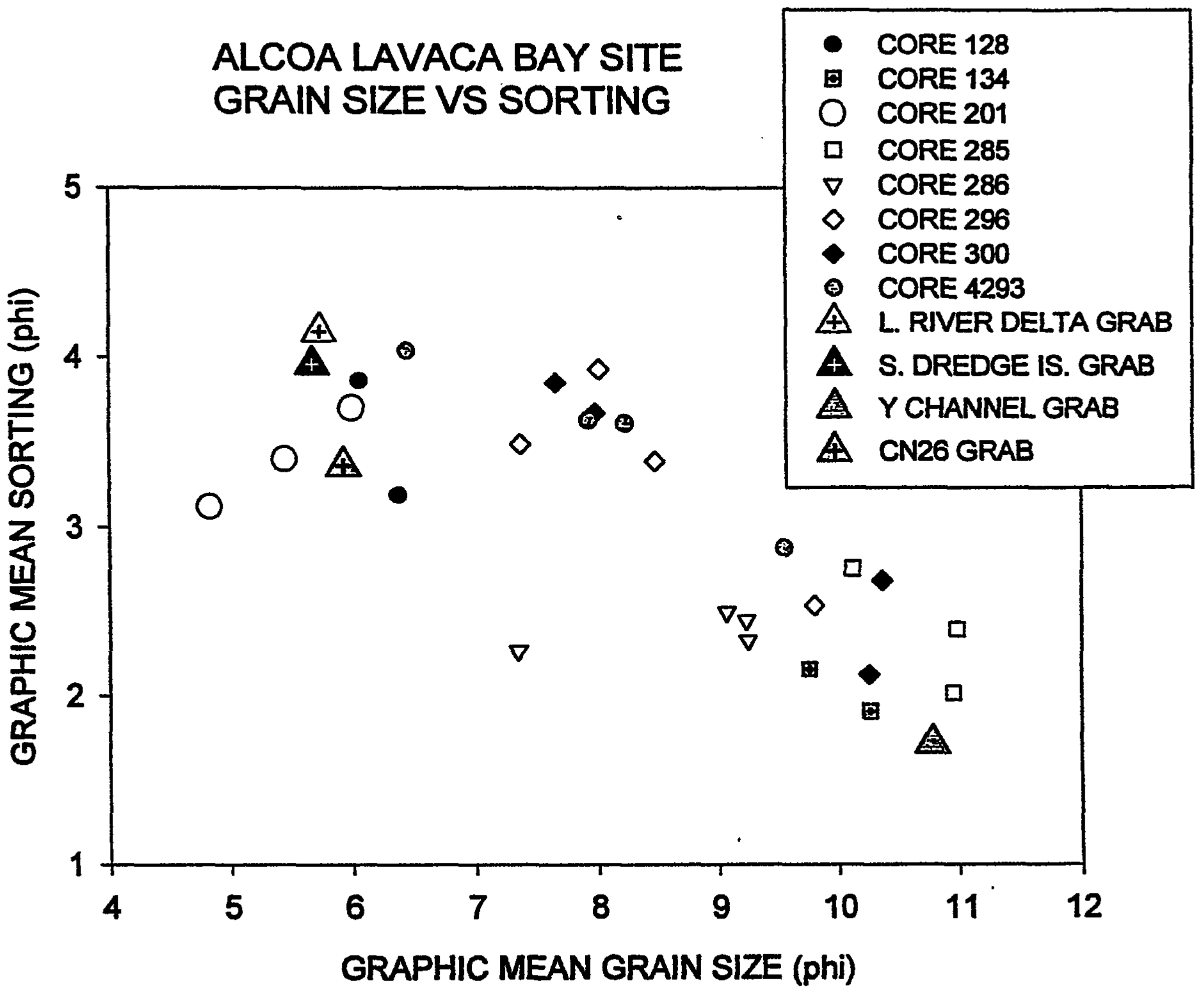

Figure C-2. Downcore plot of %sand and %clay for Core 128.

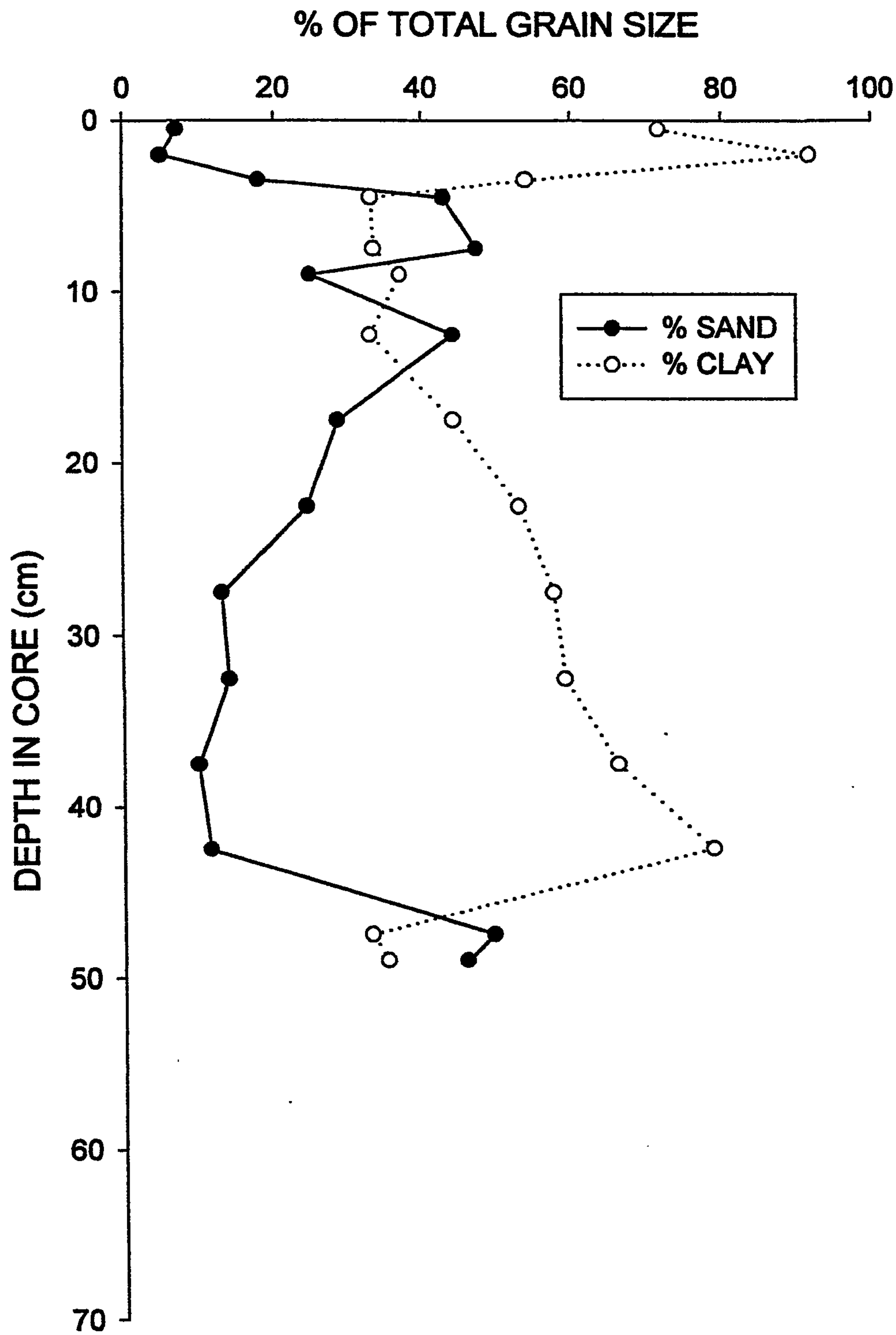

Figure C-3. Grain size histogram for Core 128, 1-3 cm depth.

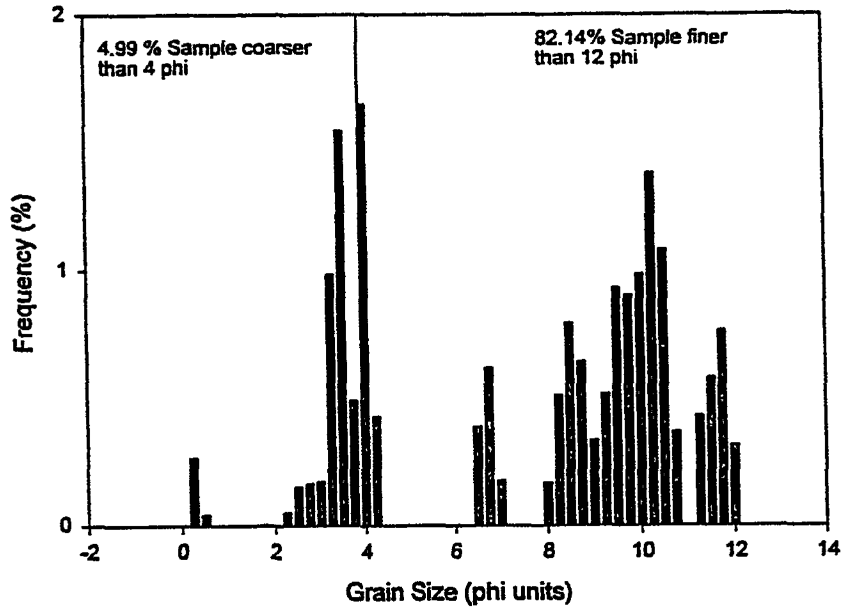

Figure C-4. Grain size histogram for Core 128, 8-10 cm depth.

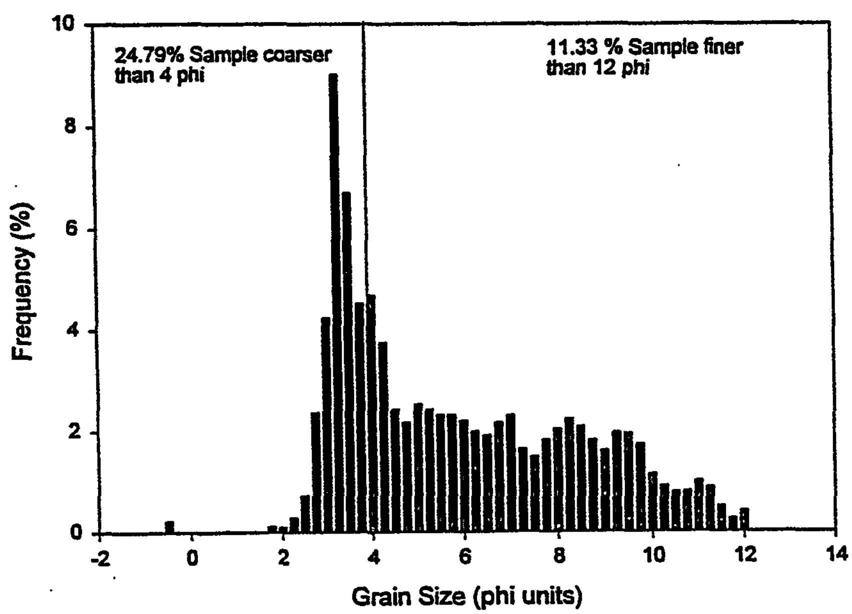

Figure C-5. Grain size histogram for Core 128, 48-50 cm depth.

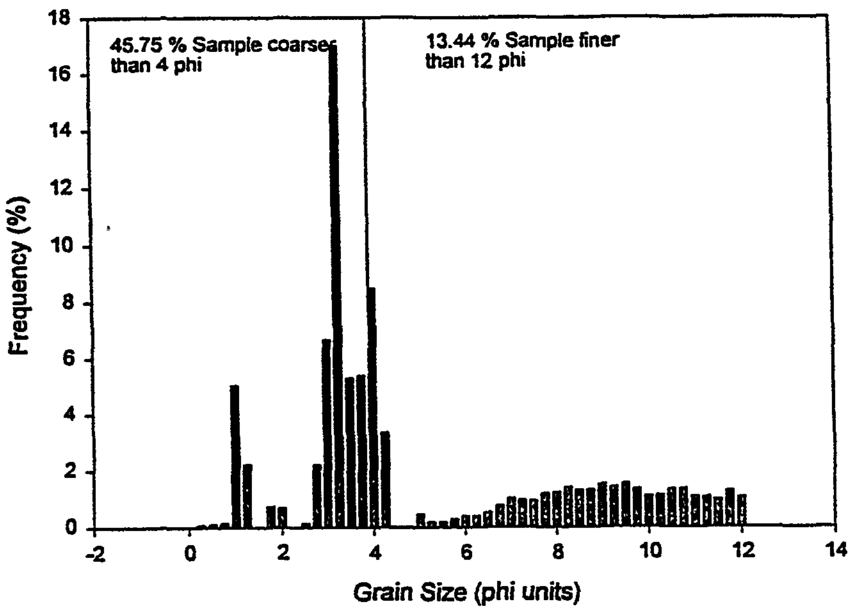

Figure C-6. Downcore plot of %sand and %clay for Core 134.

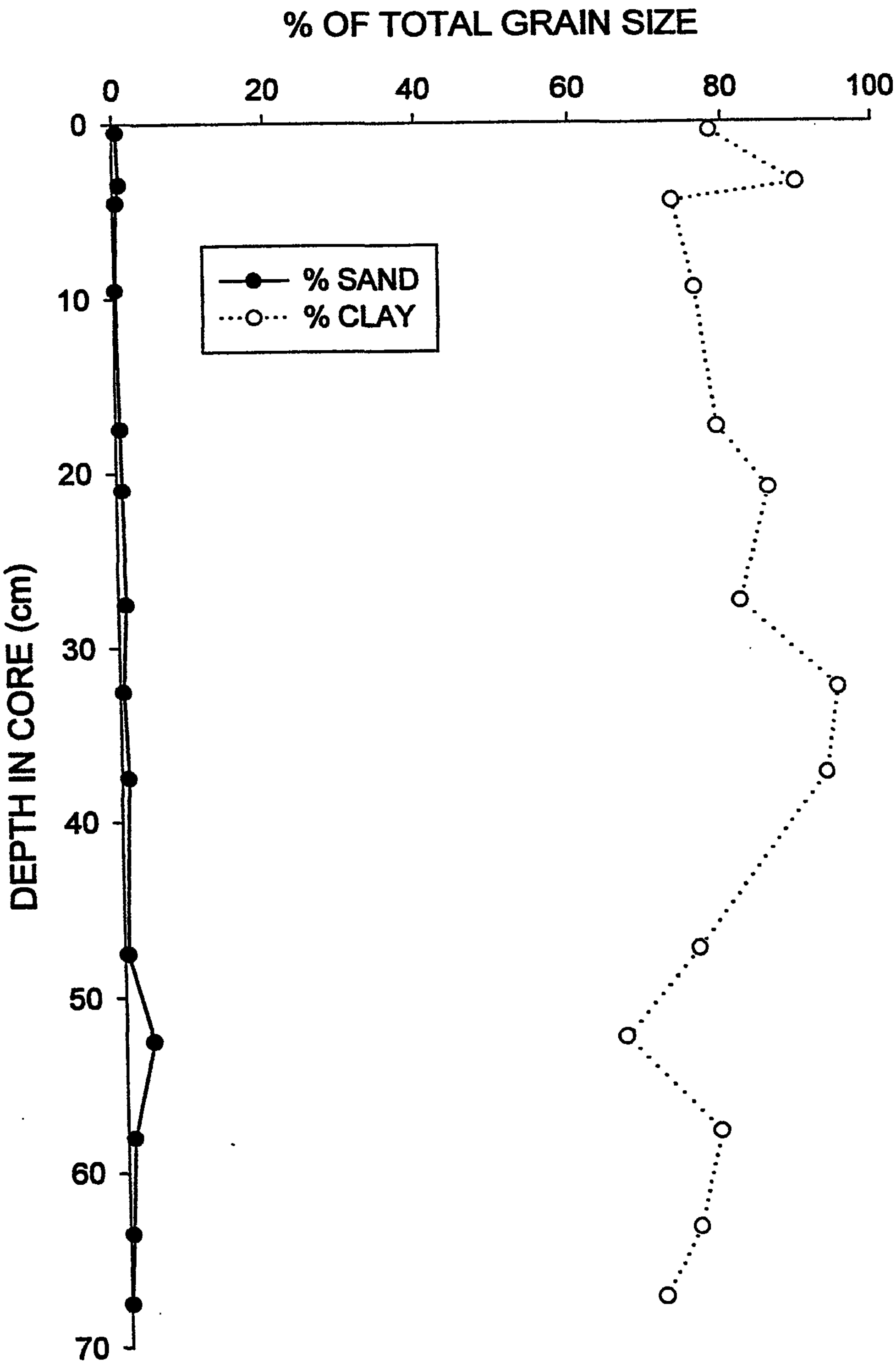

Figure C-7. Grain size histogram for Core 134, 20-22 cm depth.

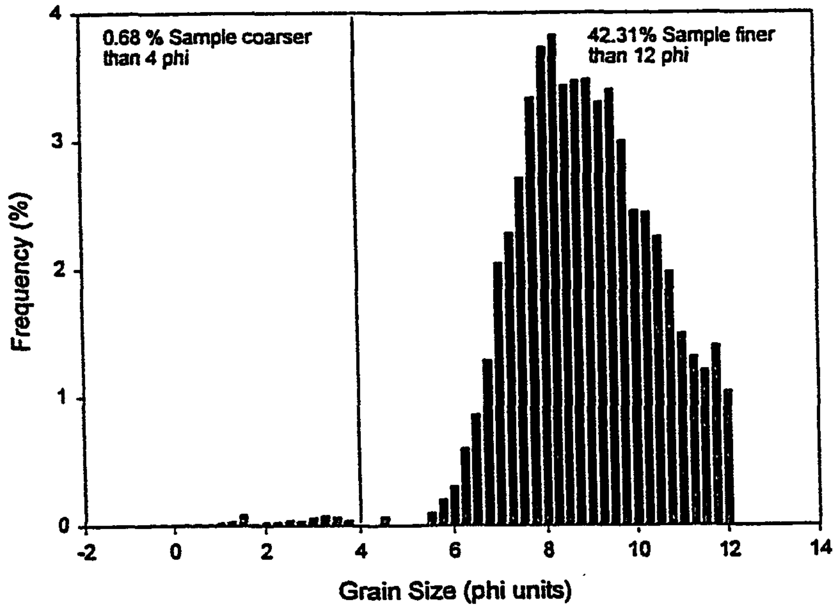

Figure C-8. Grain size histogram for Core 134, 57-59 cm depth.

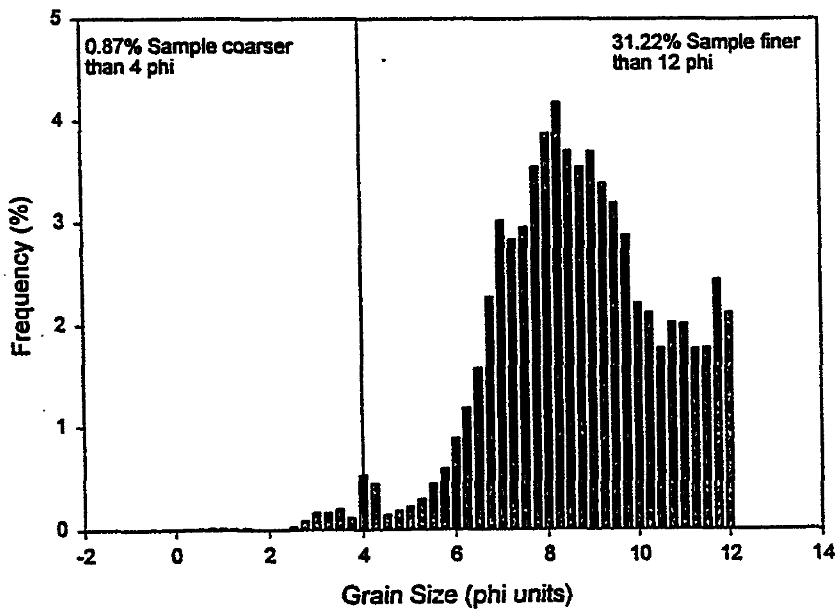

Figure C-9. Downcore plot of %sand and %clay for Core 142.

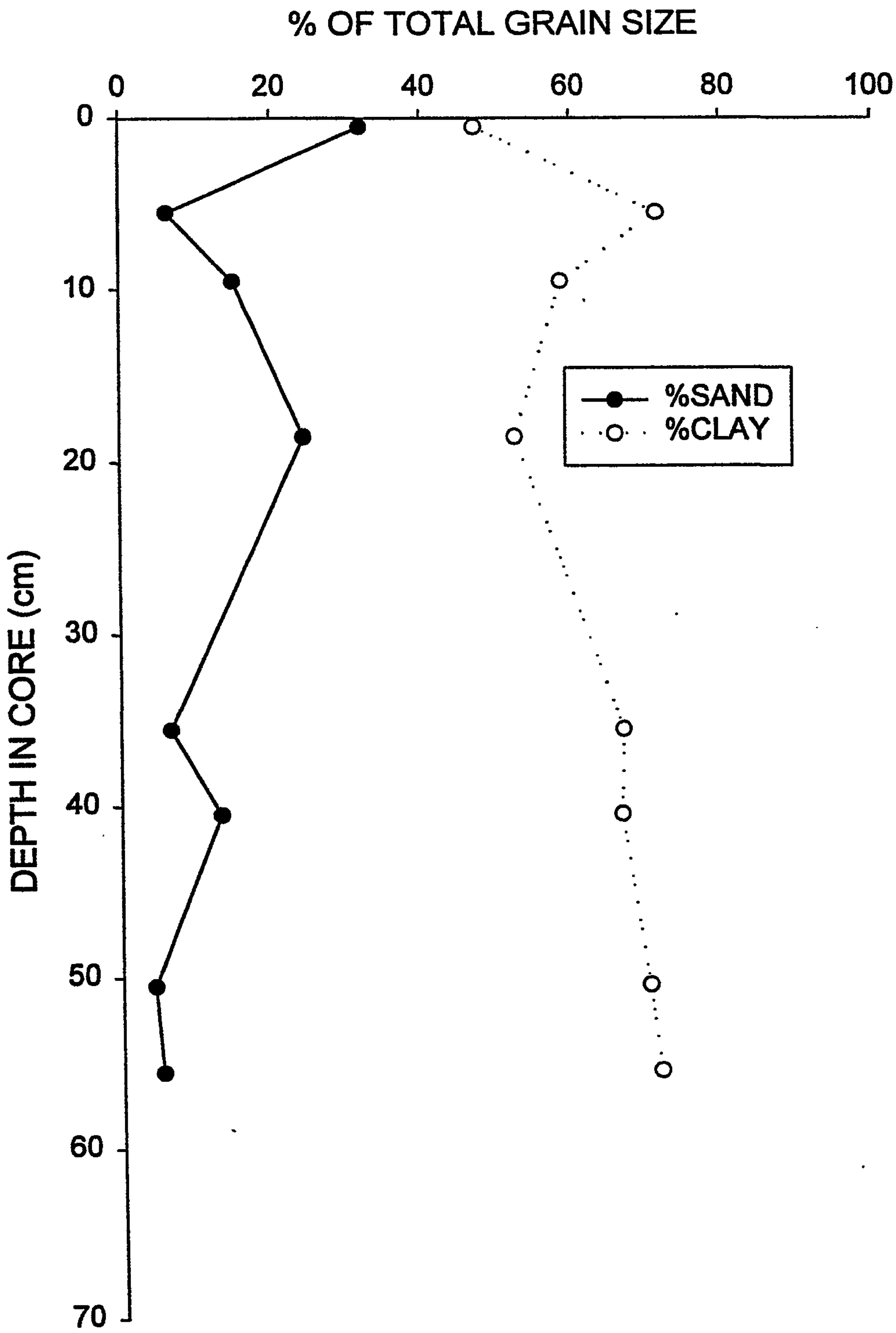

Figure C-10. Grain size histogram for Core 142, 2-4 cm depth.

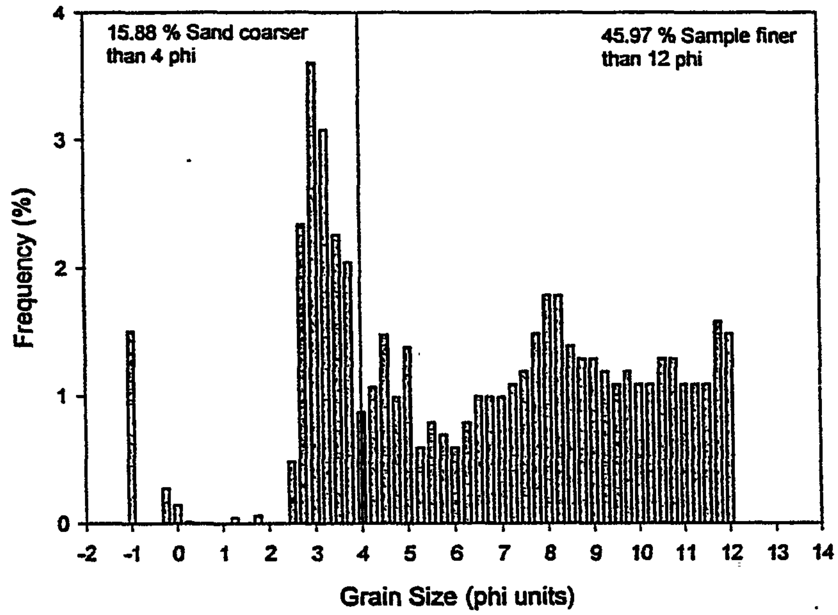

Figure C-11. Grain size histogram for Core 142, 13-15 cm depth.

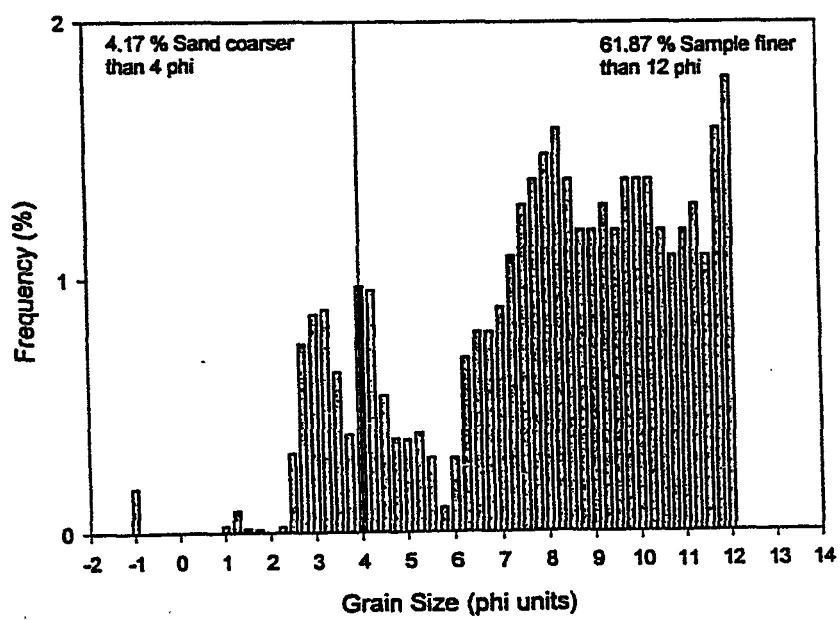

Figure C-12. Grain size histogram for Core 142, 25-27 cm depth.

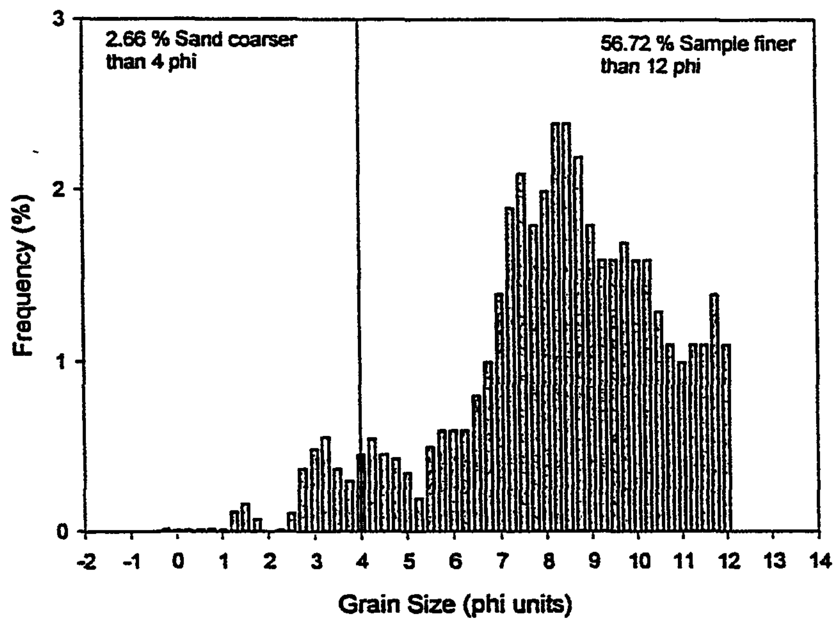

Figure C-13. Grain size histogram for Core 142, 44-46 cm depth.

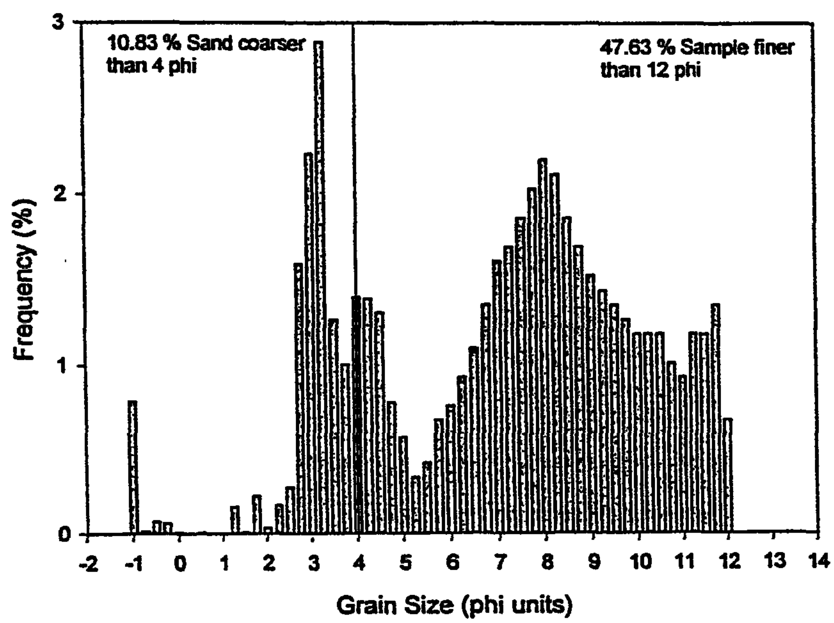

Figure C-14. Downcore plot of %sand and %clay for Core 201.

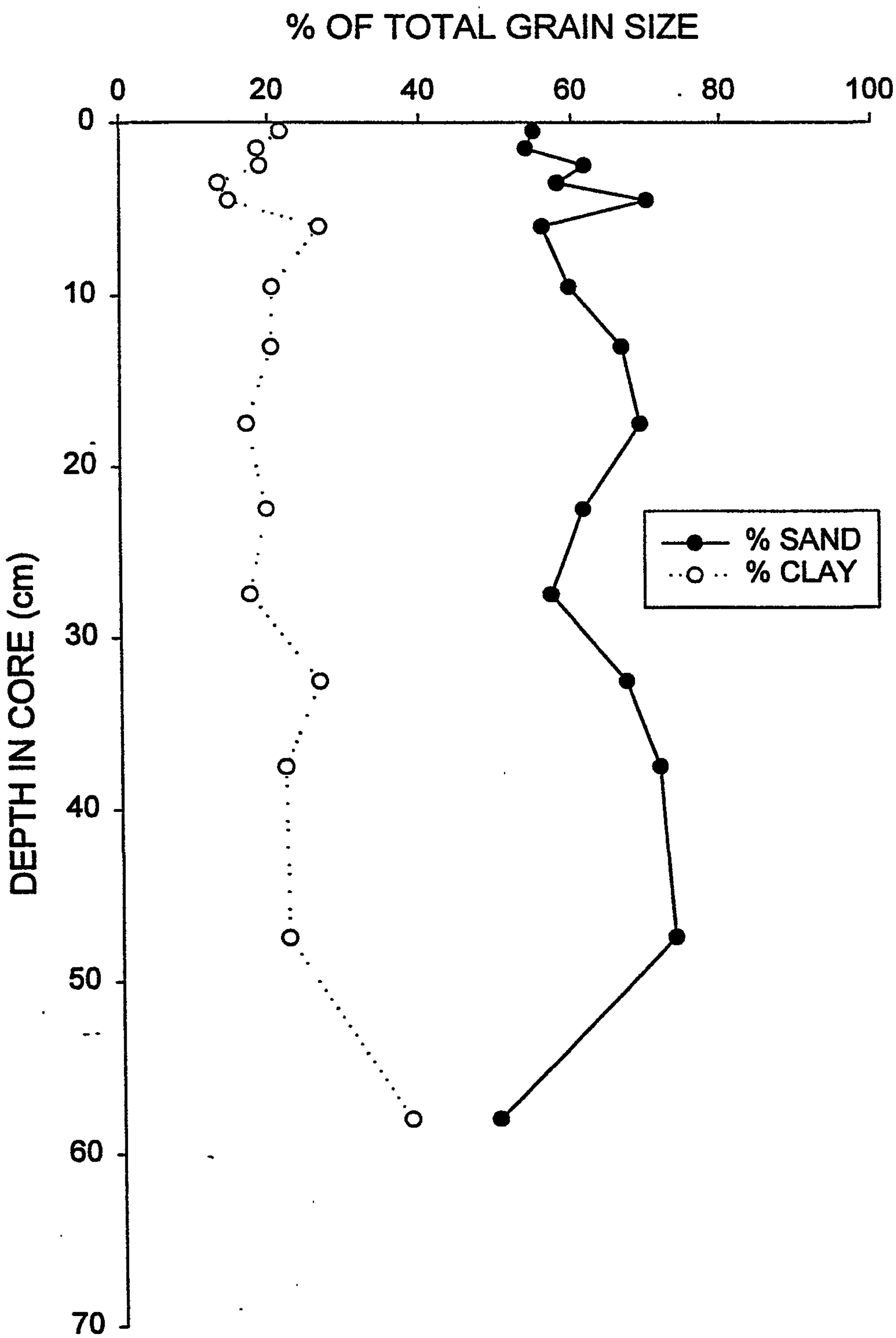

Figure C-15. Grain size histogram for Core 201, 5-7 cm depth.

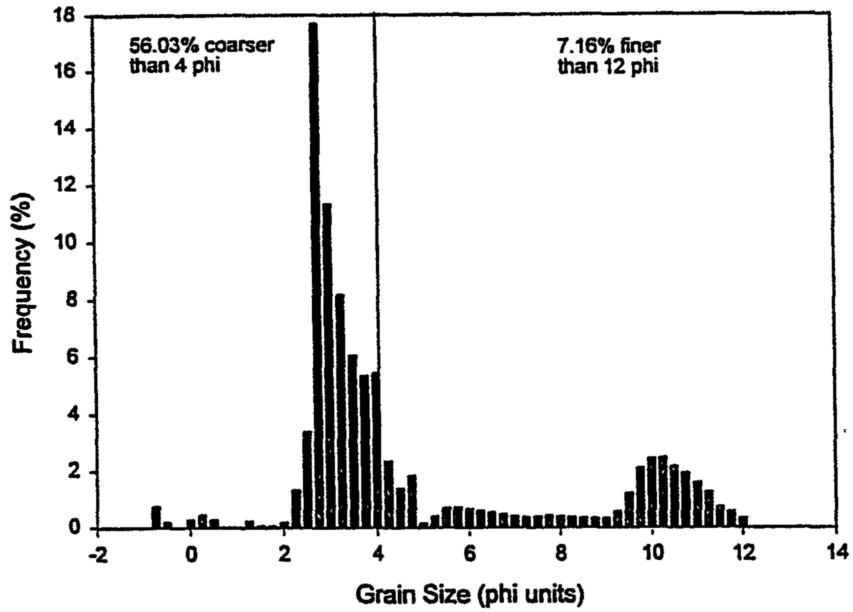

Figure C-16. Grain size histogram for Core 201, 12-14 cm depth.

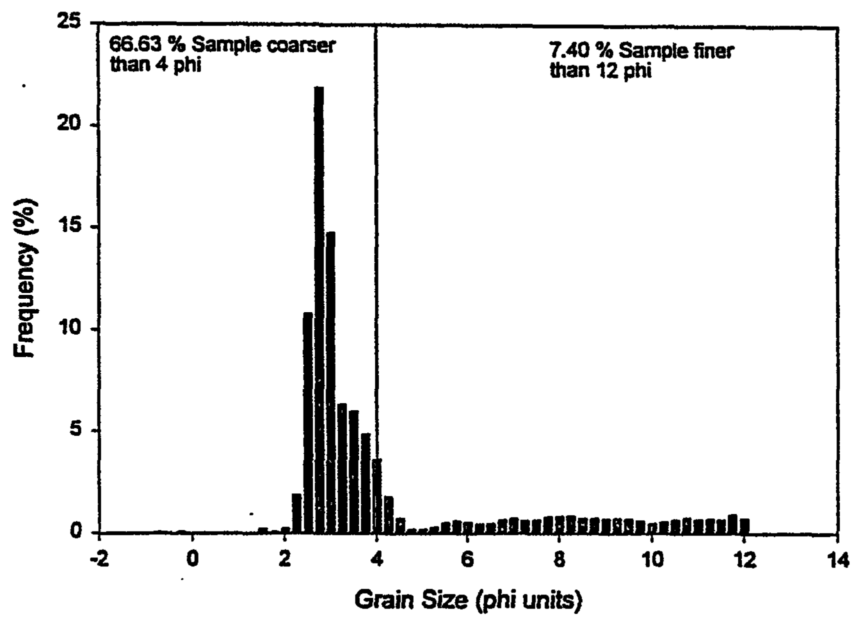

Figure C-17. Grain size histogram for Core 201, 57-59 cm depth.

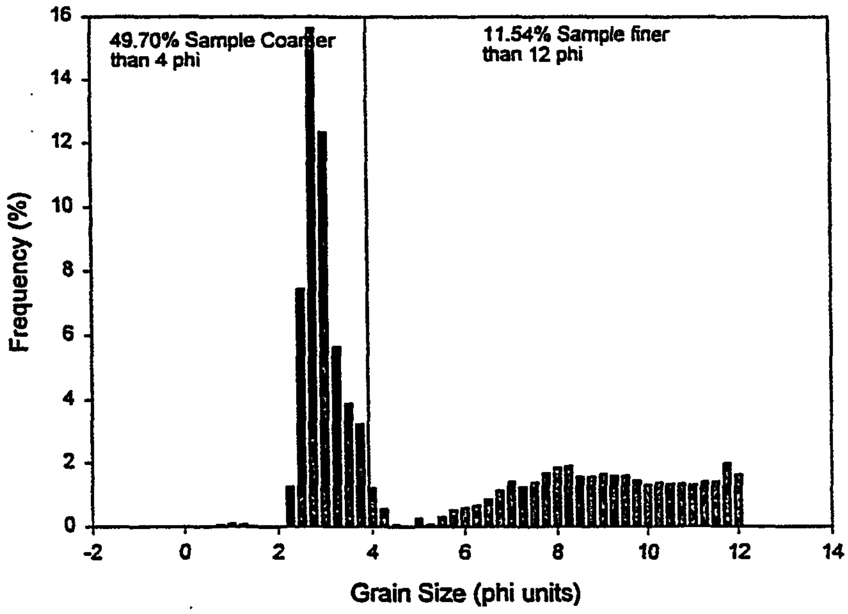

Figure C-18. Downcore plot of %sand and %clay for Core 285.

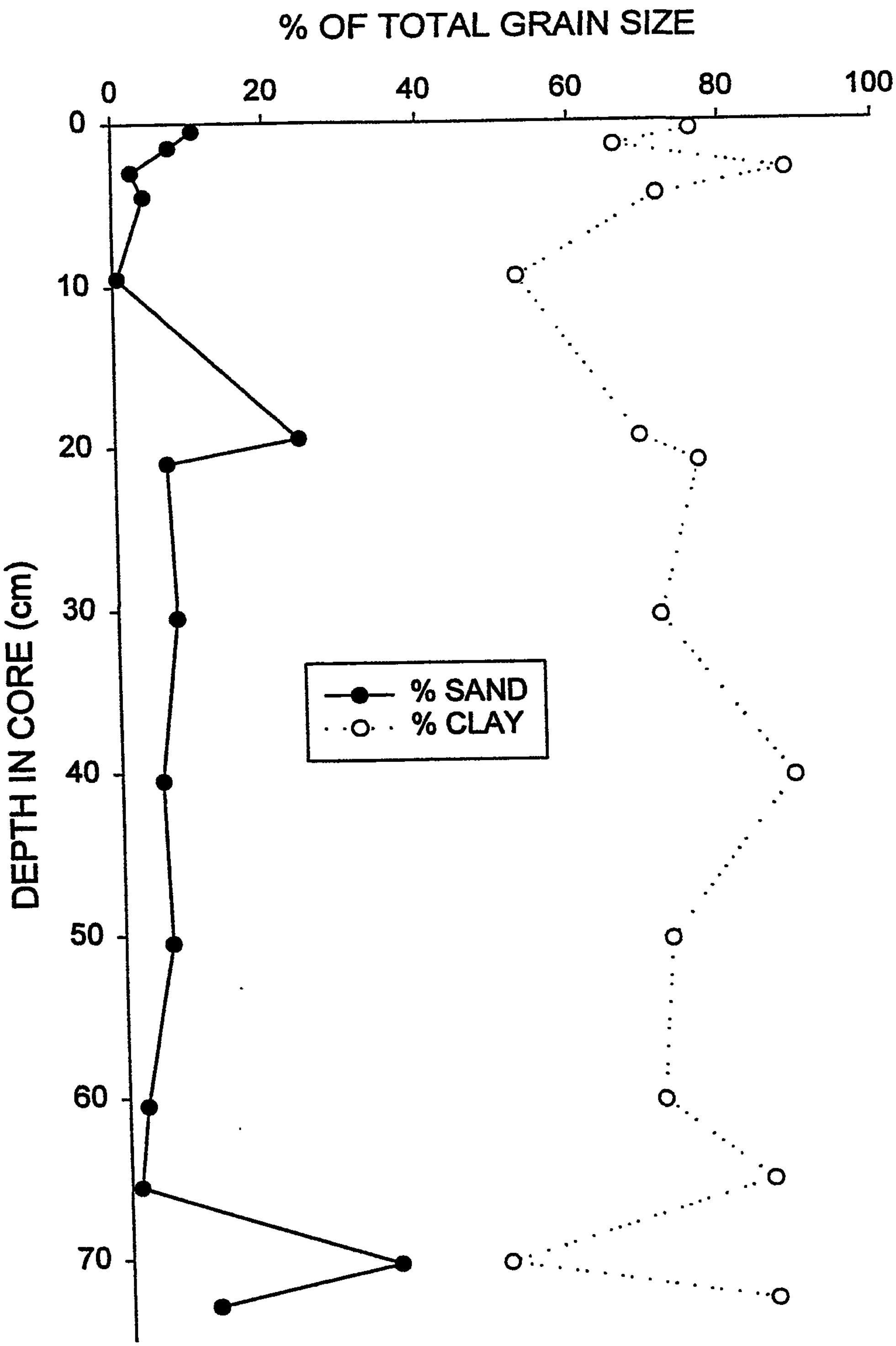

Figure C-19. Grain size histogram for Core 285, 2-4 cm depth.

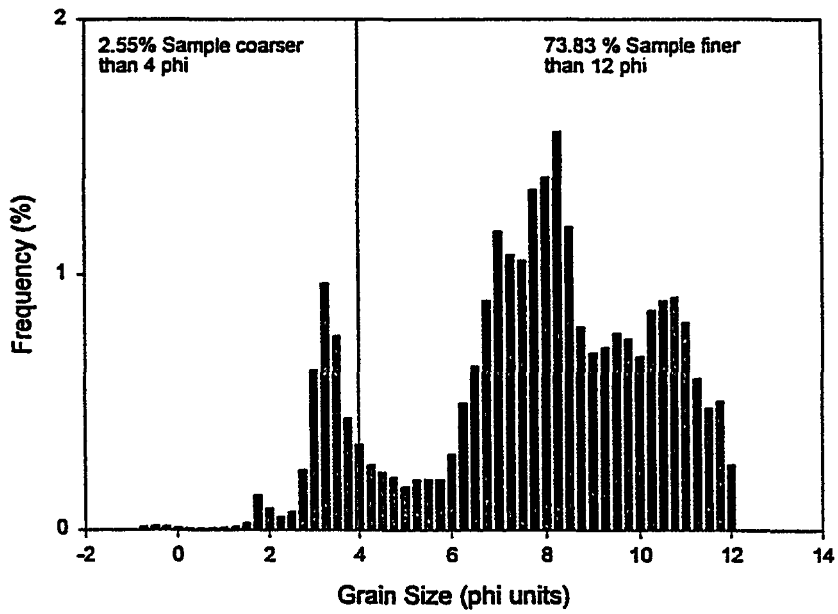

Figure C-20. Grain size histogram for Core 285, 20-22 cm depth.

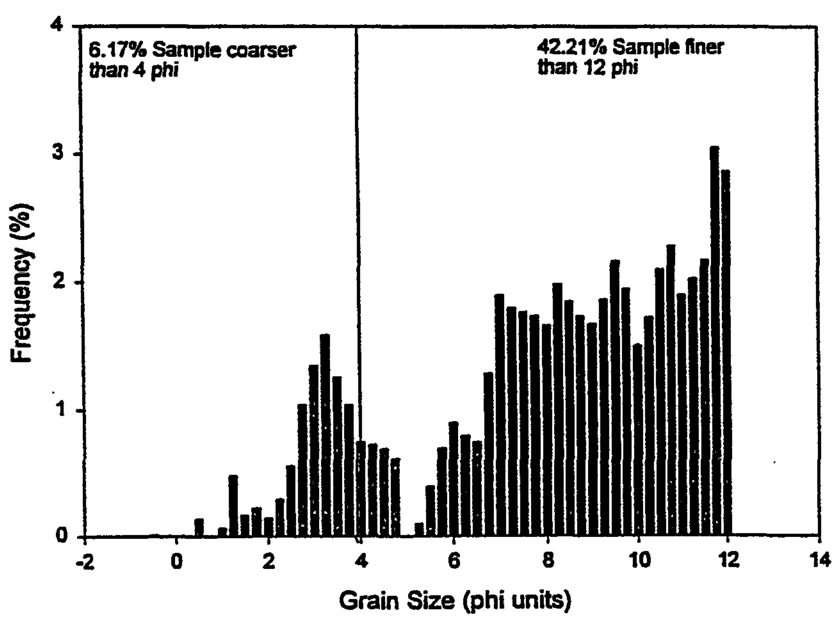

Figure C-21. Grain size histogram for Core 285, 72-74 cm depth.

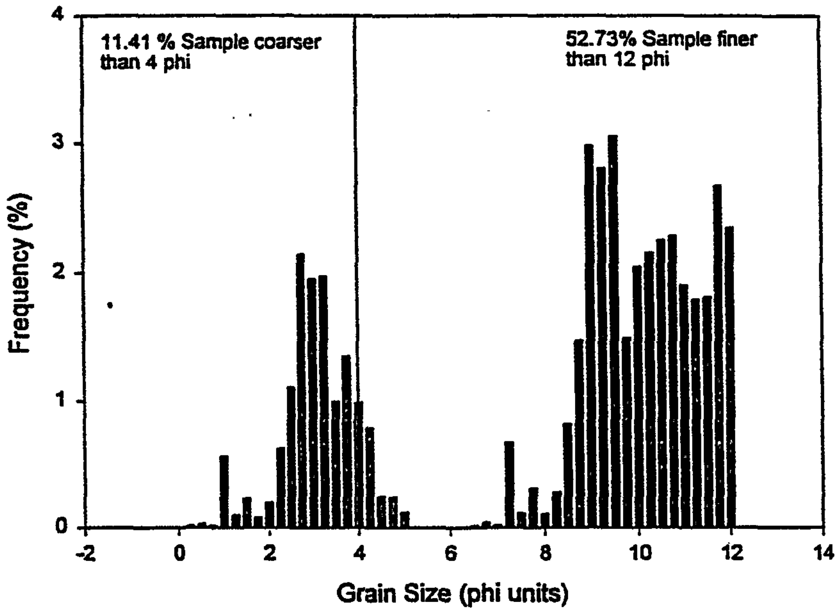

Figure C-22. Downcore plot of %sand and %clay for Core 286.

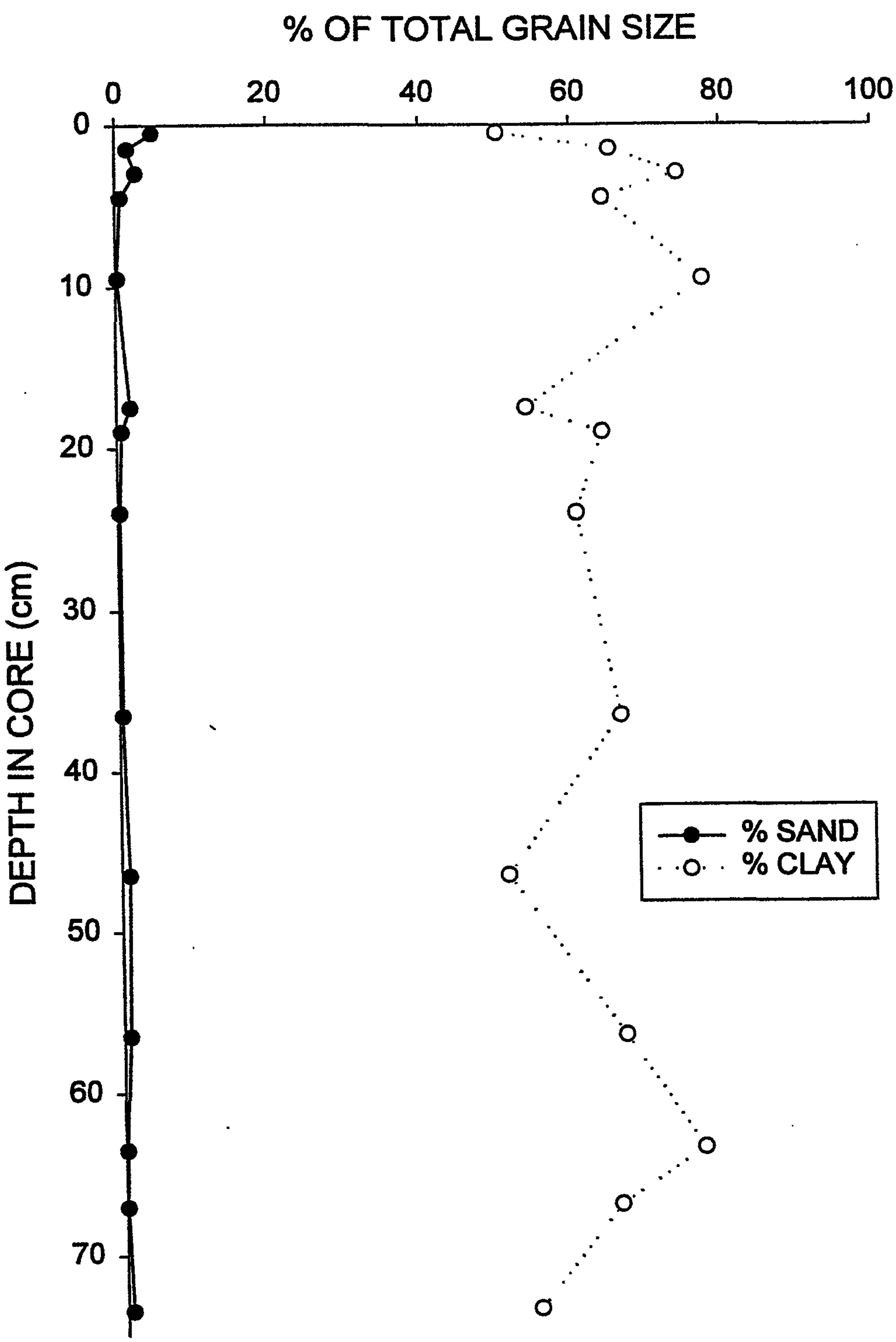

Figure C-23. Grain size histogram for Core 286, 2-4 cm depth.

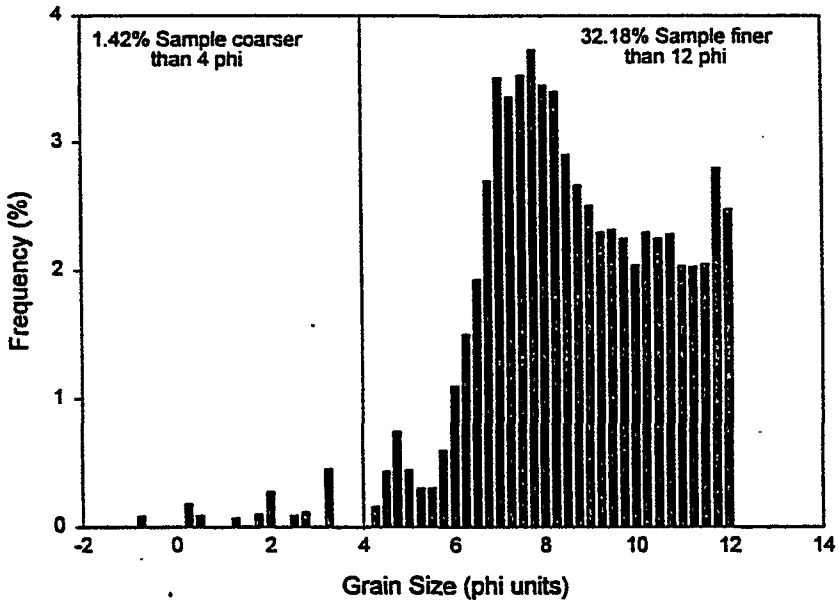

Figure C-24. Grain size histogram for Core 286, 18-20 cm depth.

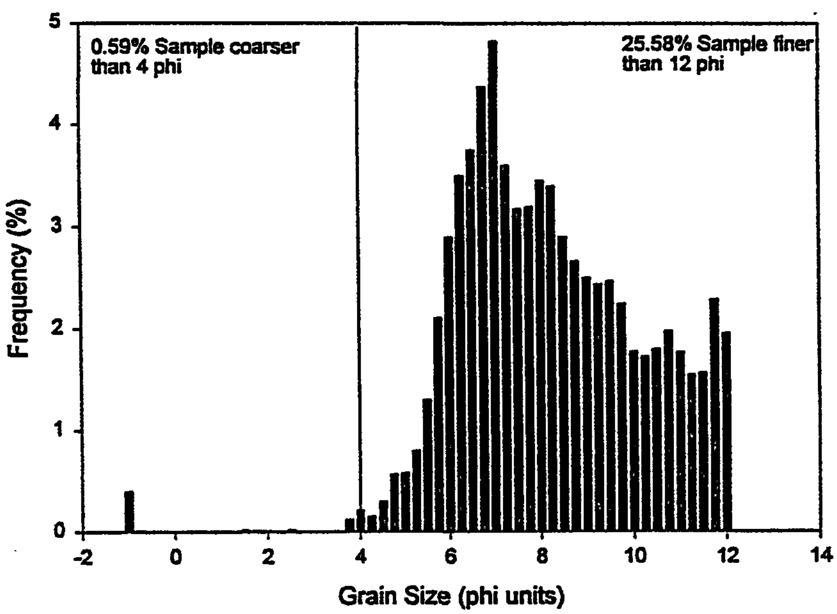

Figure C-25. Grain size histogram for Core 286, 23-25 cm depth.

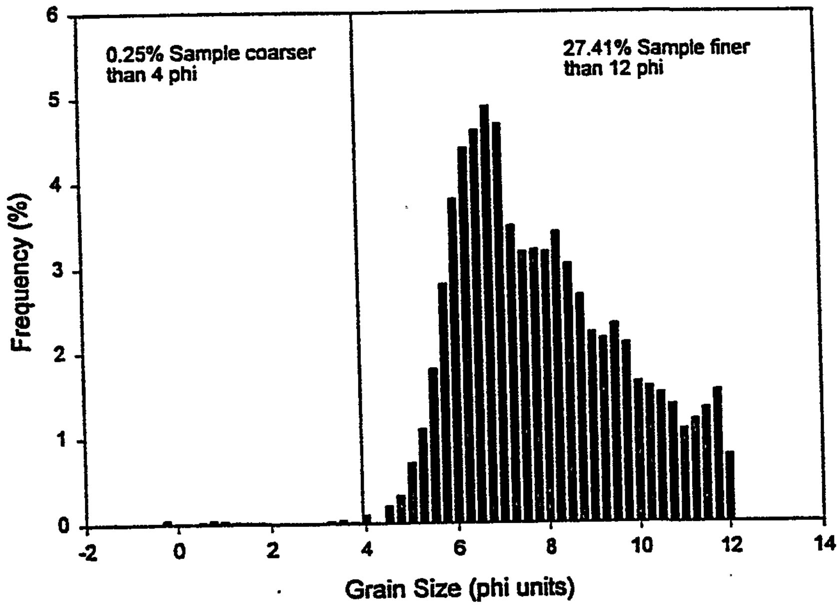

Figure C-26. Grain size histogram for Core 286, 66-68 cm depth.

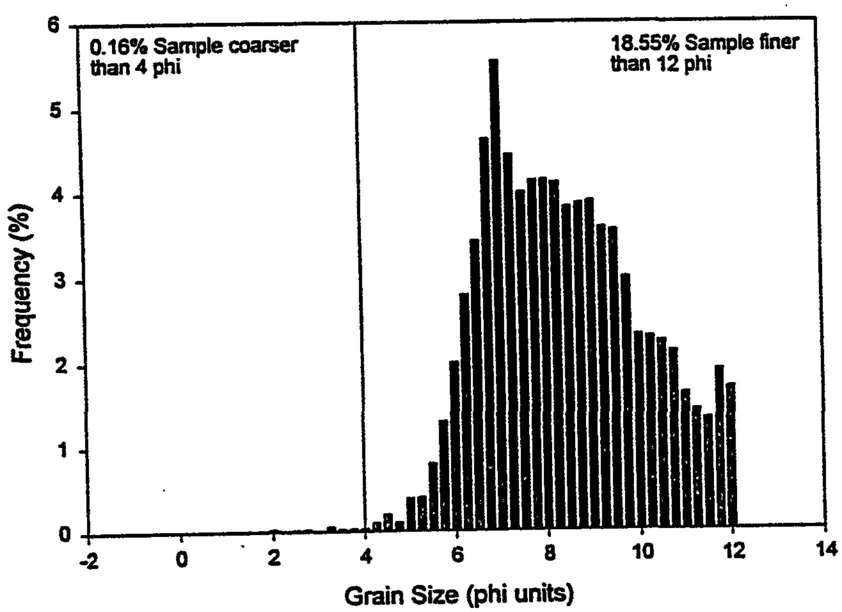

Figure C-27. Downcore plot of %sand and %clay for Core 296.

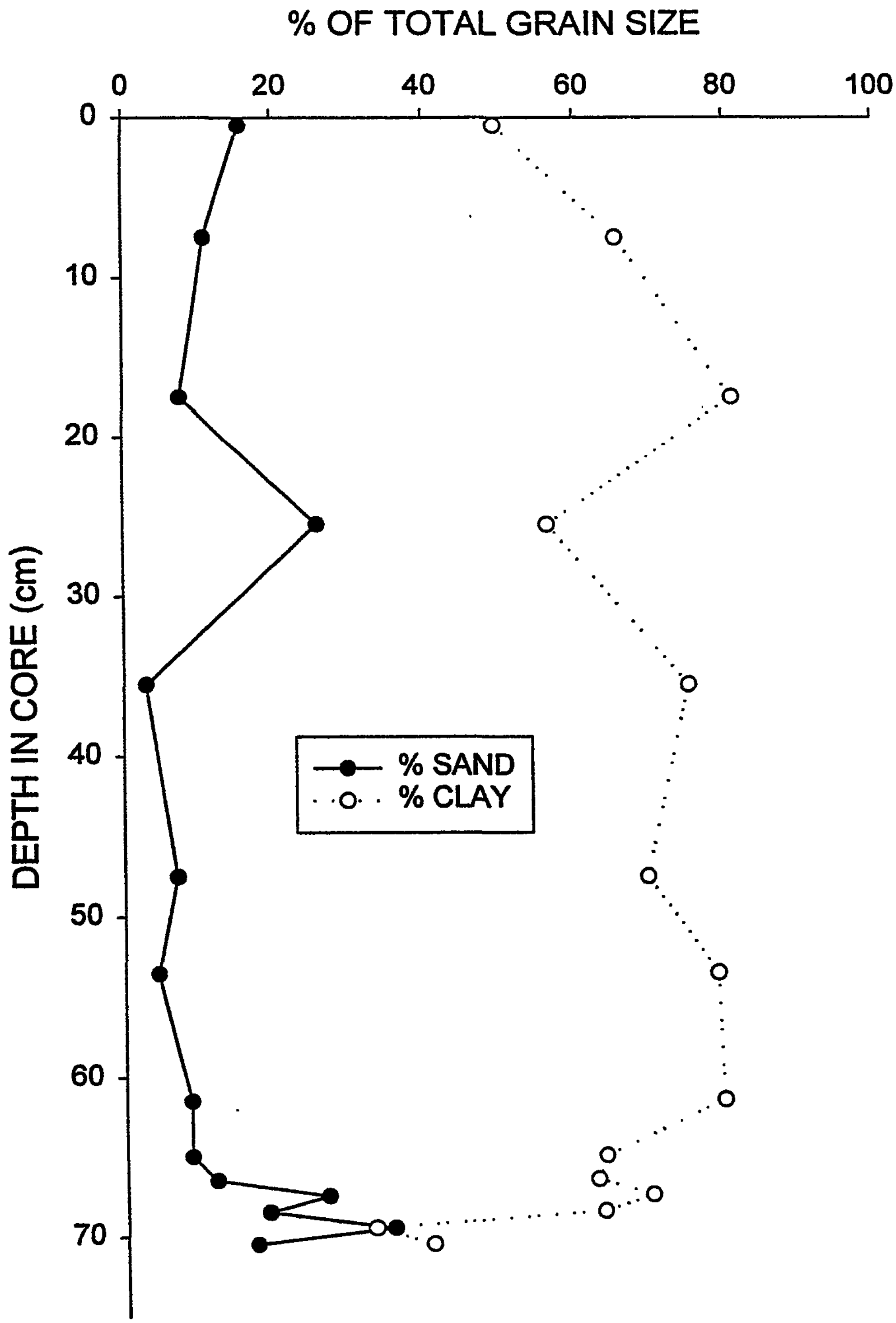

Figure C-28. Grain size histogram for Core 296, 7-8 cm depth.

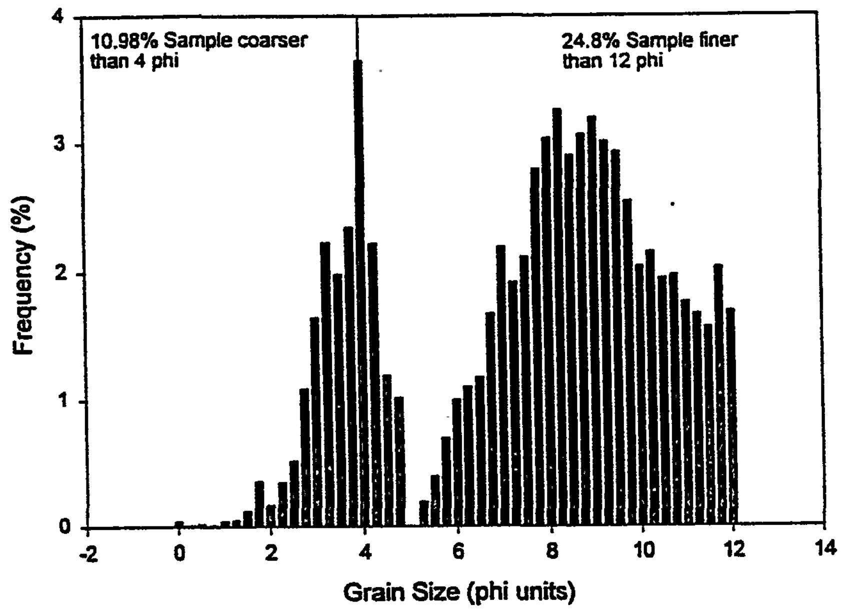

Figure C-29. Grain size histogram for Core 296, 25-26 cm depth.

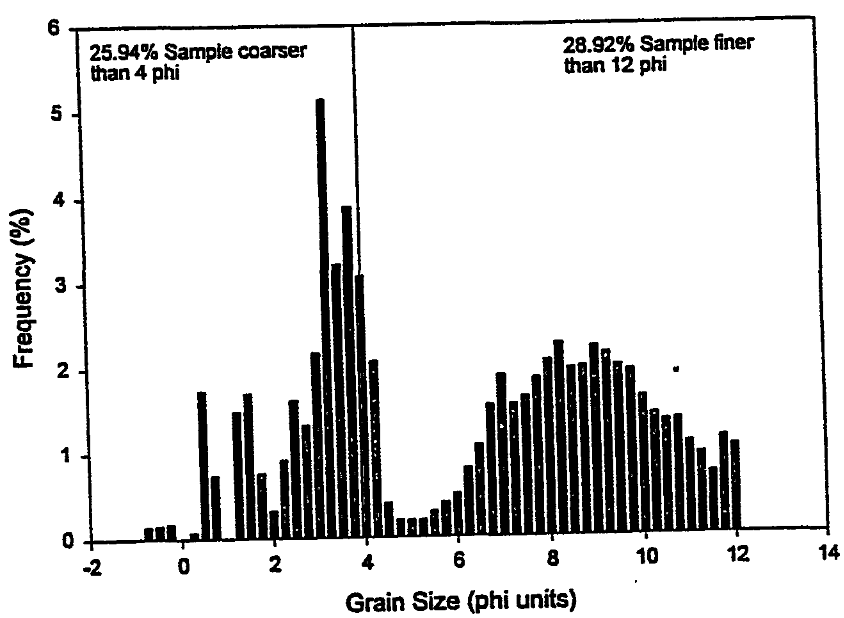

Figure C-30. Grain size histogram for Core 296, 35-36 cm depth.

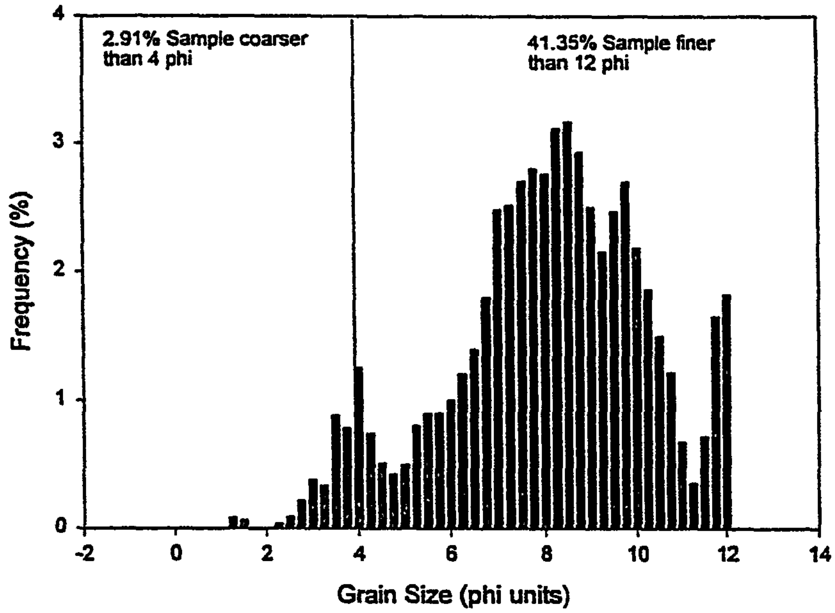

Figure C-31. Grain size histogram for Core 296, 70-71 cm depth.

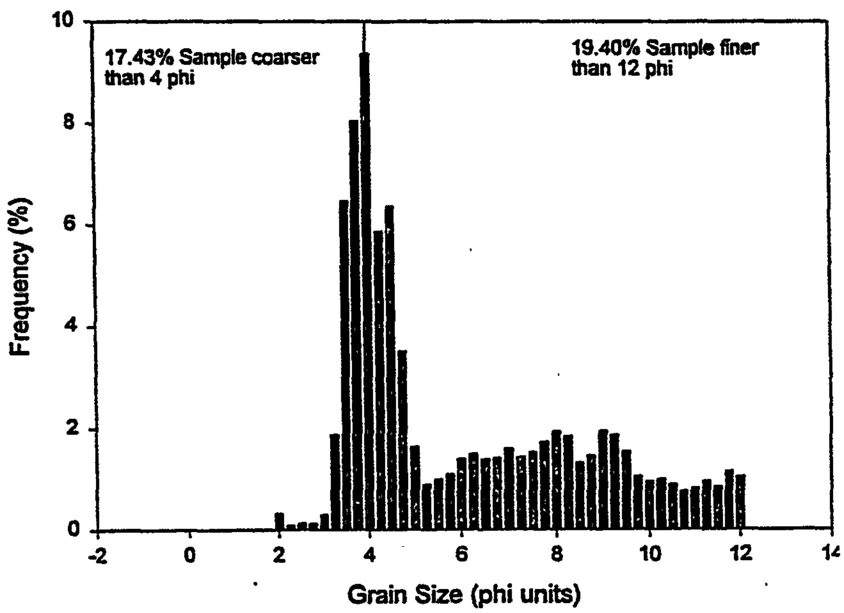

Figure C-32. Downcore plot of %sand and %clay for Core 300.

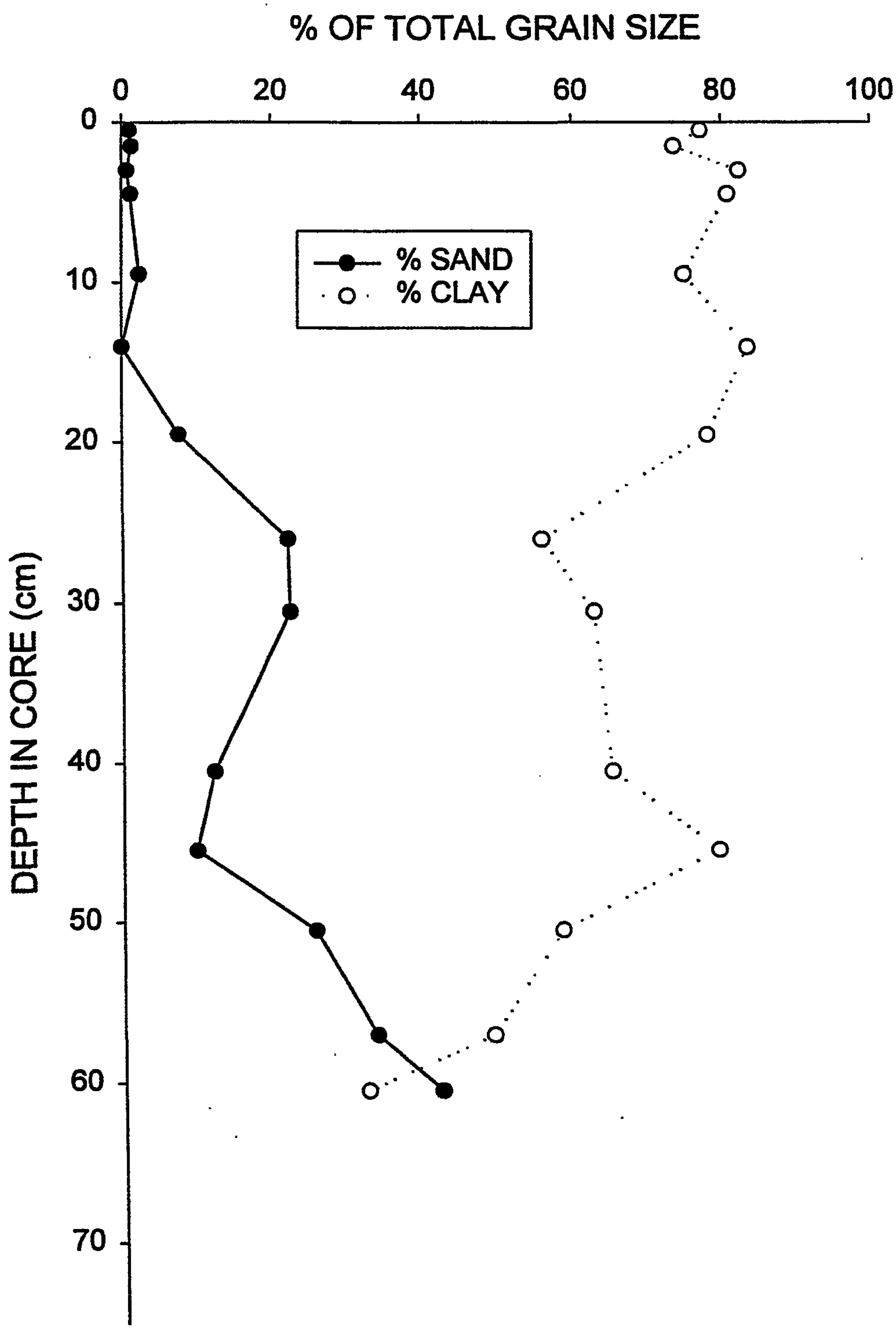

Figure C-33. Grain size histogram for Core 300, 2-4 cm depth.

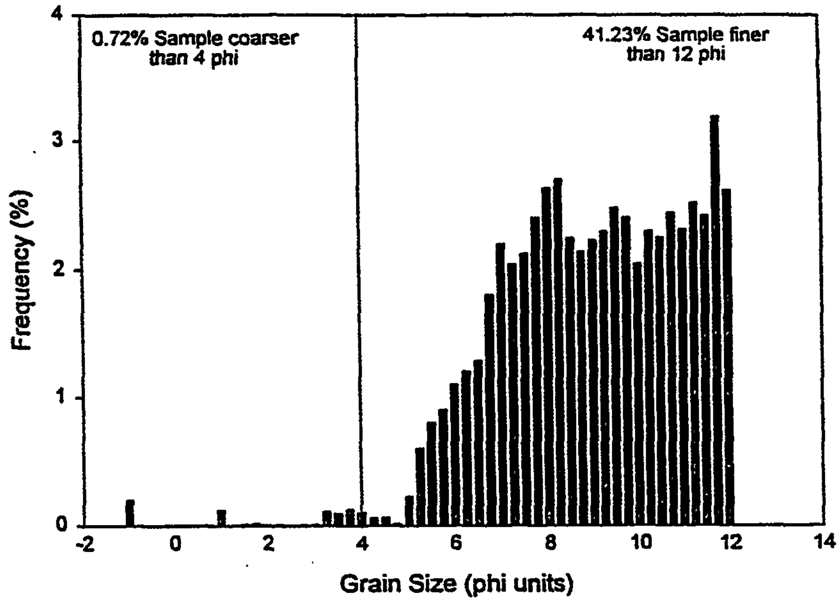

Figure C-34. Grain size histogram for Core 300, 13-15 cm depth.

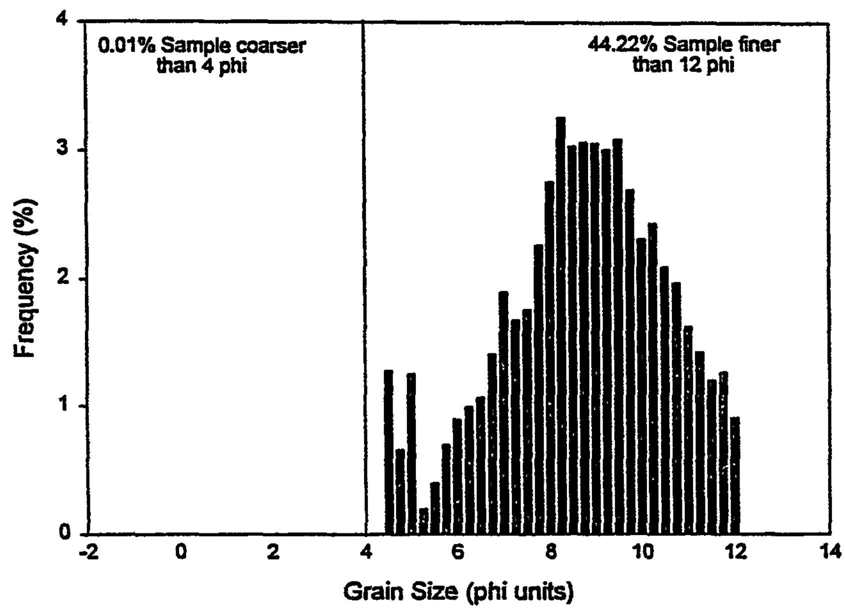

Figure C-35. Grain size histogram for Core 300, 25-27 cm depth.

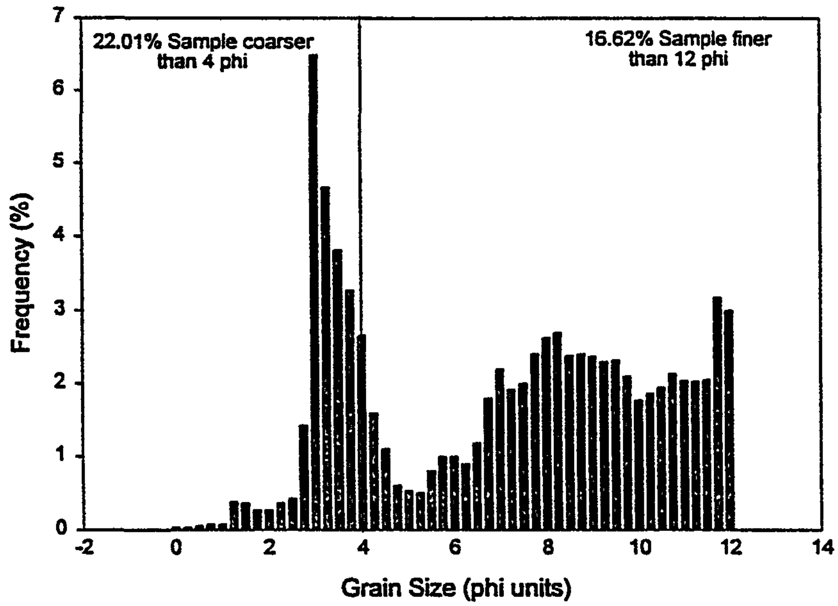

Figure C-36. Grain size histogram for Core 300, 56-58 cm depth.

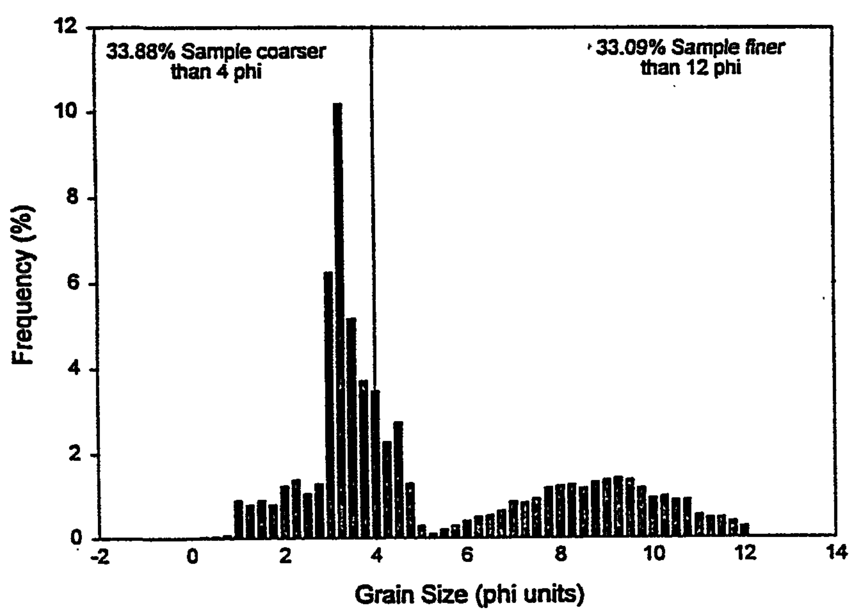

Figure C-37. Downcore plot of %sand and %clay for Core 924.

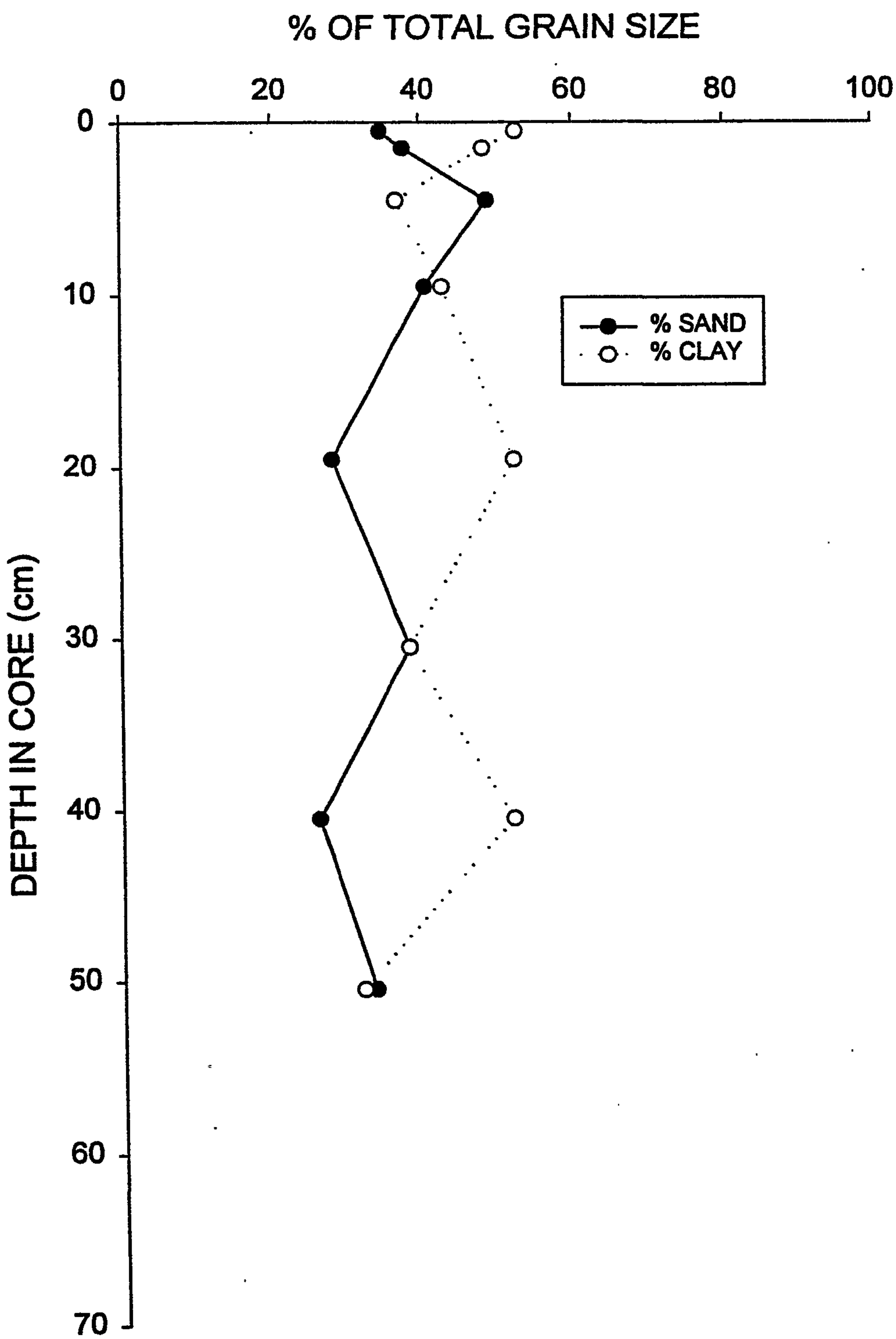

Figure C-38. Grain size histogram for Core 924, 2-4 cm depth.

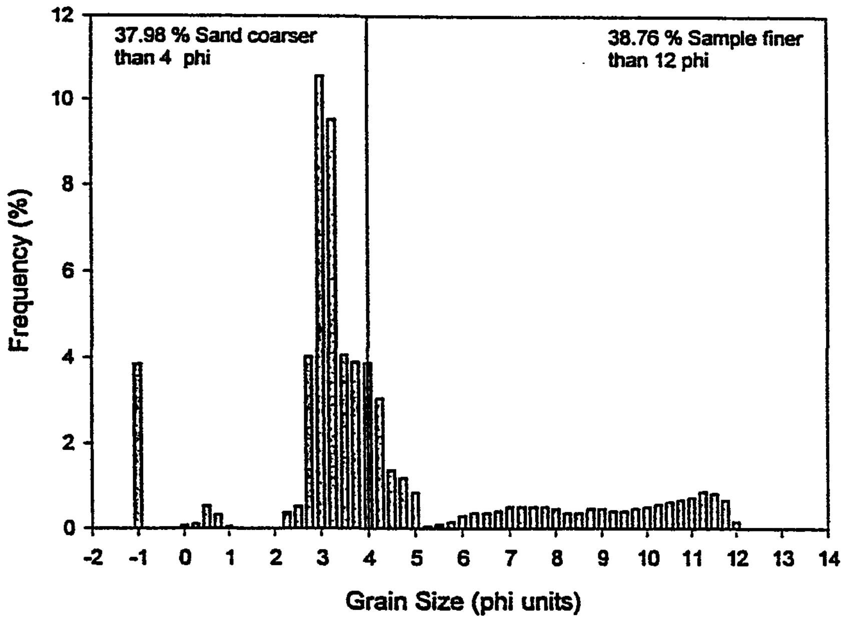

Figure C-39. Grain size histogram for Core 924, 13-15 cm depth.

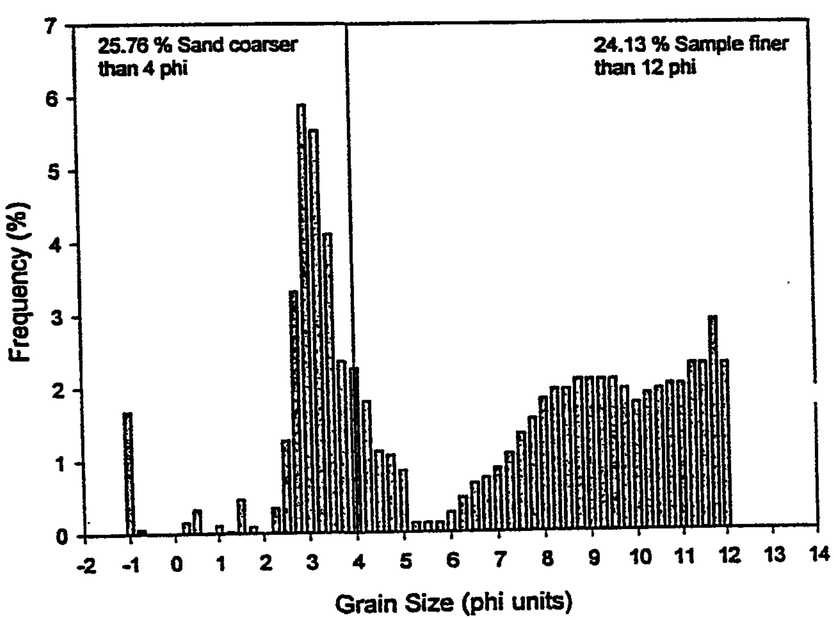

Figure C-40. Grain size histogram for Core 924, 25-27 cm depth.

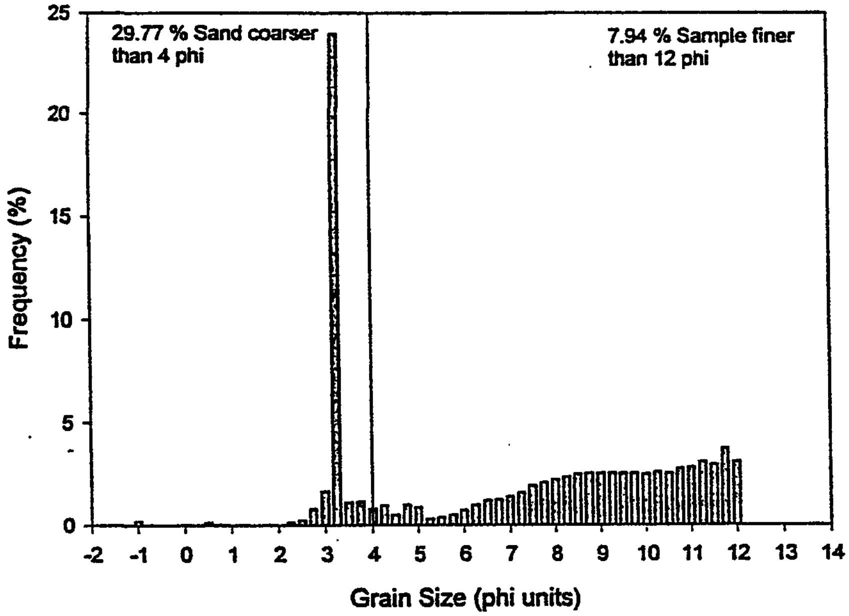

Figure C-41. Grain size histogram for Core 924, 44-46 cm depth.

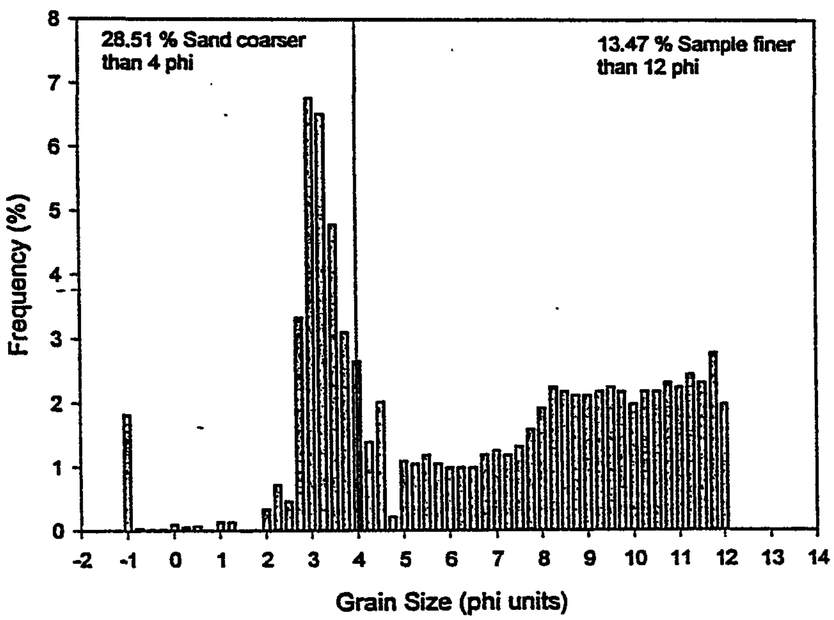

Figure C-42. Downcore plot of %sand and %clay for Core 926.

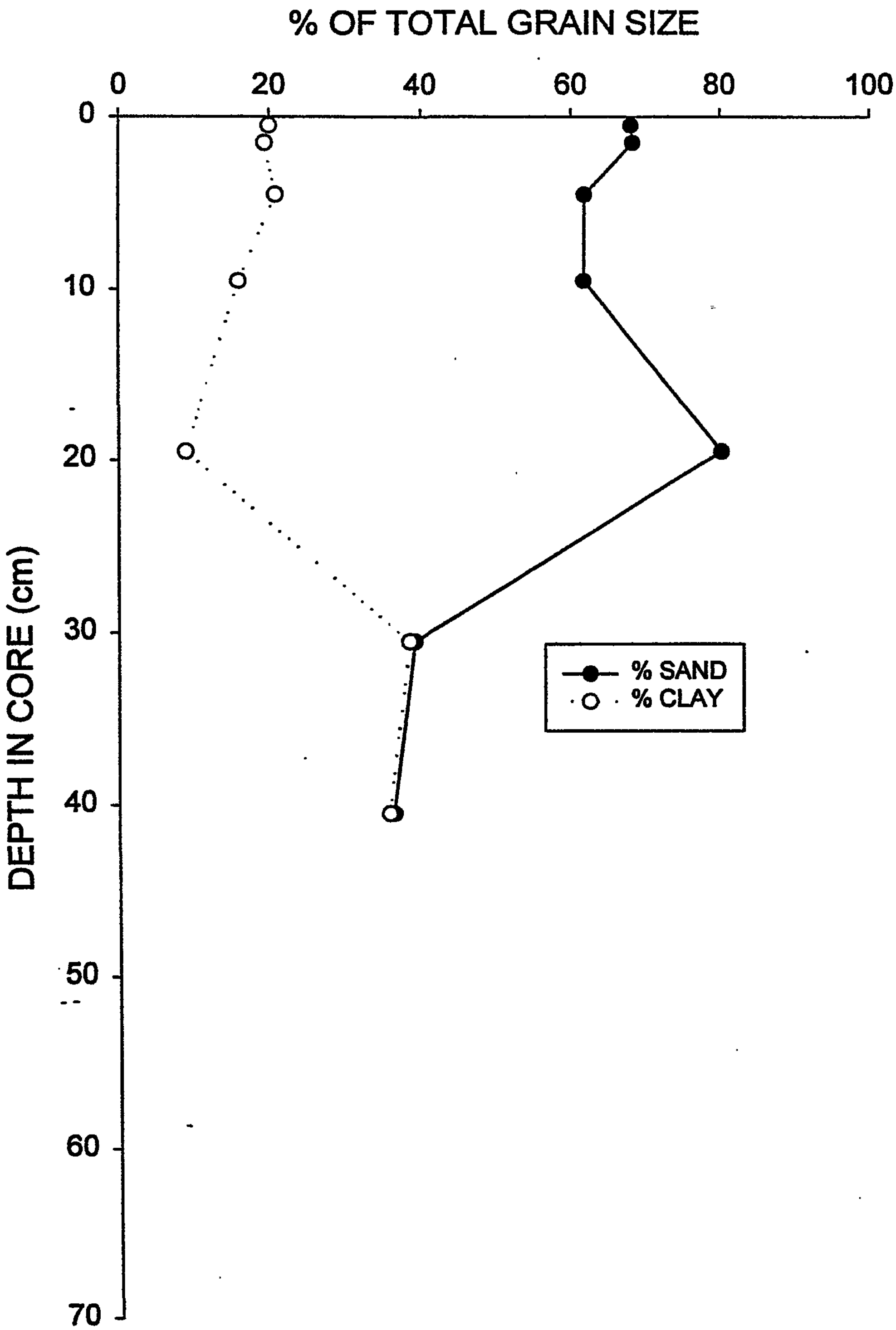

Figure C-43. Grain size histogram for Core 926, 2-4 cm depth.

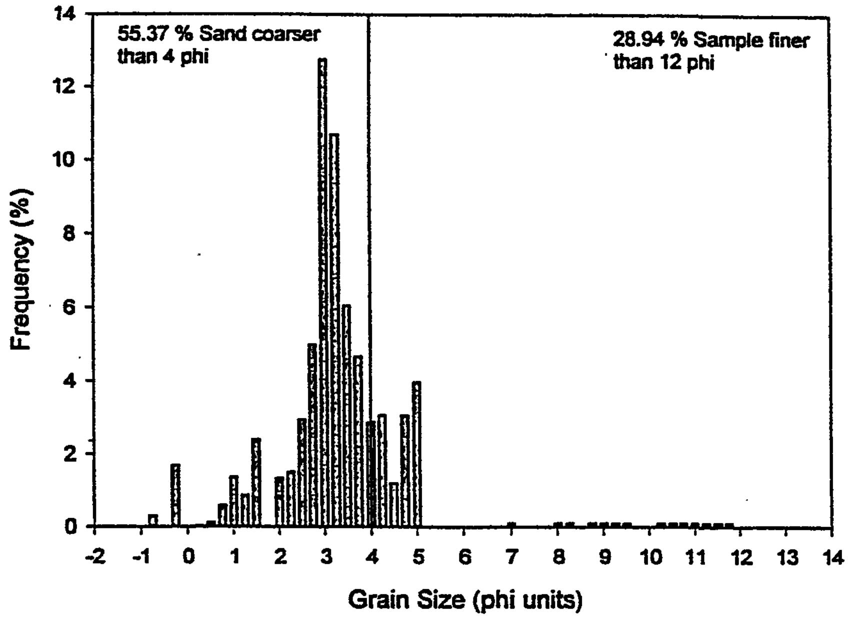

Figure C-44. Grain size histogram for Core 926, 13-15 cm depth.

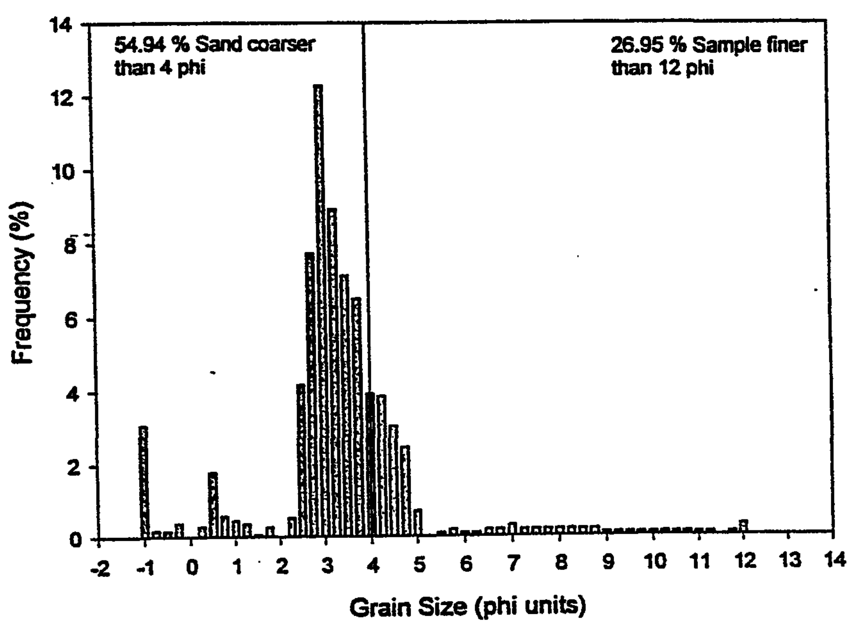

Figure C-45. Grain size histogram for Core 926, 25-27 cm depth.

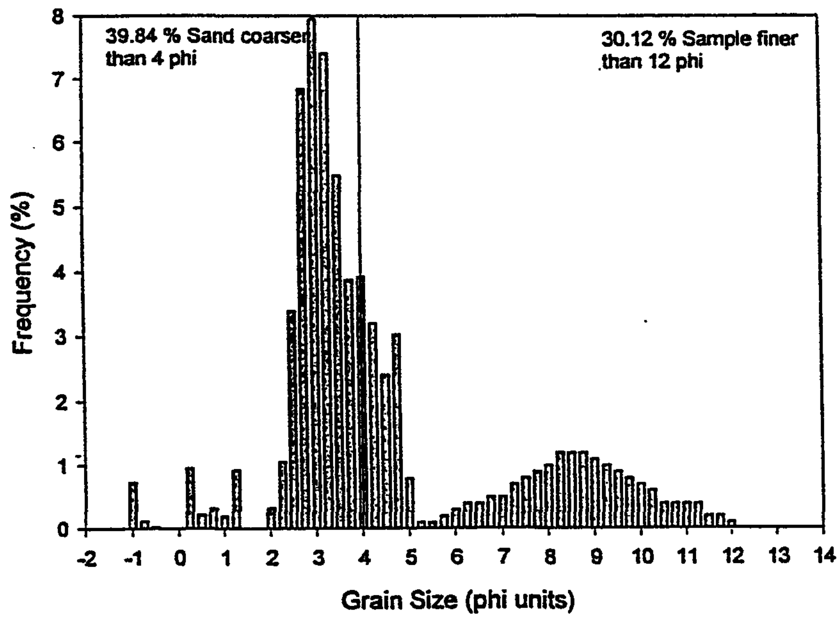

Figure C-46. Grain size histogram for Core 926, 44-46 cm depth.

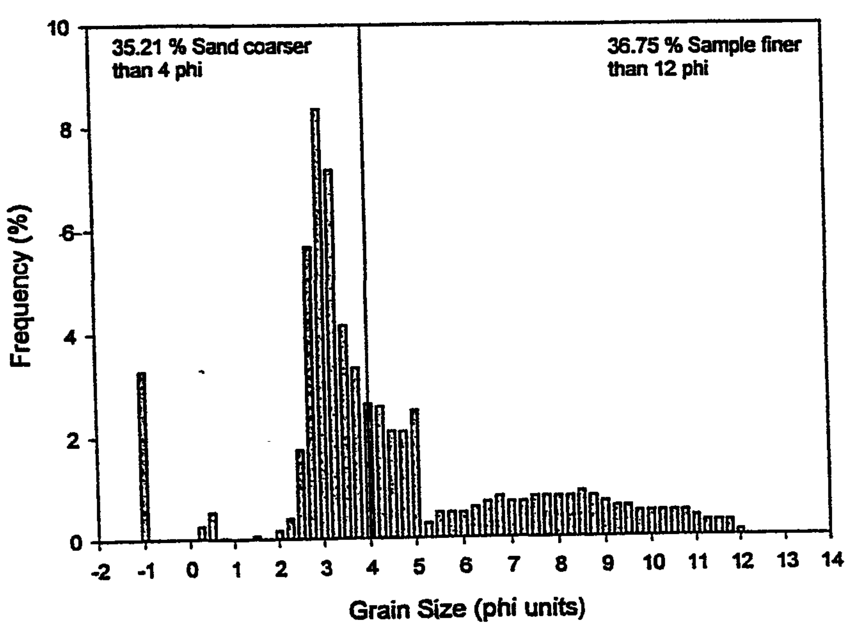

Figure C-47. Downcore plot of %sand and %clay for Core 928.

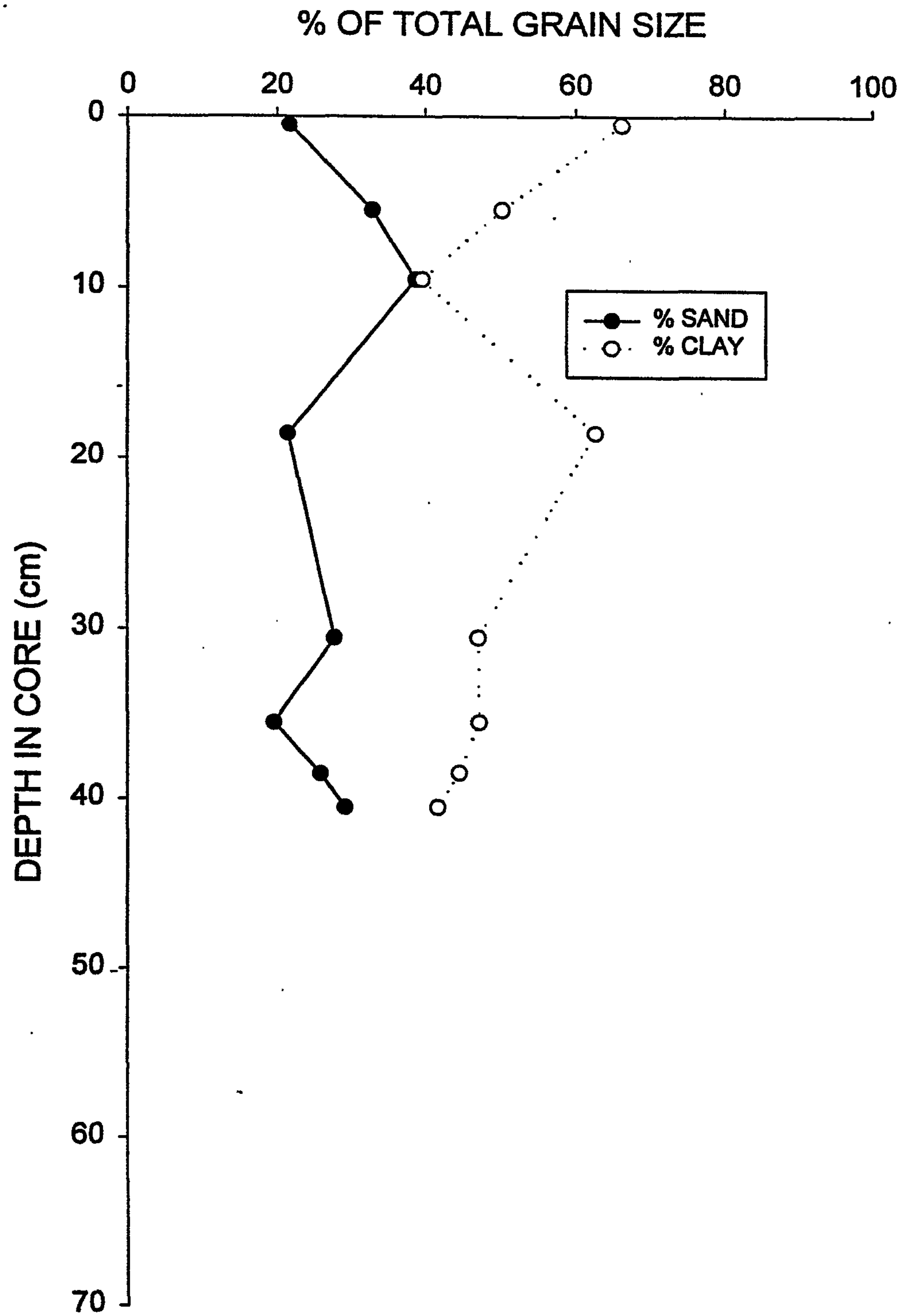

Figure C-48. Grain size histogram for Core 928, 2-4 cm depth.

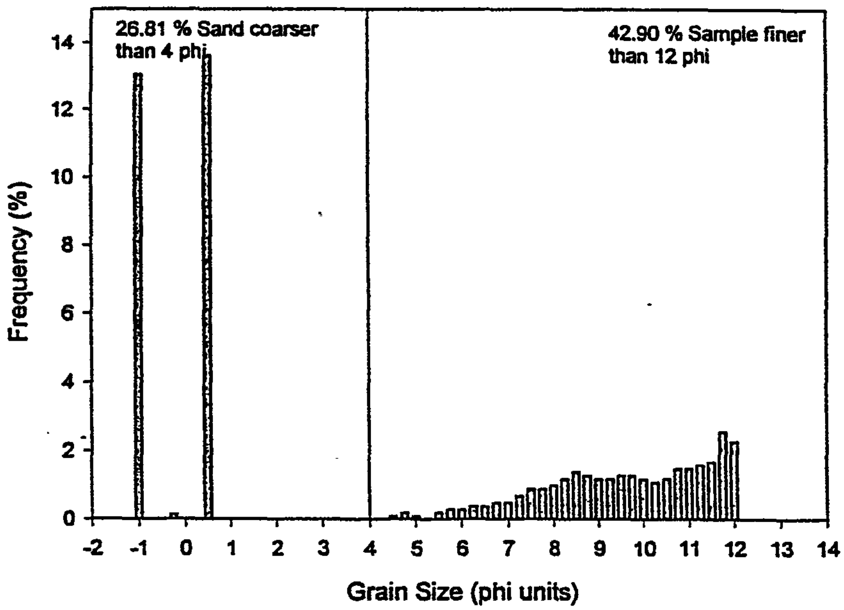

Figure C-49. Grain size histogram for Core 928, 13-15 cm depth.

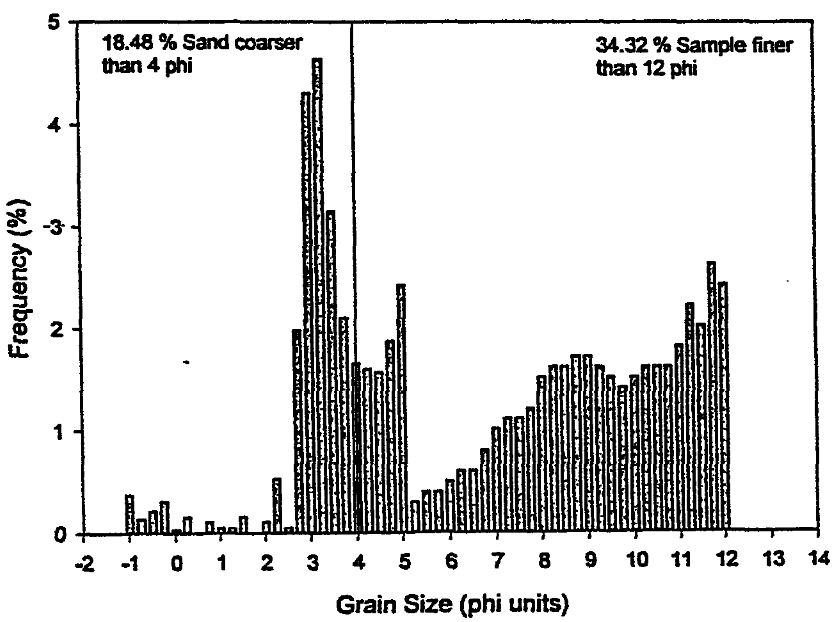

Figure C-50. Grain size histogram for Core 928, 25-27 cm depth.

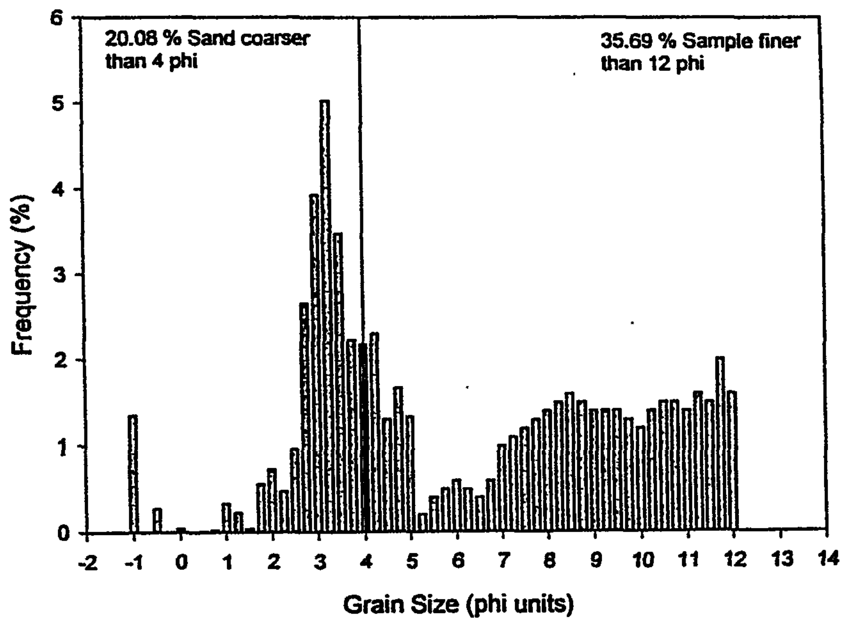

Figure C-51. Grain size histogram for Core 928, 44-46 cm depth.

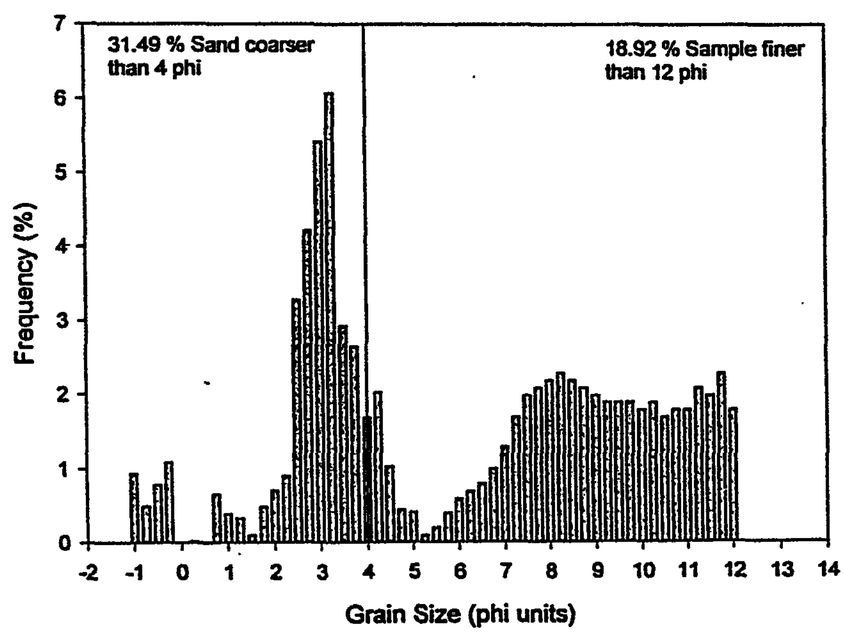

Figure C-52. Downcore plot of %sand and %clay for Core 4293.

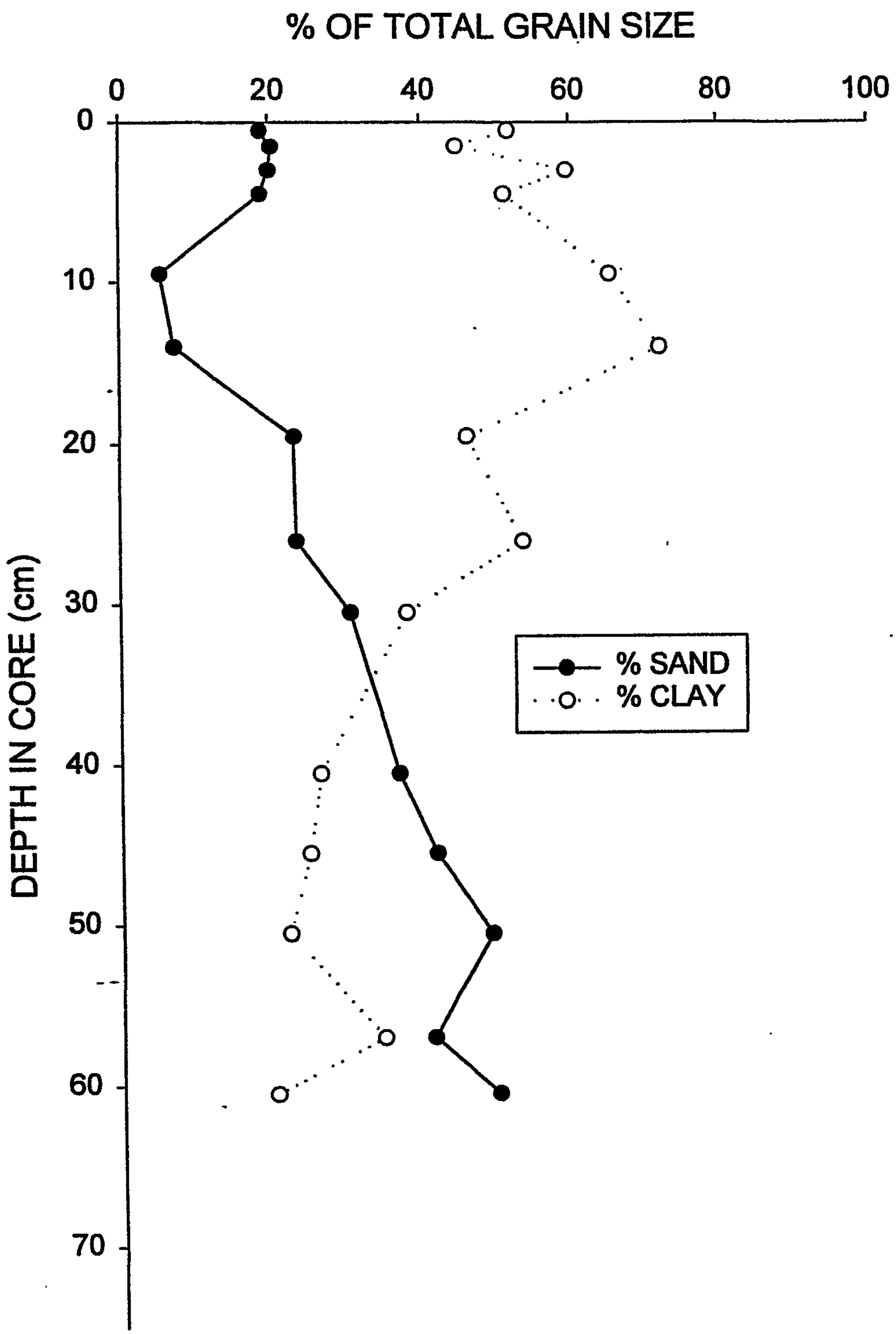

Figure C-53. Grain size histogram for Core 4293, 2-4 cm depth.

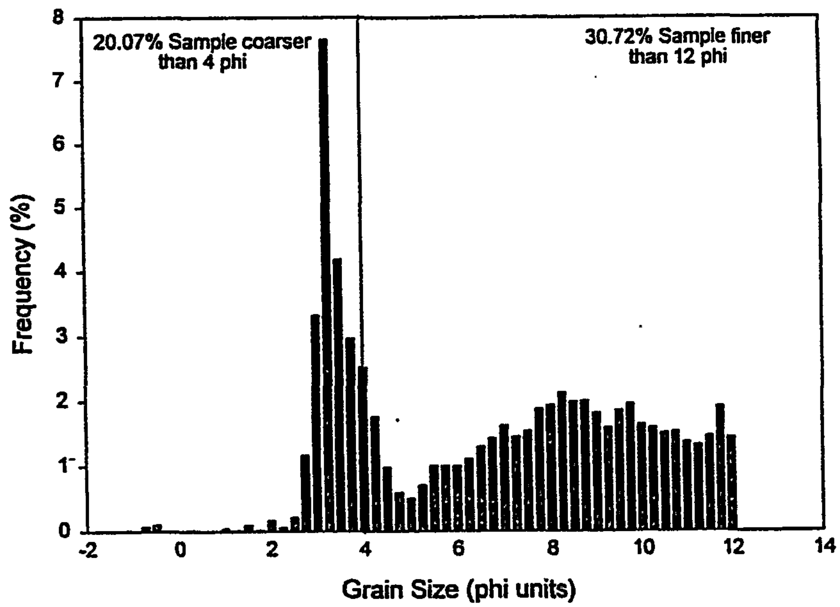

Figure C-54. Grain size histogram for Core 4293, 13-15 cm depth.

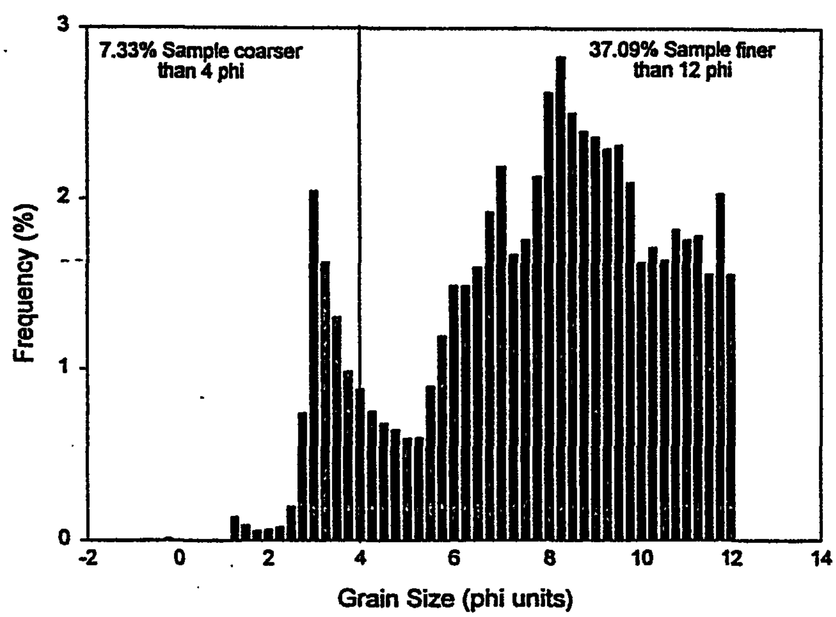

Figure C-55. Grain size histogram for Core 4293, 56-58 cm depth.

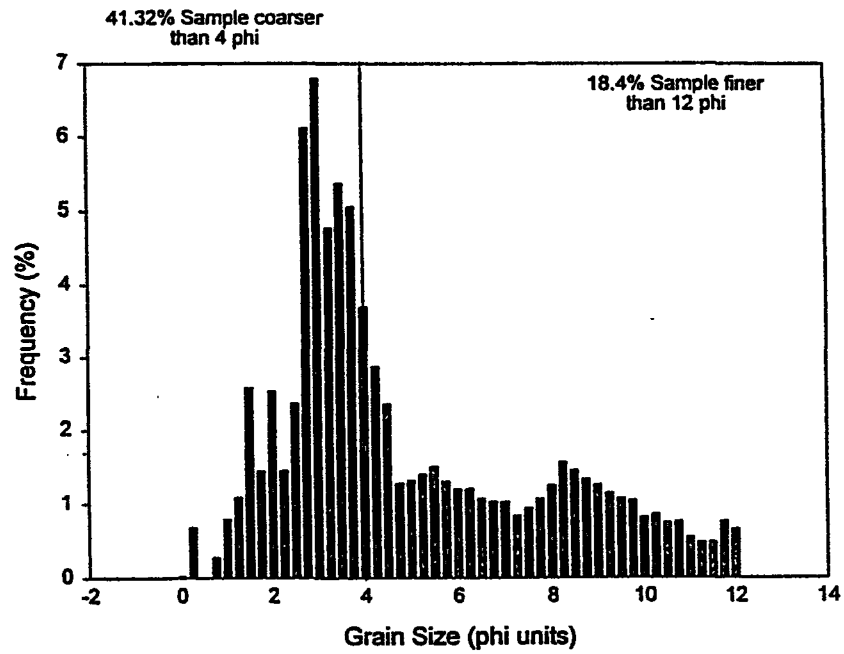

Figure C-56. Downcore plot of %sand and %clay for Core 8721.

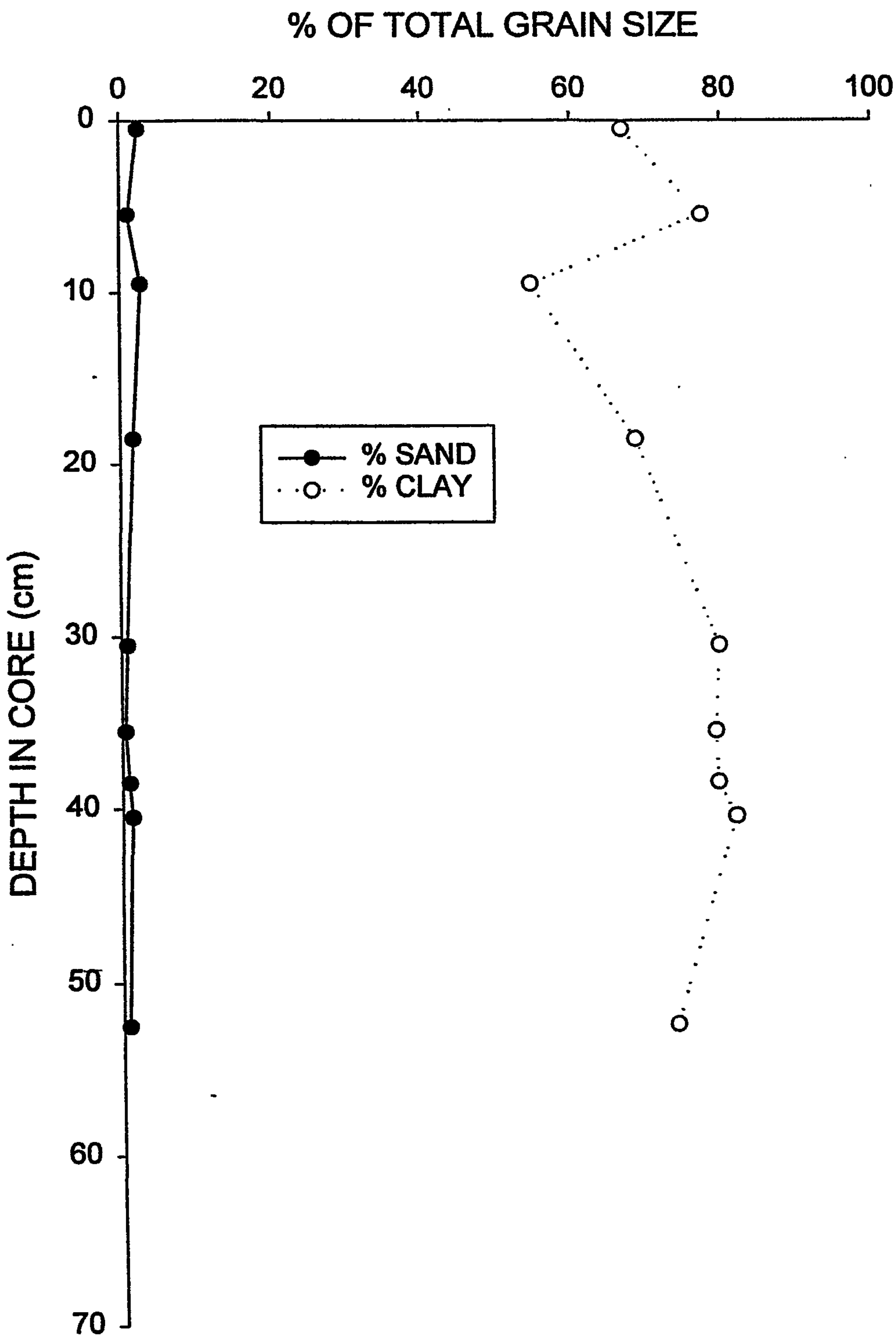

Figure C-57. Grain size histogram for Core 8721, 2-4 cm depth.

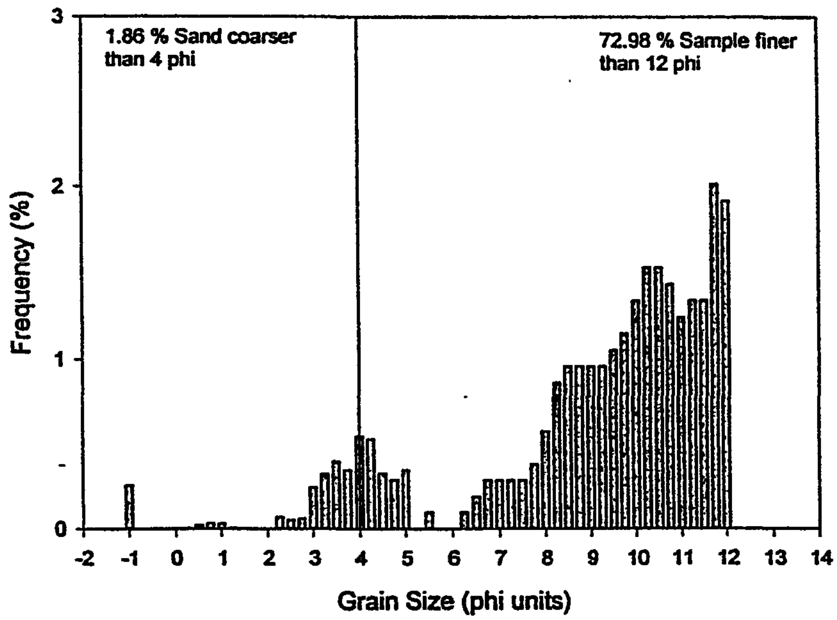

Figure C-58. Grain size histogram for Core 8721, 13-15 cm depth.

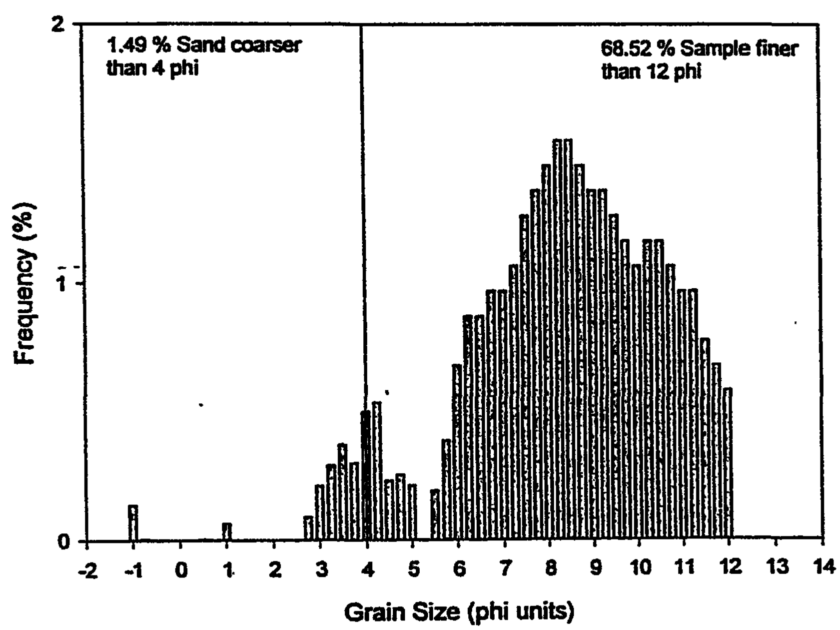

Figure C-59. Grain size histogram for Core 8721, 25-27 cm depth.

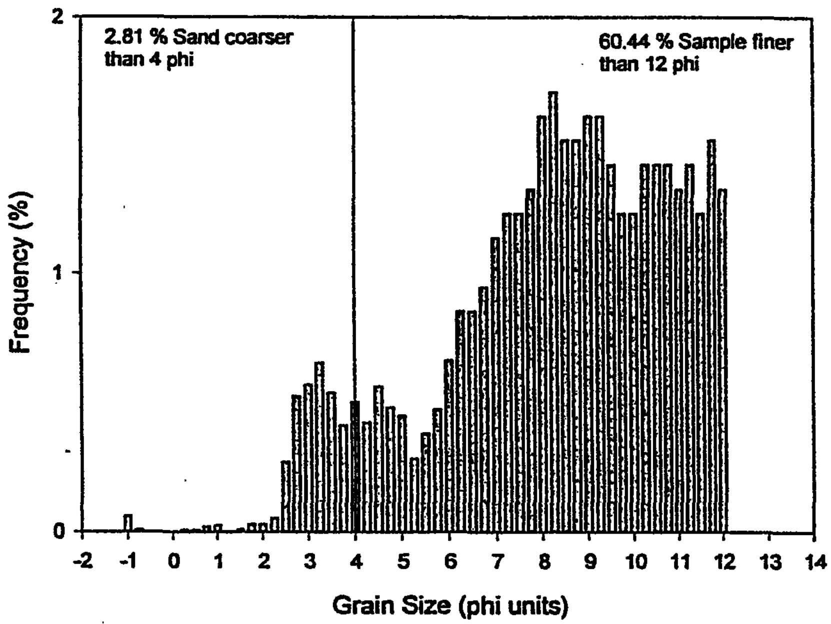

Figure C-60. Grain size histogram for Core 8721, 44-46 cm depth.

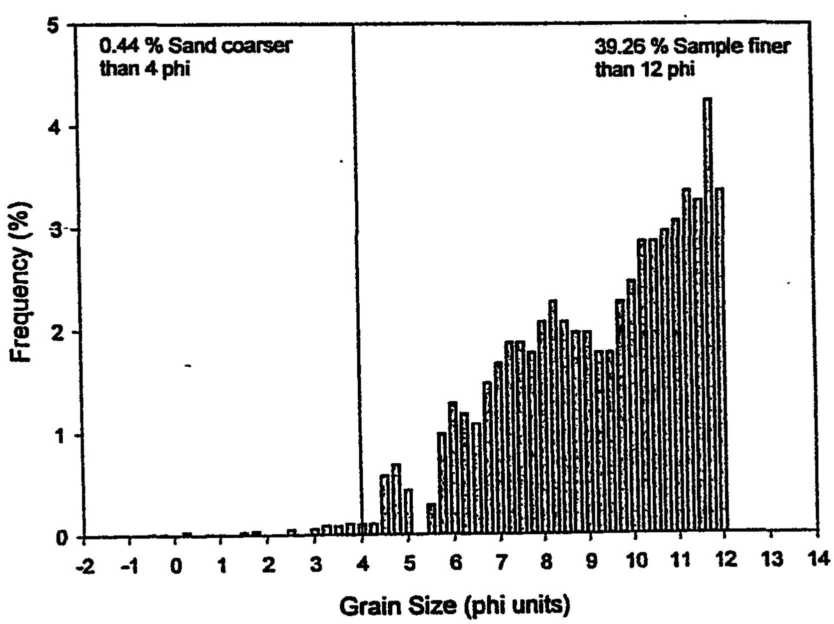

Figure C-61. Downcore plot of %sand and %clay for Core 8826.

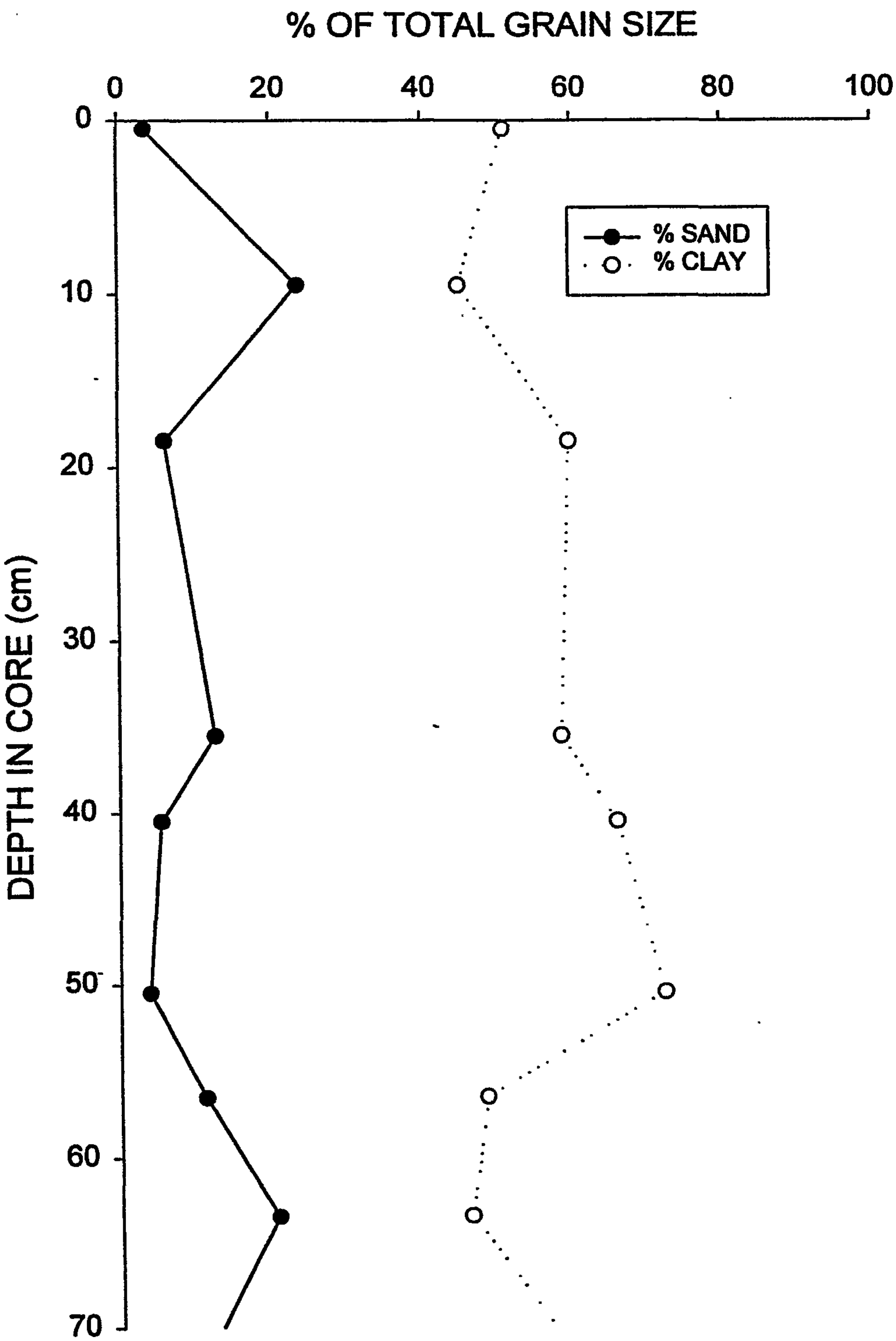

Figure C-62. Grain size histogram for Core 8826, 2-4 cm depth.

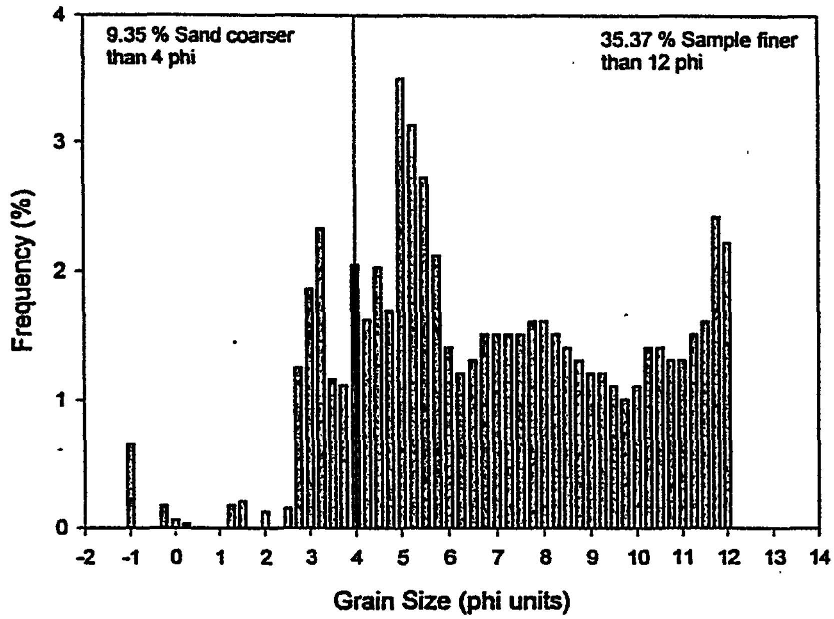

Figure C-63. Grain size histogram for Core 8826, 13-15 cm depth.

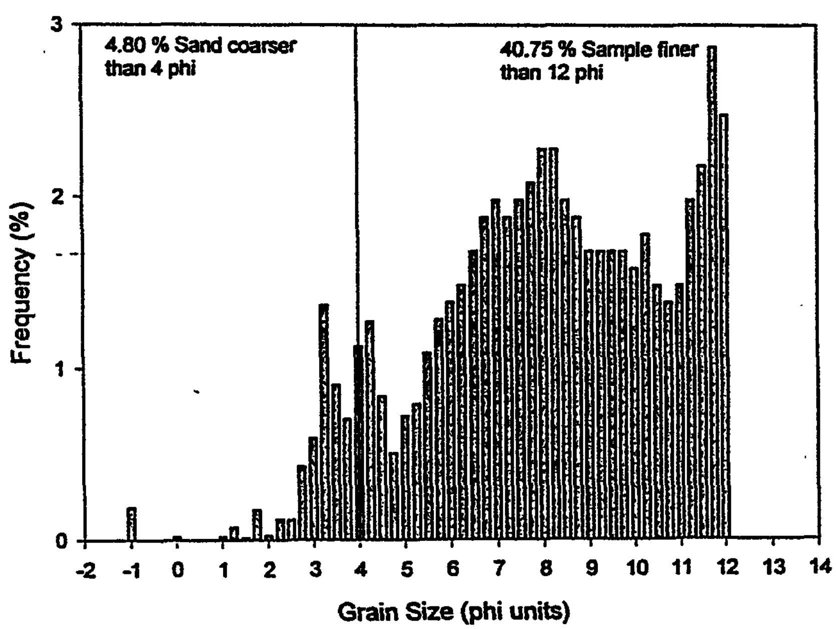

Figure C-64. Grain size histogram for Core 8826, 25-27 cm depth.

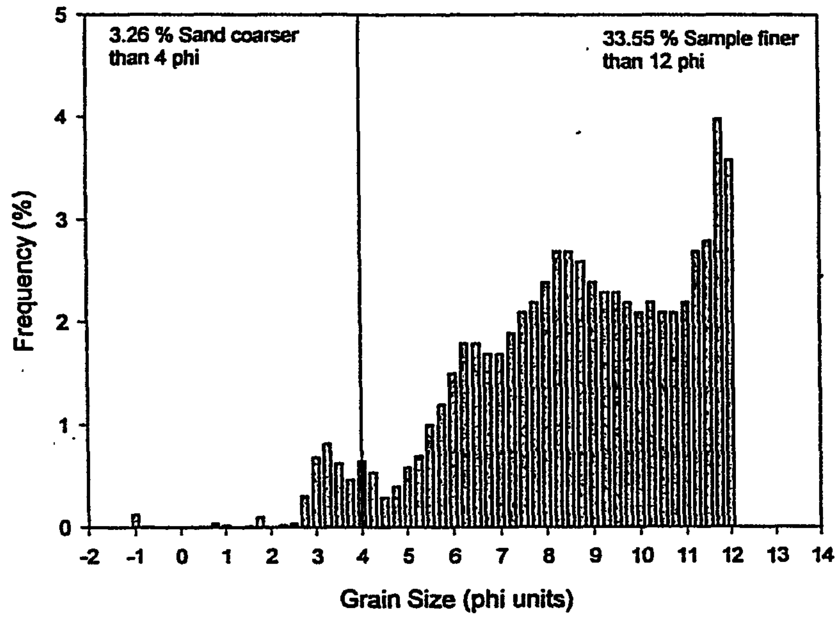

Figure C-65. Grain size histogram for Core 8826, 44-46 cm depth.

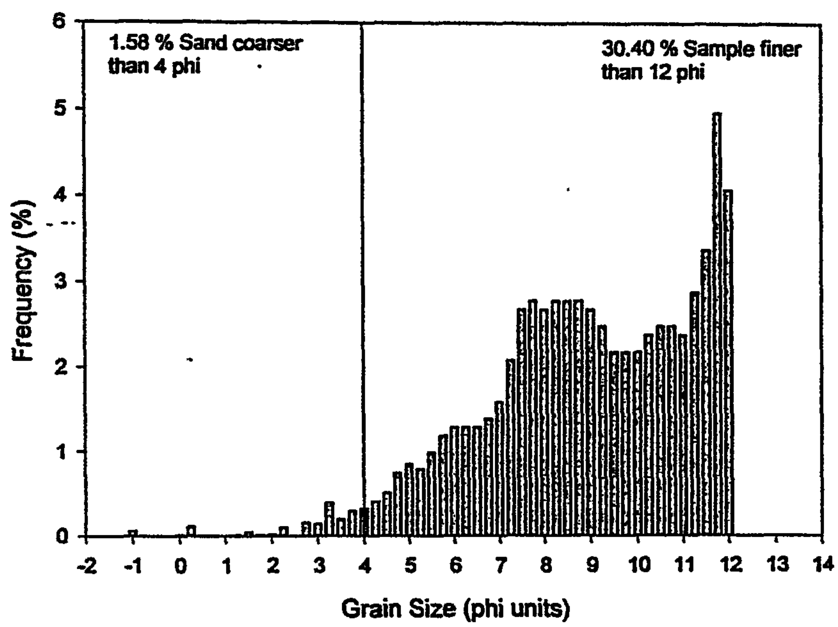

Figure C-66. Downcore plot of %sand and %clay for Core 8827.

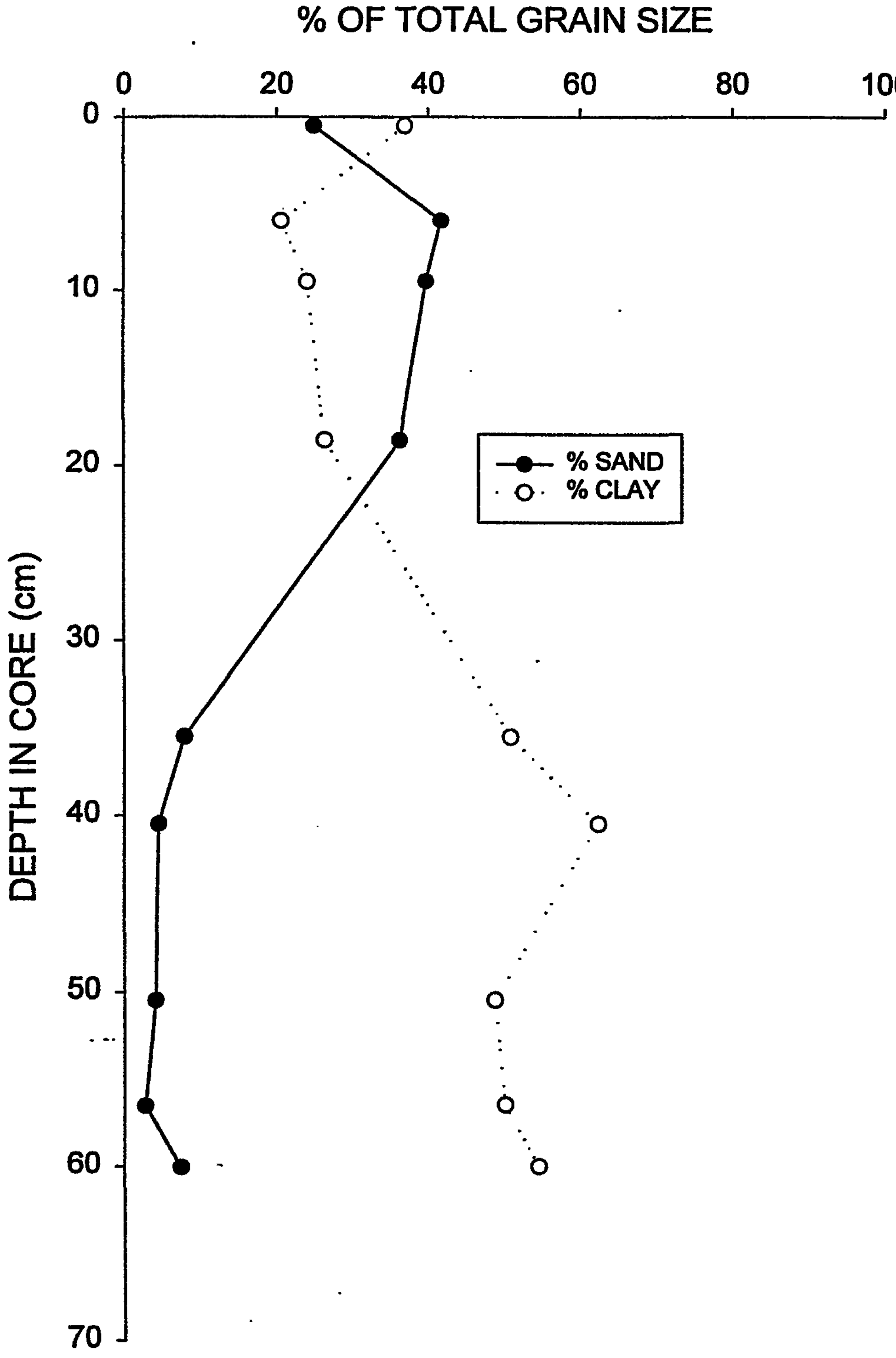

Figure C-67. Grain size histogram for Core 8827, 2-4 cm depth.

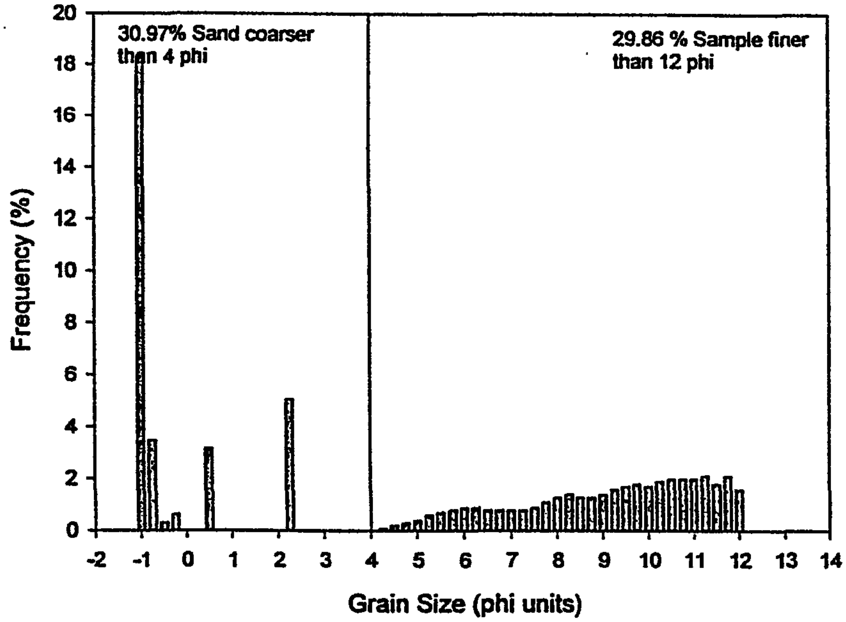

Figure C-68. Grain size histogram for Core 8827, 13-15 cm depth.

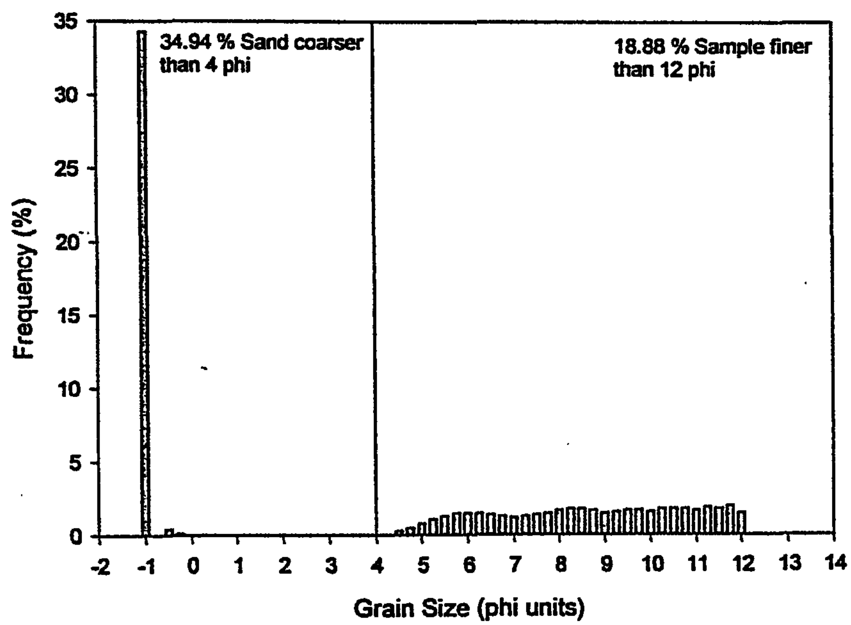

Figure C-69. Grain size histogram for Core 8827, 25-27 cm depth.

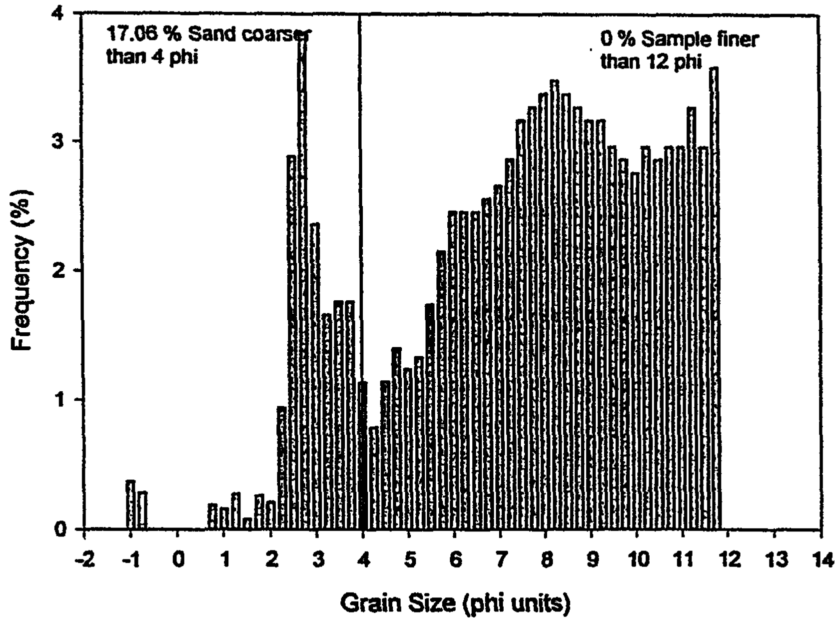

Figure C-70. Grain size histogram for Core 8827, 44-46 cm depth.

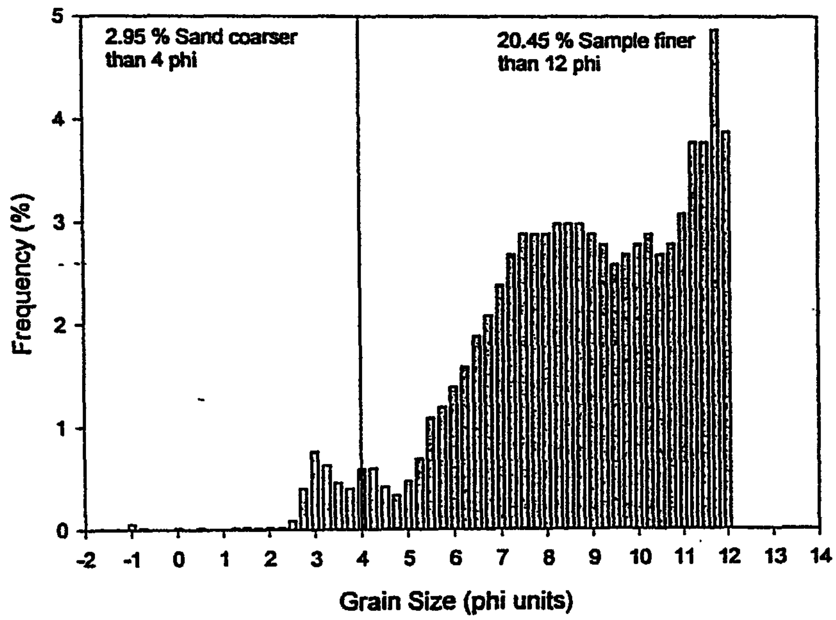

Figure C-71. Porosity depth distribution for Core 128. (Note that porosity was determined for every 5 cm homogenized section.)

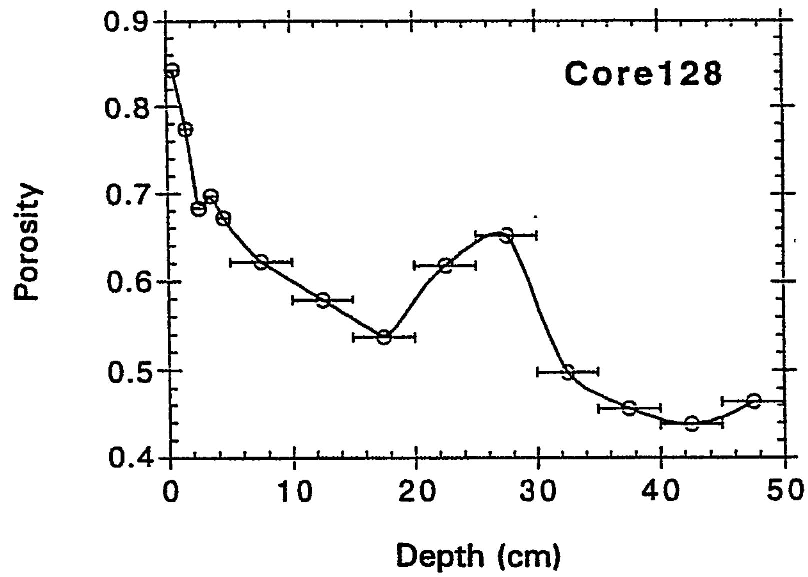

Figure C-72. Porosity depth distribution for Core 134. (Note that porosity was determined for every 1 cm homogenized section.)

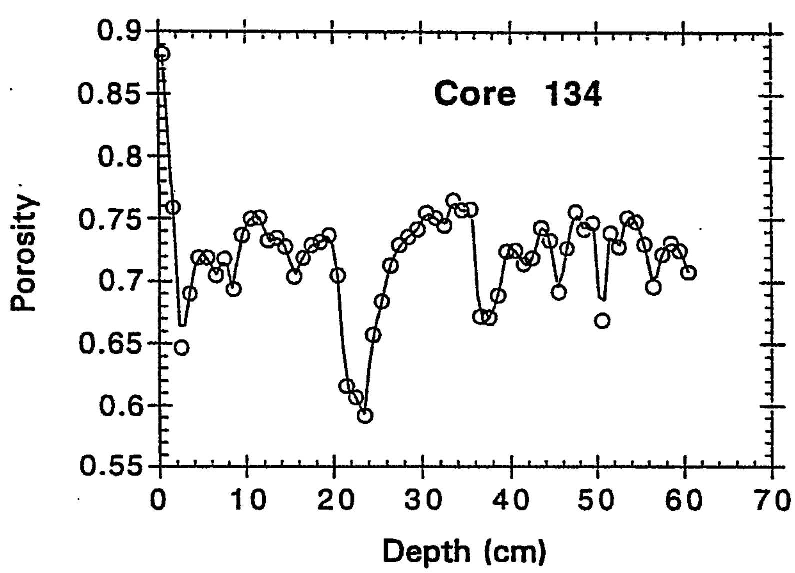

Figure C-73. Porosity depth distribution for Core 142. (Note that porosity was determined for every 1 cm homogenized section.)

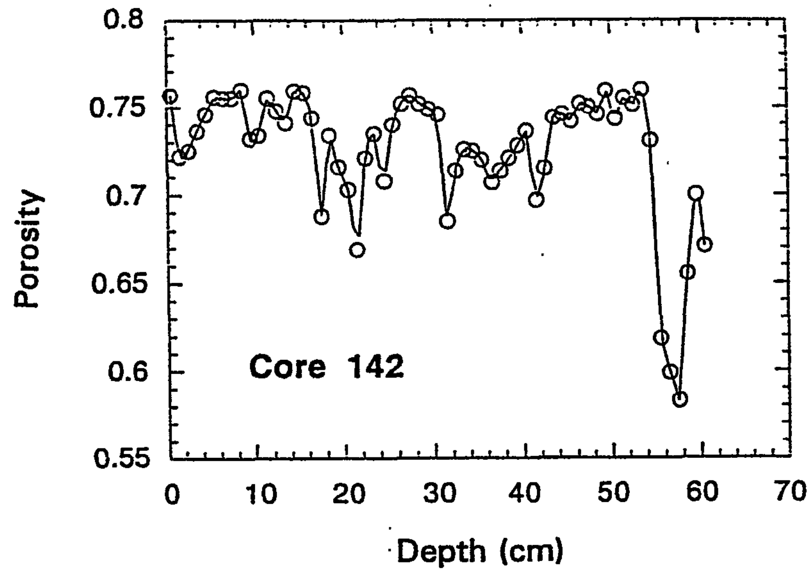

Figure C-74. Porosity depth distribution for Core 201. (Note that porosity was determined for every 1 cm homogenized section.)

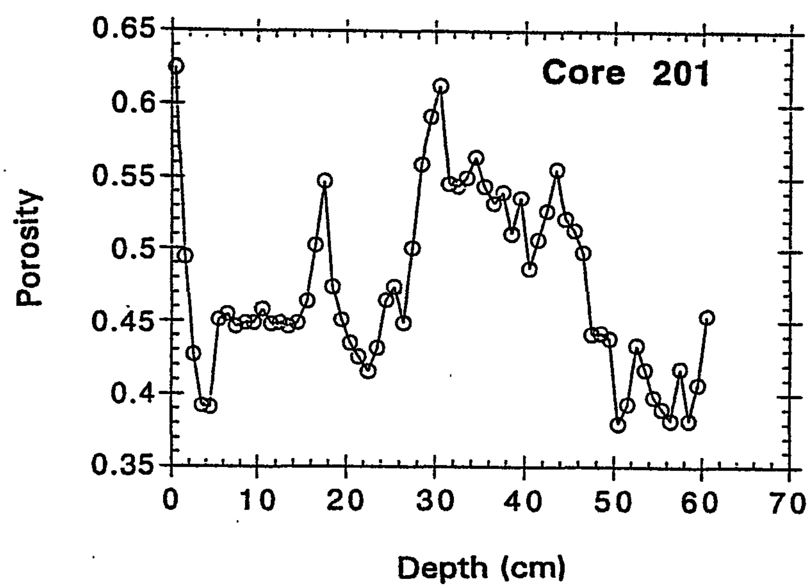

Figure C-75. Porosity depth distribution for Core 285. (Note that porosity was determined for every 1 cm homogenized section.)

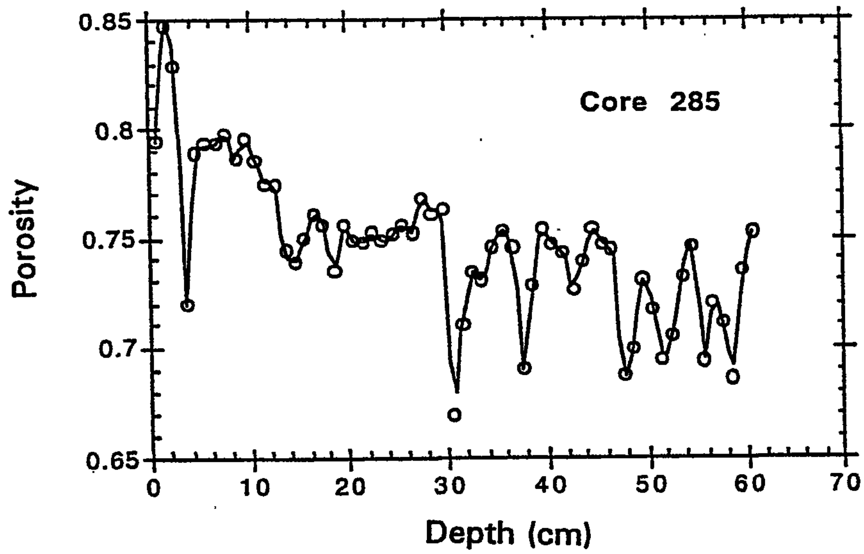

Figure C-76. Porosity depth distribution for Core 286. (Note that porosity was determined for every 1 cm homogenized section.)

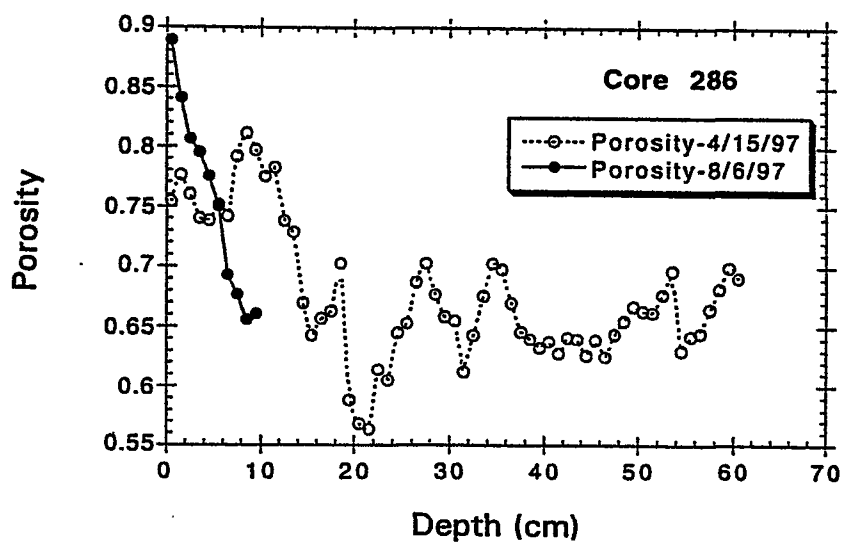

Figure C-77. Porosity depth distribution for Core 296. (Note that porosity was determined for every 1 cm homogenized section.)

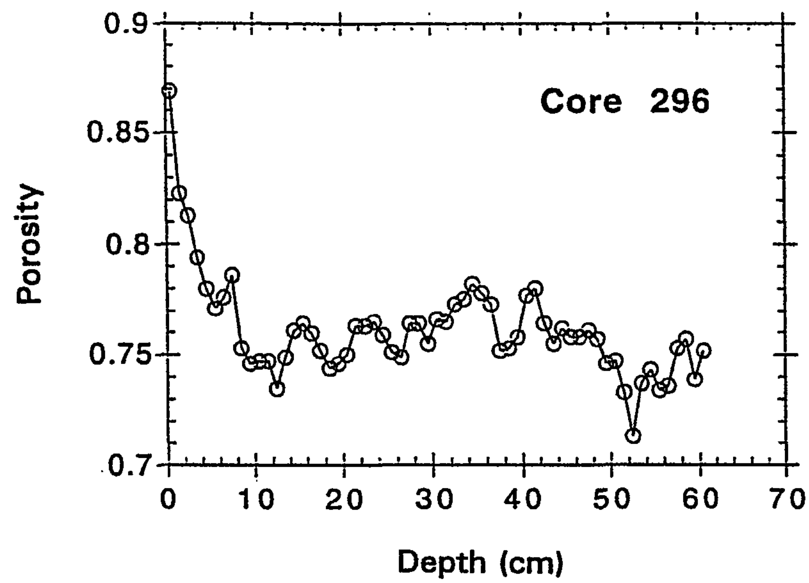

Figure C-78. Porosity depth distribution for Core 296 and 296B. (Note that porosity was determined for every 1 cm homogenized section.)

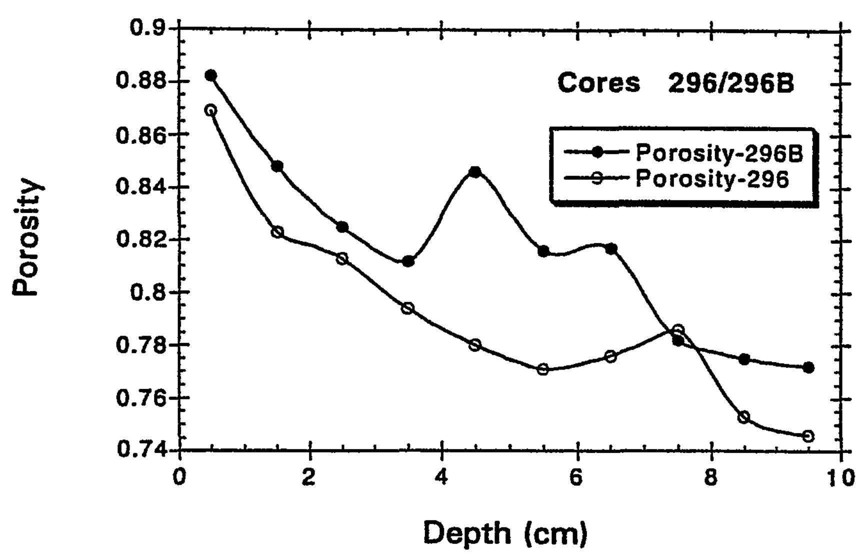

Figure C-79. Porosity depth distribution for Core 300. (Note that porosity was determined for every 1 cm homogenized section.)

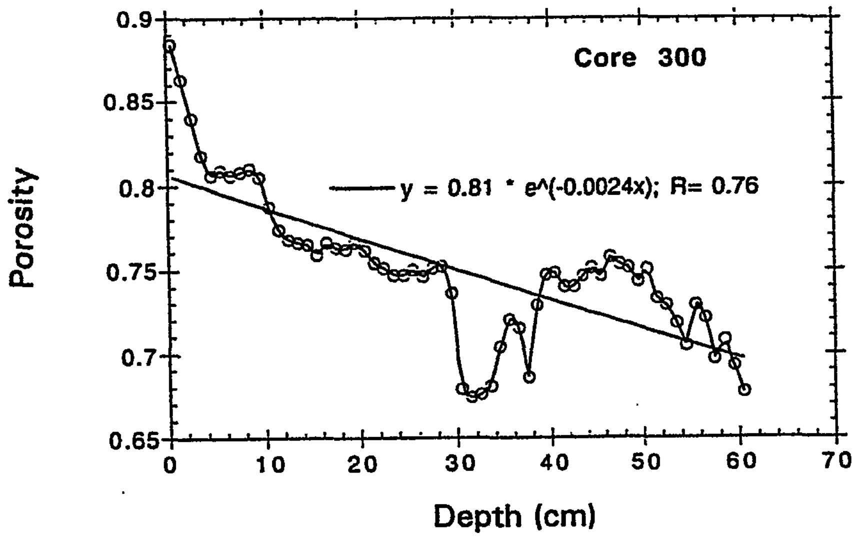

Figure C-80. Porosity depth distribution for Core 924. (Note that porosity was determined for every 1 cm homogenized section.)

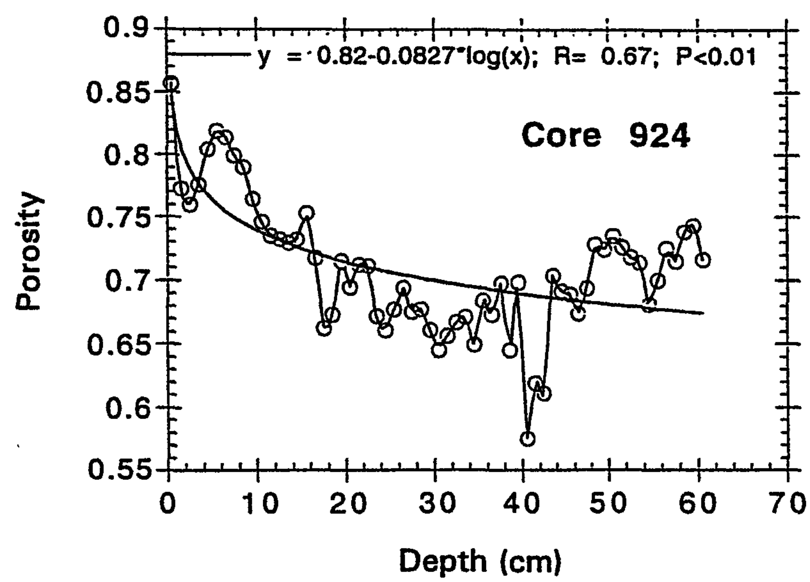

Figure C-81. Porosity depth distribution for Core 926. (Note that porosity was determined for every 1 cm homogenized section.)

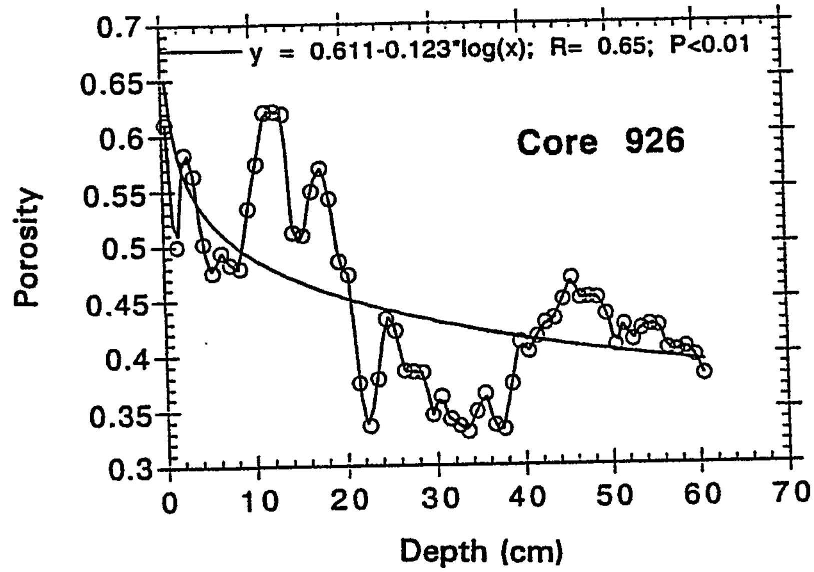

Figure C-82. Porosity depth distribution for Core 928. (Note that porosity was determined for every 1 cm homogenized section.)

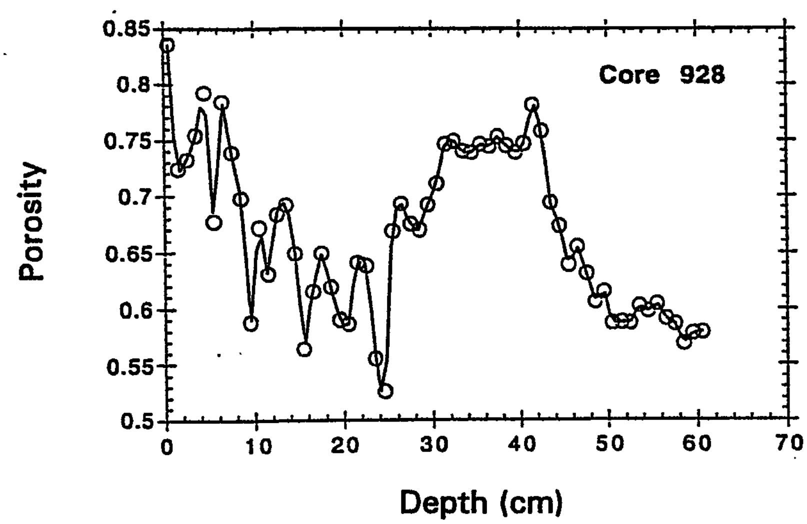

Figure C-83. Porosity depth distribution for Core 4293. (Note that porosity was determined for every 1 cm homogenized section.)

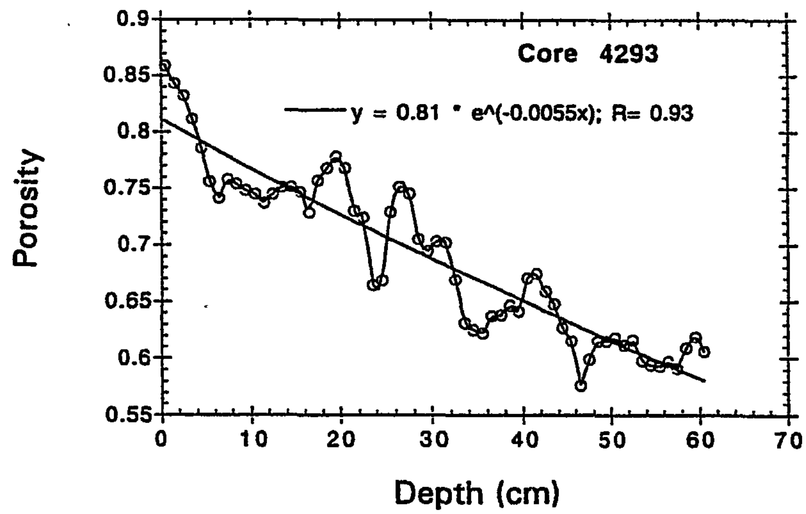

Figure C-84. Porosity depth distribution for Core 8721. (Note that porosity was determined for every 1 cm homogenized section.)

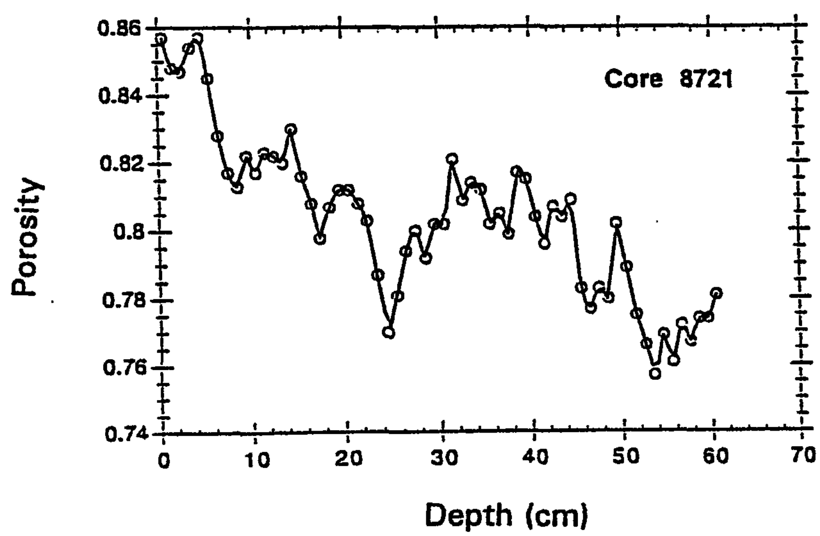

Figure C-85. Porosity depth distribution for Core 8826. (Note that porosity was determined for every 1 cm homogenized section.)

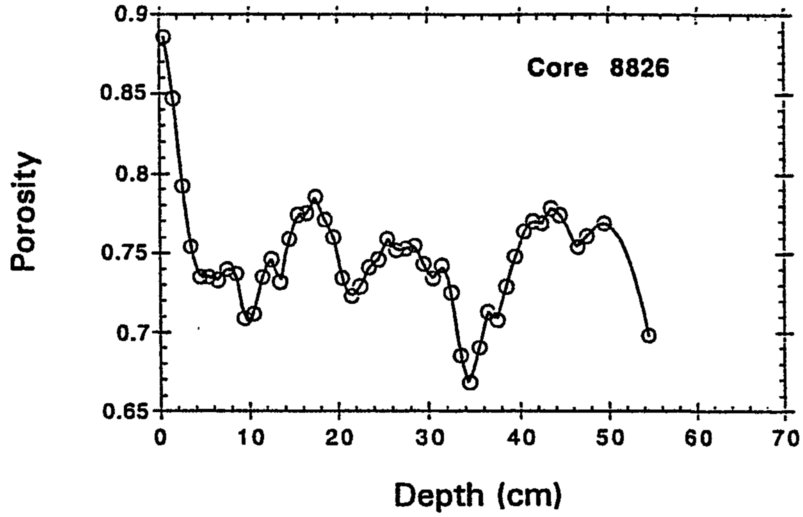

Figure C-86. Porosity depth distribution for Core 8827. (Note that porosity was determined for every 1 cm homogenized section.)

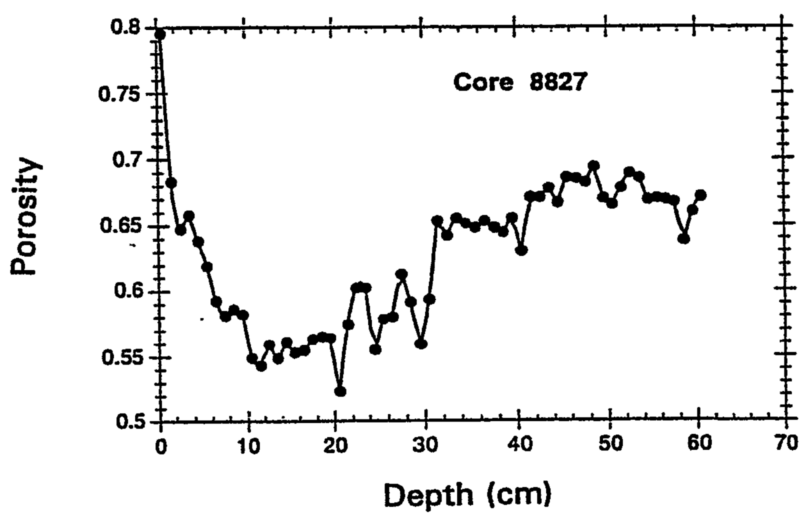

Figure C-87. Correlations between grain size and sediment porosity. Porosity in Cores 8827 and 8721 were determined in the same sections as the grain size, while in all other cores, the porosity data were measured in parallel cores which were different from those for downcore %clay distribution.

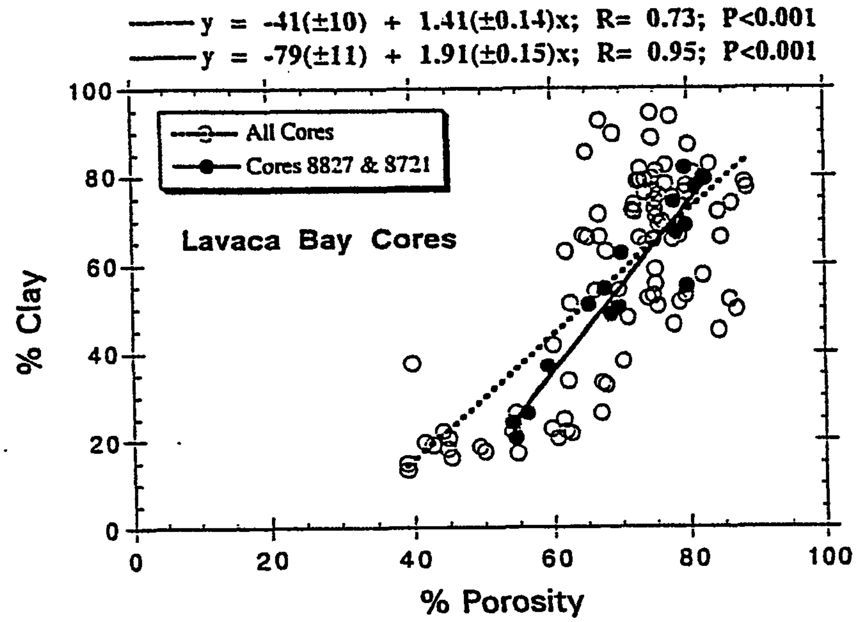

Figure C-88. Sediment profile of decay corrected ^7Be activities in Core 128. Upper and lower bounds of the value (± 1 propagated standard deviation) are depicted for every data point as "-up" and "-low").

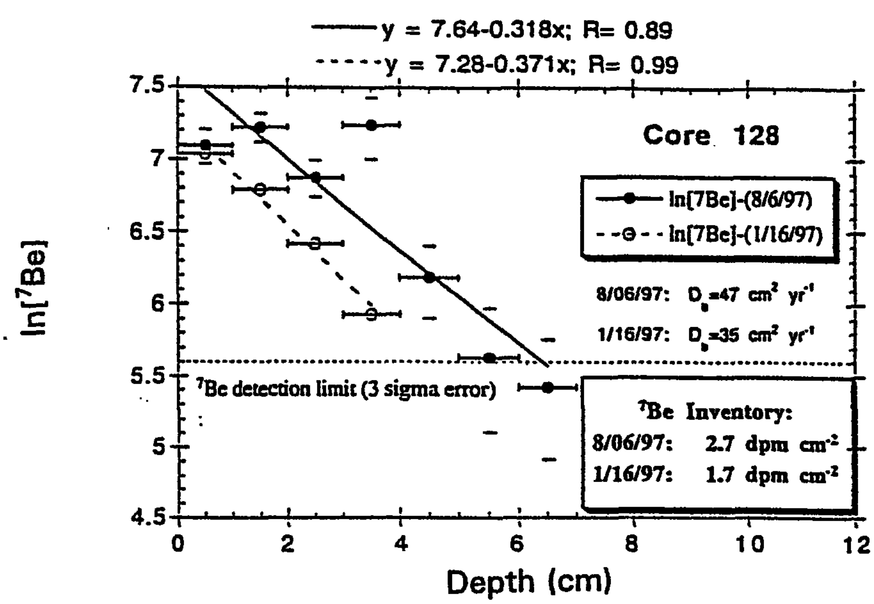

Figure C-89. Sediment profile of decay corrected ^{7}Be activities in Core 134. Upper and lower bounds of the value (± 1 propagated standard deviation) are depicted for every data point as "-up" and "-low").

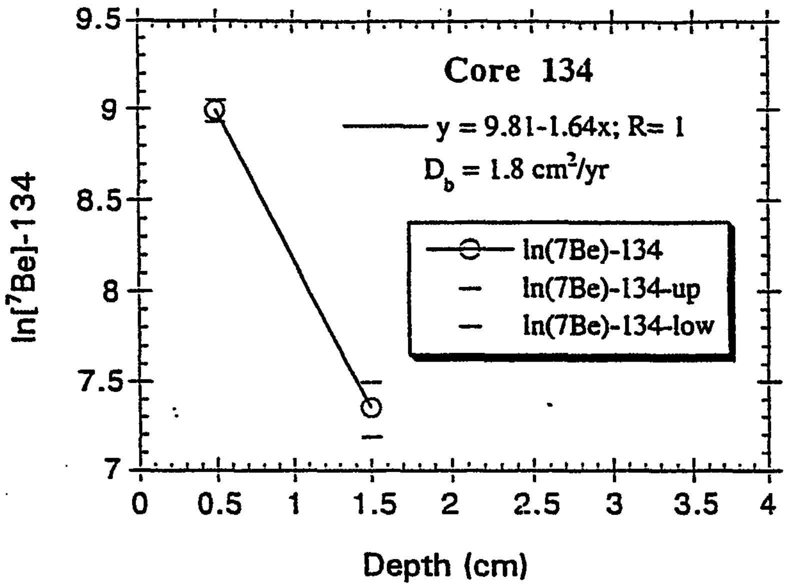

Figure C-90. Sediment profile of decay corrected ^{7}Be activities in Core 142. Upper and lower bounds of the value (± 1 propagated standard deviation) are depicted for every data point as "-up" and "-low").

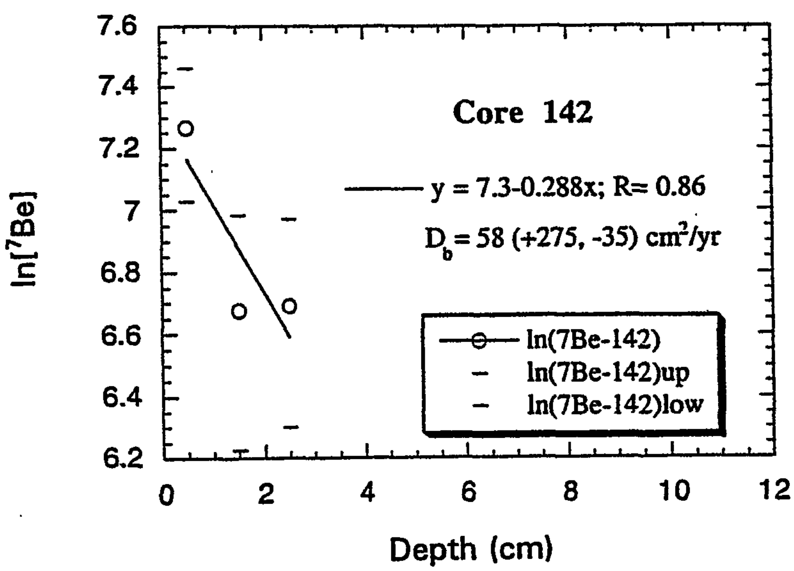

Figure C-91. Sediment profile of decay corrected ^{7}Be activities in Core 201. Upper and lower bounds of the value (± 1 propagated standard deviation) are depicted for every data point as "-up" and "-low").

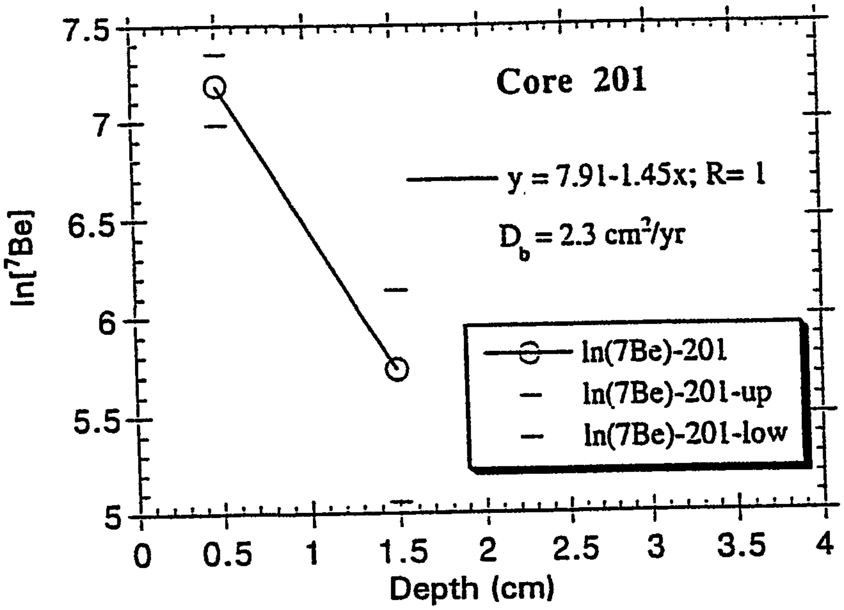

Figure C-92. Sediment profiles of decay corrected ^{7}Be activities in Core 285. Upper and lower bounds of the value (± 1 propagated standard deviation) are depicted for every data point as "-up" and "-low").

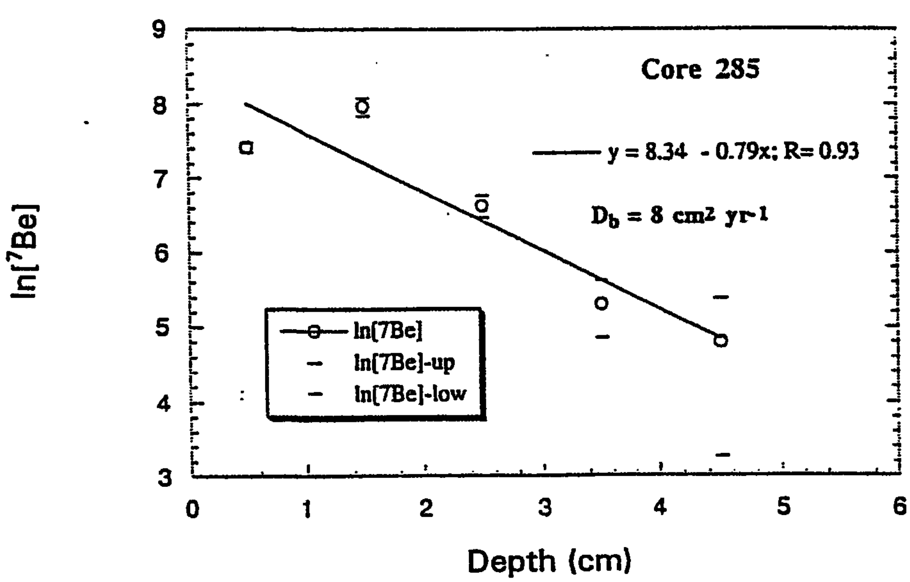

Figure C-93. Sediment profile of decay corrected ^{7}Be activities in Core 286. Upper and lower bounds of the value (± 1 propagated standard deviation) are depicted for every data point as "-up" and "-low").

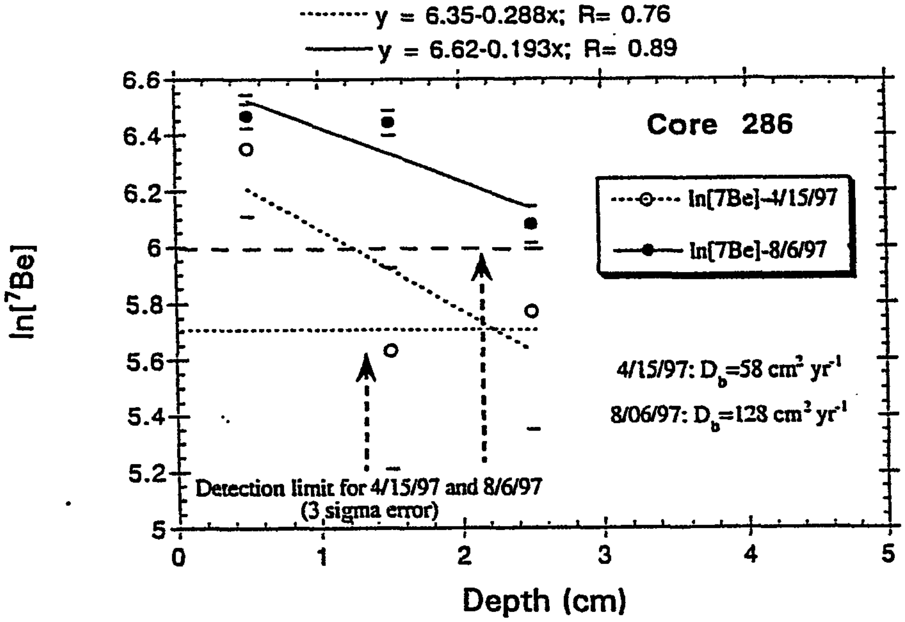

Figure C-94. Sediment profile of decay corrected ^{7}Be activities in Cores 296 and 296B. Upper and lower bounds of the value (± 1 propagated standard deviation) are depicted for every data point as "-up" and "-low").

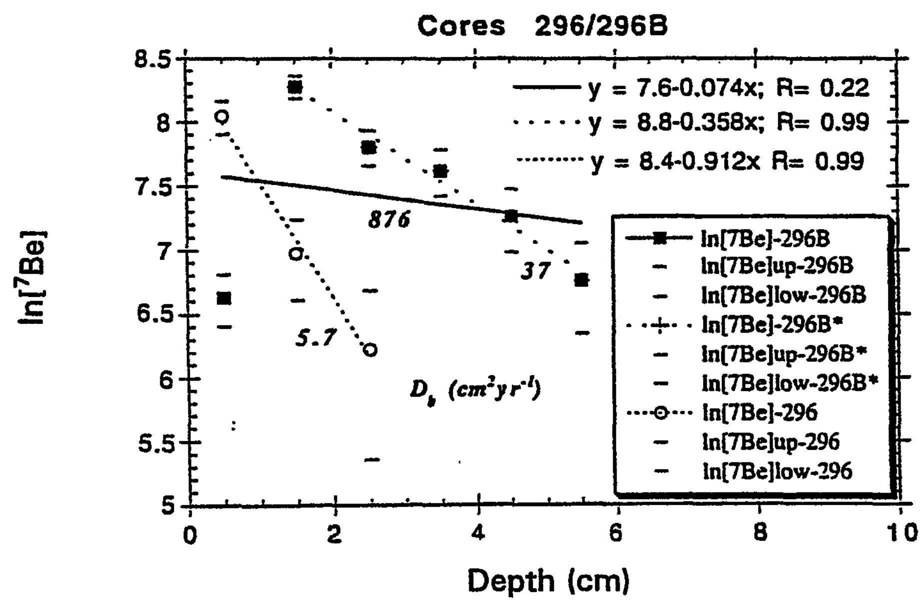

Figure C-95. Sediment profile of decay corrected ^{7}Be activities in Core 300. Upper and lower bounds of the value (± 1 propagated standard deviation) are depicted for every data point as "-up" and "-low").

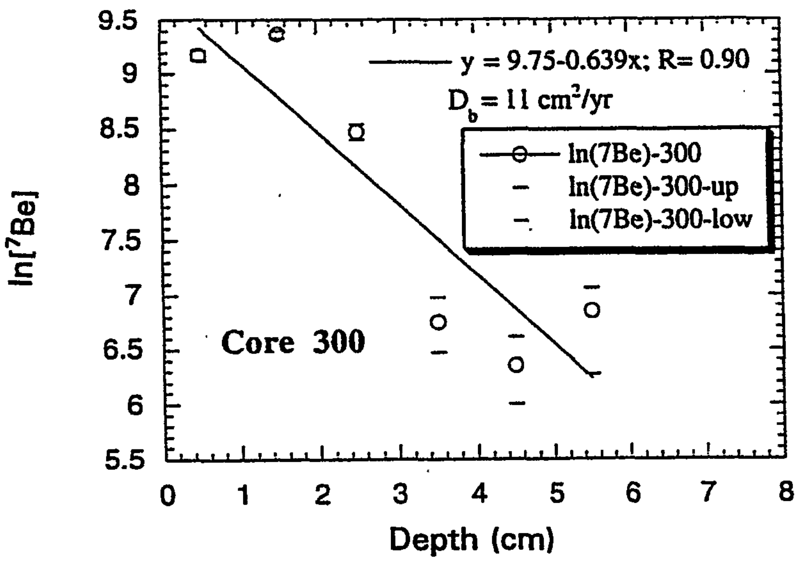

Figure C-96. Sediment profile of decay corrected ^{7}Be activities in Core 924. Upper and lower bounds of the value (± 1 propagated standard deviation) are depicted for every data point as "-up" and "-low").

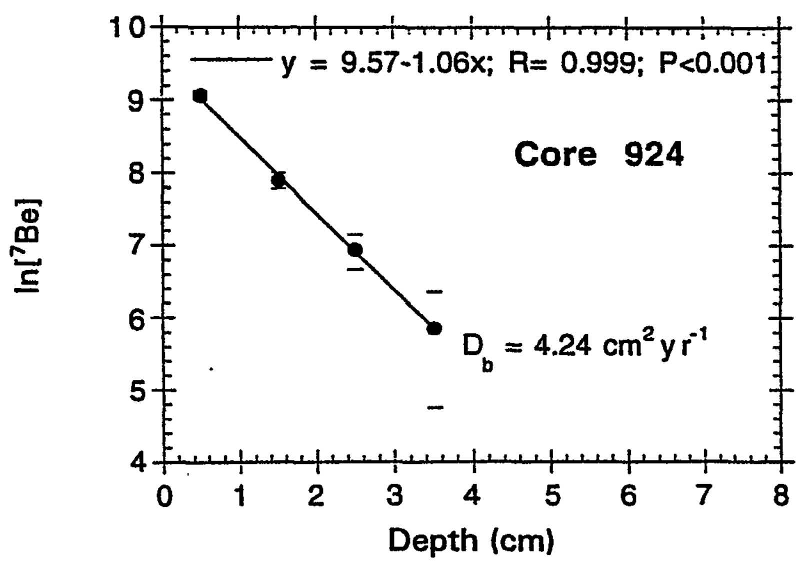

Figure C-97. Sediment profile of decay corrected ^{7}Be activities in Core 926. Upper and lower bounds of the value (± 1 propagated standard deviation) are depicted for every data point as "-up" and "-low").

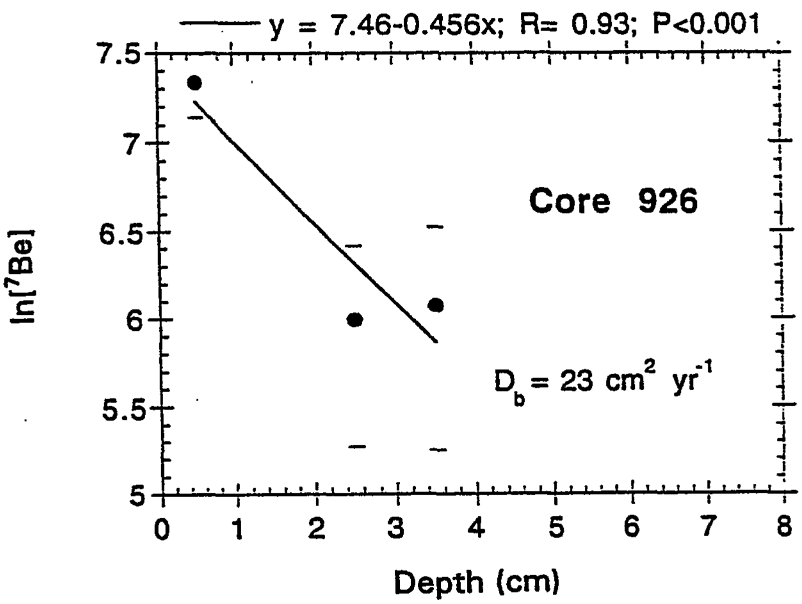

Figure C-98. Sediment profile of decay corrected ^{7}Be activities in Core 928. Upper and lower bounds of the value (± 1 propagated standard deviation) are depicted for every data point as "-up" and "-low").

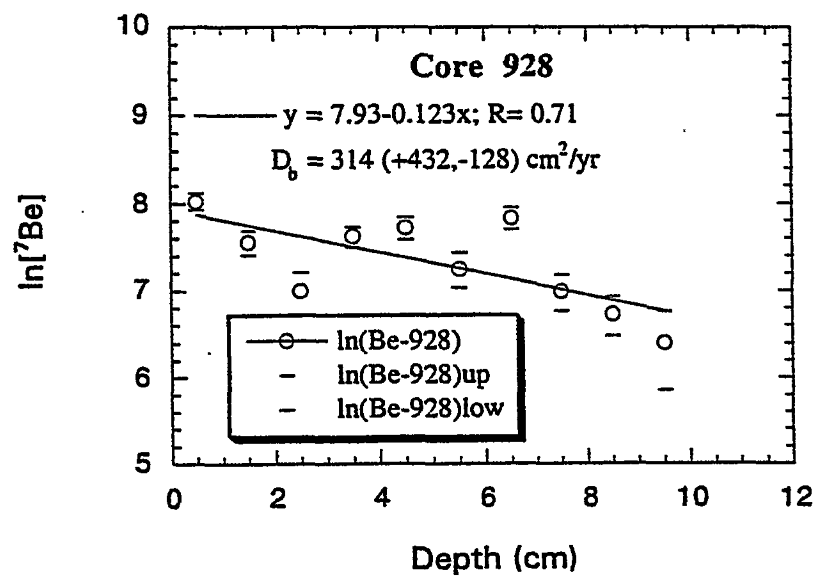

Figure C-99. Sediment profile of decay corrected ^{7}Be activities in Core 4293. Upper and lower bounds of the value (± 1 propagated standard deviation) are depicted for every data point as "-up" and "-low").

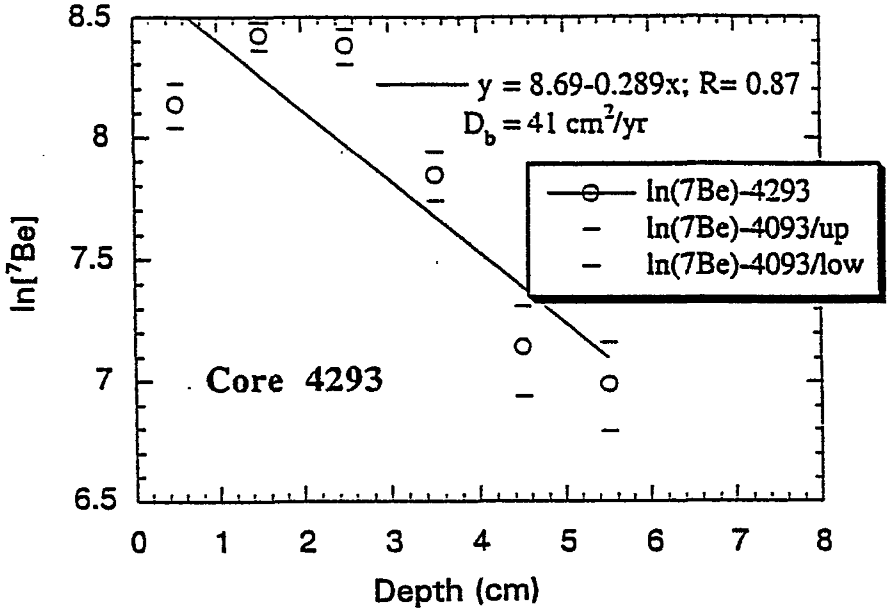

Figure C-100. Sediment profile of decay corrected ^{7}Be activities in Core 8721. Upper and lower bounds of the value (± 1 propagated standard deviation) are depicted for every data point as "-up" and "-low").

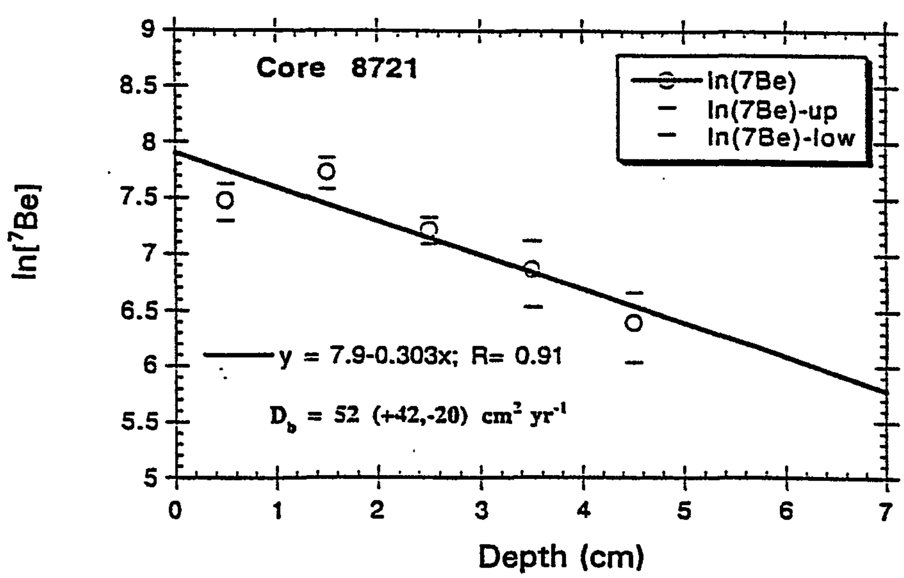

Figure C-101. Sediment profile of decay corrected ^7Be activities in Core 8826. Upper and lower bounds of the value (± 1 propagated standard deviation) are depicted for every data point as "-up" and "-low").

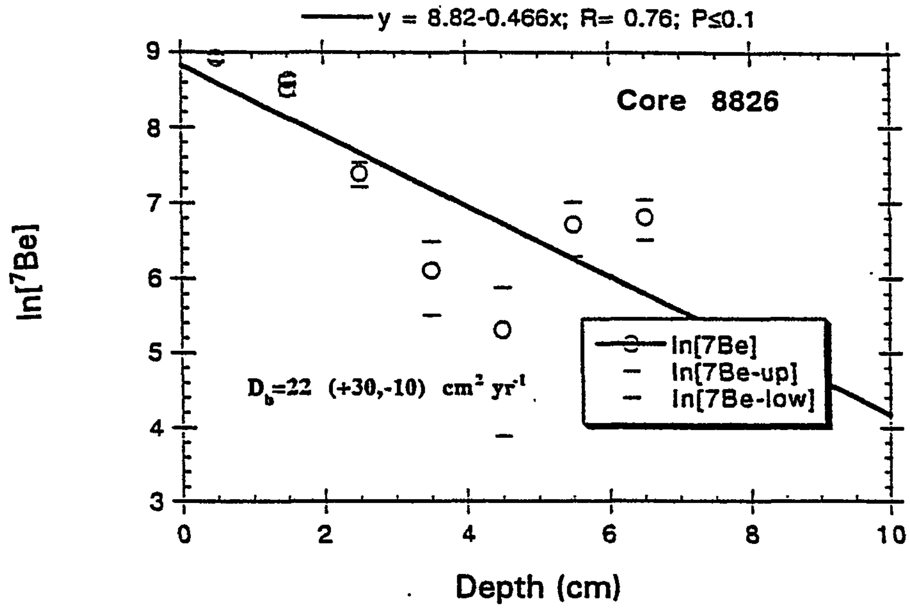

Figure C-102. Sediment profile of decay corrected ^7Be activities in Core 8827. Upper and lower bounds of the value (± 1 propagated standard deviation) are depicted for every data point as "-up" and "-low").

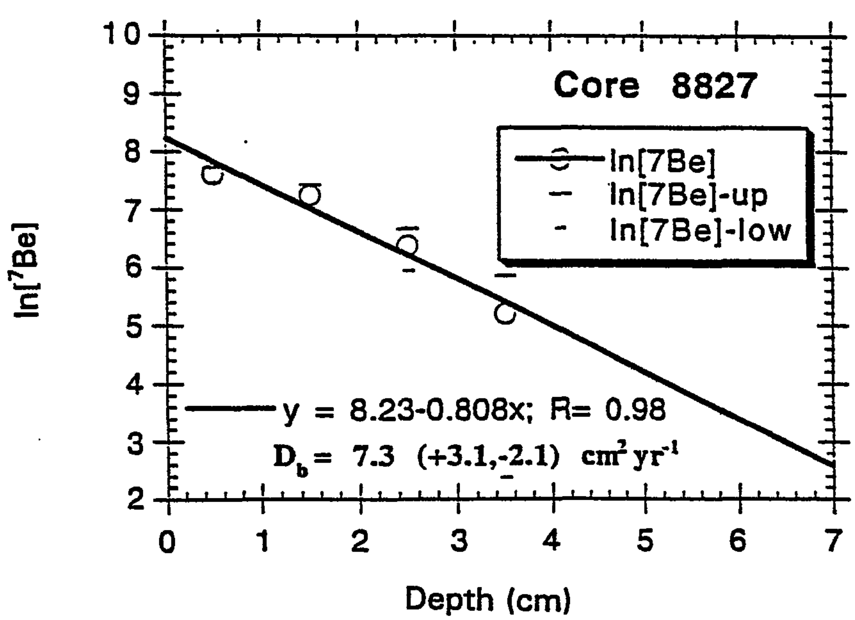

Figure C-103. Correlation of ^{7}Be inventory with mixed layer depth (z_m).

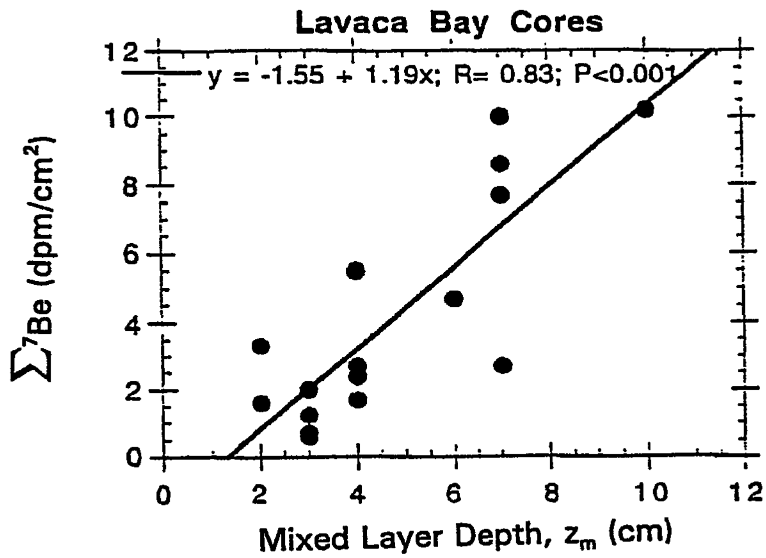

Figure C-104. Sediment profile of $^{210}Pb_{xs}$ in Core 128. Upper and lower bounds of the value (± 1 propagated standard deviation) are depicted for every data point as "-up" and "-low").

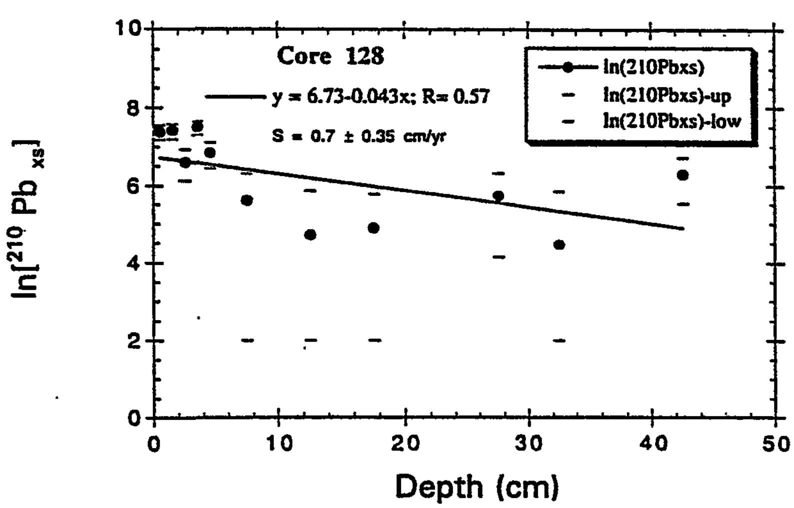

Figure C-105. Sediment profile of $^{210}Pb_{xs}$ in Core 134. Upper and lower bounds of the value (± 1 propagated standard deviation) are depicted for every data point as "-up" and "-low").

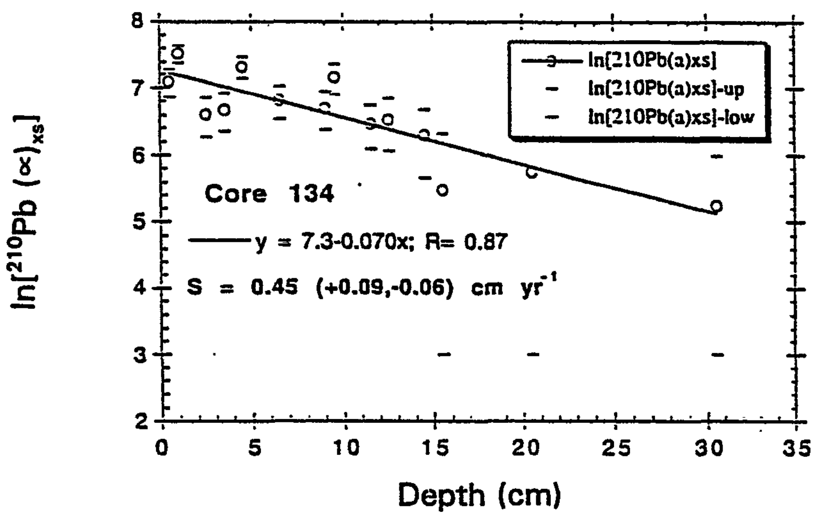

Figure C-106. Sediment profile of $^{210}Pb_{xs}$ in Core 142. Upper and lower bounds of the value (±1 propagated standard deviation) are depicted for every data point as "-up" and "-low").

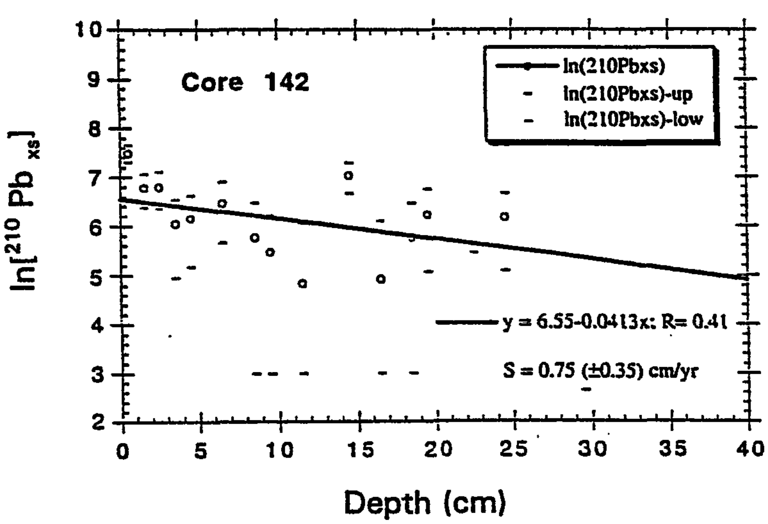

Figure C-107. Sediment profile of $^{210}Pb_{xs}$ in Core 201. Upper and lower bounds of the value (±1 propagated standard deviation) are depicted for every data point as "-up" and "-low").

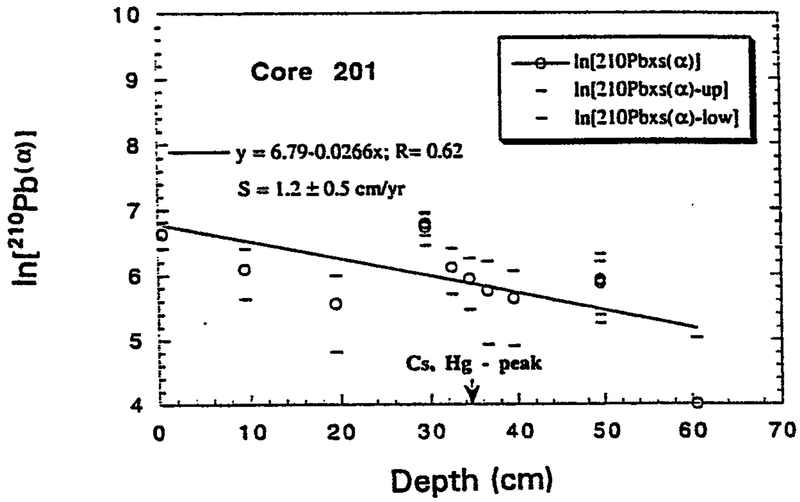

Figure C-108. Sediment profile of $^{210}Pb_{xs}$ in Core 285. Upper and lower bounds of the value (±1 propagated standard deviation) are depicted for every data point as "-up" and "-low").

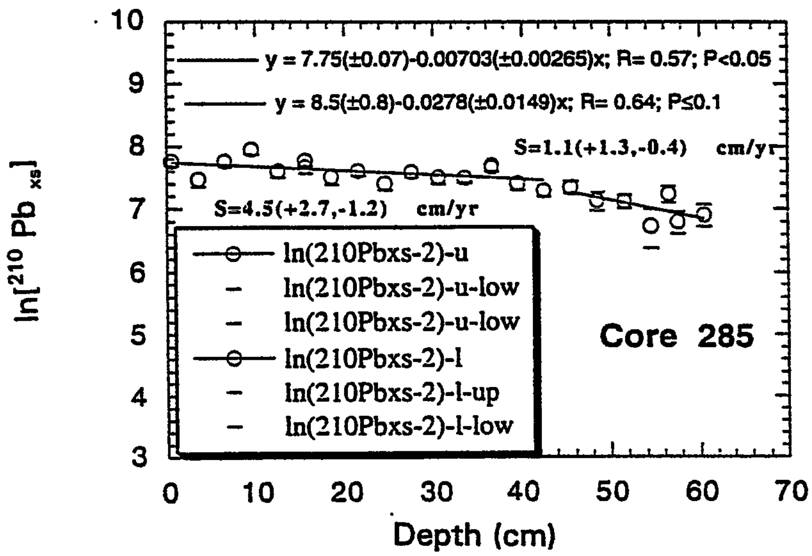

Figure C-109. Sediment profile of $^{210}Pb_{xs}$ in Core 285. Upper and lower bounds of the value (±1 propagated standard deviation) are depicted for every data point as "-up" and "-low").

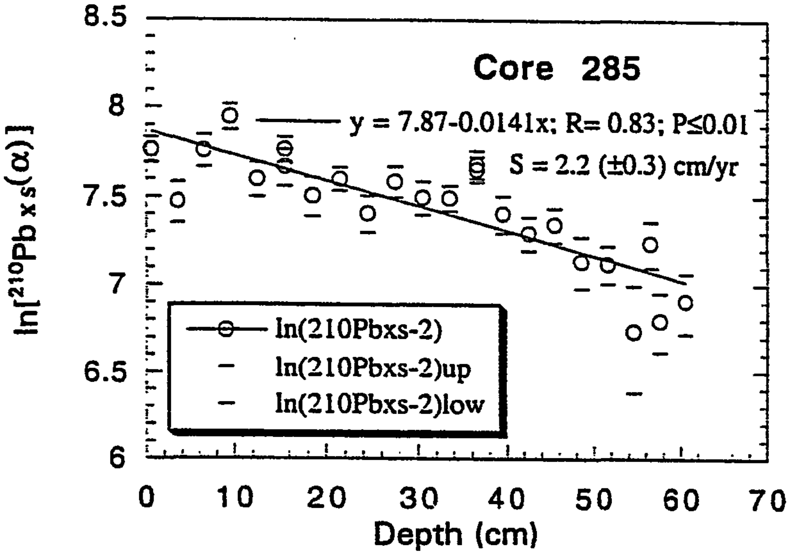

Figure C-110. Sediment profile of $^{210}Pb_{xs}$ in Core 286. Upper and lower bounds of the value (±1 propagated standard deviation) are depicted for every data point as "-up" and "-low").

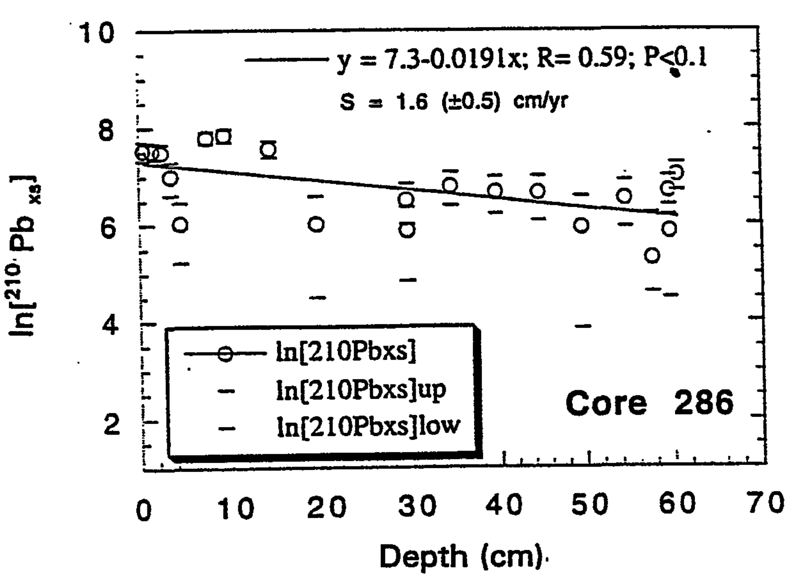

Figure C-111. **Sediment profile of $^{210}Pb_{xs}$ in Core 296. Upper and lower bounds of the value (±1 propagated standard deviation) are depicted for every data point as "-up" and "-low").**

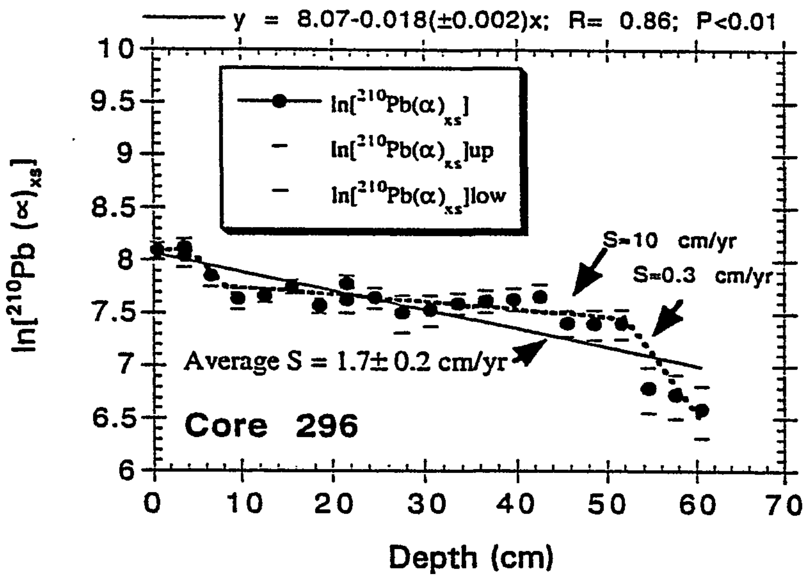

Figure C-112. **Comparison between recounted ^{210}Pb sample activity (∝ 2) and first counted activity of ^{210}Pb (∝ 1) in sediment samples from Core 296.**

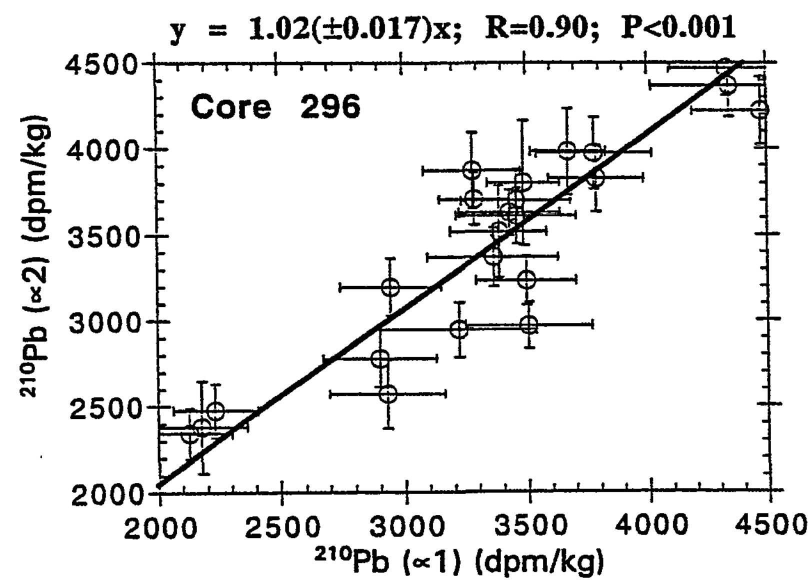

Figure C-113. Sediment profile of $^{210}Pb_{xs}$ in Core 300. Upper and lower bounds of the value (±1 propagated standard deviation) are depicted for every data point as "-up" and "-low").

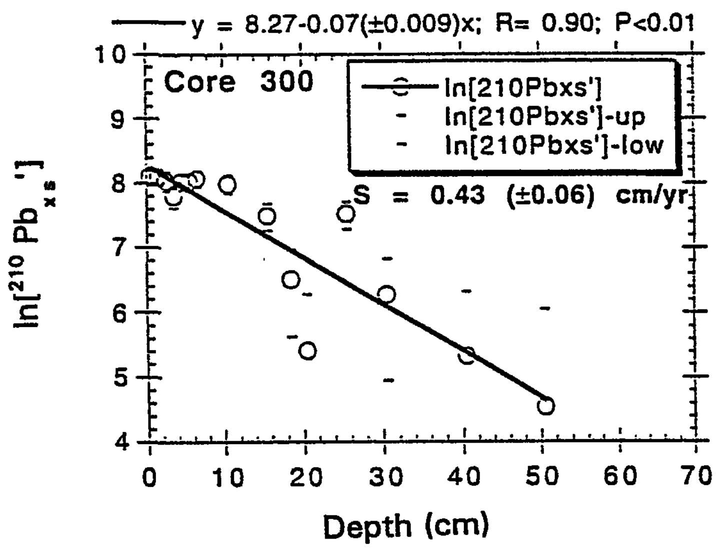

Figure C-114. Sediment profile of $^{210}Pb_{xs}$ in Core 924. Upper and lower bounds of the value (±1 propagated standard deviation) are depicted for every data point as "-up" and "-low").

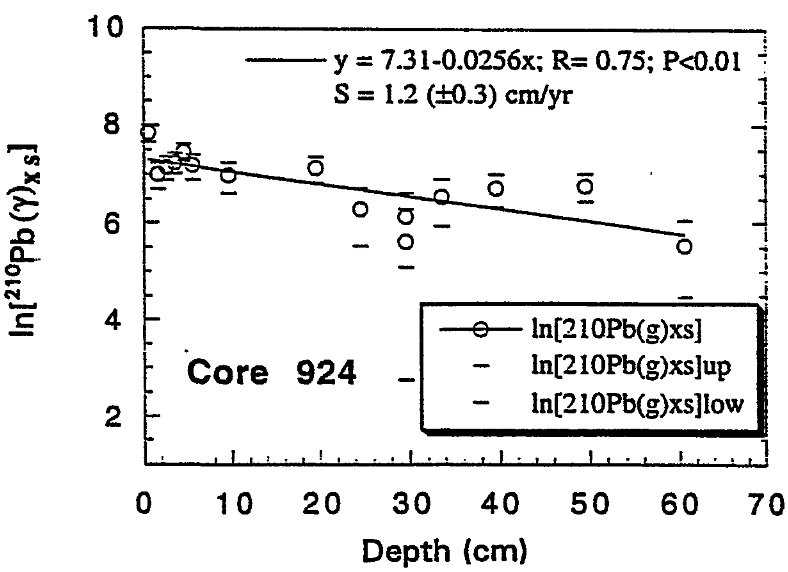

Figure C-115. Sediment profile of $^{210}Pb_{xs}$ in Core 926. Upper and lower bounds of the value (±1 propagated standard deviation) are depicted for every data point as "-up" and "-low").

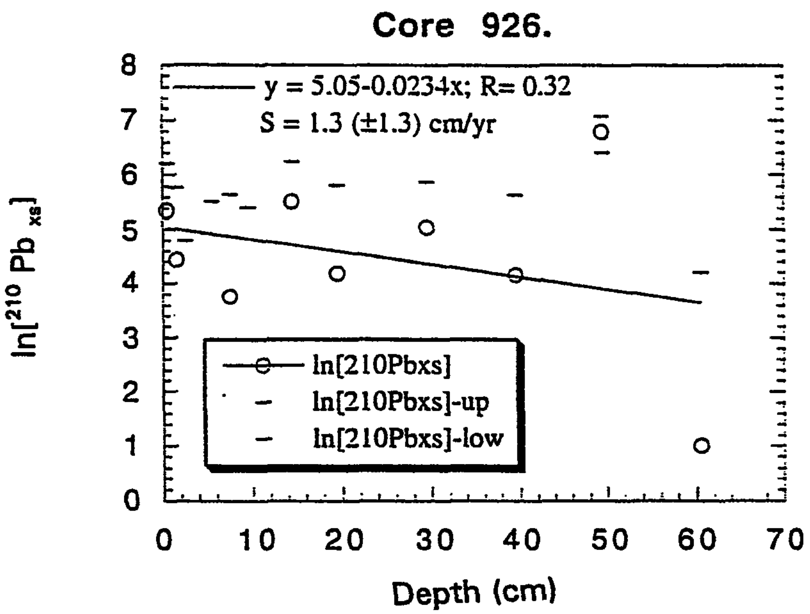

Figure C-116. Sediment profile of $^{210}Pb_{xs}$ in Core 928. Upper and lower bounds of the value (±1 propagated standard deviation) are depicted for every data point as "-up" and "-low").

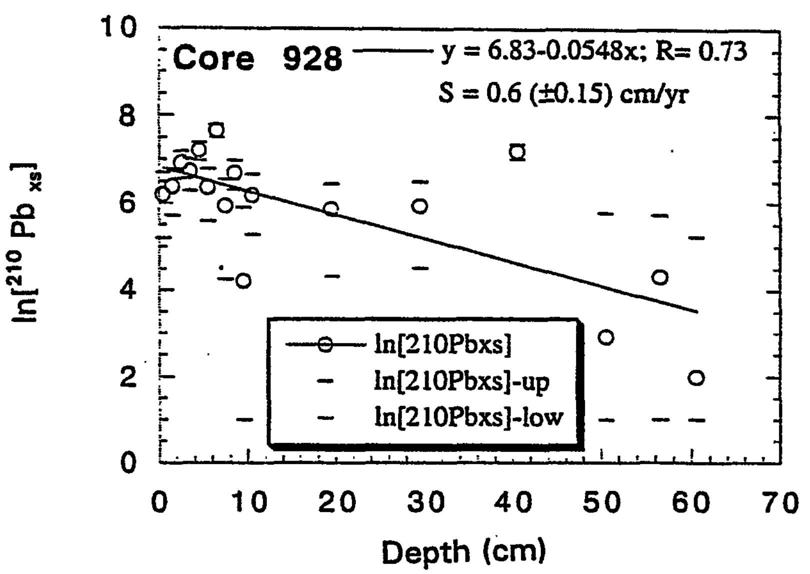

Figure C-117. **Sediment profile of $^{210}Pb_{xs}$ in Core 4293. Upper and lower bounds of the value (±1 propagated standard deviation) are depicted for every data point as "-up" and "-low").**

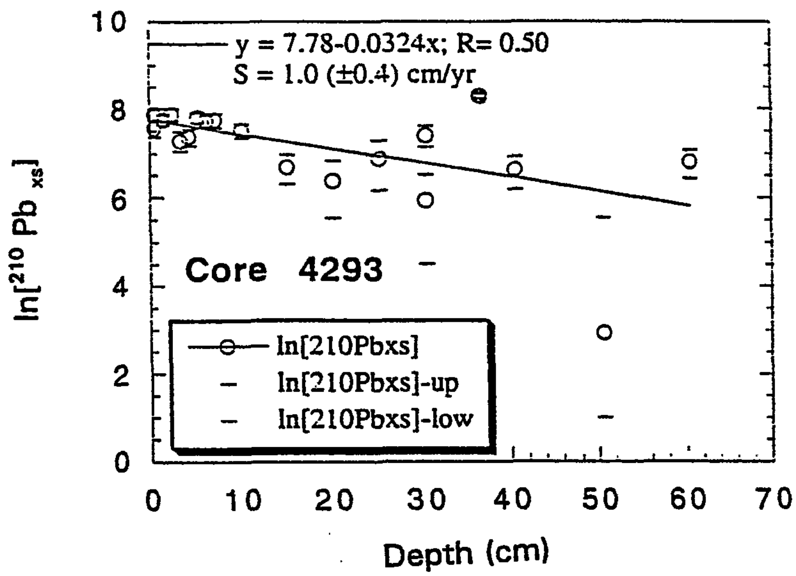

Figure C-118. **Sediment profile of $^{210}Pb_{xs}$ in Core 8721. Upper and lower bounds of the value (±1 propagated standard deviation) are depicted for every data point as "-up" and "-low").**

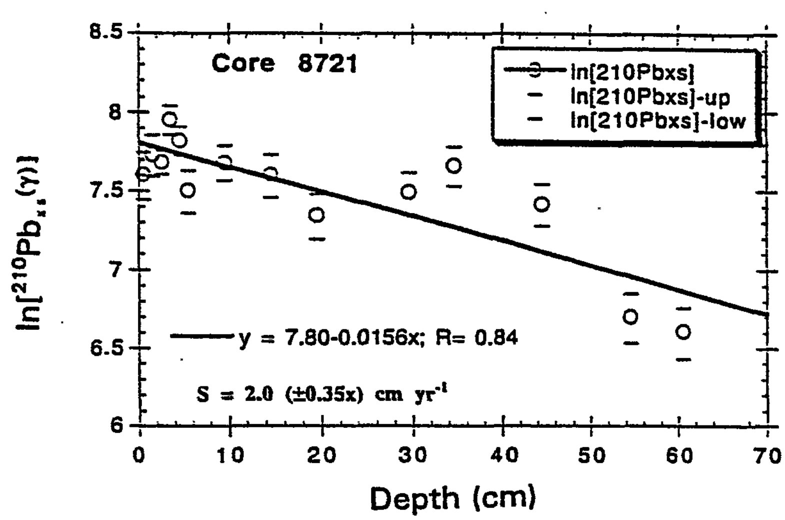

Figure C-119. Sediment profile of $^{210}Pb_{xs}$ in Core 8826. Upper and lower bounds of the value (±1 propagated standard deviation) are depicted for every data point as "-up" and "-low").

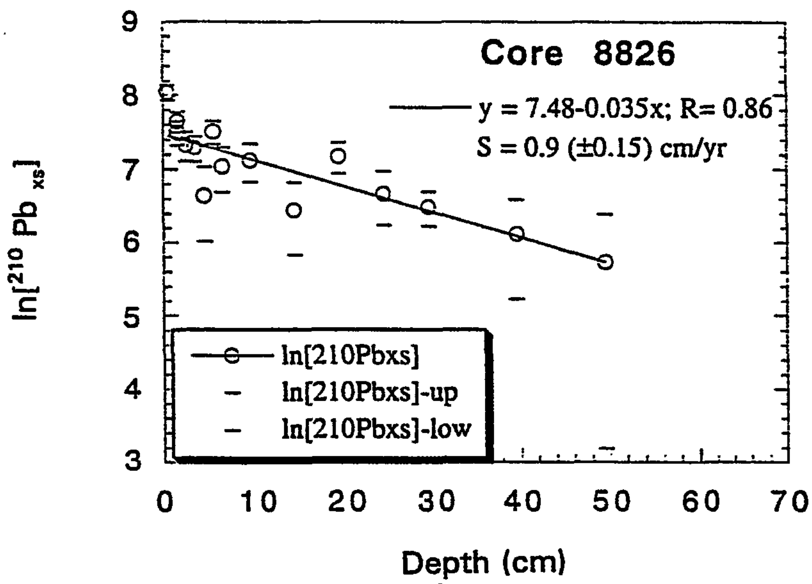

Figure C-120. Sediment profile of $^{210}Pb_{xs}$ in Core 8827. Upper and lower bounds of the value (±1 propagated standard deviation) are depicted for every data point as "-up" and "-low").

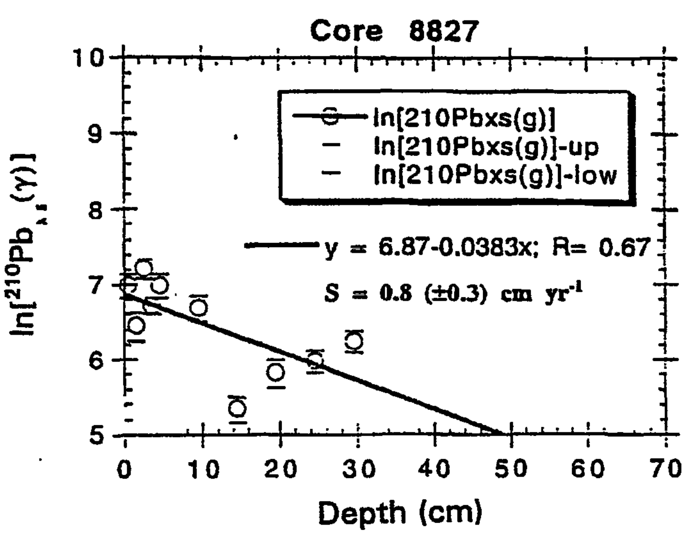

Figure C-121. Correlation of $^{210}Pb_{xs}(o)$ activity concentration in surface sediments with % organic carbon.

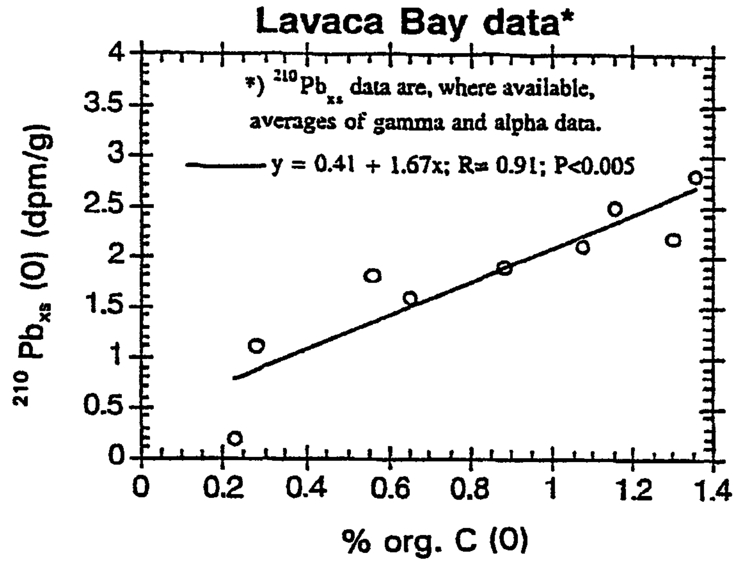

Figure C-122. Correlation of % organic carbon with porosity at the sediment surface.

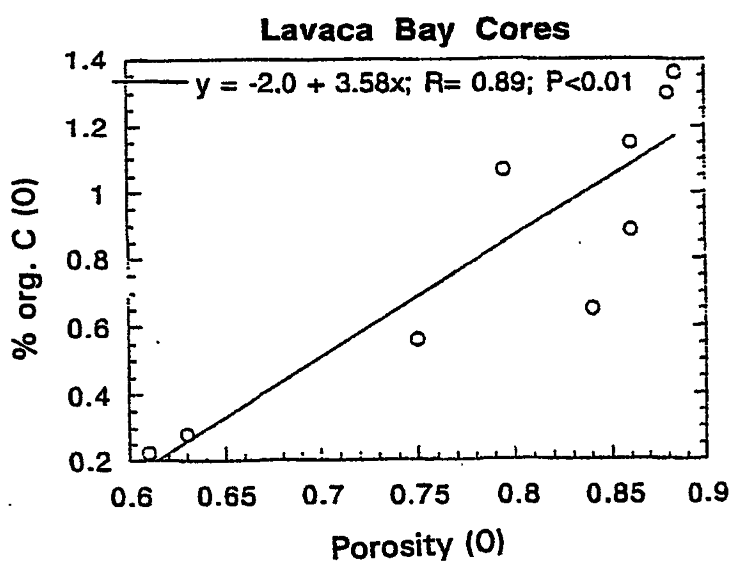

Figure C-123. Correlation of $^{210}Pb_{xs}$ inventory ($\sum$, in dpm/cm^2) with $^{210}Pb_{xs}$ based sedimentation rate (S, in cm/yr).

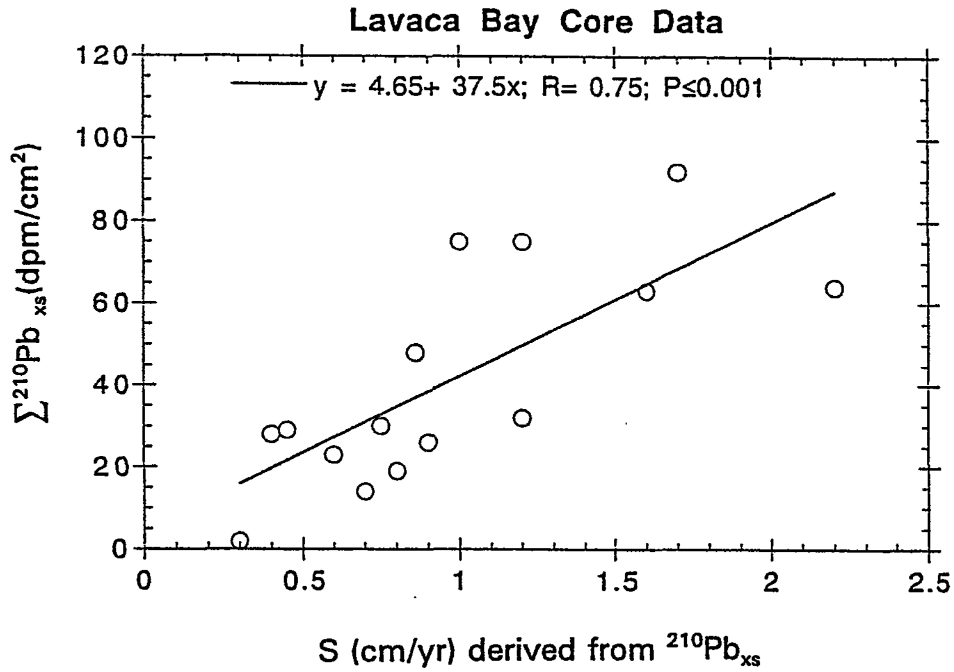

Figure C-124. Correlation of ^{137}Cs inventory ($\sum$, in dpm/cm^2) with ^{137}Cs based and sedimentation rate (S, in cm/yr).

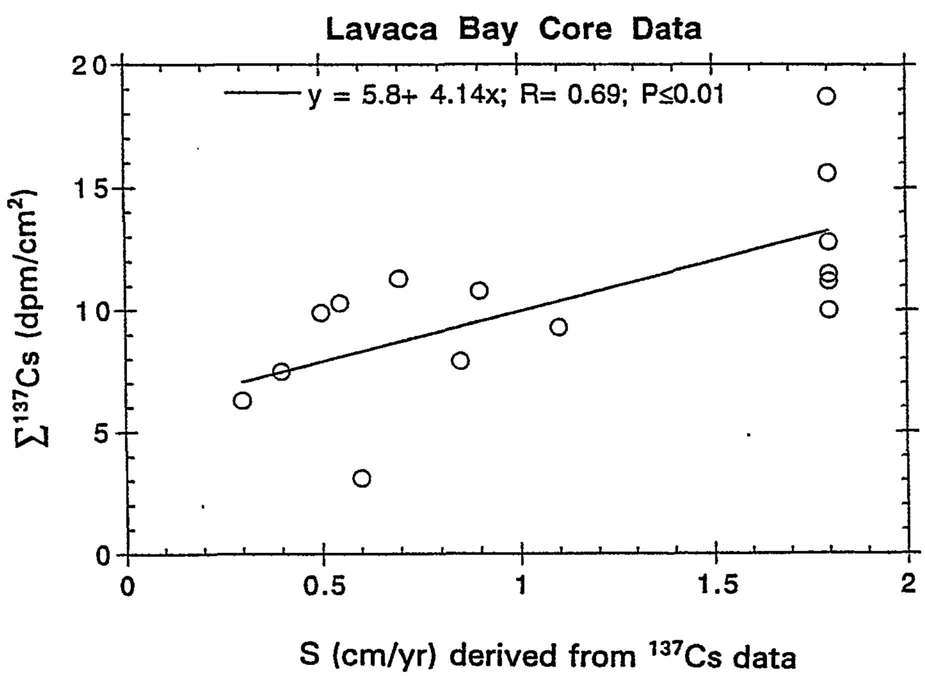

Figure C-125. Correlation of surface $^{137}Cs(o)$ activity concentration in surface sediments with porosity in the same layer.

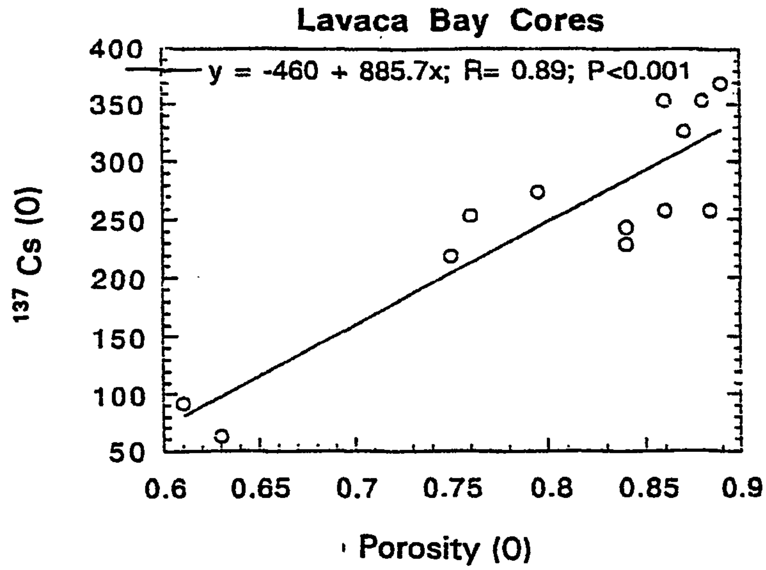

Figure C-126. Correlation of surface $^{137}Cs(o)$ activity concentration in surface sediments with % organic carbon in the same layer.

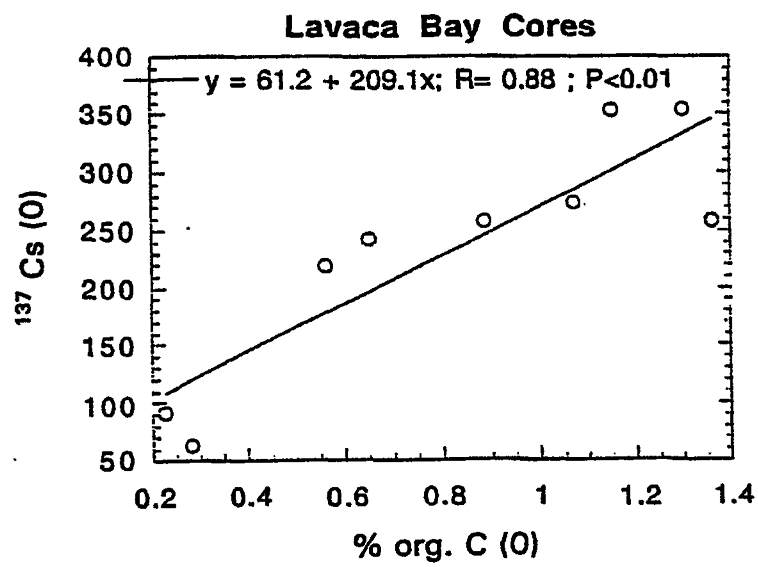

Figure C-127. X-Radiograph for Core 128.

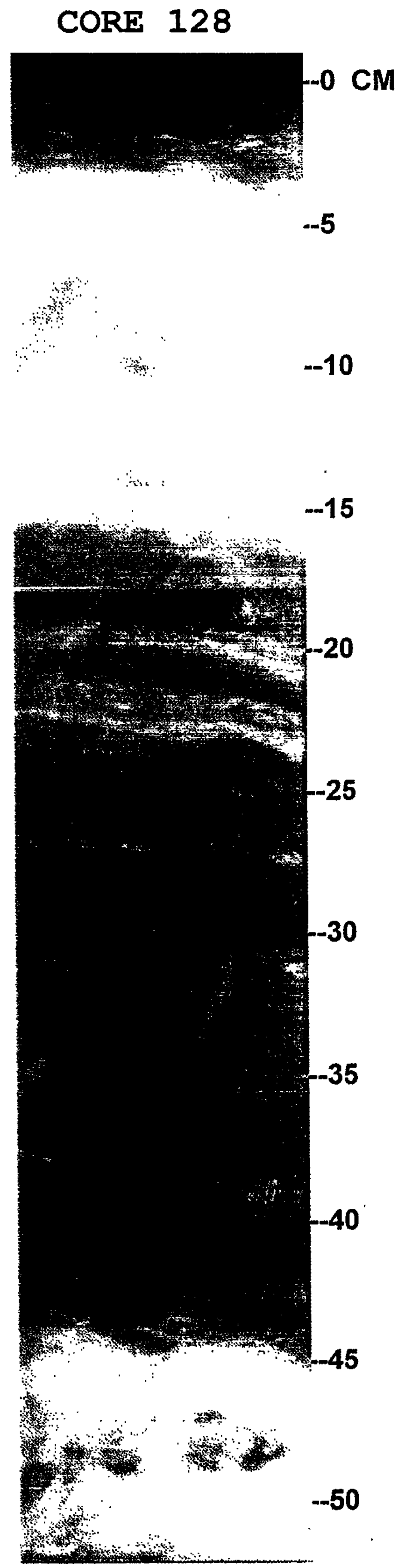

Figure C-128. X-Radiograph for Core 128b.

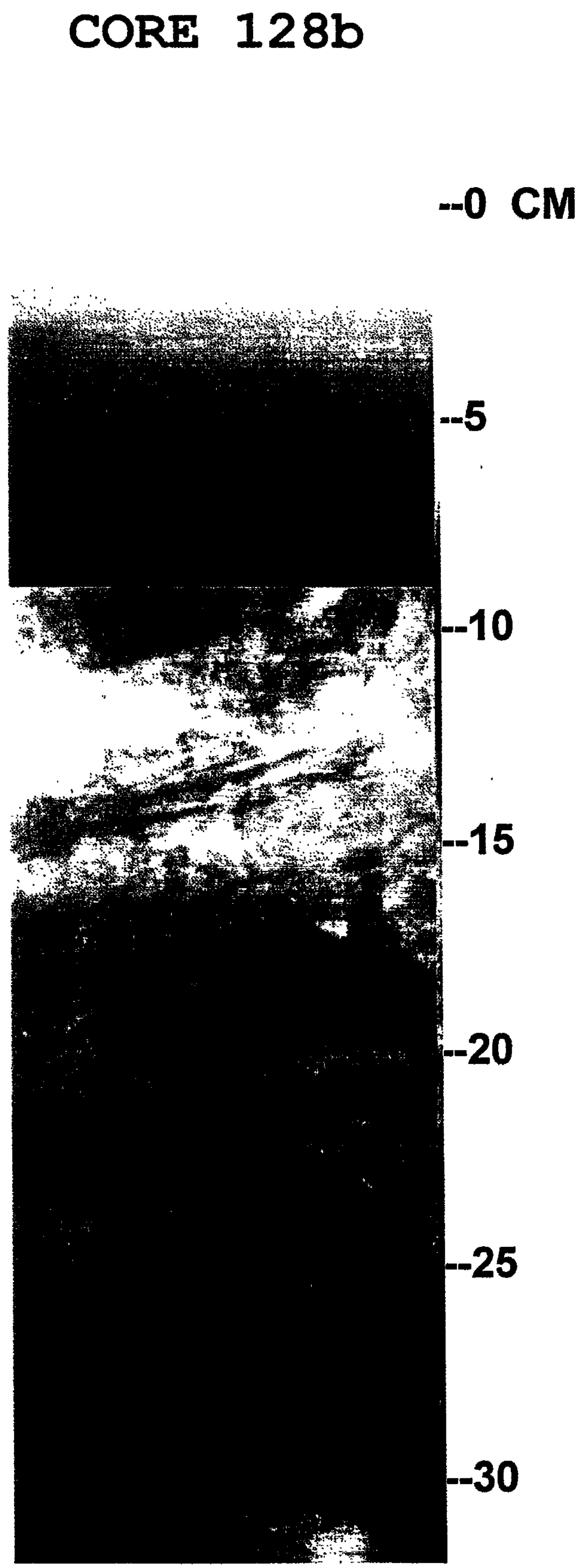

Figure C-129. X-Radiograph for Core 134.

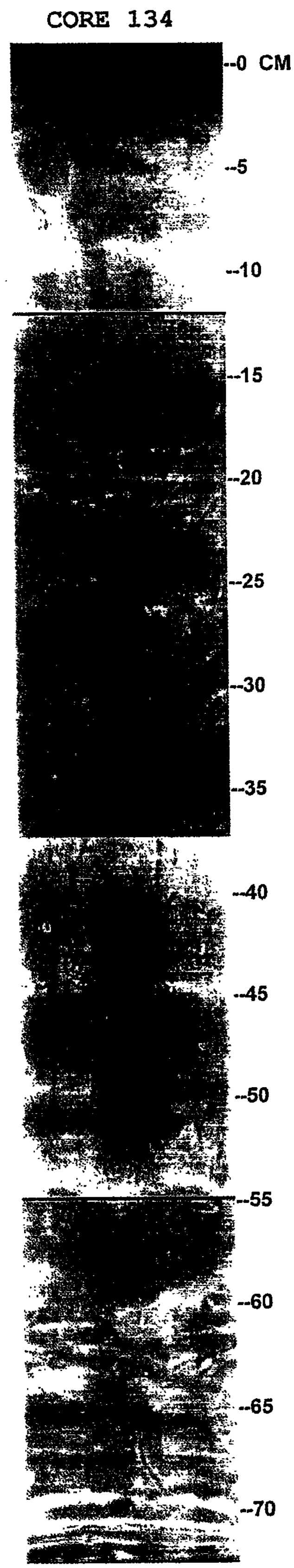

Figure C-130. X-Radiograph for Core 142.

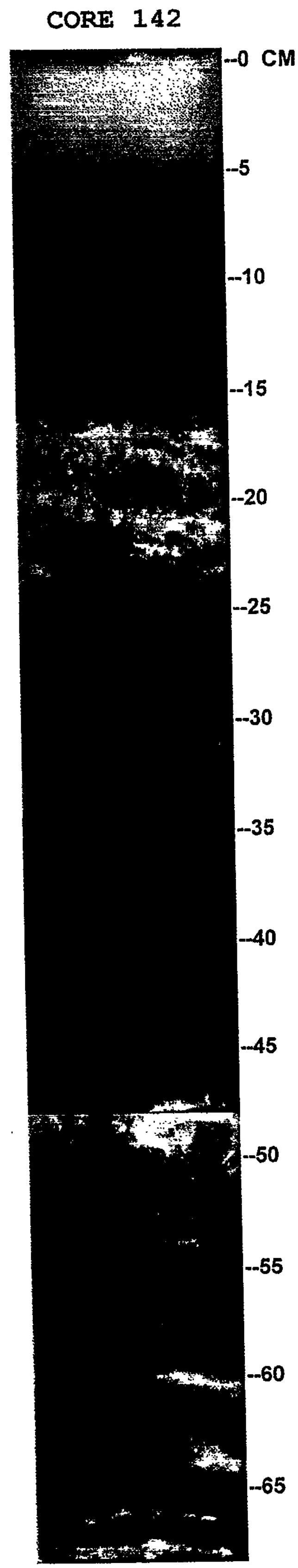

Figure C-131. X-Radiograph for Core 201a.

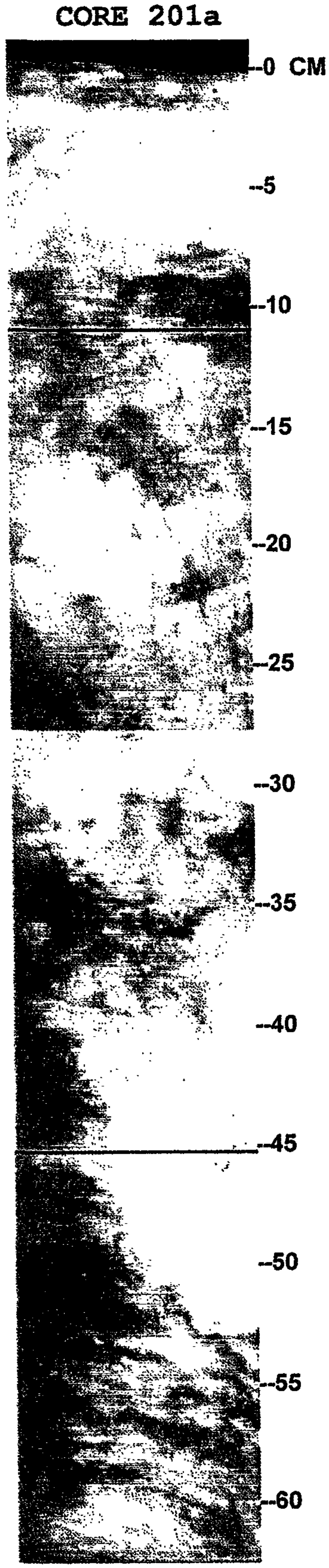

Figure C-132. X-Radiograph for Core 201b.

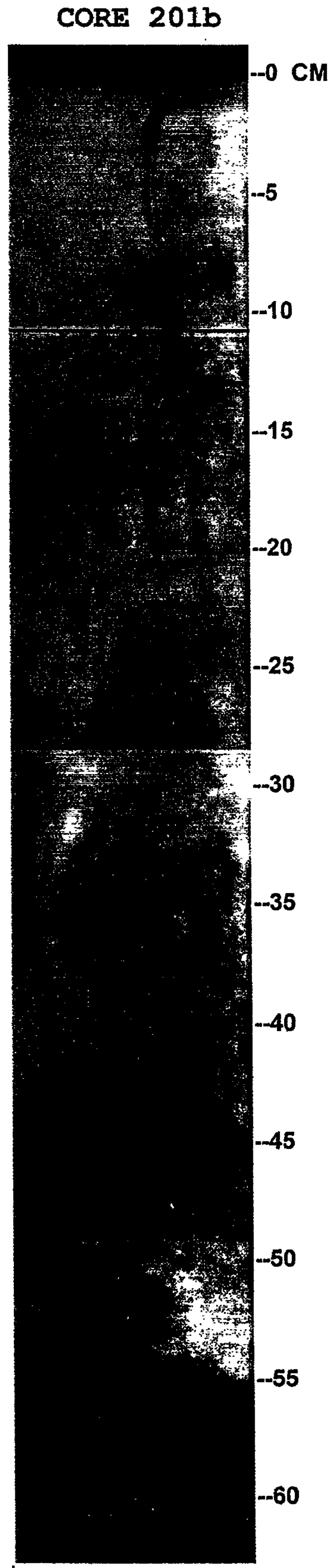

Figure C-133. X-Radiograph for Core 284.

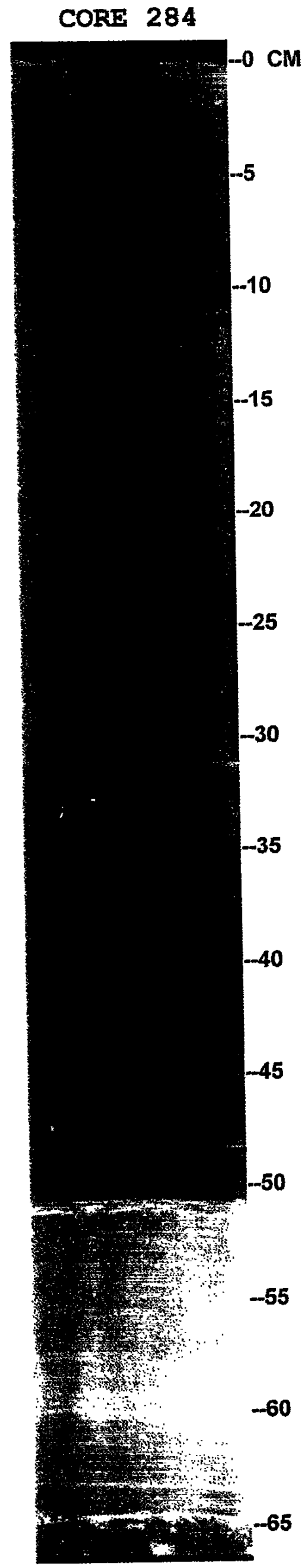

Figure C-134. X-Radiograph for Core 285.

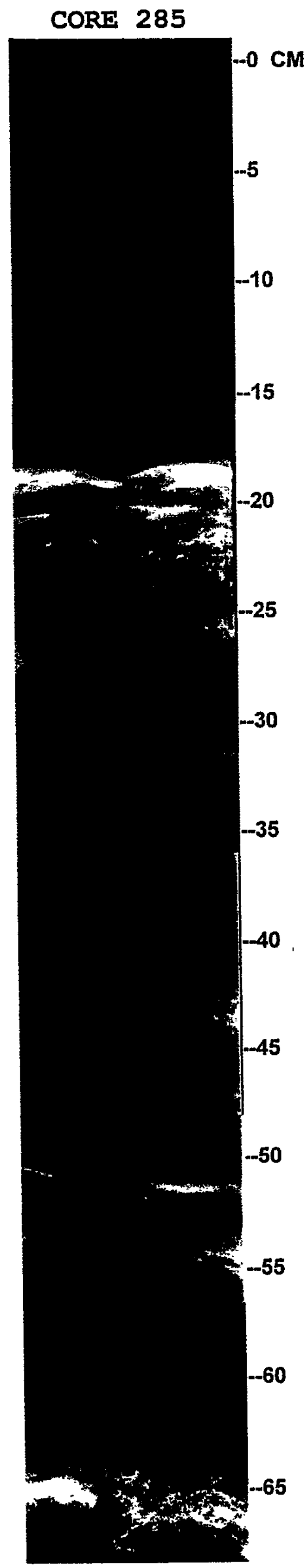

Figure C-135. X-Radiograph for Core 286.

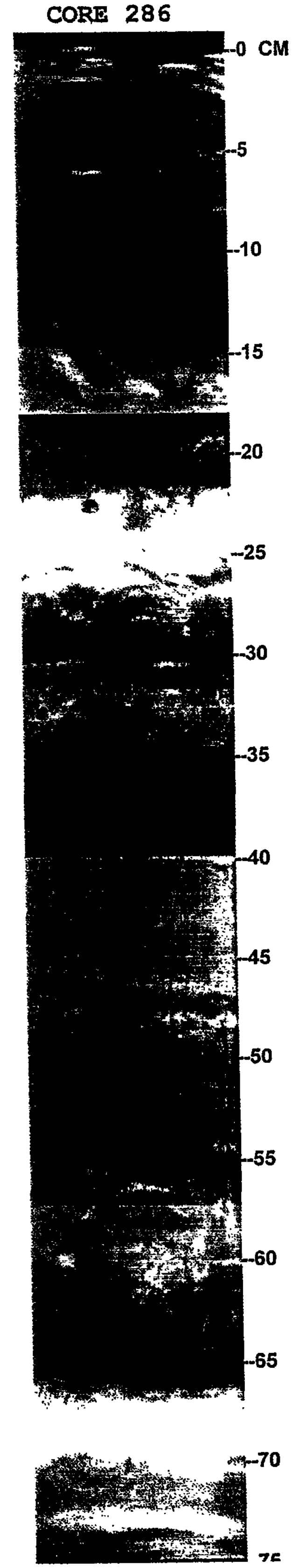

Figure C-136. X-Radiograph for Core 286b.

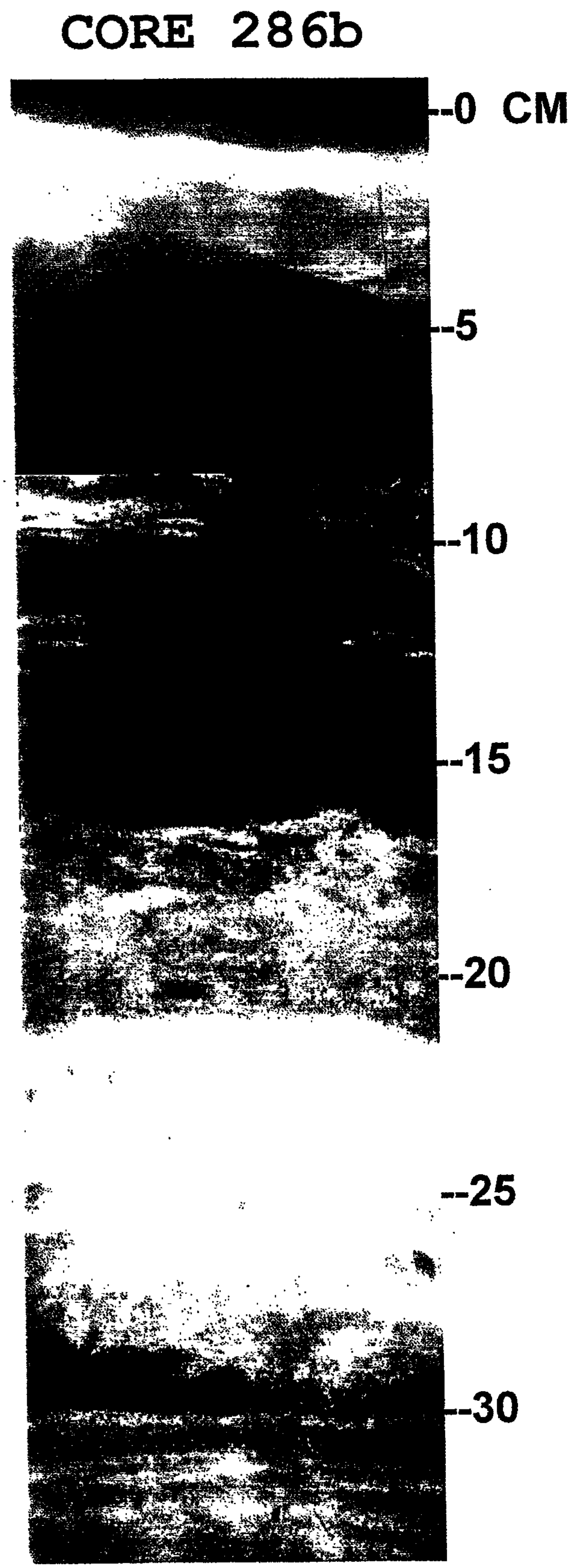

Figure C-137. X-Radiograph for Core 296.

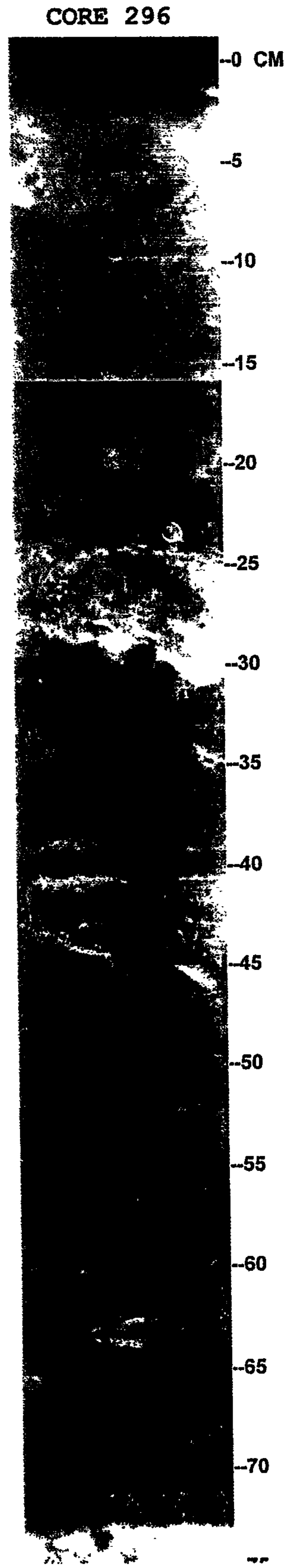

Figure C-138. X-Radiograph for Core 296N.

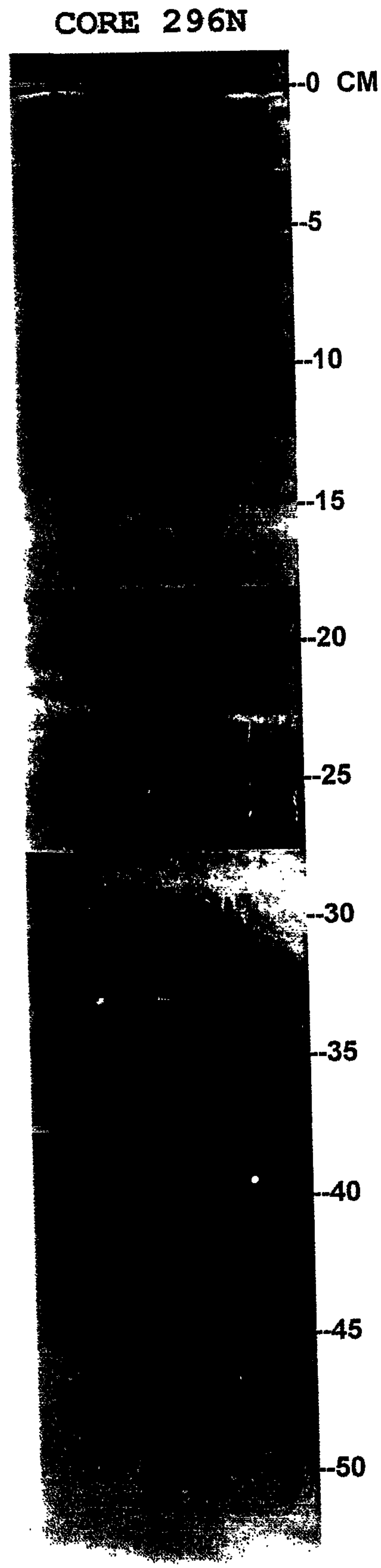

Figure C-139. X-Radiograph for Core 296S.

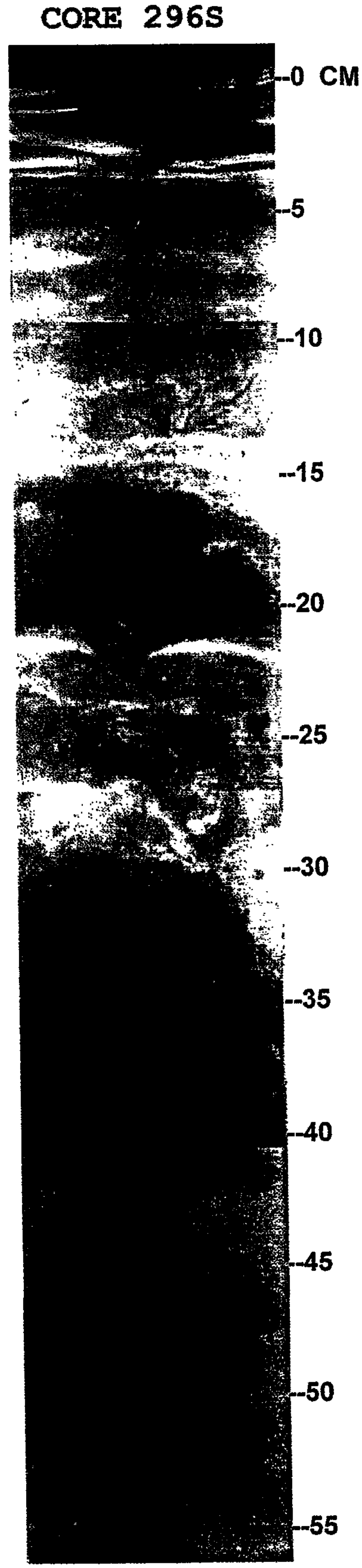

Figure C-140. X-Radiograph for Core 296E.

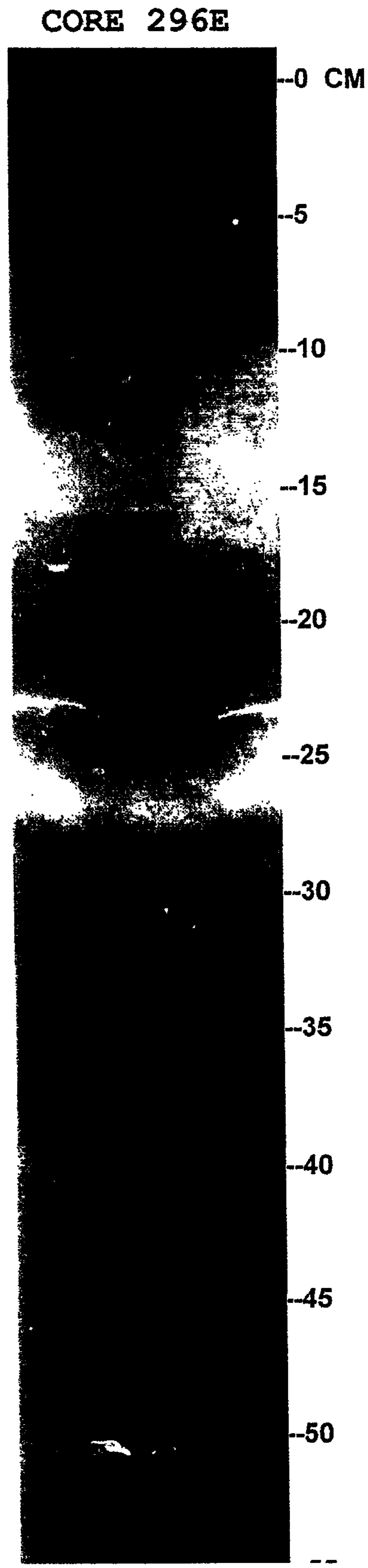

Figure C-141. X-Radiograph for Core 296W.

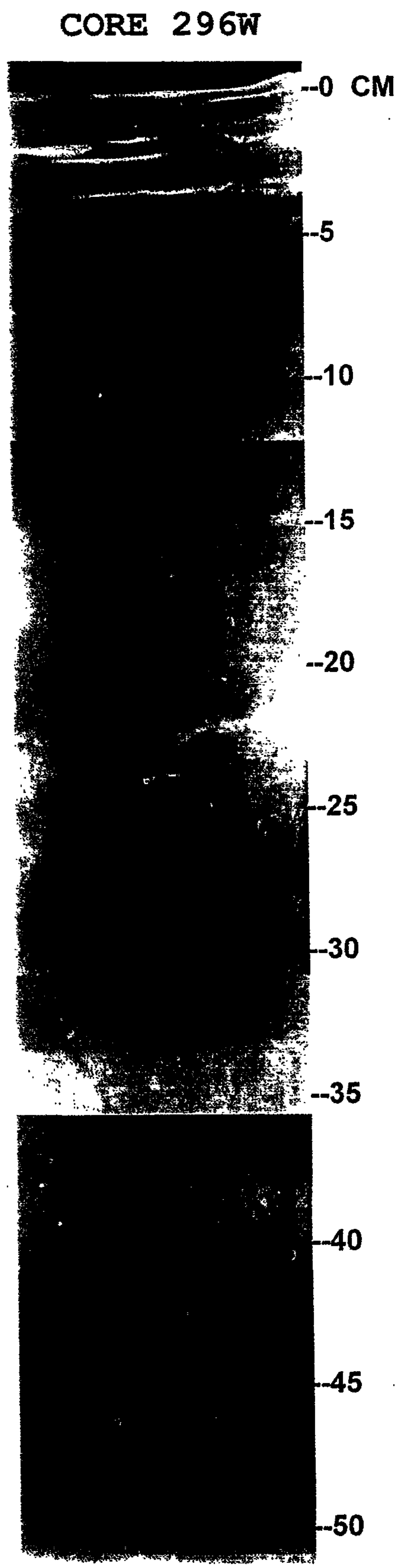

Figure C-142. X-Radiograph for Core 300.

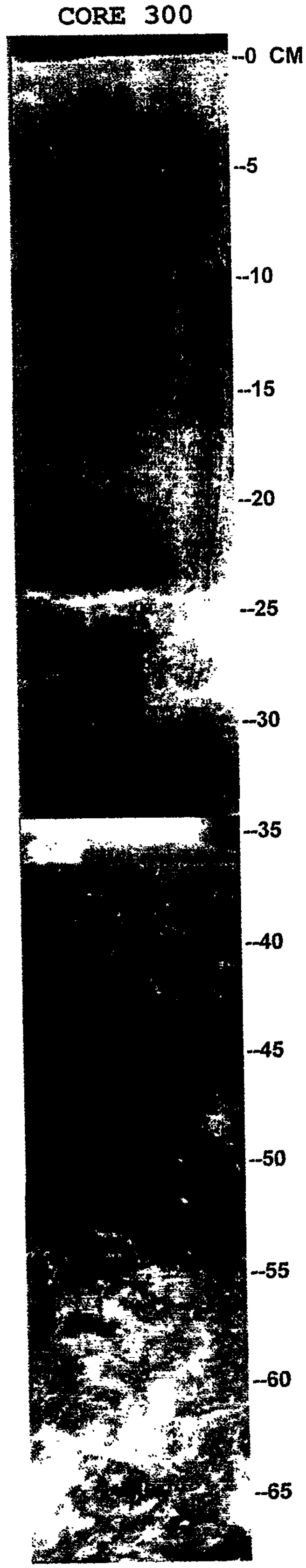

Figure C-143. X-Radiograph for Core 401.

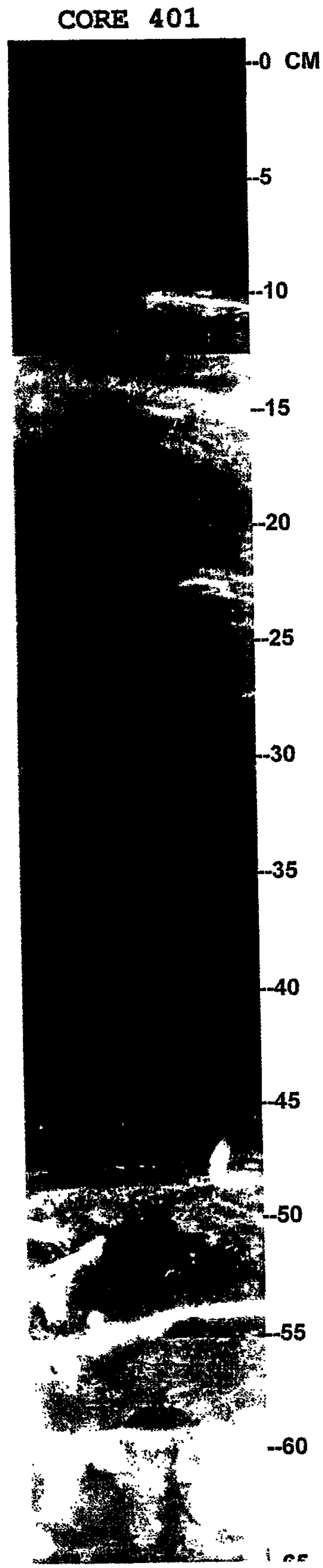

Figure C-144. X-Radiograph for Core 402.

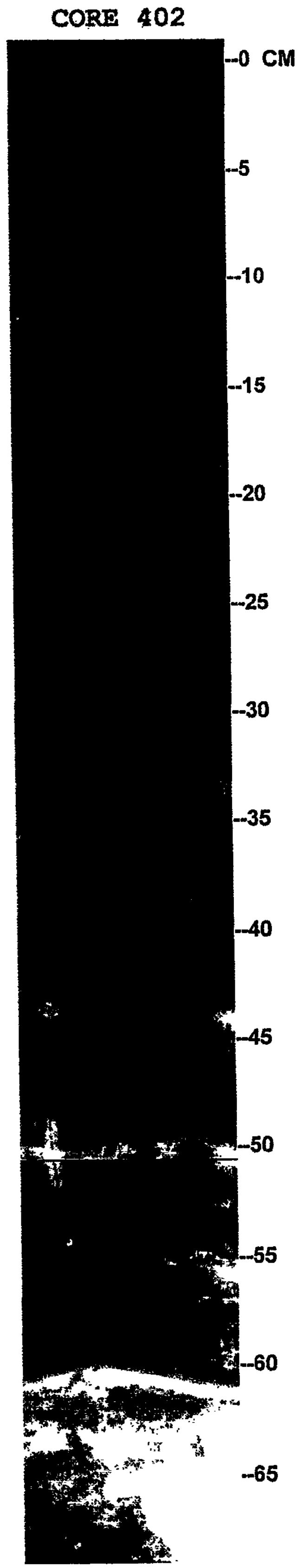

Figure C-145. X-Radiograph for Core 924.

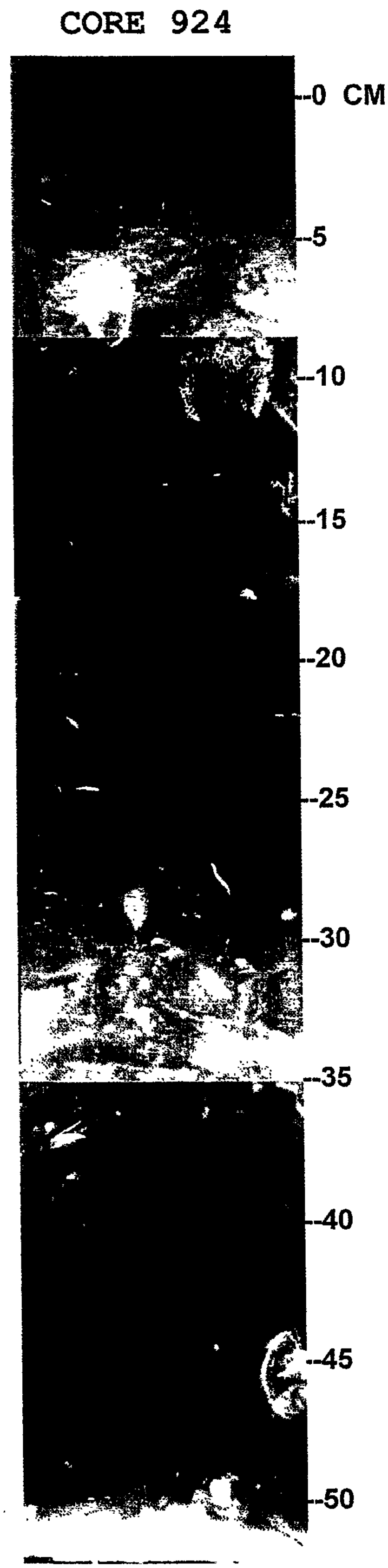

Figure C-146. X-Radiograph for Core 926.

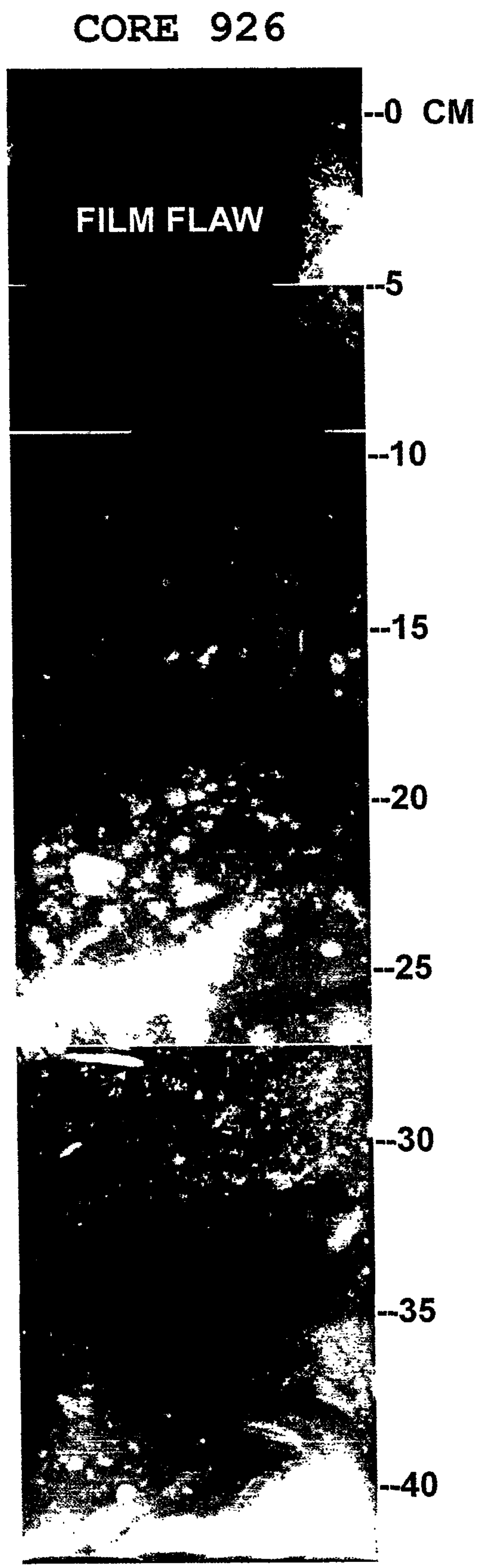

Figure C-147. X-Radiograph for Core 928.

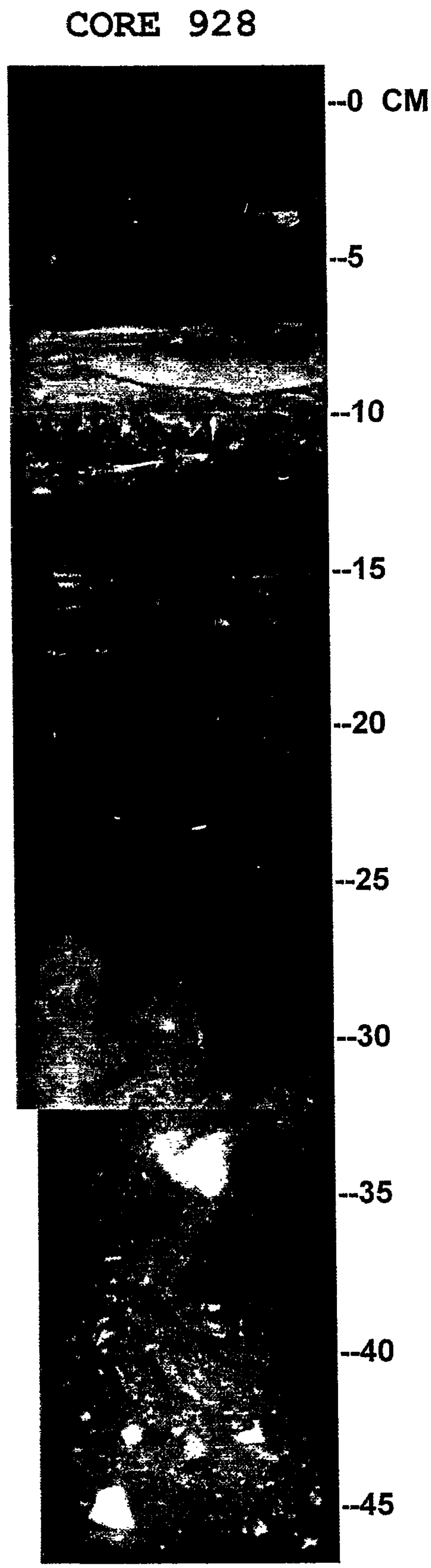

Figure C-148. X-Radiograph for Core 4293.

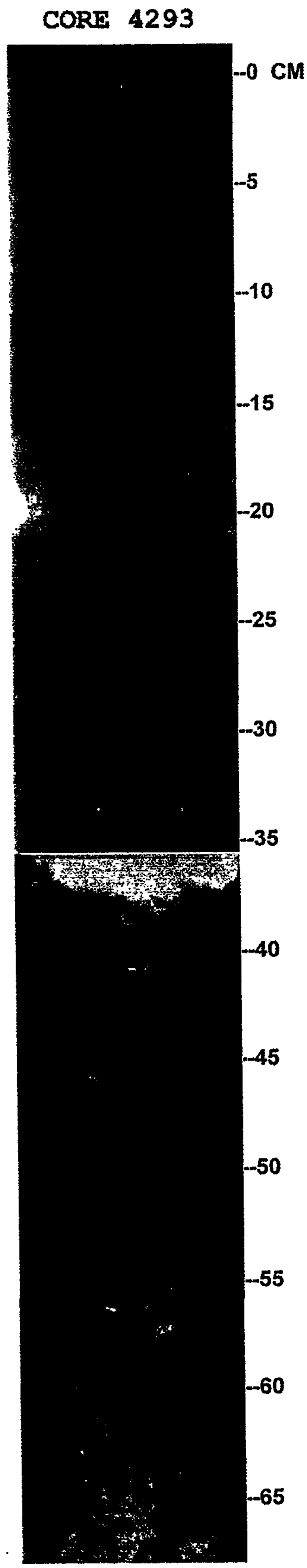

Figure C-149. X-Radiograph for Core 8271.

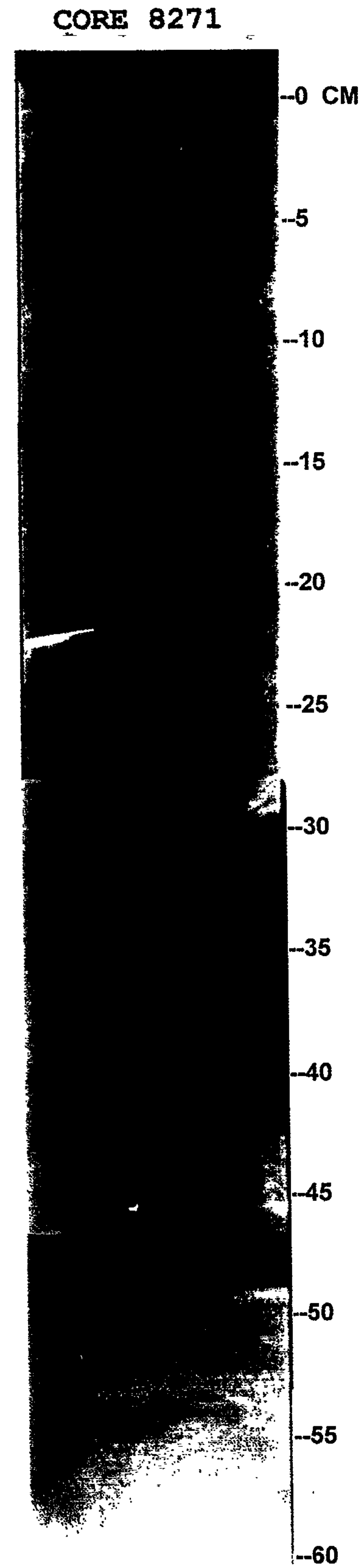

Figure C-150. X-Radiograph for Core 8826.

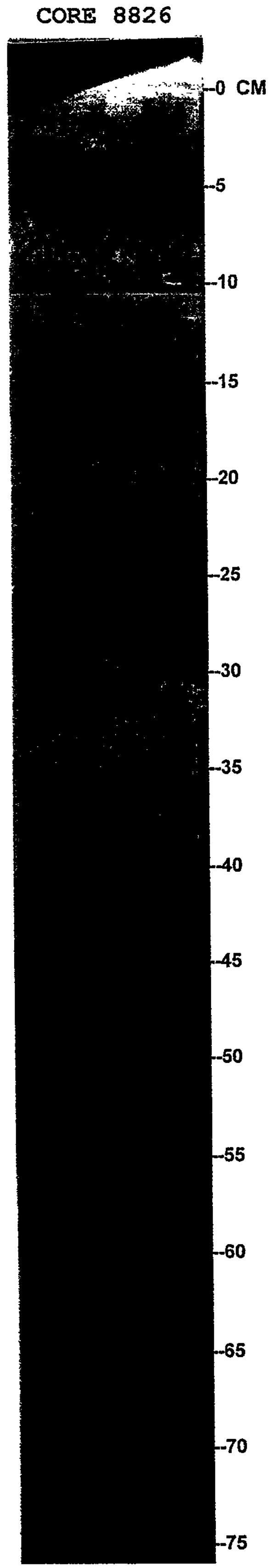

Figure C-151. X-Radiograph for Core 8827.

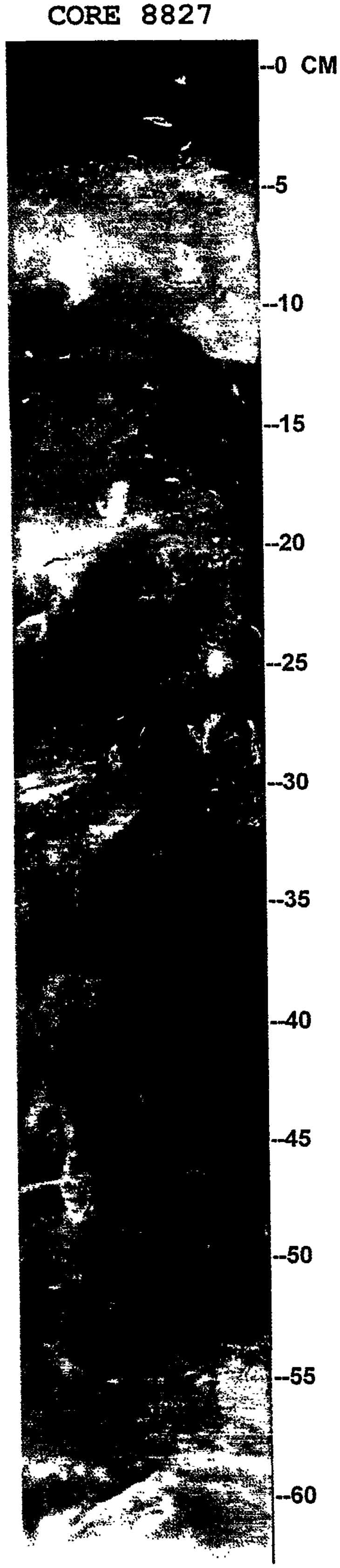

Figure C-152. Comparison of Cs-137 data and predictions from model simulations based upon parameters in the insert for Core 128. Note: two mixed areas were assumed $D_b(1)$ and a deeper mixed area $D_b(2)$. Including the deeper mixed layer based upon previous analysis does not significantly alter the model predictions compared to model simulations without this deep mixing parameter.

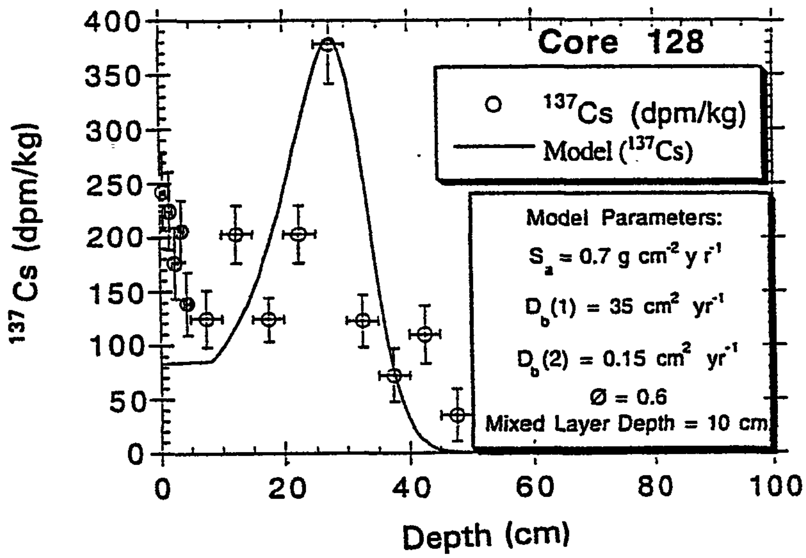

Figure C-153. Comparison of model predictions of Cs-137 at two mixing depths z_1 and z_2 for Core 128.

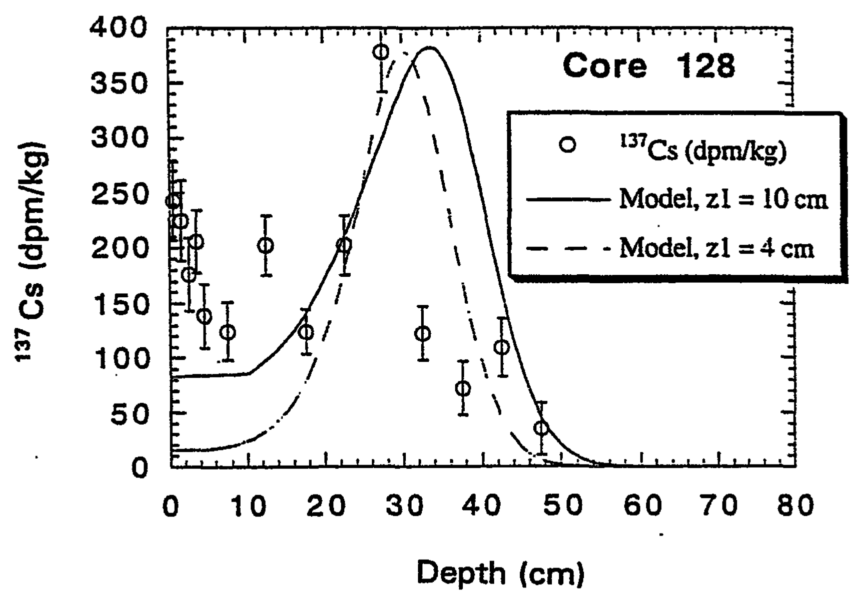

Figure C-154. Comparison of model predictions for Hg to observed Hg concentrations for Core 128.

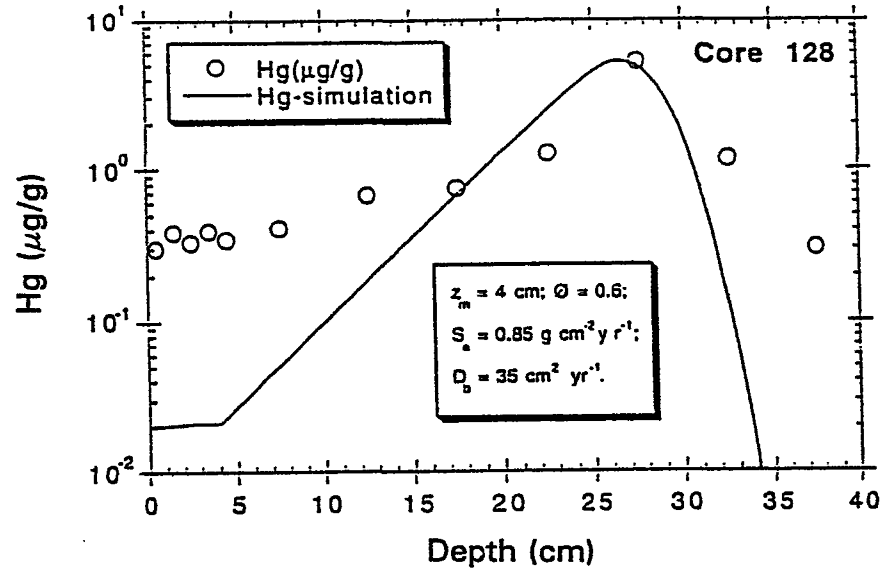

Figure C-155. Comparison of Cs-137 data and predictions from model simulations based upon the parameters in the insert for Core 134. Note: two mixed layers were assumed $D_b(1)$ and a deeper mixed area $D_b(2)$.

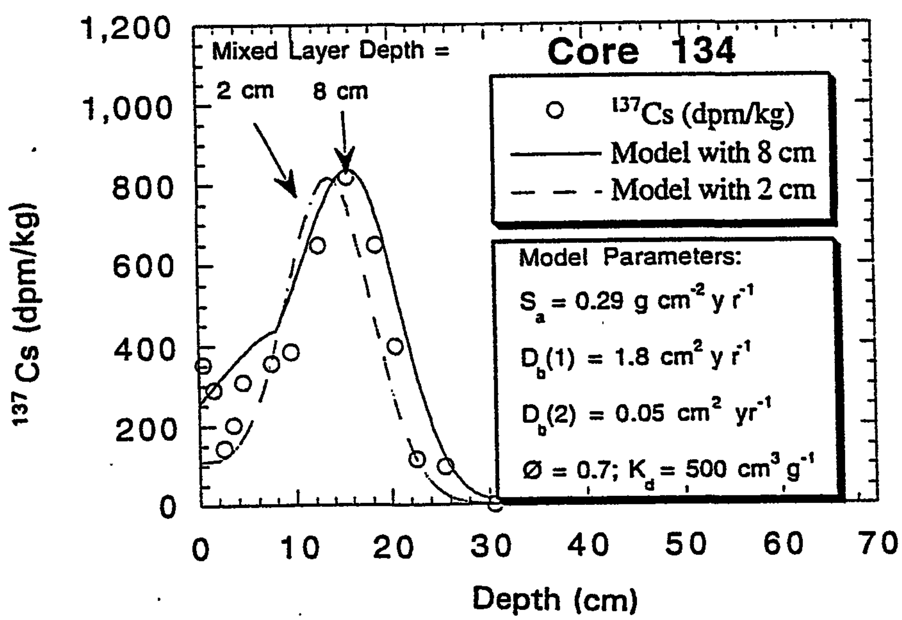

Figure C-156. Comparisons of model predictions of Cs-137 in Core 134 at two mixing depths, 2 cm and 8 cm, respectively.

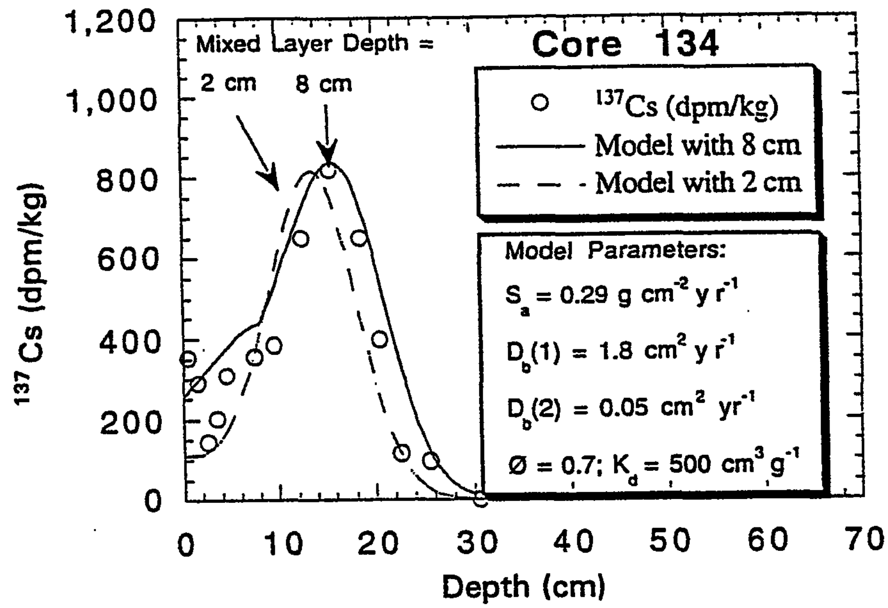

Figure C-157. Comparison of model predictions of Pu-239,240 for Core 134 to Pu concentrations observed in the core.

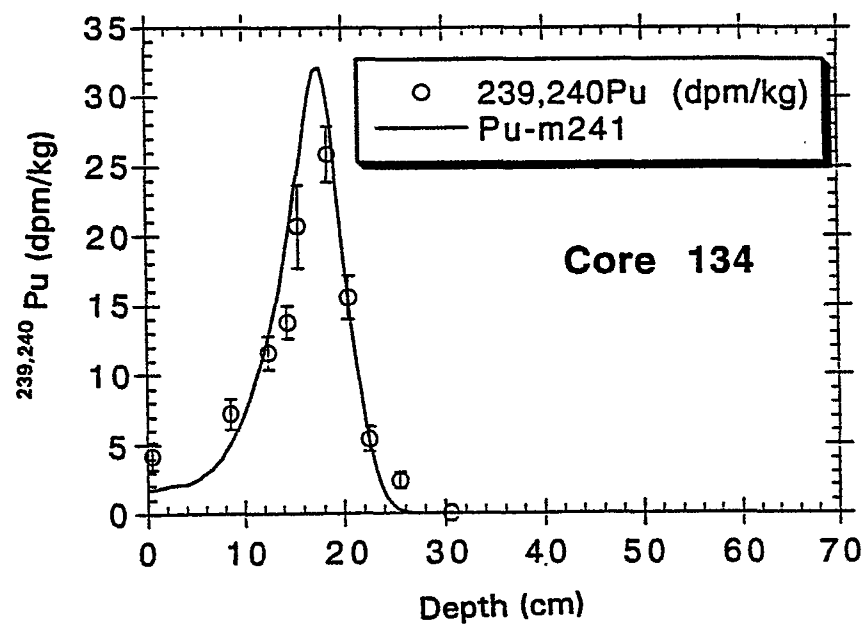

Figure C-158. **Model simulations of Hg, Pu, and ^{137}Cs profiles for Core 134.**

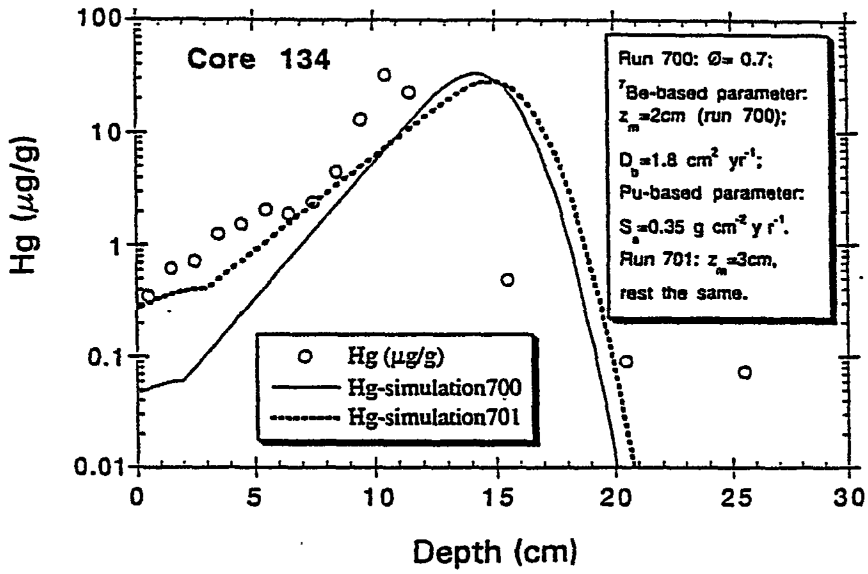

Figure C-159. **Model Simulations of Hg for Core 134.**

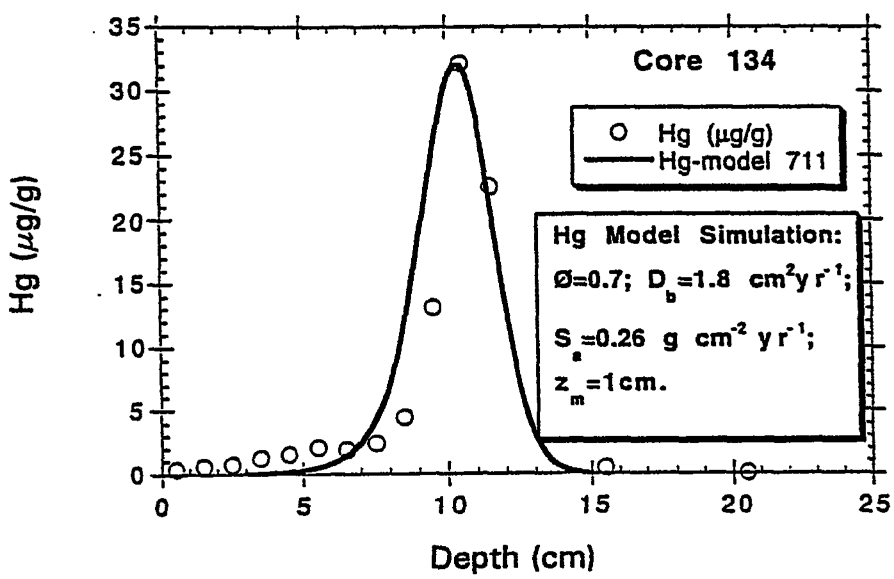

Figure C-160. Comparison of Cs-137 data and predictions from model simulations based upon parameters in the insert for Core 142.

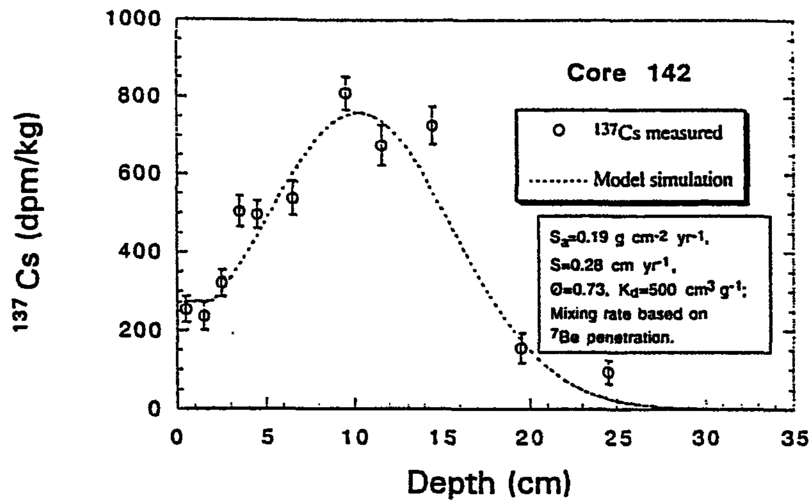

Figure C-161. Comparison of model predictions for Hg to observed Hg concentrations for Core 142.

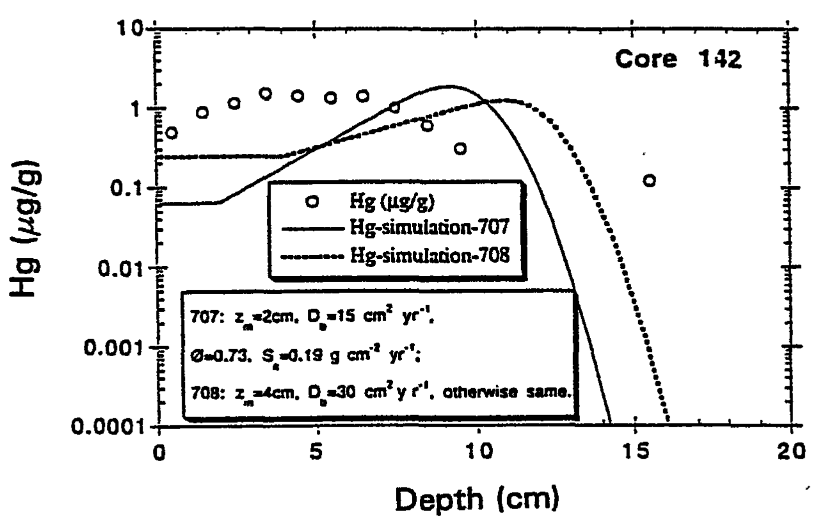

Figure C-162. **Comparison of Cs-137 data and predictions from model simulations based upon parameters in insert for Core 201. Note: two mixed layers were assumed $D_b(1)$ and a deeper mixed area $D_b(2)$. Model used a 2 cm upper mixed depth.**

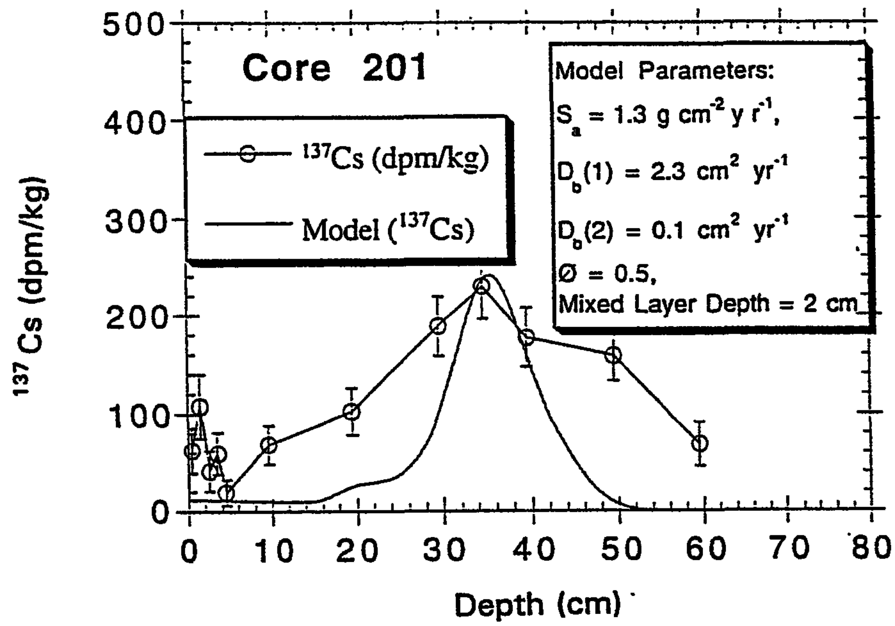

Figure C-163. **Model simulations of Hg, Pu, and ^{137}Cs profiles for Core 201.**

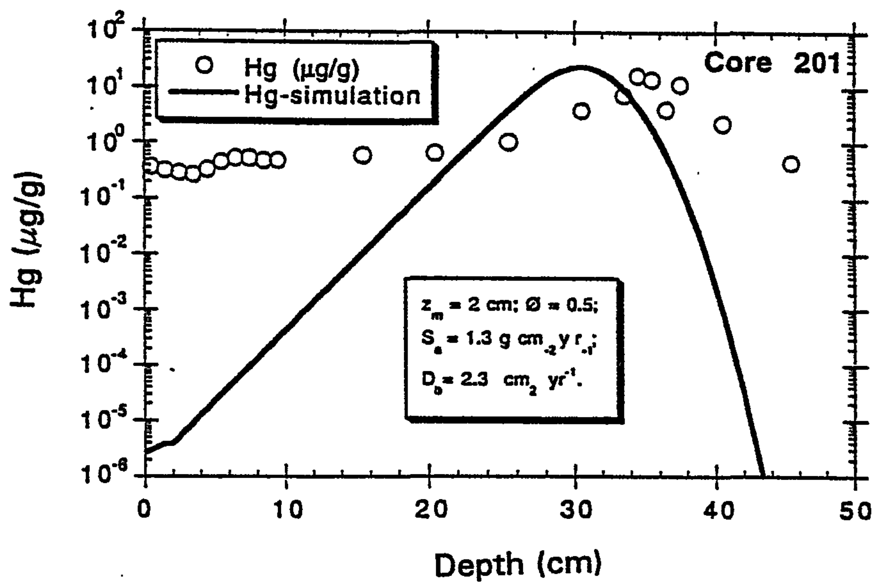

Figure C-164. Comparison of Cs-137 data and predictions from model simulations based upon parameters in insert for Core 296.

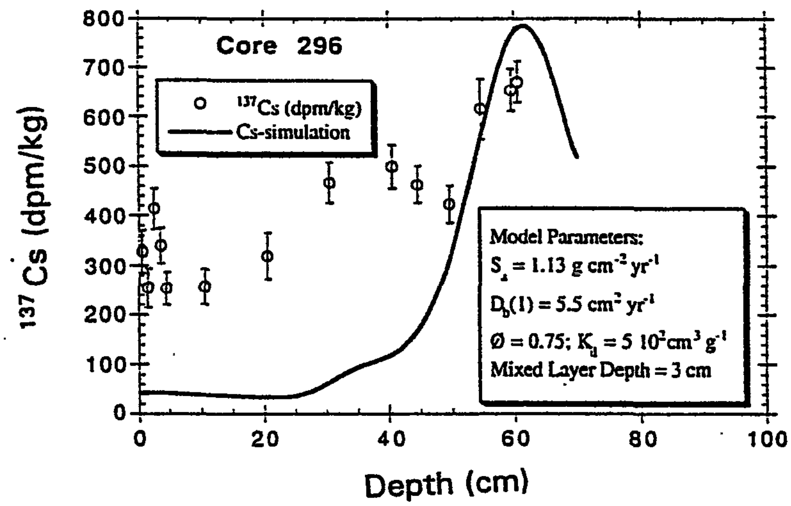

Figure C-165. Comparison of model predictions for Hg to observed Hg concentrations for Core 296.

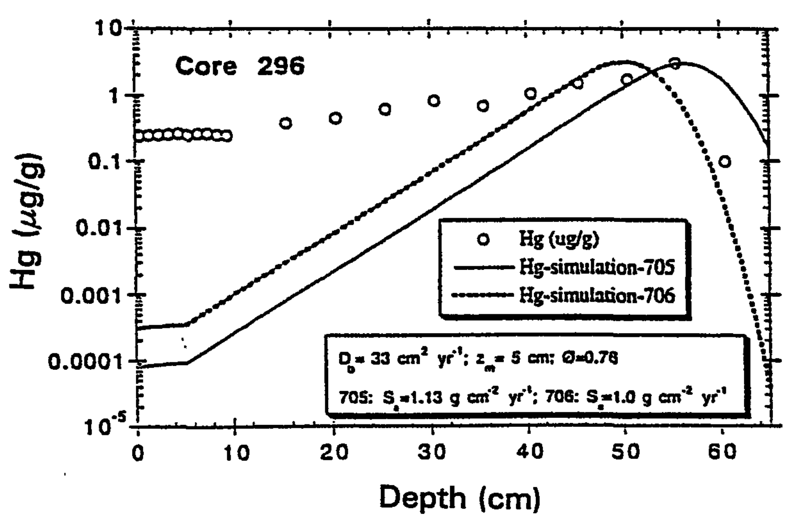

Figure C-166. Comparison of Cs-137 data and predictions from model simulations based upon parameters in the insert for Core 300.

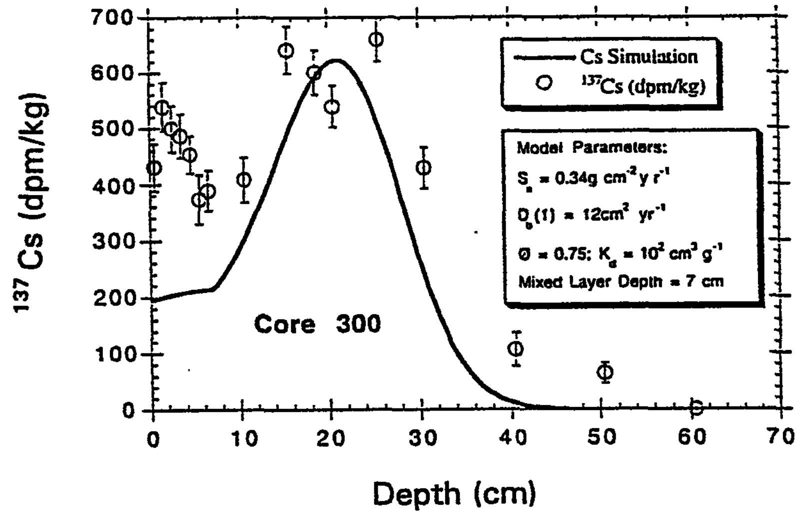

Figure C-167. Comparison of Hg data and predictions from model simulations based upon the parameters in the insert for Core 300.

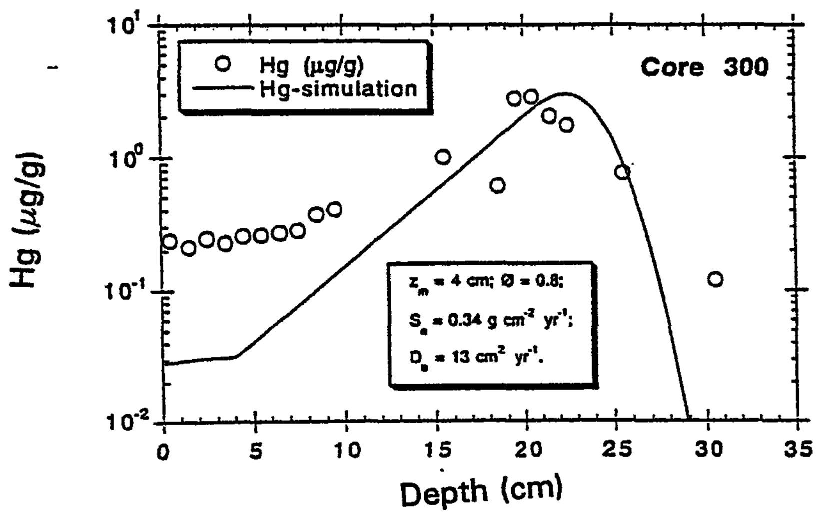

Figure C-168. Recovery rate calculation for surface sediment concentration of Hg in Core 128.

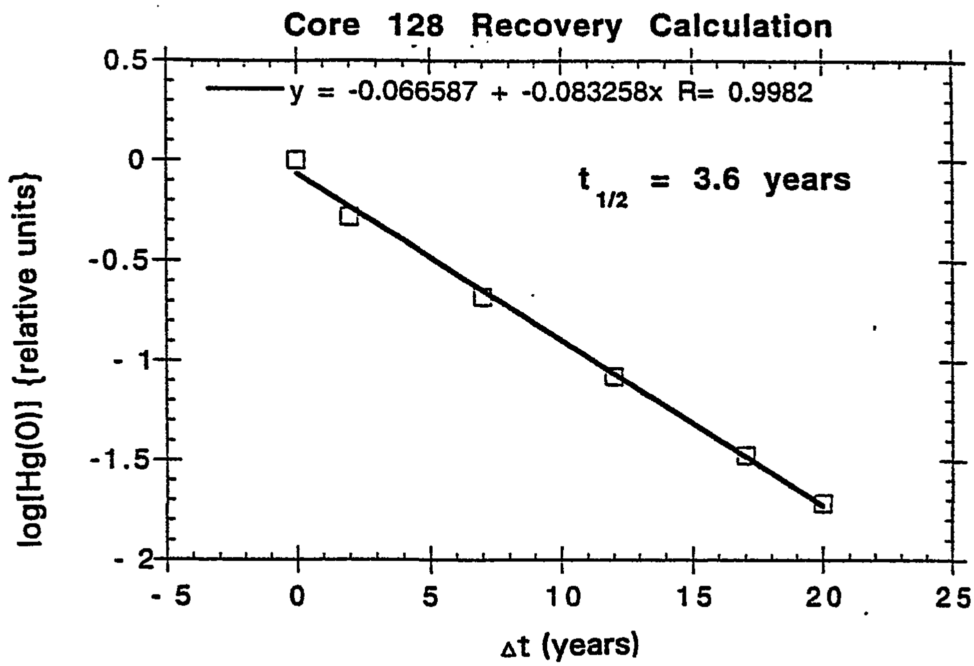

Figure C-169. Recovery rate calculation for surface sediment concentrations of Hg in Core 134.

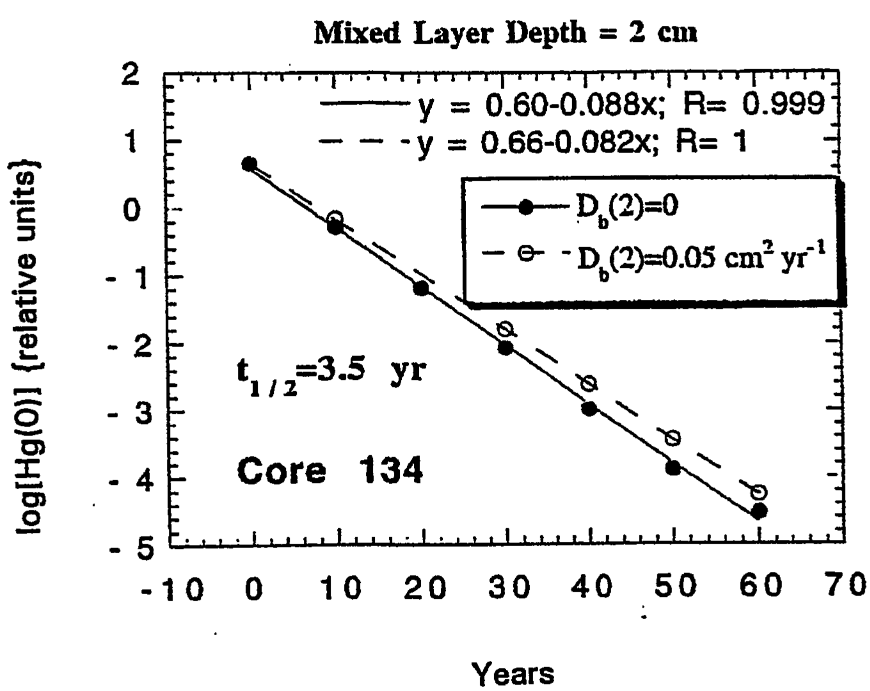

Figure C-170. **Recovery rate calculation for surface sediment concentrations of Hg for Core 134 for mixed depth of 2 cm. Figure also compares the effect of assuming a deep mixing coefficient $D_b(2)$ (which is assumed to be non-zero) on recovery rate predictions.**

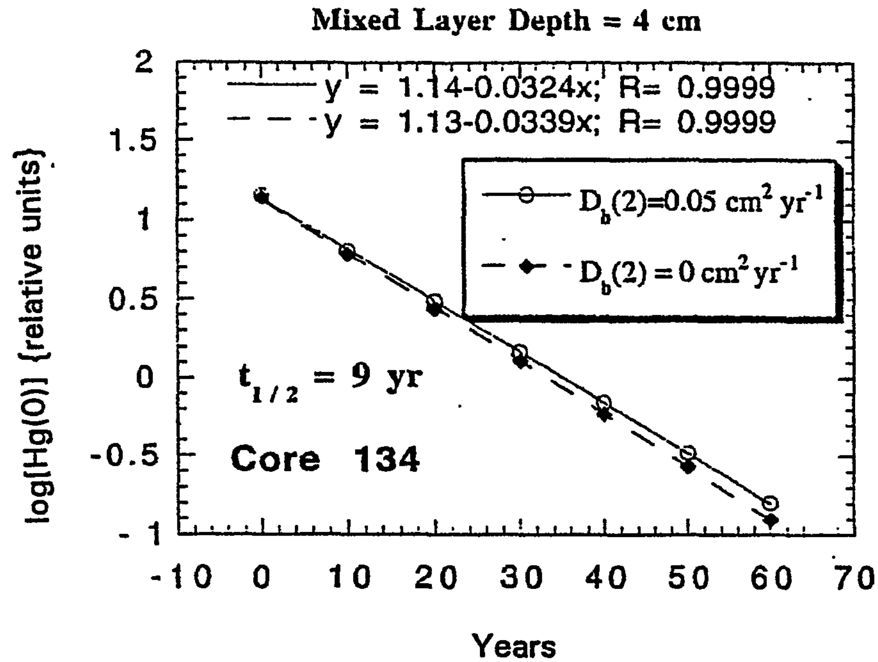

Figure C-171. **Recovery rate calculation for surface sediment concentrations of Hg for Core 201. The half life (t½) for the mercury concentrations to be reduced by half is 1 year.**

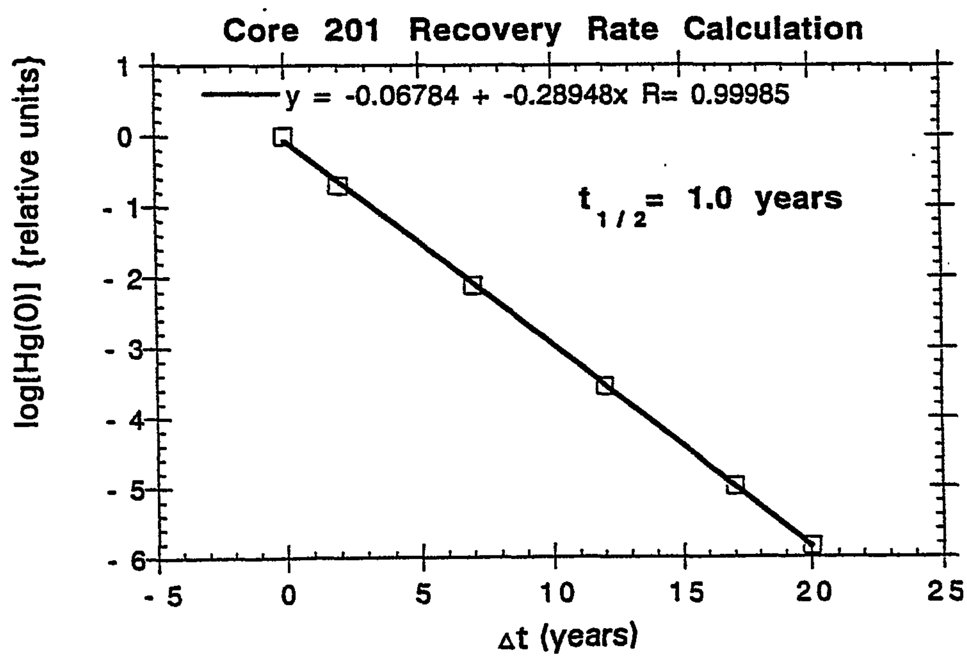

Figure C-172. Recovery rate calculation for surface sediment concentrations of Hg for Core 300.

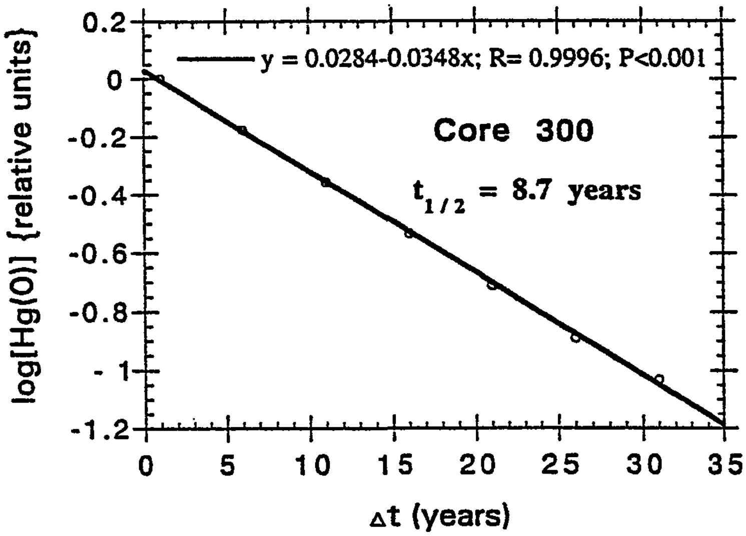

Figure C-173. Comparison of recovery half-times ($t_{½}$, in years) calculated for surface sediment concentrations of Hg to decrease to ½, determined by numerically modeling Hg distributions into the future, and a simple algorithm based on the travel time of a tracer through the mixed layer (i.e., ratio of mixed layer depth (z_m) to sedimentation rate (S), multiplied by natural logarithm of 2).